VENTRICLE-SPECIFIC FIBROTIC CARDIAC REMODELING IN THE PROGRESSION OF HEART FAILURE WITH PRESERVED EJECTION FRACTION

A Dissertation

presented to

the Faculty of the Graduate School

at the University of Missouri-Columbia

In Partial Fulfillment

of the Requirements for the Degree

Doctor of Philosophy

By

SHANNON C. KELLY

Dr. Craig A. Emter, Dissertation Supervisor

July 2022

The undersigned, appointed by the Dean of the Graduate School, have examined the dissertation entitled:

VENTRICLE-SPECIFIC FIBROTIC CARDIAC REMODELING IN THE PROGRESSION OF HEART FAILURE WITH PRESERVED EJECTION FRACTION

Presented by Shannon C. Kelly,

A candidate for the degree of Doctor of Philosophy in Biomedical Sciences, and hereby certify that, in their opinion, is worthy of acceptance.

_____

Craig A. Emter

_____

Kevin J. Cummings

_____

Laurel A. Grisanti

_____

R. Scott Rector

_____

Pilar Ruiz-Lozano

DEDICATION

To my parents, I am standing here today due to your support, encouragement, motivation, and love. I would not be where I am without you.

ACKNOWLEDGEMENTS

First and foremost, I would like to thank my advisor Dr. Craig Emter, for all of the support and guidance he has provided me over the last four years. Especially, for challenging me to expand my ideas, focus on the big picture and for pushing me out of my comfort zone numerous times. I would also like to acknowledge the countless opportunities he has provided me over the last few years.

I would also like to sincerely thank Dr. Kevin Cummings, Dr. Laurel Grisanti, Dr. Scott Rector, and Dr. Pilar Ruiz-Lozano for serving as my committee members and providing support, feedback, and guidance to explore new experimental questions and methods.

I am deeply appreciative of every member of the Emter lab for their technical support, emotional support and encouragement throughout this journey. To Pam Thorne, for your help with completing experiments, aid in trouble shooting, and providing a friendly, supportive ear when needed. To Jan Ivey, for your patience and support through cath lab days and beyond. To Kleiton Silva, for your guidance, advice, and reality checks. I would not be here without each of you. And to the newer members of the Emter Lab, Darla Tharp, Christina Mueller, and Amira Amin, thank you for your support though the end of this journey. I would also like to thank the current and past members of the Emter lab, including Jan Ivey, Dylan Olver, Jessica Hiemstra, and Jenna Edwards, who developed the animals models I utilized for this research.

To my fellow students, especially Nathan Kerr, Lauren Borkowski, and Toby Thomas, thank you for sharing office space with me, listening to me vent, providing emotional support, and much needed breaks in the day. As well as, Karol Dinwiddie and Tommy Thompson, who made any administrative task go smoothly and easily with your help and support.

To my parents, brother, sister-in-law, grandparents, aunts, uncles, cousins, and friends, thank you for encouraging me and reminding me throughout this process why I chose to take this step. I would not have made it without each one of you.

Lastly, to Olive Renee and Everly Margaret, my rays of sunshine and guiding lights through this storm. Thank you for reminding me to play, laugh, explore, sing, dance, and use my imagination throughout this process.

TABLE OF CONTENTS

LIST OF TABLES

LIST OF FIGURES

LIST OF NOMENCLATURE

α-SMA	Alpha-smooth muscle actin
AB	Aortic-banded
AB-INT	Aortic-banded intact
AB-OVX	Aortic-banded ovariectomized
ADAM	A disintegrin and metalloproteinase
ADAMTS	ADAM with thrombospondin motifs
AKT	Protein kinase B
AP-1	Activator protein 1
AU	Arbitrary units
BK_{Ca}	Large conductance calcium-activated potassium channels
BMI	Body mass index
BNP	Brain natriuretic peptide
BTEB	Basic transcription element binding protein
CDK	A-cyclin dependent kinase
cGMP	Cyclic guanosine monophosphate
CITP	Carboxy-terminal telopeptide of collagen type I
CKII	Casein kinase II
CON	Control
CON-INT	Control intact
CON-OVX	Control Ovariectomized
COPD	Chronic obstructive pulmonary disease
CSQ	Calsequestrin

DAB	diaminobenzidine
DUSP	Dual-specificity phosphatases
ECM	Extracellular matrix
EDP	End diastolic pressure
EDV	End diastolic volume
EEM	Elastin elastic modulus
EF	Ejection fraction
ELK1	ETS like-1 protein
EMSA	Electrophoretic mobility shift assay
ERα	Estrogen receptor alpha
ERβ	Estrogen receptor beta
ERK1/2	Extracellular signal-related kinase 1/2
ESR1	Estrogen receptor 1
ESR2	Estrogen receptor 2
ESV	End systolic volume
ETS1	ETS proto-oncogene 1
Fn	Fibronectin
GSK3β	Glycogen synthase kinase 3 beta
HERS	Heart and Estrogen/Progestin Replacement Study
HF	Heart failure
HFmrEF	Heart failure with mid-range ejection fraction
HFrEF	Heart failure with reduced ejection fraction
HFpEF	Heart failure with preserved ejection fraction

HRT	Hormone replacement therapy
IHC	Immunohistochemistry
IL-8	Interleukin-8; CXCL8
IPA	Ingenuity Pathway Analysis
ITGB8	β_8-integrin
JNK	c-Jun N-terminal kinase
LSD	Least significant difference
LV	Left ventricle
LIF	Leukemia inhibitory factor
MAP	Mean arterial pressure
MAPK	Mitogen-activated protein kinase
MAP2K	Mitogen-activated protein kinase kinase; MEK, MKK
MAP3K	Mitogen-activated protein kinase kinase kinase; MEKK, MKKK
MAPK1	ERK2
MAPK3	ERK1
MAPK8	JNK1
MAPK9	JNK2
MMP	Matrix metalloproteinases
MPA	medroxyprogesterone acetate
NHLBI	National Heart, Lung, and Blood Institute
NO	Nitric oxide
NPPA	Atrial natriuretic peptide
OVX	Ovariectomized

PEA-3	Polyomavirus enhancer activator 3
pERK	Phosphorylated-ERK
PGR	Progesterone receptor
PGRMC1	Progesterone receptor membrane component 1
PI3K	Phosphatidylinositol 3-kinase
PICP	Carboxy-terminal pro-peptide of procollagen I
PINP	Amino-terminal pro-peptide type I
PIIINP	Amino-terminal pro-peptide type III
pJNK	Phosphorylated-JNK
PKC	Protein kinase C
PKG	Protein kinase G
PSR	Picrosirius red
PTX3	Pentraxin 3
RCA	Right coronary artery
RV	Right ventricle
RVD	Right ventricle dysfunction
SAPK	Stress-activated protein kinase
SE	Standard error
SP1	Specificity protein 1
SV	Stroke volume
TAC	Trans aortic constriction
TGF-β	Transforming growth factor-beta
TIMP	Tissue inhibitor of matrix metalloproteinases

WD-AB	Western-diet fed, aortic-banded
WGA	Wheat germ agglutinin
WHI	Women’s Health Initiative

ABSTRACT

Heart failure with preserved ejection fraction (HFpEF) is currently the most prominent form of heart failure (HF). Despite the rising prevalence over the last few years, the pathogenesis of this disease is still unknown. Therefore, the focus of this dissertation is to investigate the molecular pathogenesis of fibrotic cardiac remodeling in swine models of HFpEF as cardiac fibrosis is a hallmark feature of this disease and hypothesized to be involved in its pathogenesis. Fibrotic cardiac remodeling can occur when there is a dysregulation between the synthesis and degradation of extracellular matrix (ECM) proteins. Additionally, the focus of this dissertation is to evaluate fibrosis in the left and right ventricles as right ventricle (RV) dysfunction can increase the risk of mortality up to 80% in individuals with HFpEF. Overall the goals of this dissertation are two-fold. First, to evaluate RV remodeling in a cardio-metabolic swine model of HFpEF. Second, to investigate the differences between the regulation of cardiac fibrosis in left ventricle (LV) and RV in a swine model subject to chronic pressure overload and/or the loss of female sex hormones. With the cardio-metabolic swine model, RV transcriptome analysis identified MAPK8/JNK1 as a hub gene associated with ECM remodeling that included an increase in fibronectin in the right coronary artery (RCA). This increase in fibronectin was potentially due to a regulatory imbalance between JNK and matrix metalloproteinase-14 (MMP-14). Additionally, this increase in fibronectin was associated with an increase in vascular stiffness. With the second goal of this study, it was demonstrated that the regulation of cardiac fibrosis occurs in a chamber-specific manner. In the LV, there was an increase in total collagen

levels due to the loss of sex hormones but this increase in fibrosis was not a result of linear alterations in synthesis or degradation. In the RV, though, there was an increase in total collagen levels due to chronic pressure overload and independent of the loss of sex hormones. This increase in fibrosis was due to an increase in synthesis associated with increases in JNK activation and myofibroblast activation. Taken together, these results demonstrate differences in the regulation of ECM remodeling that occur in the LV, RV, and RCA in two swine models with relevance to HFpEF. This emphasizes the need to further explore the regulation of ECM remodeling at multiple levels of the heart in order to fully understand the pathogenesis of HFpEF.

CHAPTER 1: INTRODUCTION

Heart Failure

Heart failure (HF) is growing epidemic that is expected to increase from 6 million to 8 million cases with an economic burden more than doubling from $30.7 billion to $69.8 billion by the year 2030 (1, 2). The lifetime risk of developing HF can range from 20% to 45% in individuals aged 45 to 95, respectively. Currently, heart disease is the leading cause of death in the US. 1 in 8 deaths have HF mentioned on the death certificate and the number of deaths with an underlying cause of HF has increased 52.8% over the last decade (1).

HF occurs when there is a lack of cardiac reserve either through contraction or relaxation impairment resulting in exercise intolerance, dyspnea, fatigue, and edema (3, 4). There are three HF subclasses that are categorized based on ejection fraction: HF with reduced ejection fraction (HFrEF), HF with mid-range ejection fraction (HFmrEF), and HF with preserved ejection fraction (HFpEF). While the classification of HF based on ejection fraction is not definitive, it is typically thought of as HFrEF having an ejection fraction below 35-40%, HFmrEF having an ejection fraction between 40-49%, and HFpEF having an ejection fraction above 50% (5, 6). In addition to the lack of cardiac reserve and symptoms mentioned previously, each subtype of HF presents with elevated brain natriuretic peptide (BNP) levels and left ventricular (LV) remodeling (7). With HFrEF, the LV remodeling consists of eccentric hypertrophy with chamber dilation and thinning of the ventricle wall (3). This eccentric remodeling can occur with HFmrEF in addition to left atrial enlargement (5, 7). HFpEF presents with LV concentric hypertrophy

with an increase in wall thickness without a change in chamber dimensions. Previously, HFrEF was known as systolic HF while HFpEF was known as diastolic HF but these classifications are no longer utilized as all three HF subtypes can present with both systolic and/or diastolic impairments (3).

While HFrEF was the most prominent form of HF, the rates of HFpEF have steadily been increasing over the past few decades making it the most prominent form of HF with morbidity and mortality rates similar to values observed in HFrEF (8). This rise in the prevalence of HFpEF is often attributed to an aging population and an increase in comorbidities such as hypertension and diabetes (9). Despite the increased incidence of HFpEF, conventional HF treatments have failed to improve the prognosis of this HF sub-group illustrating the need to understand its specific pathophysiology (6). While the pathogenesis of HFrEF stems from myocardial injury, such as myocardial infarction, the pathogenesis of HFpEF is not well defined (10). It has been hypothesized that HFpEF arises from a chronic inflammatory state associated with comorbidities like metabolic syndrome and hypertension that lead to left ventricular dysfunction and remodeling (10, 11). Since the pathogenesis of HFpEF is not completely defined, the National Heart, Lung, and Blood Institute (NHLBI) working group has recommended that the study of the molecular pathogenesis of HFpEF be a focus over the next ten years in order to develop novel treatment strategies (10).

Heart Failure with Preserved Ejection Fraction

As previously mentioned, HFpEF was formerly classified as diastolic HF, as diastolic dysfunction was a hallmark feature of this subclass of HF. The clinical

classification has since expanded and now HFpEF is clinically classified as having symptoms of HF including a lack of cardiac reserve and exercise intolerance, an ejection fraction greater than 50%, and either LV hypertrophy, left atrial enlargement, or diastolic dysfunction (7). However, HFpEF is a complex and heterogenous disease that is influenced by multiple other clinical parameters including cardiac impairments and comorbidities. Other cardiac impairments seen in HFpEF include: chronotropic incompetence, elevated left atrial pressure, abnormal E/A or E/e' ratio, right ventricle (RV) dysfunction, diffuse myocardial fibrosis, increased vascular stiffness, and impaired vascular and coronary microvascular function (4, 6, 12-14). Individuals with HFpEF may have multiple comorbidities with as much as 50% of patients having more than 5 comorbidities. Comorbidities often seen with HFpEF include: obesity, insulin resistance, diabetes mellitus, hypertension, atrial fibrillation, pulmonary hypertension, kidney disease, skeletal muscle weakness, chronic lung disease, liver disease, and cancer (4, 13, 15-18). Individuals with HFpEF are also older in age and tend to be female (15).

HFpEF is hypothesized to arise from a chronic inflammatory state due to the multiple comorbidities present such as obesity, hypertension, diabetes mellitus, chronic obstructive pulmonary disease (COPD), and kidney disease (11). This increase in inflammation is systemic as it can affect skeletal muscle, pulmonary vasculature and the kidneys in addition to the heart; therefore, HFpEF is a multi-organ disease. This increase in systemic inflammation can lead to an increase in myocardial stiffness through multiple mechanisms and an increase in LV filling pressures. First, individuals with HFpEF see increases in proinflammatory

signaling with increases of growth differentiation factor-15, interleukin 1 receptor-like 1, c-reactive protein, and interleukin 6. This increase in proinflammatory signaling can be due to comorbidities like obesity or alterations in the hemodynamic load. This can lead to increases in the activation of immune cells such as macrophages and fibroblasts which are pro-fibrotic. Individuals with HFpEF have an increase in the volume of collagen leading to a less compliant, stiffer ventricle which would affect the passive stiffness (11). Myocardial stiffness is also altered in individuals with HFpEF due to alterations in titin, which is a sarcomeric protein responsible for passive stiffness. This can occur through a decrease in the more compliant titin isoform N2BA, decreased phosphorylation of titin, or an increase in the noncompliant isoform N2B, all of which would decrease the distensibility (8). However, LV end-diastolic pressure does not correlate with titin-based stiffness, but does correlate with collagen-based stiffness suggesting that collagen plays a more prominent role in the development of diastolic dysfunction (19). This increase in inflammatory signaling due to multiple comorbidities can also alter paracrine signaling between endothelial cells and cardiomyocytes which would decrease nitric oxide (NO) and cyclic guanosine monophosphate (cGMP). This decrease in signaling can lead to an increase in cardiomyocyte hypertrophy and concentric remodeling of the heart (11, 18).

The five-year mortality rate in individuals with HFpEF is between 65-75% (4, 14). The cause of death in individuals with HFpEF is not always attributed to cardiac symptoms. In reality, 30-40% of deaths in individuals with HFpEF is attributed to comorbidities such as renal dysfunction, respiratory dysfunction,

infections, or cancer (20). The other 60-70% of deaths are attributed to cardiac events such as sudden death, myocardial infarction, aortic aneurysm, pulmonary embolism, stroke, progressive pulmonary hypertension and right heart failure (20).

There are currently no treatment options available for individuals with HFpEF as HFpEF is a heterogenous systemic disease that affects multiple organ systems. Drugs utilized to treat HFrEF including angiotensin-converting enzyme inhibitors, angiotensin-receptor blockers, aldosterone-receptor blockers, and beta blockers have not been shown to be efficacious (20). Recommended treatment strategies focus on treating symptoms such as reducing LV filling pressures with diuretics or treating the comorbidities to improve quality of life (18, 20). However, there have been a few studies conducted to determine if exercise is a beneficial treatment strategy for individuals with HFpEF. Studies that have evaluated exercise training via biking or treadmill exercise have shown improvements in cardiorespiratory fitness evaluated by VO_2 peak, six-minute walk distance, time to exhaustion, HR reserve and oxygen pulse (21-24). However, there are conflicting results on whether exercise directly improves LV function, diastolic function or quality of life in individuals with HFpEF. In a study that evaluated caloric restriction and exercise, caloric restriction reduced LV mass and LV wall thickness as well as improved E/A ratio, a measure of diastolic function, while exercise alone did not alter any cardiac parameters. Most studies have evaluated overall cardiorespiratory fitness of LV function. However, one study evaluated RV global longitudinal strain and reported improvements after high intensity interval training for 4 weeks with no alterations in LV function (25). Therefore, while exercise may

not alter heart morphology or function alone, it did improve exercise capacity, which is often compromised in individuals with HFpEF. In addition to the lack of effective treatment for HFpEF, myocardial biopsies from individuals with HFpEF are not readily available which limits gene expression, protein expression, and subsequent -omics analyses that would aid in the understanding of the pathogenesis of this disease and development of possible therapeutics. Since these biopsies are not readily available, the development of animal models with clinical relevance to HFpEF is crucial for the understanding of the development of this disease.

The Left and Right Ventricles

The heart can be divided into the left heart and the right heart. The left heart pumps oxygenated blood into the systemic circulation while the right heart pumps deoxygenated blood into the pulmonary circulation (26). The RV is a crescent-shaped, thin-walled ventricle compared to the more spherical, thick-walled LV. The RV also has smaller cardiomyocytes and a smaller mass but with 30% more collagen. Little research has been conducted on protein and gene expression differences between the two ventricles but due to differences in morphology and function seen in the RV and LV, the processes and pathways altered in LV in the progression of HF cannot be generalized to the RV.

The RV can be thought of as the “forgotten ventricle” as the general focus of HFpEF is on LV dysfunction and most research has solely evaluated the LV even though right ventricular dysfunction (RVD) has been associated with more frequent hospitalization as well as increases in mortality (27, 28). RVD occurs

when the RV is not able to meet the body's metabolic demands. The pathogenesis of RVD in HFpEF is unknown but it is hypothesized to arise from comorbidities such as pulmonary hypertension, atrial fibrillation, obesity, or renal dysfunction (28, 29). Specifically, the development of RVD can occur through an increase in afterload due pulmonary hypertension, a common comorbidity seen with HFpEF, or through an increase in pulmonary vascular resistance via other HFpEF comorbidities such as COPD, hypertension, or obesity. This increase in afterload can result in an RV dilation and hypertrophy to compensate for the increase in pressure gradient but over time this can deteriorate into RVD (28). The development of RVD can also occur though interventricular dependence. The LV and RV share a septal wall in addition to muscle fibers; therefore, contraction in the LV can aid in contraction in the RV. When there is an increase in RV afterload, such as with pulmonary hypertension, the RV can dilate and protrude towards the LV thus hindering LV filling and lead to an increase in RV size and dysfunction (28, 30).

A meta-analysis of clinical studies looking at RVD estimates 18-28% of individuals with HFpEF also have RVD (31). However, this number could be an underestimate. In these studies, echocardiography measurements are taken at rest when the RV may be functioning normally. In most HFpEF patients, cardiac function becomes compromised during stress, such as exercise. From these clinical studies, those with RVD had increased renal dysfunction, more severe pulmonary vascular disease, atrial fibrillation, coronary artery disease, higher body-mass index (BMI), higher RV filling pressures, increased RV mass, RV

remodeling, and reduced RV ejection fraction (EF) (31-34). Overall individuals with RVD have a more severe phenotype that can lead to decreased survival rates but little research has been conducted targeting the pathology of this dysfunction or possible treatment strategies (35). In a clinical study that evaluated the four-year progression of LV and RV function in individuals with HFpEF, RVD was shown to increase over time with increase in RV diastolic area and decreases in RV fractional area change. In comparison, only minor changes were seen in the LV. In those individuals that developed RVD, the risk of death was increased by 80% (34). However, in another retrospective analysis of individuals with HFpEF, the risk of death was associated with an increase in LV mass and LV fibrosis but not associated with LV end diastolic volume (EDV), LV end systolic volume (ESV), LV stroke volume (SV), LV EF, RV EDV, RV ESV, RV SV, RV EF, or RV mass (36). This study did not specify the length of time since diagnosis of HFpEF while the previous study was reported after a 4 year follow up; therefore, these studies may represent different prognostic markers of HFpEF and how they can change over the progression of the disease.

As previously mentioned, no effective therapeutics have been reported for HFpEF and traditional HFrEF treatments, such as beta blockers, have not been found to be efficacious in individuals with HFpEF. This is also true for individuals with HFpEF and RVD (28). However, recently beta blocker treatment for HFpEF was evaluated in individuals with HFpEF and preserved RV function or RVD. Beta blocker treatment in individuals with HFpEF and preserved RV function produced

less cardiac events compared to those with HFpEF and RVD suggesting that RVD may play a role in the efficacy of treatments for HFpEF (37).

Sex Differences with Heart Failure

HF has been shown to affect males and females differently depending on age. Under 75 years of age, HF prevalence and mortality rates have been shown to be greater in males than females but as the population ages, HF prevalence and mortality rates are similar between sexes while women report a lower quality of life (16, 38, 39). This discrepancy between age and sex is hypothesized to be due to cardioprotective effects of female sex hormones (i.e. progesterone and estrogen) as the onset of heart disease typically occurs ten years later in females than males (40). Postmenopausal women have a greater incidence of ventricular diastolic stiffness, ventricular systolic stiffness, vascular stiffness, increased cardiac fibrosis, and impaired diastolic function compared to men regardless of cardiovascular disease status (39, 41, 42). Both diastolic dysfunction and cardiac fibrosis have been associated with increased risk of HF, specifically HFpEF, and death (43, 44). Additionally, the increased risk of death or adverse cardiac events in individuals with HFpEF was independently associated with female sex (45).

In addition to an increase in death for females with HFpEF compared with males, females also have a decreased LV EDV and LV mass compared with males while no differences are seen in LV EF, LV end diastolic pressure (EDP), or LV ESV (46). However, another clinical study saw that RV mass, RV EDV, RV SV, LV EDV and LV ESV decrease with increasing age and men had higher RV mass, RV EDV, and RV SV than women, suggesting a possible role of sex hormones in the

regulation of the RV (47, 48). This role of female sex hormones in the regulation of the RV is further supported by another study that evaluated hormone replacement therapy in postmenopausal women. This study found that hormone replacement therapy correlated with higher RV EF and lower RV ESV. This correlation was absent in men and postmenopausal women who are not taking hormone replacement therapy (49). Besides differences in LV and RV function between males and females with HFpEF, there are also differences in the prevalence of comorbidities due to sex. Females have an increased prevalence of comorbidities including diabetes, hypertension, renal disease, and anemia (7). Additionally, these comorbidities increase the risk of HF in females compared with males. Females with diabetes or hypertension have a five-fold increased risk or a 3.4-fold increased risk of developing heart failure, respectively, while males with diabetes or hypertension have a two-fold increased risk (7).

Cardiac Fibrosis

One common feature of HFpEF that has been hypothesized to contribute to the pathogenesis of the disease is cardiac fibrosis. One study demonstrated 93% of individuals with HFpEF have cardiac fibrosis (50). Individuals with HFpEF often demonstrate an increase in perivascular and interstitial fibrosis (10, 18, 50), which is associated with impaired cardiac function and an increase in mortality (36, 51). Specifically, interstitial myocardial fibrosis is correlated with diastolic and systolic function in individuals with HFpEF but not in individuals with HFrEF (52). Cardiac fibrosis occurs when there is an accumulation of extracellular matrix (ECM) proteins, specifically collagen. The accumulation of ECM proteins can be beneficial

for structural scaffold, force distribution and wound healing; however, excessive accumulation of ECM protein can lead to a stiffer ventricle, contractile impairments, and diastolic dysfunction (42, 53-56). Collagen type I and III are the prominent ECM proteins in the myocardium that lead to cardiac fibrosis, but collagen type IV, V, and VI, elastin and fibronectin can also play a role (53, 54, 56). In addition to an excess accumulation of collagen, fibrosis can occur when there are alterations in collagen content that affect ventricular compliance, such as with a shift in the ratio between collagen I and collagen III (57). Collagen I fibers are stiffer than collagen III fibers which are more elastic, or compliant (58). When there is more collagen III compared to collagen I then the ventricle is more elastic and more compliant and when there is a shift towards an increase in collagen I, this is associated with an increase in myocardial stiffness. An example of this shift in collagen isoforms occurs with aging in which there is an increase in collagen I levels compared with collagen III levels leading to a stiffer ventricle (59).

The excess accumulation of collagen that leads to cardiac fibrosis can occur through a dysregulation of synthesis and degradation of ECM proteins. ECM proteins as well as their regulators, matrix metalloproteinases (MMPs) and tissue inhibitors of MMPs (TIMPs), are secreted by multiple cell types including myofibroblasts. Myofibroblasts differentiate from fibroblasts upon activation by inflammatory cytokines, ischemia, or stress such as that induced by pulmonary hypertension (4, 59-61). Therefore, an increase in synthesis of collagen and ECM proteins occurs in the pro-fibrotic environments after the differentiation of fibroblasts to myofibroblasts. Collagen is secreted from myocardial fibroblasts as

a procollagen in which it must be cleaved to form insoluble collagen. It will then undergo posttranslational modifications followed by eventual degradation (18). Degradation of ECM proteins are regulated by MMPs, as well as TIMPs, which inhibit MMPs. TIMPs inhibit MMPs in a 1:1 ratio (62). The balance of MMPs and TIMPs is crucial for the maintenance of the ECM as an imbalance can lead to fibrosis (63). There are multiple MMPs and they each degrade a different set of ECM proteins. MMP-1, -2, -3, -9, -13, and -14 degrade collagen I and/or III and are located in the myocardium (64-66). There are four TIMPs (TIMP-1, -2, -3, -4) which inhibit all MMP family members, except TIMP-1 weakly inhibits MMP-14 (63). MMP-1 has a high affinity for collagen and is often the first MMP to degrade the protein as it must be broken down prior to further processing by other MMPs such as MMP-2, -3, or -9 (67).

Previous studies have shown that collagen synthesis is increased while collagen degradation is decreased in individuals with HFpEF and overall collagen content is increased in HFpEF compared with controls (12, 18). There is an increase in collagen turnover in individuals with diastolic dysfunction and diastolic heart failure. This was previously documented through elevated serum markers of collagen synthesis including increased levels of carboxy-terminal pro-peptide of procollagen I (PICP) and amino-terminal pro-peptide type III (PIIINP) as well as increases in serum markers of collagen degradation including carboxy-terminal telopeptide of collagen type I (CITP), MMP-2 and MMP-9 (68). Recent studies have been conducted evaluating potential biomarkers for HFpEF. Biomarkers for collagen homeostasis, including markers for synthesis and degradation, were

shown to be more useful in identifying HFpEF than other classic biomarkers of HF including BNP (8, 69). However, elevated plasma markers of fibrosis are not indicative of cardiac specific fibrosis but they could be representative of a systemic increase in fibrosis that would be imperative to know in treating individuals with HFpEF (70). This highlights the need for further investigation into the regulation of fibrosis in individuals with HFpEF to understand how these potential biomarkers are involved in the pathogenesis of the disease. Additionally, a more complete understanding of fibrosis is crucial for development of novel therapeutics. For example, in individuals with aortic stenosis that underwent valve replacement and in mice subject to trans aortic constriction (TAC) that was reversed three weeks later, there was a reduction in the levels of fibrosis, suggesting that fibrosis can be reversed (71-74). This provides further rationale for investigating the pathogenesis of fibrosis as it is hypothesized to be reversible.

Degradation of collagen is an important step in the regulation of fibrosis and is shown to be altered in individuals with clinical relevance to HFpEF. In patients with chronic pressure overload, there were increased plasma levels of TIMP-1 and MMP-9 which correlated with ECM remodeling and increases in MMP-2 and TIMP-4 that correlated with diastolic HF (62). In individuals with hypertension, there was a decrease in serum levels of MMP-1 and increased serum levels of TIMP-1 suggesting a decrease in collagen degradation (75). However, in individuals with hypertension and diastolic HF, there was an increase in plasma MMP-2 levels (76). Additionally, cardiac biopsies from individuals with aortic stenosis showed increased collagen content, increased TIMP-1, increased TIMP-2 with no change

in MMP-1, -2, or -9 (77). Similarly, pressure overload in pigs has been shown to increase plasma levels of TIMP-1 and TIMP-4 and increase total collagen content (78). Overall, TIMP levels have been shown to be increased in multiple disease models such as hypertension with HF, aortic stenosis, and chronic pressure overload which would lead to an increase in the inhibition of the degradation of collagen. Whereas, MMP levels vary depending on the specific MMP and the disease model (57, 62, 78-80).

While most of the research on cardiac fibrosis has been conducted in the LV or by measuring serum levels of potential biomarkers, few clinical studies have been conducted on the remodeling of the RV in individuals with HFpEF. In individuals with pulmonary hypertension and HFpEF, diffuse RV fibrosis was correlated with RV ESV, RV EDV, RV diastolic stiffness, and RV longitudinal strain but not correlated with RV EF. These results indicate that remodeling of the RV may precede functional changes, making RV fibrosis a potential therapeutic target to prevent RVD (81). In regards to RV remodeling with common comorbidities seen with HFpEF, obese individuals without HF demonstrate increased RV volume, mass and dysfunction compared with normal weight individuals (82). Individuals with HFpEF and obesity display greater RV remodeling, higher filling pressures and pulmonary vascular dysfunction during exercise (29).

Sex Hormones and Fibrosis

Estrogen is the main female sex hormones that is involved in multiple biological processes including regulation of the menstrual cycle and female sex characteristics (83). Estrogen is produced in the ovaries and the adrenal gland and

binds to estrogen receptor alpha (ERα) and estrogen receptor beta (ERβ). These receptors can be found in cells throughout the body, including cardiac myocytes and cardiac fibroblasts (84, 85). After menopause, circulating estrogen levels decline. While ERα and ERβ protein levels in the heart of postmenopausal women have not been evaluated, the protein levels of these receptors have been shown to be decreased in the heart of ovariectomized rats (86-88). Estrogen's actions on the cardiovascular system are known to be cardioprotective, due to its ability to reduce inflammation, decrease fibrosis, inhibit collagen synthesis, decrease infarct size post myocardial infarction, reduce hypertrophy, reduce atherosclerosis, and increase cell survival (85, 89-95).

Progesterone, the other primary female sex hormone, is crucial for the preparation and maintenance of pregnancy but after menopause, circulating levels of the hormone decline. Even though progesterone is produced by the ovaries and adrenal gland, there are PGRs in cells throughout the body, including cardiac fibroblasts and cardiac myocytes (84, 96). Following menopause, progesterone receptor (PGR) levels have been shown to decline in the brain, breast cancer tissue, and epidermal skin (83, 97-99). However, it is unknown how the loss of sex hormones affects progesterone receptor levels in the heart of postmenopausal women or ovariectomized animals. Progesterone's role in the cardiovascular system has not been as extensively evaluated as estrogen. Another PGR is the progesterone receptor membrane component 1, or PGRMC1, which has been implicated in cardiac fibrosis, inflammation and heart failure development (100). It is hypothesized that progesterone, like estrogen, has cardioprotective effects as

physiological concentrations of progesterone have been shown to reduce arrhythmias, increase coronary blood flow, as well as improve cardiac output after hemorrhagic shock (101-103). Additionally, progesterone has been shown to decrease blood pressure in ovariectomized ewes (104). The hormone has also been shown to inhibit collagen synthesis in cardiac fibroblasts to a greater extent than estrogen *in vitro*, further suggesting a cardioprotective effect (90, 105).

In a small, case control study, hormone replacement therapy (HRT) showed promising results in primary cardiac outputs and HRT resulted in a decrease in cardiac hypertrophy (106). The women were on HRT ~15 years with no adverse cardiac events and were either taking estrogen or estrogen with progesterone. However, large-scale HRT studies, such as the Women's Health Initiative (WHI) and the Heart and Estrogen/Progestin Replacement study (HERS), have not shown improvement in cardiovascular endpoints (107, 108). The WHI and HERS studies provided women with HRT of estrogen plus synthetic progesterone, or progestin (41, 92). These studies employed synthetic progesterone, specifically medroxyprogesterone acetate (MPA), which has been shown to produce contradictory effects on the cardiovascular system compared to natural progesterone, such as vasoconstriction instead of vasodilation (109). Additionally, MPA can reduce cardioprotective effects seen with estradiol treatment (90, 110). Progesterone, alone or with estrogen, has yet to be evaluated as a preventative measure or treatment for cardiovascular disease. Overall, these studies suggest that the lack of improvement in cardiovascular outcomes seen in large-scale HRT trials may be due to the use of synthetic progestin rather than a more natural form

of progesterone. Synthetic progestin disrupts progesterone's molecular mechanisms and while the physiological cardioprotective effects of progesterone have been shown, the molecular mechanism behind these functions has not been evaluated. In a recent retrospective analysis of the WHI which suggests that HRT with estrogen alone that begins in participants shortly after the start of menopause, ages 50-59, decreased the risks for breast cancer, coronary heart disease and mortality. Interestingly, these benefits were eliminated in the age-matched estrogen + MPA groups (111).

While progesterone's role in cardiovascular disease has not been evaluated, individuals subject to chronic pressure overload via aortic stenosis showed an increase in both ERα and ERβ mRNA levels (93). Additionally, female ERβ knockout mice that underwent an increase in pressure overload via TAC saw increases in fibrosis (94) and a separate study saw decreases in fibrosis with ERα agonists (95). These results suggest that alterations in estrogen receptor levels or activation could be involved in protection against cardiac fibrosis in chronic pressure overload as a tissues responsiveness to a hormone is dependent upon the number of receptors as well as the amount of circulating hormones (99). From this information, alterations in sex hormone receptor levels could be due to the loss of sex hormones and/or aortic banding highlighting a need to elucidate the role of each condition in the alteration of these sex hormone receptor levels.

Female sex hormones are hypothesized to play a cardioprotective role against the development of fibrosis. Postmenopausal women have increased levels of cardiac fibrosis, specifically increased collagen I and III protein levels,

compared to men and premenopausal women. Additionally, postmenopausal women demonstrated increases in TIMP-1, -2, and -3 protein levels without changes in MMP-2, and -9 levels suggesting that cardiac fibrosis could be due to an increase in the inhibition of collagen degradation (42). Similarly, to postmenopausal women, ovariectomized (OVX) rats demonstrate increases in cardiac fibrosis without changes to MMP-2 levels, or decreases in MMP-2 levels (87, 88, 112). Lastly, in individuals with HFpEF, plasma levels of MMP-3 were decreased in females compared to males (113). Overall, the increase in collagen in postmenopausal women could be due to an alteration in the degradation of collagen. In contrast, from a synthesis perspective, there are differences seen in cardiac fibroblasts. For example, cardiac fibroblasts are more abundant in female mice compared with male mice and these differences due to sex were no longer present after gonadectomy suggesting alteration in the fibroblast population after the loss of sex hormones. Estrogen can also protect fibroblasts from differentiating into myofibroblasts thus inhibiting the synthesis of ECM proteins and regulators (61). This is one possible mechanism to explain the decrease in collagen synthesis seen in cardiac fibroblasts with treatment of estrogen. This decrease in collagen synthesis by estrogen is also enhanced in the presence of progesterone (90). Estrogen can also decrease collagen I and collagen III mRNA and protein levels through an ERα, but not an ERβ, dependent mechanism in cardiac fibroblasts *in vitro* (112). While progesterone and estrogen have been shown to decrease collagen synthesis in cardiac fibroblasts, only progesterone was shown to alter fibronectin mRNA levels in cardiac fibroblasts (114).

The studies reported so far connecting sex hormones and fibrosis have been completed *in vitro*, but there are *in vivo* studies that further demonstrate this link between the two variables. Estrogen treatment reduced myocardial fibrosis in mice that underwent TAC to increase pressure load on the heart (115). This regulation in fibrosis after pressure overload is hypothesized to occur through ERβ as ERβ knockout animals demonstrated a further increase in fibrosis compared with controls; however, this was not evaluated in ERα knockout animals (94). In another animal model of HF induced by angiotensin-II, animals subject to OVX followed by estrogen treatment demonstrated reduced fibrosis that was blunted in ERβ knockout mice while ERα mice demonstrated similar results to controls (116). These results suggest that *in vivo* reduction of collagen through estrogen is mediated through ERβ. Most research on the cardioprotective role of sex hormones in mitigating fibrosis is completed through supplementation of estrogen while little research has evaluated progesterone's role *in vivo*. There is one study that evaluated PGRMC1 knockout mice fed a high fat diet and these mice demonstrated an increase in the number of fibroblasts as well an increase in cardiac fibrosis, highlighting progesterone's possible cardioprotective role *in vivo* (100). This research has all been completed on the LV, but some animal research has been conducted on the RV of OVX animals with pulmonary hypertension. In these animals, progesterone supplementation reduced RV hypertrophy, RV peak systolic pressure, RV EDP and mortality (117) while estrogen supplementation reduced fibrosis and improved RV systolic pressure through a ERβ-dependent pathway (60, 118). While this was evaluated in an animal model of pulmonary

hypertension, pulmonary hypertension is a comorbidity commonly seen in HFpEF and a hypothesized mechanism for the development of RVD.

Regulation of Fibrosis through Mitogen-Activated Protein Kinases

Mitogen-activated protein kinases (MAPKs) are a family of protein kinases heavily involved in cell signaling and many cell processes such as proliferation, metabolism, motility, survival and apoptosis (119). There are four main subfamilies of MAPKs: ERK1/2; JNK-1, -2, and -3; p38 kinase; and ERK5. The activation of MAPKs occurs via a signaling cascade that begins with phosphorylation of MAPK kinase kinase (MAP3K, MEKK, MKKK). The MAPKKK then phosphorylates MAPK kinase (MAP2K, MEK, MKK) to then activate the MAPK. The regulation of this signaling cascade occurs through tyrosine, serine/threonine, or dual-specificity phosphatases (DUSPs) (119). Each MAPK has its role in different biological processes and are stimulated by different signals, such as hormones, growth factors, or stress. However, there is cross talk between subfamilies, convergence on similar effector targets, and even negative-feedback regulation between MAPK families.

Extracellular signal-related kinase 1/2 (ERK1/2) is activated by hormones and growth factors and then proceeds through a Ras, Raf, MEK1, ERK signaling cascade (119). Once activated, ERK can translate to the nucleus to phosphorylate and activate many proteins, including transcription factors such as specificity protein 1 (SP1), ETS like-1 protein (Elk1), ETS proto-oncogene 1 (ETS1), and c-myc or c-jun, which are components of activator protein 1 (AP-1) (119-121). ERK1/2 is involved in many cellular processes including proliferation, transcription,

differentiation, cell death, and cell adhesion (119). ERK1/2 has also been implicated in many pathological processes such as cardiovascular disease, specifically cardiac fibrosis. However, ERK1/2's role is still debated as the fibrotic response varies depending on the physiological or pathological stressor. An overexpression of MEK1 for 6 months did not alter cardiac fibrosis or cardiac function even though hypertrophy was induced, suggesting ERK1/2 did not play a role in fibrosis (122). However, in another model where ERK1 was activated in the heart for 3 months, there was less fibrosis accumulation after TAC suggesting that activation of ERK1 is cardioprotective as it was able to reduce fibrosis (123). Additionally, one study demonstrated an increase in fibrosis after 4 weeks correlated with a decrease in activation of ERK in mice subject to pressure overload via TAC. While the increase in fibrosis also correlated with a decrease in the activation of protein kinase B (AKT) and glycogen synthase kinase 3 beta (GSK3β), the correlation does encourage further investigation (124). However, the addition of the ERK1/2 inhibitor PD98059 for 4 weeks in an animal model of dilated cardiomyopathy resulted in a decrease in total fibrosis as well as a decrease in collagen I and fibronectin mRNA levels (125). Therefore, ERK1/2's role in cardiac fibrosis may be dependent upon the timing of activation as well as the pathological stimulus.

c-Jun N-terminal kinase (JNK) is a member of the stress-activated protein kinase (SAPK) family and is activated by physical, chemical, and physiological stressors such as inflammatory cytokines, oxidant stress, ER stress, stretch, and to a lesser extent, growth factors. JNK is activated through a MEKK1/2/3, MKK4/7,

JNK signaling cascade to phosphorylate many downstream proteins, including similar transcription factors mentioned previously that are activated by ERK1/2 (121, 126). JNK is involved in multiple cell processes such as proliferation, differentiation, apoptosis, cell survival, and metabolism (119). JNK has been implicated in the pathogenesis of many diseases including obesity, diabetes, and cardiovascular disease. The role of JNK in cardiac fibrosis is a subject of debate, similarly to ERK1/2. JNK has been shown to play a role in selective extracellular matrix remodeling where increases in the activation of MKK upstream of JNK resulted in an increase in fibronectin but not collagen (119, 127). In another study, the deletion of JNK resulted in an increase in fibrosis after pressure overload via TAC suggesting that JNK is cardioprotective against fibrosis (128). JNK inhibition prior to the development of dilated cardiomyopathy resulted in an increase in cardiac fibrosis (129). However, addition of the JNK inhibitor SP600125 for 4 weeks in an animal model of dilated cardiomyopathy resulted in a decrease in total fibrosis as well as a decrease in collagen 1 and fibronectin mRNA levels (125). The addition of the JNK inhibitor C66 to a diabetic mouse model reduced cardiac fibrosis, cell death and hypertrophy; therefore, JNK's role in fibrosis is dependent upon timing as well as pathological disease state (130). Lastly, upstream activation of ERK1/2 and JNK in the heart and subsequent microarray analysis demonstrated that ECM remodeling is common pathway altered between these two MAPK families (131). Specifically, upstream ERK1/2 activation resulted in an increase in collagen I, collagen III, fibronectin, and TIMP-1 with a decrease in MMP-2 while upstream activation of JNK resulted in an increase in collagen I, fibronectin, TIMP-

1 and MMP-2. This could be due to the transition of fibroblasts to myofibroblasts which is dependent upon the MAPK pathway as inhibiting both the ERK1/2 and JNK pathway has blocked this differentiation (70). Overall, both ERK1/2 and JNK's role in fibrosis appears to depend heavily on timing and disease state reflecting its diverse role in this process.

Estrogen has been shown to inhibit cardiac fibrosis and this can occur through multiple mechanisms including ER activation of the MAPK pathway which lies upstream of collagen transcription and MMP/TIMP transcription (93). Both progesterone and estrogen receptors have similar signaling transduction mechanisms. Sex hormone receptor signaling can occur through two main pathways: genomic and non-genomic. In the genomic pathway, the sex hormone binds to its receptor in the cytoplasm, dimerizes and translocates to the nucleus. There it will bind to either the estrogen response element or the progesterone response element on DNA and act as a transcription factor (132, 133). In the non-genomic pathway, estrogen binds to membrane-bound estrogen receptors and can activate signal transduction pathways including mitogen-activated protein kinase (MAPK) pathways (133). PGRs are also linked to cardiac fibrosis through MAPK pathways and can participate in non-genomic signaling pathways. Progesterone receptor B (PGR-B) has been reported to be involved in extra-nuclear signaling whereas progesterone receptor A (PGR-A) has not been shown to be involved in extra-nuclear signaling (134). One molecular mechanism of progesterone action is through the p60-Src kinase and subsequent MAPK pathway, specifically ERK1/2 (135). Similarly, to PGR-B, PGRMC1 has binding

domains for SRC homology, suggesting that this receptor could also be involved in the ERK1/2 signaling cascade (132). ERs are also involved in cell signaling where estrogen binding to its receptor can mediate downstream signaling pathways such as the MAPKs, ERK1/2 and JNK (40, 93, 136). ERs can also influence transcription as the receptors contain binding sites for AP-1 and SP1 transcription factors (137) while progesterone has also been linked to these transcription factors (132). In this transcriptional cross-talk estrogen has been shown to both activate and inactivate AP-1 transcription while progesterone in complex with SP1 has been shown to increase transcription (137, 138).

The transcriptional regulation of ECM proteins, MMPs, and TIMPs, is very complex and there are multiple binding sites for transcription factors that can be altered by MAPKs. For example, AP-1 has binding sites located in the promoter regions of ECM proteins, MMPs, and TIMPs and is essential for their transcriptional activation (53, 56, 62, 63). Of the MMPs located in the heart that degrade collagen I and/or III, MMP-1, -3, -9, and -13 have AP-1 binding sites in their promoter regions, whereas MMP-2 and -14 are lacking AP-1 binding sites and are not under AP-1 control (58, 65). Of the four TIMPs, TIMP-1 and -2 have AP-1 binding sites whereas TIMP-3 and -4 do not (65). Additionally, TIMPs, specifically TIMP-1, have multiple AP-1 binding sites as well as regulatory sites upstream of AP-1 that could play an additional role in the regulation of its transcription that differs from MMPs (63, 65). Other transcription binding sites include polyomavirus enhancer activator 3 (PEA-3), which can be altered via phosphorylation by ERK, and have binding sites in the same MMP and TIMP promoters as AP-1 (139-141).

Lastly, transcription factor SP-1 can be altered by ERK1/2 and JNK as well as estrogen and progesterone receptors directly (93, 142). MMP-2, -9, -14 as well as all four TIMPs have binding sites for SP1; therefore, there are multiple points of regulation of ECM biomarkers that can occur through MAPKs (65). Overall these previous studies provide a possible mechanism as to the regulation of fibrosis due to the loss of sex hormones and chronic pressure overload as ECM proteins and their regulators lie downstream of MAPKs which can be altered by sex hormone receptors.

From this information the purpose of this dissertation is to evaluate how the synthesis and degradation of ECM proteins is altered in two previously completed animal models from our lab. This first study evaluates JNKs role in remodeling in the RV and right coronary artery of a cardio-metabolic swine model of HF. The second study investigates how the loss of female sex hormones alters cardiac fibrosis in a swine model with aortic-banding induced HF. This latter study will also compare differences in fibrotic remodeling between the LV and RV through analysis of pathways upstream and downstream of collagen regulation including sex hormone receptors, MAPK signaling, MMPs and TIMPs. Overall, the goal of this dissertation is to provide insight into the development of cardiac fibrosis and how it can be altered due to diet, sex hormones, heart failure, and tissue type.

CHAPTER 2: THE RIGHT VENTRICULAR TRANSCRIPTOME SIGNATURE IN OSSABAW SWINE WITH CARDIO-METABOLIC HEART FAILURE: IMPLICATIONS FOR THE CORONARY VASCULATURE

Shannon C. Kelly[1], Christoph D. Rau[2], An Ouyang[3], Pamela K. Thorne[1], T. Dylan Olver[4], Jenna C. Edwards[1], Timothy L. Domeier[5], Jaume Padilla[6,7], Laurel A. Grisanti[1], Bradley S. Fleenor[8], Yibin Wang[9], R. Scott Rector[6,10,11], and Craig A. Emter[1].

[1]Department of Biomedical Sciences
[5]Department of Medical Pharmacology and Physiology
[6]Department of Nutrition and Exercise Physiology
[7]Dalton Cardiovascular Research Center
[10]Department of Medicine - Gastroenterology and Hepatology
[11]Research Service - Harry S Truman Memorial VA Hospital
University of Missouri- Columbia
Columbia, MO 65211

[2]Department of Computational Medicine and Genetics
University of North Carolina School of Medicine
Chapel Hill, NC

[3]Department of Neurology
Massachusetts General Hospital and Harvard Medical School
Boston, Massachusetts

[4]Department of Biomedical Sciences, Western College of Veterinary Medicine,
University of Saskatchewan,
Saskatoon, SK, Canada

[8]Human Performance Laboratory, School of Kinesiology,
Ball State University,
Muncie, Indiana

[9]David Geffen School of Medicine
University of California, Los Angeles
Los Angeles, CA

Running Head: RV Transcriptome in Swine with Cardio-Metabolic HF

Key Words: Cardio-metabolic; Heart Failure; Right Ventricle Transcriptome; Ossabaw Swine; Right Coronary Artery

This research was published in Physiological Genomics, 2021.

Abstract

Heart failure (HF) patients with deteriorating right ventricular (RV) structure and function have a nearly two-fold increased risk of death compared to those without. Despite the well-established clinical risk, few studies have examined the molecular signature associated with this HF condition. The purpose of this study was to integrate morphological, molecular, and functional data with the transcriptome dataset in the RV of a pre-clinical model of cardio-metabolic HF. Ossabaw swine were fed either normal diet without surgery (lean control, n=5) or Western Diet and aortic-banding (WD-AB; n=4). Postmortem RV weight was increased and positively correlated with lung weight in the WD-AB group compared to CON. Total RNA-seq was performed and gene expression profiles were compared and analyzed using Principal Component Analysis, Weighted Gene Co-Expression Network Analysis, Module Enrichment Analysis, and Ingenuity Pathway Analysis. Gene networks specifically associated with RV hypertrophic remodeling identified a hub gene in MAPK8 (or JNK1) that was associated with the selective induction of the extracellular matrix (ECM) component fibronectin. JNK1 and fibronectin protein were increased in the right coronary artery (RCA) of WD-AB animals and associated with a decrease in matrix metalloproteinase 14 protein, which specifically degrades fibronectin. RCA fibronectin content was correlated with increased vascular stiffness evident as a decreased elastin elastic modulus in WD-AB animals. In conclusion, this study establishes a molecular and transcriptome signature in the RV using Ossabaw swine with cardio-metabolic HF. This signature

was associated with altered ECM regulation and increased vascular stiffness in the RCA, with selective dysregulation of fibronectin.

Introduction

Recently, there has been an increased focus on right ventricular (RV) structural and/or functional impairment in heart failure (HF) patients regardless of ejection fraction (28, 143-145). A meta-analysis of clinical studies estimates 18-28% of individuals with HF also have RV disease (31). Heart failure patients with RV pathology have increased renal dysfunction, higher natriuretic peptide levels, more severe pulmonary vascular disease, and coronary artery disease. These individuals also have a higher incidence of atrial fibrillation, increased RV filling pressures, larger RV and atrial volumes, decreased RV and LV ejection fraction, and increased RV diastolic stiffness (28, 32, 33). Importantly, this more severe pathological phenotype is associated with an increased risk of death (34, 35), highlighting the need to understand mechanisms influencing the negative synergy between RV disease and HF.

We recently developed a pre-clinical swine model of cardio-metabolic HF that showed aortic-banded Ossabaw pigs fed a Western Diet display an increase in postmortem RV weight compared to lean controls, similar to HF with deterioration of RV structure and function (146). We hypothesized that gene networks associated with hypertrophic remodeling would be activated in the RV of these same animals. Accordingly, we performed total RNA-sequencing analyses in the RV homogenate and interrogated the dataset to identify differentially expressed genes associated with chronic pressure-overload and metabolic challenge. Unbiased Ingenuity Pathway Analysis (IPA) from the differentially expressed genes detected specific molecular signatures indicative of cardiac

hypertrophy and fibrosis in the RV. The initial gene-network analysis also identified a HF-associated gene module centered around a number of hub genes. We specifically focused on stress-activated protein kinase 8 (MAPK8; also known as JNK1), which after targeted validation we demonstrate was significantly increased in the RV.

After initial findings failed to confirm the transcriptome signature in the RV at the protein level, we extended our examination of the regulation of MAPK8/JNK1 signaling into the right coronary artery (RCA). The RV homogenate assessed herein is composed of a number of cell types including vascular and immune cells, cardiomyocytes, and fibroblasts. Given our laboratory has extensively studied vascular contributions to HF (146-153), the extension of this study to the coronary vasculature was a logical choice. Our results indicate an increase in JNK1 protein in the RCA that was associated with dysregulation of fibronectin, an extracellular matrix (ECM) component that is a selective target of MAPK8/JNK1 signaling (119, 127). These molecular and structural changes in the RCA were functionally correlated to an increase in coronary vascular stiffness. These results highlight the potential value of this pre-clinical RV transcriptome dataset to uncover novel insights and molecular targets potentially relevant to the mechanistic understanding of cardio-metabolic HF with pathological RV remodeling.

Methods

Experimental Design

This was an analysis of the total RV homogenate (cardiomyocytes, fibroblasts, coronary blood vessels) and right coronary artery (RCA) harvested from the same animals previously used in a recently published study from our laboratory (146). Briefly, intact, female Ossabaw swine (15-20 kg; 2 mo. old) were randomly assigned to either a non-sham sedentary control group (CON; n=5) that ingested a standard chow diet (5L80, Lab Diet; 3.03 $kcal \cdot g^{-1}$, carbohydrate=71%, protein=18.5% and fat=10.5%; 500 g per day) or a Western Diet-fed aortic-banded heart failure group (WD-AB; n=4) that consumed a diet high in fat, high fructose corn syrup, and cholesterol (5B4L, Laboratory Diet; 4.14 $kcal \cdot g^{-1}$; carbohydrate, 40.8% [17.8% of total calories from high fructose corn syrup]; protein, 16.2%; fat, 43%, 2% cholesterol wt/wt) (154-159). At 6 months of age, an aortic band was placed on the ascending aorta to increase afterload on the heart as previously described (149-151, 154, 160-164). A trans-stenotic systolic gradient was set to ≈70 mmHg (72 ± 2 mmHg) under anesthesia using phenylephrine (I.V. 1-3 ug/kg/min) to set equivalent hemodynamic conditions defined as a mean aortic pressure (MAP) of ≈90 mmHg (87 ± 2 mmHg) and a heart rate of ≈85 beats/min (84 ± 3 bpm). After 6 months of chronic cardiac pressure overload and 10 months of Western Diet feeding, terminal experiments were performed at 1 year of age. Animals were anesthetized with a telazol (5 mg/kg)/xylazine (2.25 mg/kg) mix and maintained on propofol (6-10 $mg \bullet kg^{-1} \bullet min^{-1}$ with bolus as needed) for previously

published *in vivo* hemodynamic experiments before euthanasia and tissue harvest as previously described (154, 155).

RV Gross and Cellular Morphology

Gross RV morphology was calculated by postmortem weight. Cardiomyocyte morphology was determined using cross-sections of RV that were formalin fixed, embedded in paraffin for analysis, and stained for measurement of cross-sectional area. After dewaxing and rehydrating, antigen retrieval was performed using 10 mM sodium citrate buffer at 98°C for 30 minutes. Samples were incubated in 6 μg/mL Alexa Fluor 488-conjugated wheat germ agglutinin (WGA; Invitrogen) for 30 minutes (165). Sections were imaged under 400x magnification with fluorescence microscope (Nikon Eclipse E600) with camera (Olympus DP72). A minimum of 50 cells from 4 cross-sectional views/animal were analyzed using Image J software (National Institute of Health, Bethesda, MA).

RNA-seq, Principal Component Analysis, Weighted Gene Co-Expression Network Analysis, Module Enrichment Analysis, and Ingenuity Pathway Analysis:

Total RNA was extracted from the complete RV homogenate (a transmural section of the RV including cardiomyocytes, fibroblasts, and coronary blood vessels dissected from the midwall) using Trizol (Thermo Fisher Scientific) and RNA-seq libraries were prepared using a standard Illumina protocol as previously described (154, 166-168). Transcript abundances were calculated using the 0.8.2 version of the Salmon algorithm (169) and the Ensembl SusScrofa 10.2 build of the pig genome with correction for both sequence biases and GC biases in the reads. Principle component analysis was performed on all expressed and varying genes

(FPKM >1, Coefficient of Variation >5%) using the prcomp R function and the ggbiplot R package (170). Differentially expressed genes were calculated using DESEQ2 (171) and GeneAnalytics (172) was used to identify enriched biological categories in these differentially expressed genes. Significance was determined by a Bejamini-Hochberg corrected binomial test reported at the $P < 0.05$ level. Networks were generated through the use of Ingenuity Pathway Analysis (IPA, Ingenuity Systems, **www.ingenuity.com**) based on the list of differentially expressed genes, and subject to statistical analysis as previously described (154, 156, 158, 173).

qRT-PCR

Total RV homogenate was flash frozen in liquid nitrogen and stored at -80°C until processed. Quantitative Real Time-PCR (qRT-PCR) was performed as previously described using the $2^{-\Delta\Delta}$Ct method (149, 174, 175). Primers for analysis of 18S, Fibronectin, collagen I, collagen III, matrix metalloproteinase-2 (MMP2), MMP9, tissue inhibitor of matrix metalloproteinase-1 (TIMP1), and TIMP4 mRNA levels were previously published (149). Primers used for MAPK8, MMP14, TIMP2, dual specificity phosphatase-1 (DUSP1), DUSP4, and DUSP10 to measure mRNA levels are listed in **Table 1**.

Table 1. Primer sequences (5' to 3')

Target Gene	Forward Primer	Reverse Primer
MAPK8	CAGCCCTCTCCTTTAGCACA	TGTATCCGAGGCCAAAGTCG
MMP14	CTTCGAACATTGGCCTTGAT	TGCAGCAGTATGGCTACCTG
TIMP2	CCAGTACGAAATCAAGCAGATA	GGCCGTGTAGATAAACTCTATG
DUSP1	GGGAGTGCCTACCATGCTTC	ATGTCCGCCTTGTGGTTGT
DUSP4	GTCACCAACCACAGATGAATA	CTGATCTGCATCCAGGTAAAT
DUSP10	CAGCCATCCTCCTGTCATCG	TGTCCTTGTCGTAAGTTGCCA

Western Blot

Western blot analysis was used to determine RV (from the total RV homogenate) and RCA protein levels as previously described (149, 160, 176, 177). RV tissue was homogenized in buffer containing 150 mM NaCl, 50 mM Tris pH 8.0, 2 mM EDTA, 1% Triton X-100, 0.5% Sodium Deoxycholate and protease/phosphatase inhibitors (Halt, Thermo Scientific). After homogenization in TissueLyser (Qiagen), the RV lysates were incubated on ice for 30 minutes and then centrifuged at 12,000*g* for 10 min. Protein from right coronary arteries were extracted in Laemmli buffer (62.5 mM Tris, pH 6.8, 6 M urea, 160 mM dithiothreitol, 2% SDS, and 0.0001% bromophenol blue) using sonication (150). Protein concentration was determined by Bradford assay (Bio-Rad) or NanoOrange assay (ThermoFisher). 10 μg of protein in SDS loading buffer were run on 4-20% SDS/PAGE acrylamide gels (GeneScript) before transfer to PVDF membranes (GE Life Sciences). After blocking in 2.5% non-fat milk, membranes were incubated overnight at 4°C in primary antibodies: SAPK/JNK (46 kDa; Cell Signaling Technologies, 1:1000), phospho-SAPK/JNK (46 & 54 kDa, Thr 183 / Thr 185; Cell Signaling Technologies, 1:1000), Fibronectin (262 kDa; Sigma-Aldrich, 1:5000), Elastin (70 kDa, Abcam,

1:1000), MMP14 (65 kDa; Invitrogen, 1:1000), TIMP2 (24 kDa; Abcam, 1:1000), and β-actin (42 kDa, Sigma, 1:5000). The appropriate horseradish peroxidase-linked secondary antibodies (Cell Signaling, 1:1000) were then applied to the membrane prior to imaging on a Kodak image station (4000R) using Luminata Forte Western Chemiluminescent HRP substrate reagent (EMD Millipore). β-actin was utilized as a loading control. No statistical differences in the loading control was observed between groups, thus, absolute protein levels normalized relative to the CON group were used for analysis.

RV Fibrosis

Total RV collagen levels were determined through the biochemical quantification of collagen-specific hydroxyproline using a commercially available kit (Cedarlane, QuickZyme Total Protein and Collagen, Leinden, The Netherlands), and reported as the ratio of total collagen: total protein as previously described (146). Visualization of RV fibrosis was accomplished using Masson's trichrome stain (146, 149, 176, 177).

Immunohistochemistry (IHC)

IHC was performed by standard procedures as previously described (148, 164, 178). Segments of RCA were embedded with optimal cutting temperature (O.C.T.) and frozen. Arteries were cross-sectioned (8μm), fixed on glass slides with acetone and stained using Dako Envison+ system HRP-DAB kit (Agilent). An elastin primary antibody was used (Abcam, ab21607) with slides incubated at 4°C overnight at a 1:300 dilution. The secondary HRP conjugated labeled polymer was

applied for 30 minutes at room temperature followed diaminobenzidine (DAB) application for approximately 2 minutes until the appropriate darkness was achieved. Images were acquired using a Nikon 80i microscope with a 4x objective. Densitometry analysis was performed by ImageJ (NIH) and the data are presented as relative density in arbitrary units (AU).

Elastin Elastic Modulus

Right coronary artery stress-strain curves were utilized to calculate the elastin elastic modulus (EEM), an indicator of vascular stiffness, as previously described (148, 164). The RCA was cleaned of adipose tissue and cut into ~1.5-mm segments. The RCA rings were placed in a myograph (DMT 620) with preheated (37°C) Ca^{2+}- and Mg^{2+}-free phosphate-buffered saline. The RCA was then stretched every 3 min by 1 mm increments until mechanical failure. The elastic modulus was calculated as the greatest r^2 value from the stress-strain curve. The stress-strain curve was generated in which stress (t) was calculated as $t = \lambda L/2HD$ and strain (λ) was defined as $\lambda = \Delta d/d$(i), where L = one-dimensional load applied, H = wall thickness, D = length of vessel, and Δd = change in diameter, d(i) = initial diameter. Wall thickness and diameter were assessed via histology and length was assessed under a dissecting microscope.

Zymography

Activity and abundance of MMP2 was analyzed by gelatin zymography (149, 179). Frozen RV tissue was homogenized in lysis buffer (100 mM NaCl, 25 mM Tris-HCl, 1% Triton X-100, and 1x HALT protease inhibitor) with stainless steel beads

(Next Advance) using a TissueLyser (Qiagen). Samples were then centrifuged at 16,000*g* for 10 min at 4°C. Protein concentration was quantified with BCA protein assay. 100 µg total protein from each animal was prepared in 4x sample buffer (250 mM Tris-HCl, pH 6.8, 40% v/v glycerol, 8% SDS w/v, 0.01% w/v bromophenol blue) and ran on 10% zymography gel (Invitrogen) for 110 minutes at 125 V. Gels were then incubated in zymography renaturing buffer (Invitrogen) for 30 minutes at room temperature with gentle agitation. This process was followed by incubation in zymography developing buffer (Invitrogen) for 30 minutes at room temperature and subsequent exposure to fresh developing buffer for 36 hours at 37°C with gentle agitation. After incubation, gels were stained with Coomassie blue (0.5% w/v Coomassie, 5% v/v methanol, and 10% v/v acetic acid in H_2O) for one hour. The gels were then destained with buffer (10% v/v methanol and 5% v/v acetic acid in H_2O) until adequate resolution of bands was observed. Gels were imaged with Azure Biosystems c600 Imager and quantified with ImageJ software.

Statistical Analysis

Statistical analysis was performed using SigmaPlot 14 (SysStat Software, San Jose, CA) and RStudio software (R version 3.5.3, Boston, MA). Linear regression was used to examine the relationship between: 1.) RV postmortem weight and postmortem lung weight; and 2.) EEM and fibronectin protein levels. Group comparisons were completed using Student's t-test (180). Power analysis for this study was described previously (154, 181) and indicate 4 swine per group is sufficient to detect group differences. All data is presented as mean ± standard

error (SE) and significance is reported at the $P < 0.10$ and $P < 0.05$ levels (182, 183).

Results

Right Ventricular Morphological Remodeling

A comprehensive description of whole animal morphological and functional characteristics for the same animals used in the current study was recently published by our laboratory in the *Journal of the American College of Cardiology: Basic to Translational Science* (154). Herein, we provide a brief summary of these results. Normal resting systolic function (ejection fraction >50%) was observed in parallel with global hypertrophic remodeling in the LV, atria, and RV. The combination of diastolic dysfunction (increased slope of the end diastolic pressure-volume relationship and abnormal diastolic strain), atrial hypertrophy, increased aortic systolic and pulse pressure, and increased wet lung weight in WD-AB animals support a theory of backward hemodynamic transmission that could increase RV mechanical stress (184, 185). Significant comorbidities were present including metabolic derangement indicated by obesity, inactivity, insulin resistance, dyslipidemia, and systemic inflammation. Extensive vascular dysfunction was present in multiple organ systems including the heart, brain, and skeletal muscle. Finally, the LV transcriptome showed substantial enrichment of gene signatures associated with HF, fibrosis, metabolic syndrome, and chronic inflammation. Collectively, the outcomes observed in the WD-AB group are consistent with a series of integrated physiological, morphological, and genetic phenotypes evocative of cardio-metabolic HF.

To evaluate RV hypertrophy, postmortem RV weight was measured. Tibia length was examined to determine if normalization of the morphometric data was

necessary (186, 187). As previously reported in these same animals, tibia length was not different between groups (154). Therefore, absolute RV weights were used for group morphological analyses (188). As shown in **Figure 1A**, postmortem RV weight was significantly increased in WD-AB animals compared to CON and positively correlated to postmortem lung weight, demonstrating a right and upward shift in the group mean along the regression line (**Figure 1B**). Wheat germ agglutinin staining was utilized to further evaluate hypertrophy in individual cardiomyocytes (representative images are shown in **Figure 1C**). Cross-sectional area of individual myocytes was significantly increased in WD-AB animals compared to CON (**Figure 1D**) indicating RV hypertrophy at the organ and cellular level the WD-AB group. Additional evidence from the transcriptome supporting cardiopulmonary integration linking RV remodeling and lung disease is presented in **Table 2**, where gene ontology analysis in the RV shows enrichment of mRNA signatures related to pulmonary hypertension, fibrosis, and edema.

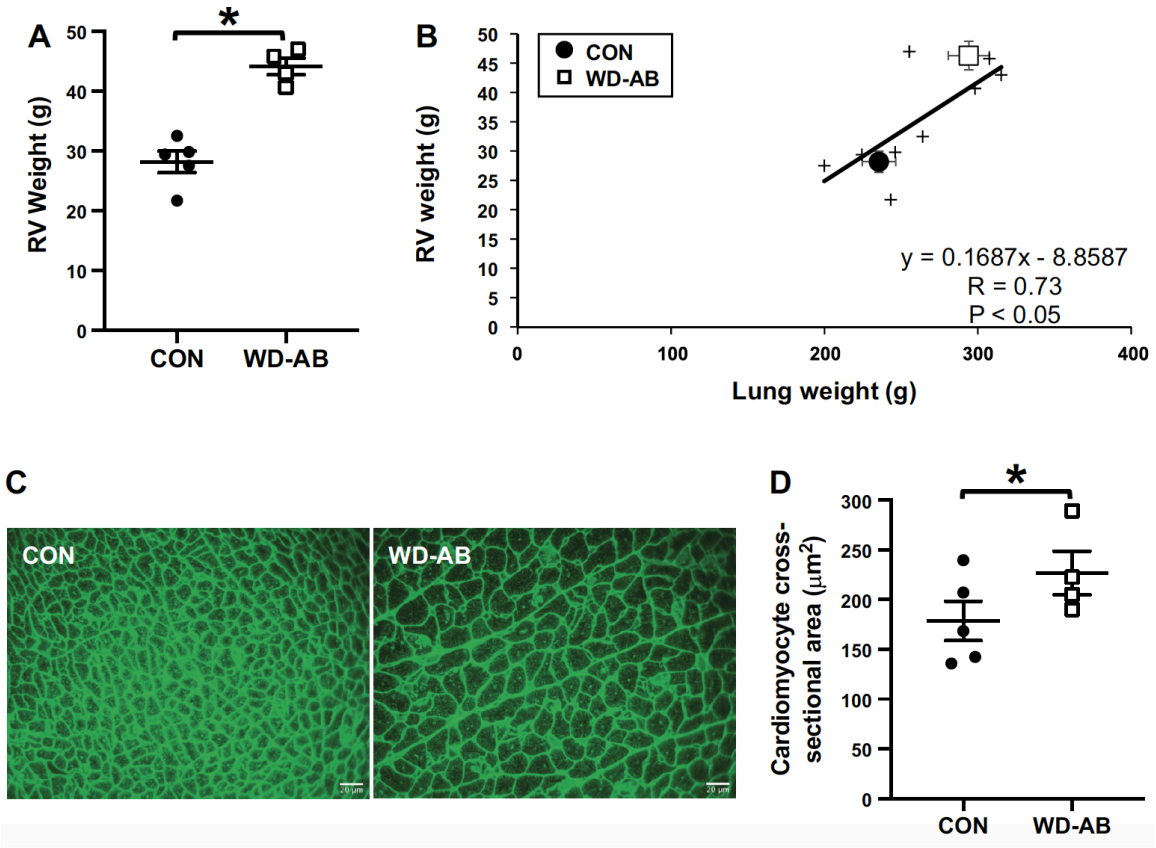

Figure 1. *Western diet-fed, aortic banded Ossabaw swine demonstrate right ventricular (RV) hypertrophy.* **(A)** Postmortem RV weight was increased in WD-AB animals and **(B)** positively correlated to postmortem lung weight. **(C-D)** Cardiomyocyte cross-sectional area was increased in WD-AB animals compared to CON as demonstrated by quantification of representative cross-sectional images stained for wheat-germ agglutinin (green, scale bar = 20 μm). *t-test vs. CON (P<0.05). n=5 animals, 50 cells/animal in the CON group; n=4 animals, 50 cells/animal in the WD-AB group.

Table 2. Gene Ontology Analyses of Induced Pulmonary Disease Pathways Expressed between CON and WD-AB Right Ventricle

Gene Ontology, Diseases

Name	Matched genes (symbol)	p-value
Pulmonary Hypertension	ACE, ADORA3, BMP4, C10orf10, EDNRB, NPPA, PLAT, PTGIR, SLC6A4, SMAD9, TNFAIP3	3.43e-4
Pulmonary Fibrosis	CCL2, CD24, CTGF, CXCL8, FASN, IL1B, MYRF, RGS1, SPP1, TNFAIP3, UBD, VCAM1	5.34e-4
Pulmonary Edema	ACE, CXCL8, IL1B, NOS2, NPPA	1.43e-02
Chronic Pulmonary Heart Disease	CP, HP, PTGIR, SLC6A4	2.32e-02

Right Ventricular Transcriptome

To evaluate the molecular signature present in the total RV homogenate, the transcriptome was profiled using RNA-seq and IPA. Unbiased IPA detected top gene expression changes in the WD-AB heart including Cardiac Hypertrophy and Cardiac Fibrosis, the #1 and #2 top significant Toxicology Lists (**Table 3**).

Table 3. Ingenuity Pathway and Gene Ontology Analyses of Differences in Heart Failure, Cardiac Hypertrophy, and Fibrosis Gene Pathways between CON and WD-AB Right Ventricle

Ingenuity Pathway Analysis, Top Toxicology Lists

Name	p-value
Cardiac Hypertrophy	3.83e-12
Cardiac Fibrosis	5.73e-10

Gene Ontology, Molecular Function

Name	Matched genes (symbol)	p-value
Protein Tyrosine/Threonine Phosphatase Activity	DUSP2, ***DUSP1***, ***DUSP4***	1.94e-04
Fibronectin Binding	PLEKHA2, IGFBP3, THBS1, CTGF, CTSL, VEGFA	6.18e-04

Gene Ontology, Phenotype

Name	Matched genes (symbol)	p-value
Abnormal Macrophage Physiology	ABCG1, ***DUSP4***, PLAU, SOCS2, ADGRE1, MYD88, SPP1, PTGS2, IL1B, MB21D1, IL4R, LCP1, LGALS3, PTX3,GPR65, IRF1, NFKB1, SGMS2, SERTAD2, NOS2, STAT3,TCIRG1, TLR2, TLR4, TNFRSF1A, BCL3, CCR1, CD14	3.78e-10
Decreased T Cell Proliferation	HRH1, PLAU, MYC, ***MAPK8***, LRFN2, IL4R, IL2RG, IL1R1, LIF, IL15RA, PTPN9, PTPRC, FYB, NFKB1, SELL, JAK3, CD44, TYROBP, VAV1, BCL10, BHLHE40, CCL5, CDK6, CD4, CD86	4.62e-10
Abnormal Cytokine Secretion	DUSP2, ***DUSP1***, ABCG1, LITAF, IFIH1, MYD88, ***MAPK8***, SPRED1, IL4R, PTPRC, NFKB1, SELP, NFKBIZ, TLR2, TLR4, TNFRSF1A, TRAF3IP2, STX11, TNFAIP3, BCL10, BCL3, CD14	7.34e-08
Lung Inflammation	***DUSP1***, ABCG1, SMAD9, ACKR3, LGALS3, PTX3, PTPRC, NFKB1, SHARPIN, CD44, THBS1, TLR4, TNFRSF1A, CSF2RB, RUNX1, ATF3, CCR1	4.41e-06
Abnormal T Cell Activation	IFIH1, ***MAPK8***, IL15RA, PTPRC, IL6ST, JAK3, PFDN1, VAV1, BCL10, BHLHE40	1.82e-04
Abnormal Heart Right Ventricle Pressure	HIF3A, NOS2, ***NPPA***, BMP4	2.28e-04
Heart Right Ventricle Hypertrophy	ABCA1, SLIT3, ADAMTS6, ADORA2A, ***NPPA***, SLC6A4, BMP4	2.34e-04

Further IPA analysis showed significant interactions between gene networks centered around MAPK8 (or JNK1), leukemia inhibitory factor (LIF), Interleukin-8 (IL-8 or CXCL8), and pentraxin 3 (PTX3) (**Figure 2**). Gene ontology analysis indicated a significant enrichment of molecular functions related to protein tyrosine/threonine phosphatase activity, including dual-specificity phosphatases (DUSP) and fibronectin binding, both of which regulate or are regulated by MAPK8/JNK1 (119, 127). Significant enrichment of several other gene networks related to RV hypertrophy and cardiac fibrosis are also listed in **Table 3**, including

traditional molecular indicators of HF such as atrial natriuretic peptide (NPPA). The increase in MAPK8 mRNA level reported by RNA-seq was verified independently using qRT-PCR. As shown in **Figure 3A**, there was a significant increase in MAPK8 mRNA levels in WD-AB animals compared to CON. Significant differences were not observed for LIF, CXCL8, or PTX3 mRNA levels between CON and WD-AB animals (**Figure 3B**), thus, subsequent analyses were focused on MAPK8/JNK1.

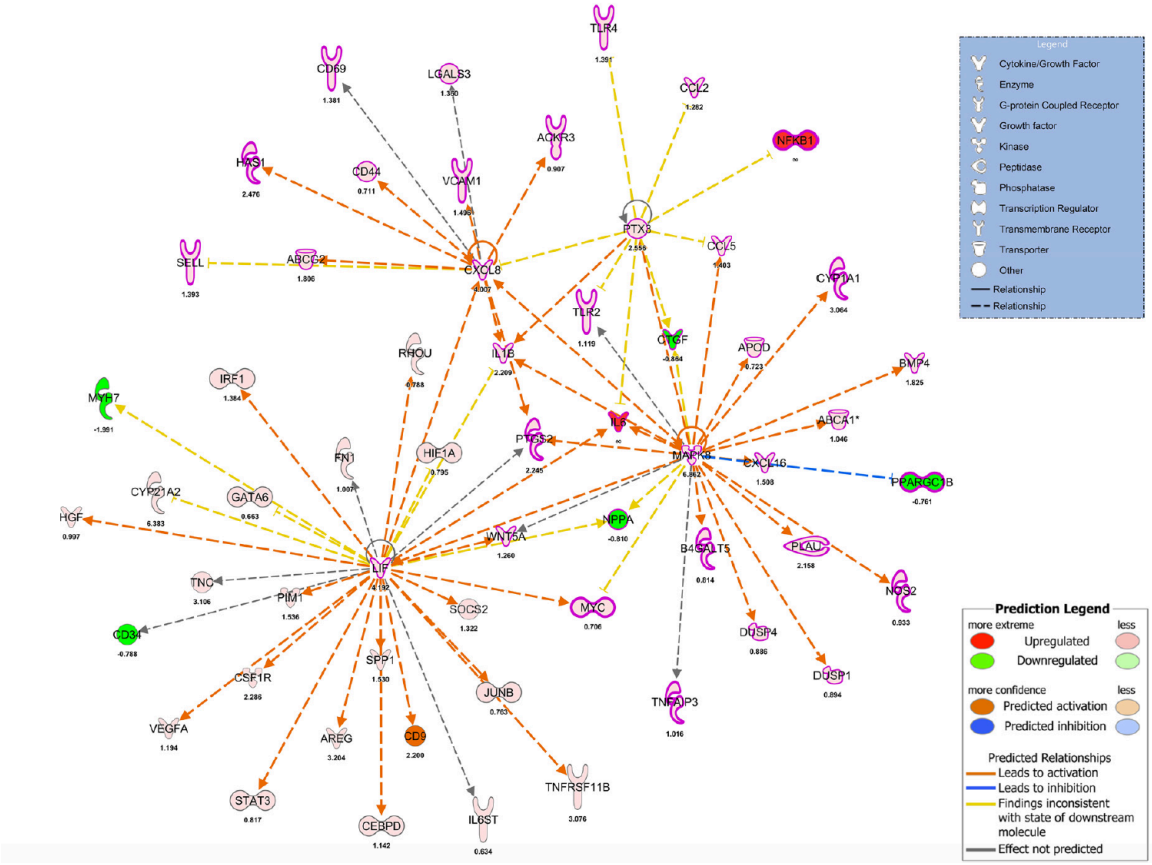

Figure 2. *Ingenuity Pathway Analysis demonstrates the activation of stress-activated protein kinase-8 (MAPK8 or JNK1), leukemia inhibitory factor (LIF), pentraxin 3 (PTX3), and interleukin-8 (CXCL8 or IL-8) in Western diet-fed, aortic banded Ossabaw swine.* Graphic illustration showing the interactions between MAPK8, LIF, PTX3, and CXCL8 in the RV of WD-AB animals compared to CON. Specified number represents fold-change in gene expression per RNA-seq analysis. n=3 for CON and WD-AB groups.

Additional verification by qRT-PCR showed increased mRNA levels of DUSP1 and DUSP4 in WD-AB compared to CON animals, suggesting an imbalance in the regulation of MAPK8 activation (**Figure 3C**). MAPK8/JNK1 signaling is linked to selective extracellular matrix (ECM) remodeling characterized by an increase in fibronectin, but not collagen, deposition (119, 127). Fibronectin mRNA level measured by qRT-PCR was increased in the WD-AB group compared to CON (**Figure 3D**), while collagen I and III mRNA levels were not significantly different between groups (**Figure 3E**).

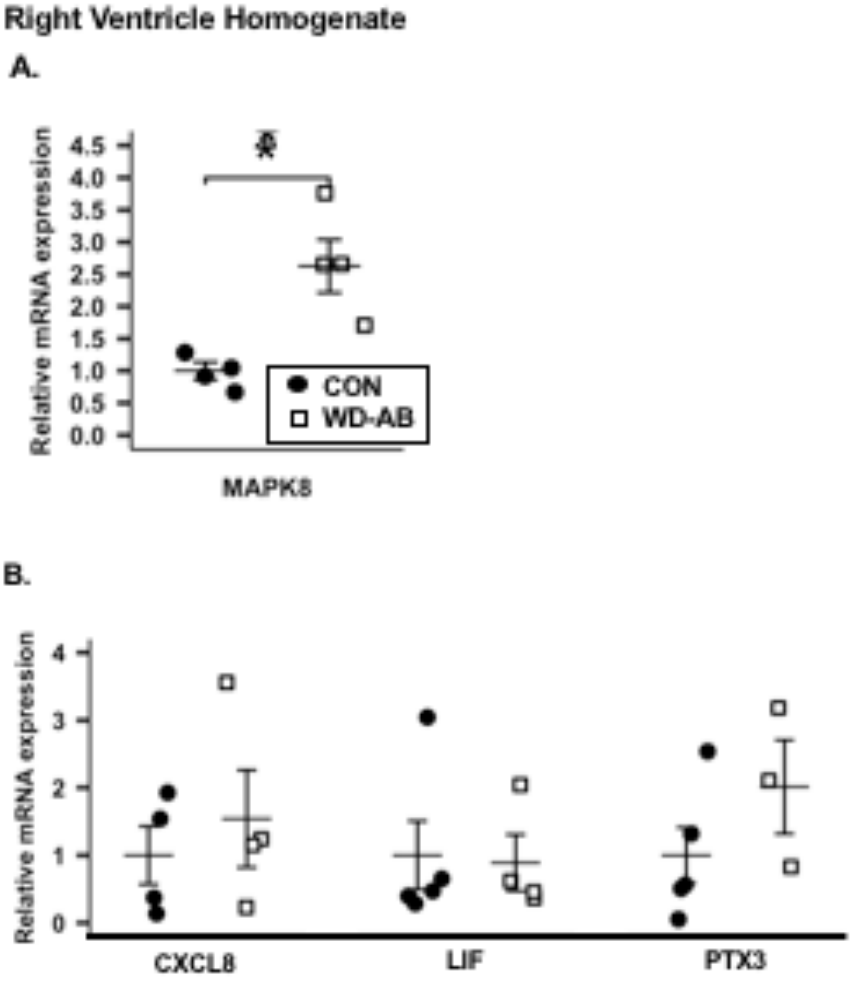

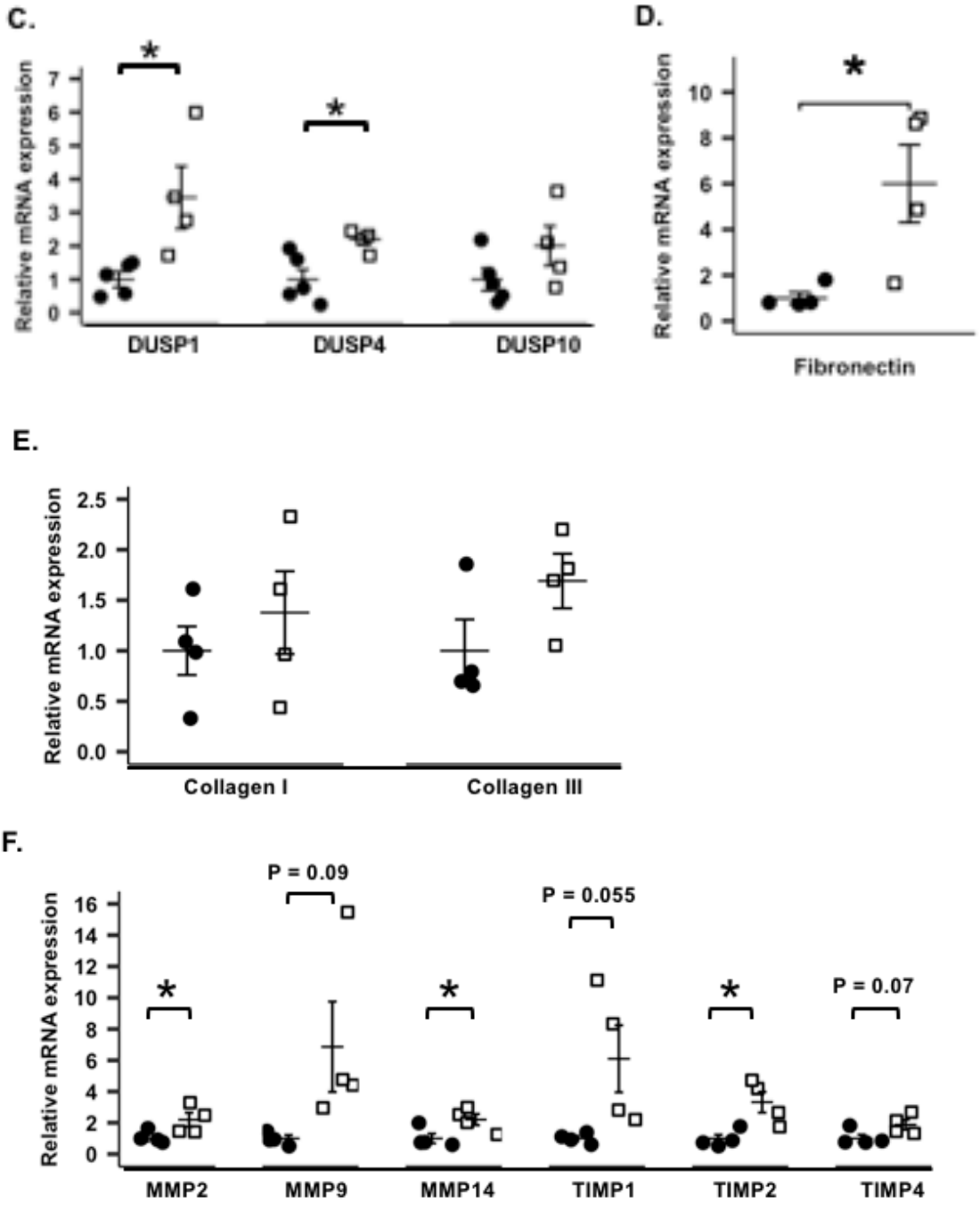
C.
Relative mRNA expression
DUSP1
DUSP4
DUSP10
D.
Relative mRNA expression
Fibronectin
E.
Relative mRNA expression
Collagen I
Collagen III
F.
Relative mRNA expression
P = 0.09
P = 0.055
P = 0.07
MMP2
MMP9
MMP14
TIMP1
TIMP2
TIMP4

Figure 3. *Independent verification of RNA-seq by qRT-PCR in Western diet-fed, aortic banded Ossabaw swine demonstrate increased MAPK8, DUSP, fibronectin and matrix metalloproteinase (MMP) and tissue inhibitors of matrix metalloproteinase (TIMP) mRNA levels that are associated with RV hypertrophy.* **(A)** MAPK8 mRNA levels were increased in WD-AB swine compared to CON. **(B)** Right ventricular CXCL8, LIF, and PTX3 mRNA levels measured by qRT-PCR are not different between groups. **(C)** The WD-AB group showed an increase in DUSP1 and DUSP4 mRNA levels compared to CON. **(D)** Fibronectin mRNA levels were increased in the RV of WD-AB animals compared to CON. **(E)** Collagen I and Collagen III mRNA levels were not different between groups. **(F)** MMP2, MMP9, MMP14, TIMP1, TIMP2, and TIMP4 mRNA levels were increased in WD-AB animals compared to CON. *t-test vs. CON ($P<0.05$). n=4 for CON and WD-AB in Figures 3A, D, and F. n=5 for CON and n=4 for the WD-AB group in Figures 3B, C.

To further evaluate regulation of the ECM in the RV, mRNA levels of MMPs and TIMPs were also measured using qRT-PCR. Our results indicate an imbalance of these regulatory biomarkers of the ECM in the RV, as multiple MMP and TIMP isoforms were elevated in the WD-AB group (**Figure 3F**). Specifically, a significant increase in MMP14 mRNA (which degrades fibronectin) was observed in parallel with increases in both TIMP2 and TIMP4 mRNA levels, which inhibit MMP14 (189-191).

To determine if these changes in mRNA levels translated to changes in protein level, western blot was utilized to evaluate phosphorylated-JNK, total JNK, fibronectin, MMP14, TIMP2, and elastin (**Figure 4A**). There were no significant differences between CON and WD-AB animals regarding the activation of JNK, phosphorylated JNK, or total JNK levels (**Figure 4B, 4C**). Protein levels were not significantly different between the two groups for fibronectin (**Figure 4D**), MMP14 (**Figure 4E**), TIMP2 (**Figure 4F**), elastin (**Figure 4G**), or calsequestrin (loading control; **Figure 4H**). Total RV collagen was evaluated biochemically with no

differences seen in protein level between groups (**Figure 4I**) and that was confirmed visually via Masson's trichrome stain (**Figure 4J**).

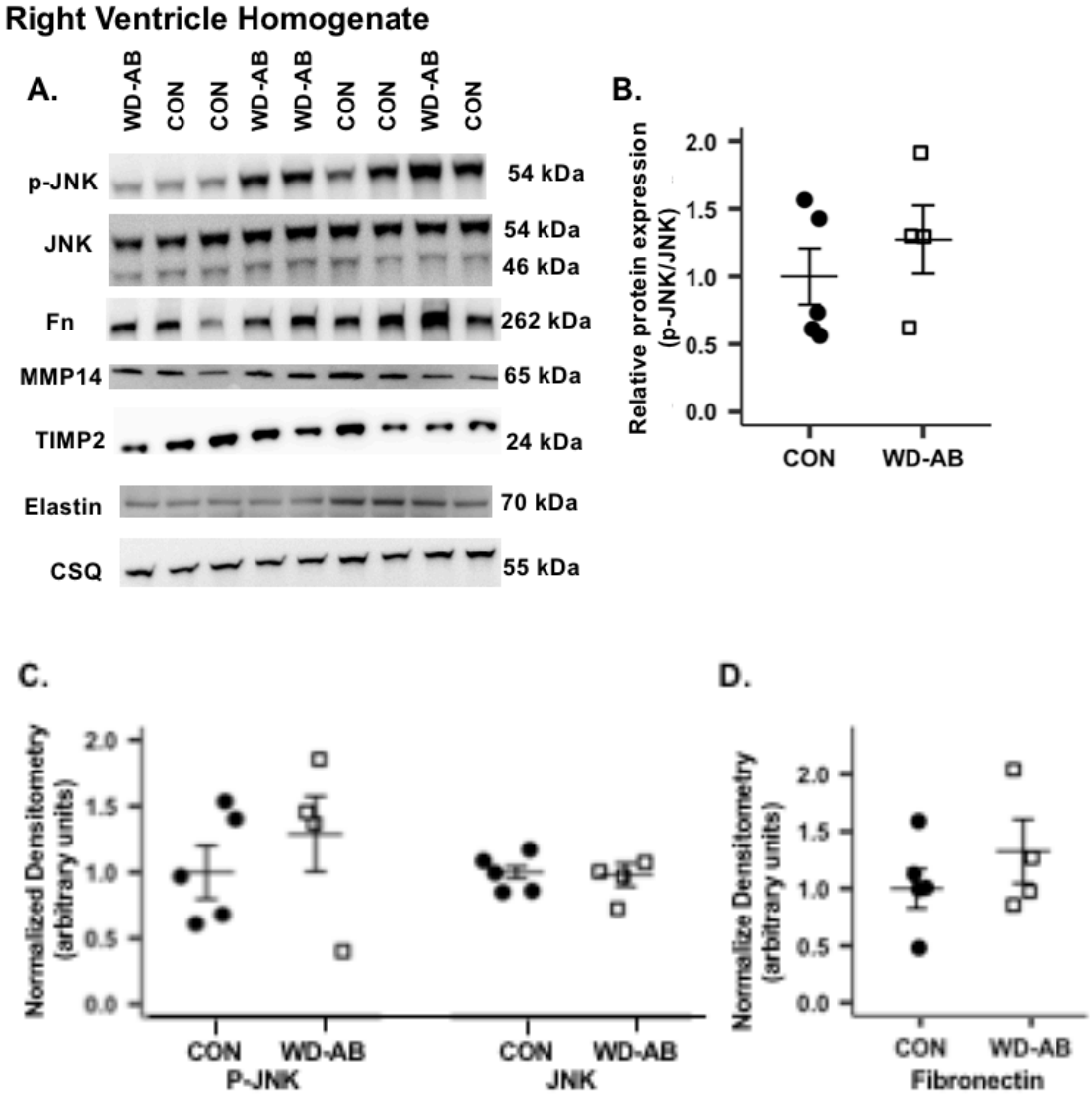

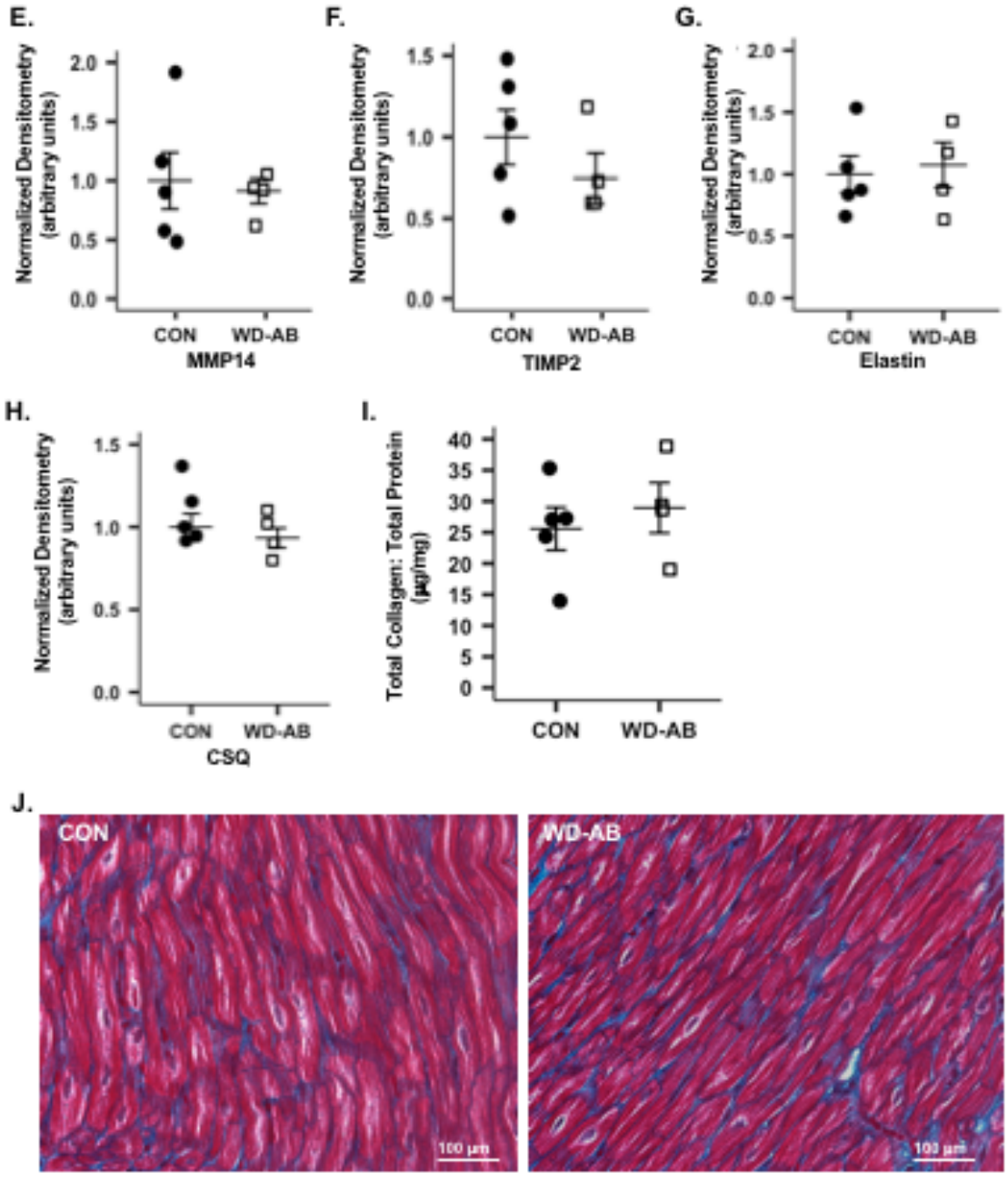
E.
Normalized Densitometry (arbitrary units)
2.0
1.5
1.0
0.5
0.0
CON
WD-AB
MMP14
F.
Normalized Densitometry (arbitrary units)
1.5
1.0
0.5
0.0
CON
WD-AB
TIMP2
G.
Normalized Densitometry (arbitrary units)
2.0
1.5
1.0
0.5
0.0
CON
WD-AB
Elastin
H.
Normalized Densitometry (arbitrary units)
1.5
1.0
0.5
0.0
CON
WD-AB
CSQ
I.
Total Collagen: Total Protein (µg/mg)
40
35
30
25
20
15
10
5
0
CON
WD-AB
J.
CON
100 µm
WD-AB
100 µm

Figure 4. *Western diet-fed, aortic banded Ossabaw swine show no differences in RV protein levels of p-JNK, JNK, fibronectin (Fn), MMP14, TIMP2, or elastin.* **(A)** Western blot images of p-JNK, JNK, Fn, MMP14, TIMP2, elastin, and CSQ for the RV. **(B)** Quantification of the p-JNK:total JNK ratio showed no difference between CON and WD-AB animals. **(C)** Both p-JNK and total JNK did not show significant differences in WD-AB animals compared to CON after individual analyses. **(D)** Fn, **(E)** MMP14, **(F)** TIMP2, **(G)** Elastin, and **(H)** CSQ protein level were not different in WD-AB animals compared to CON. **(I)** Biochemically measured total collagen protein levels were not different between the two groups and visually supported by **(J)** representative Masson's trichrome images (Magnification x40, scale bar = 100 μm). *t-test vs. CON ($P<0.05$). n=5 for CON and n=4 for the WD-AB group.

Right Coronary Artery Structure

When deciding how to further explore the molecular resources identified in the transcriptome from the total RV homogenate in this study given initial findings failed to confirm gene signatures in the RV at the protein level, we considered that fibroblasts, immune cells, cardiomyocytes, or vascular cells could be involved in the gene network oriented around MAPK8 (184). Our laboratory has focused on vascular contributions to HF (147-151, 154, 162, 164), and our initial examination of the RCA found structural adaptations in the WD-AB group. Specifically, a decrease in the RCA elastin elastic modulus (EEM) was found in WD-AB animals compared to CON (**Figure 5A**; stress-strain curves are presented in **Figure 6**) that was accompanied by a predicted reduction in vascular elastin protein level (**Figure 5B**; representative immunohistochemistry images of the RCA are shown in **Figure 5C**). The combination of these findings is consistent with increased vascular stiffness. Additionally, elastin is a target for degradation by MMP2, an MMP isoform that is regulated by both MMP14 and TIMP2 (190, 191). Quantification of MMP2 activity/abundance by gelatin zymography (Zymography gel presented in **Figure 5D**) showed an increase in the WD-AB group compared to CON (**Figure 5E**),

suggesting decreased vascular elastin protein level may be the result of increased degradation.

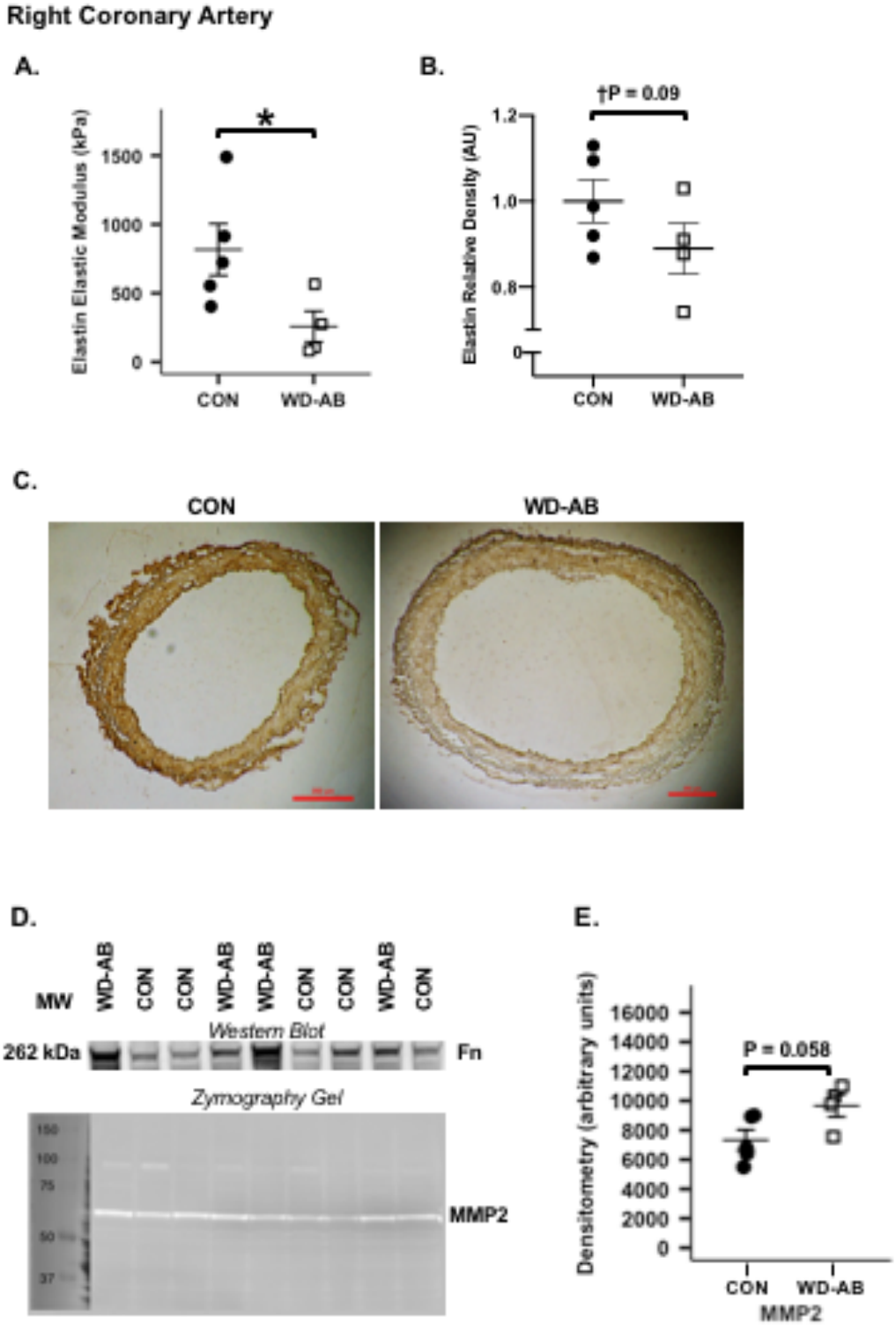

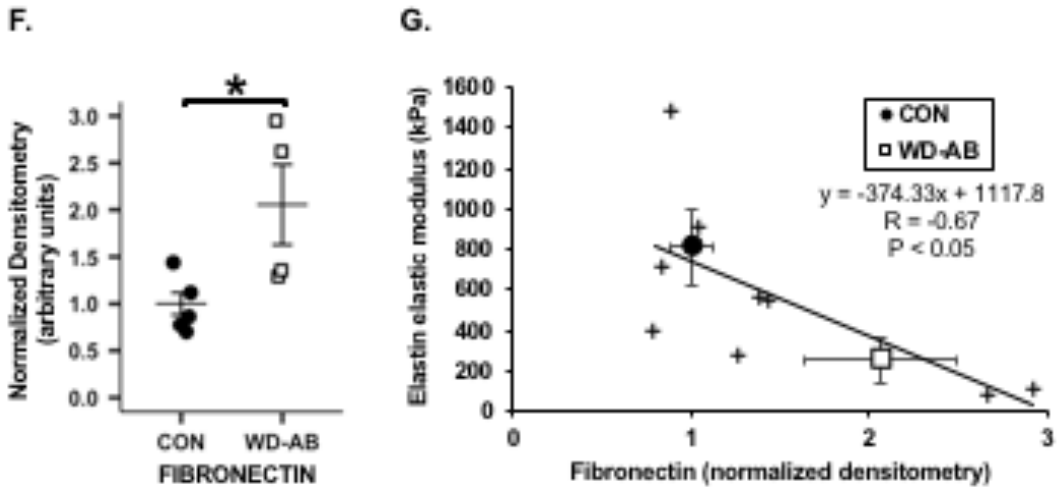

Figure 5. *Increased RCA vascular stiffness and elastin regulation is associated with fibronectin in Western diet-fed, aortic banded Ossabaw swine.* **(A)** The elastin elastic modulus was significantly decreased in the RCA of WD-AB animals compared to CON and **(B)** associated with a decrease in elastin protein level (**C**, representative immunohistochemistry images of RCA elastin staining; scale bar = 250 μm). **(D)** Western blot (top) and zymography gel (bottom) images of Fibronectin (Fn) and MMP2, respectively. (**E**) MMP2 activity/abundance was increased in WD-AB animals compared to CON. **(F)** Fn protein level in the RCA was increased in the WD-AB group compared to CON. (**G**) Increased coronary vascular stiffness, represented by a decrease in the elastin elastic modulus, was negatively correlated with fibronectin protein levels. *t-test vs. CON (P<0.05); †one-tailed t-test vs. CON. n=5 for CON and n=4 for the WD-AB group.

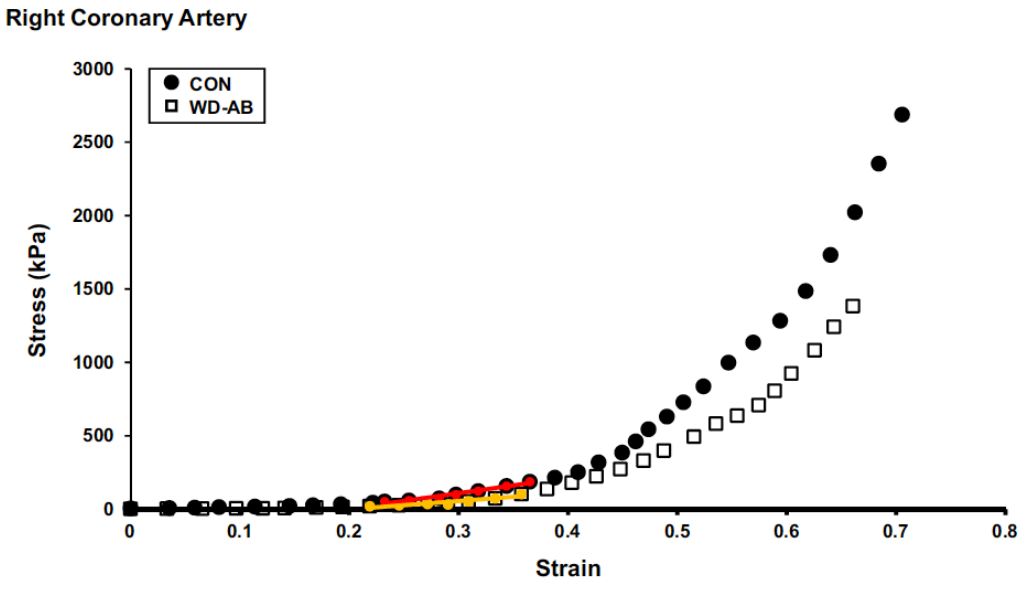

Figure 6. *Stress-strain curves*. Right coronary artery stress-strain curves showing mean group data for the CON and WD-AB groups. The linear region indicates where the elastin elastic modulus, an index of mechanical stiffness, was calculated for CON (red) and WD-AB animals (yellow).

Given these vascular observations, we chose to verify protein levels of JNK1, fibronectin, MMP14, and TIMP2 in the RCA. The first indication that findings from the RV transcriptome may relate to functional increases in coronary vascular stiffness was supported by data showing an increase in RCA fibronectin protein level in WD-AB animals (**Figure 5F;** Western blot presented in **Figure 5D**) that was negatively correlated to the EEM, with a right and downward shift in the group mean along the regression line in the WD-AB group compared to CON (**Figure 5G**). Further assessment of protein in the RCA (Western blots presented in **Figure 7A**) demonstrated the ratio of p-JNK:total JNK was not different, suggesting JNK activation was similar between groups (**Figure 7B**). However, separate evaluation of the two proteins normalized to the CON group indicated p-JNK and total JNK protein levels were increased in WD-AB animals compared to CON (**Figure 7C**). MMP14 protein level in the RCA was significantly decreased in the WD-AB group compared to CON (**Figure 7D**) and observed alongside no differences for TIMP2 (**Figure 7E**) or β-actin protein levels (loading control; **Figure 7F**). Complete Western blot gel images for all RCA and RV proteins assessed are presented in **Figure 8**.

Right Coronary Artery

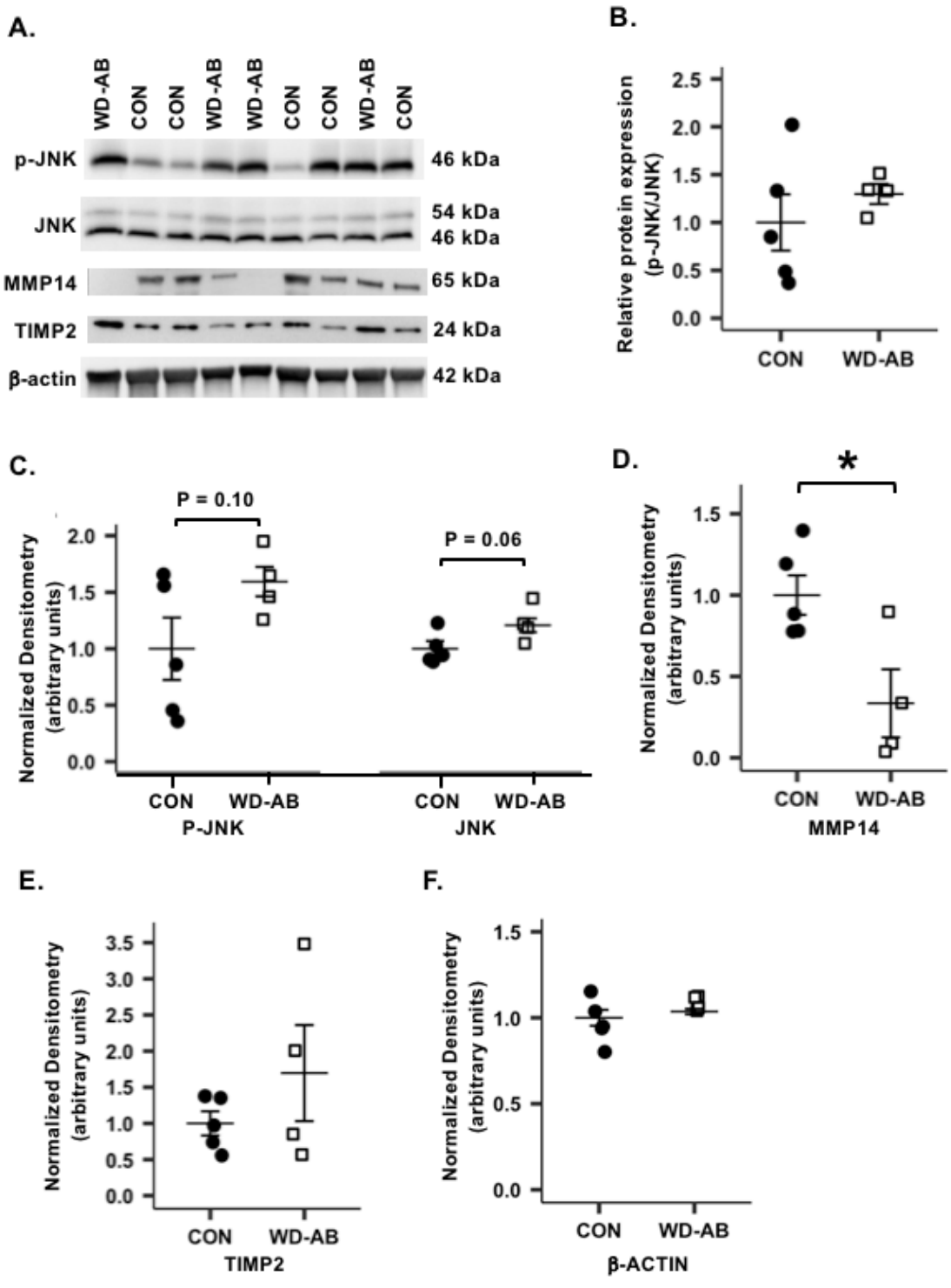

Figure 7. *Western diet-fed, aortic banded Ossabaw swine show increased p-JNK and total JNK protein levels, in addition to decreased MMP14 protein levels, in the RCA.* **(A)** Western blot images of p-JNK, JNK, MMP14, TIMP2, and β-actin for the RCA. **(B)** Quantification of the p-JNK:total JNK ratio showed no difference between CON and WD-AB animals. **(C)** Both p-JNK and total JNK were increased in WD-AB animals compared to CON after individual analyses. **(D)** MMP14 protein level was decreased in WD-AB animals compared to CON. **(F-G)** No differences in TIMP2 or β-actin protein levels were observed. *t-test vs. CON ($P<0.05$). n=5 for CON and n=4 for the WD-AB group.

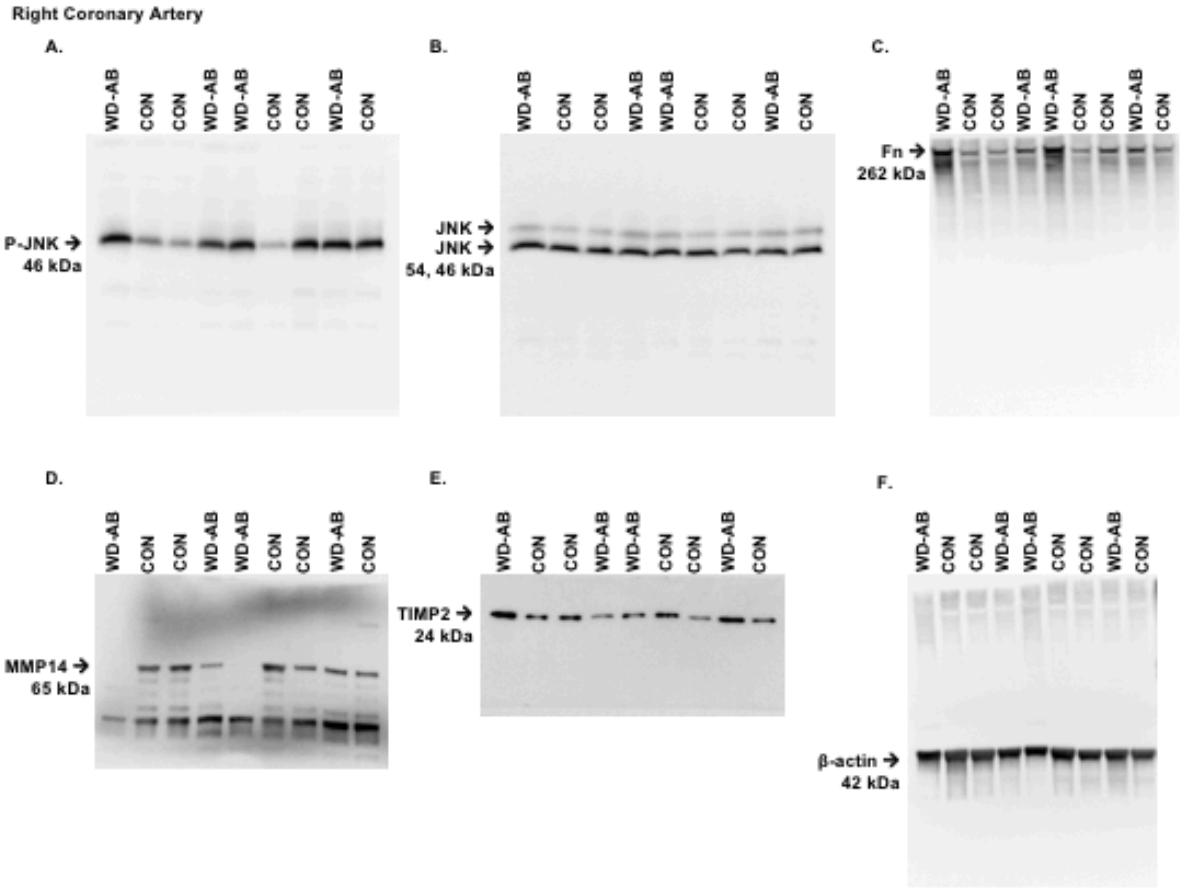

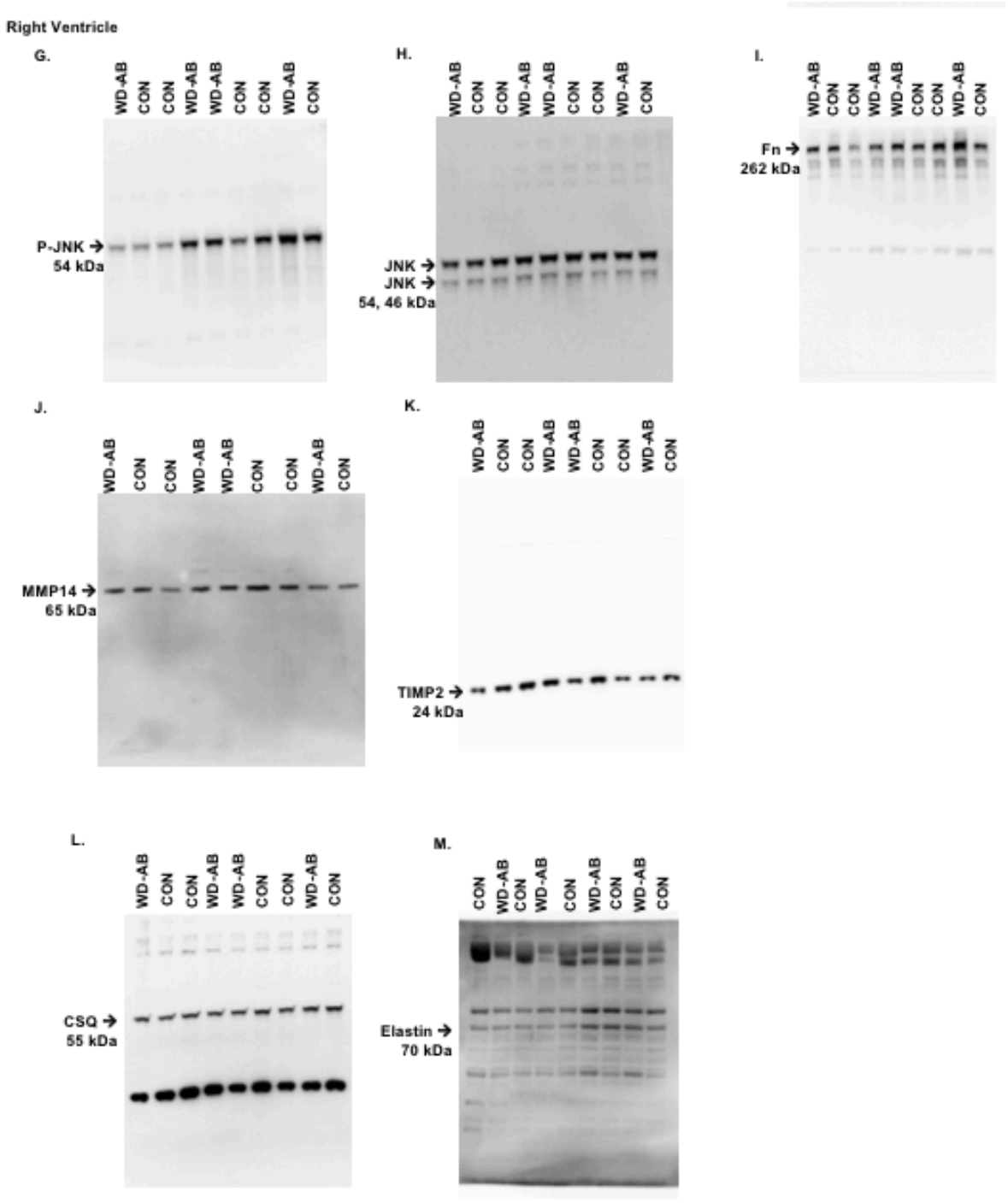

Figure 8. *Full images of western blots for the RCA (A-F) and RV (G-M)*. RCA: **(A)** p-JNK, **(B)** total JNK**, (C)** fibronectin (Fn), **(D)** MMP14, **(E)** TIMP2, and **(F)** β-actin. RV: **(G)** p-JNK, **(H)** total JNK**, (I)** fibronectin (Fn), **(J)** MMP14, **(K)** TIMP2, **(L)** calsequestrin (CSQ), and **(M)** elastin.

Discussion

Metabolic derangement is known to disrupt regulatory mechanisms controlling ECM remodeling, resulting in increased myocardial stiffness and enhanced risk for the development of HF (184). However, specific alterations to the balance between synthesis and degradation of ECM components leading to cardiac dysfunction in a setting of HF with RV disease remain unresolved. Critical gaps to our understanding include a lack of clarity regarding how alterations to the ECM contribute to the development of HF in patients with comorbidities such as diabetes (51). While a great deal of experimental focus has been centered on evaluation of the LV, significantly increased mortality in HF patients with RV pathology suggests mechanisms regulating fibrosis in the RV may also play a key pathological role in their overall health (28, 35, 143, 145). Indeed, recent evidence indicates structural and functional disease develops much more rapidly in the RV compared to the LV over the same time frame in HF patients, while almost doubling the risk of death (34). Therefore, the purpose of this study was to use the RV transcriptome signature from a recently established pre-clinical swine model of cardio-metabolic HF (154) as a first step towards elucidating potential mechanisms relevant to the pathogenesis of HF with associated RV remodeling.

Initial evaluation of the RV transcriptome indicated an increase in MAPK8 mRNA levels in the WD-AB group. This finding led to the exploration of localized remodeling centered around the regulation of the ECM component fibronectin as previous work in mice demonstrated that activation of MAPK8/JNK in the LV can lead to ECM remodeling resulting in the selective induction of fibronectin, but not

collagen, deposition (127). The initial finding that the transcriptome profile was not conserved at the protein level in the total RV homogenate guided the extension of this study into the coronary vasculature. Our subsequent findings in the RCA suggest changes to both the synthesis and degradation of fibronectin may play a role in its accumulation in this coronary conduit artery as summarized in **Figure 9**. Specifically, an increase in both total and phosphorylated JNK protein considered with a parallel decrease in MMP14 protein (a critical regulator of fibronectin turnover) (189) outline a scenario of regulatory imbalance potentially contributing to the increased fibronectin protein levels observed in the RCA. The RV transcriptome signature included herein complements recent work by Hahn et al. (192) examining RNA-seq from human RV-septal biopsies collected in heart failure with preserved ejection fraction patients and provides new perspective into vascular-related genes that may have important ramifications regarding perfusion of the myocardium in cardio-metabolic HF.

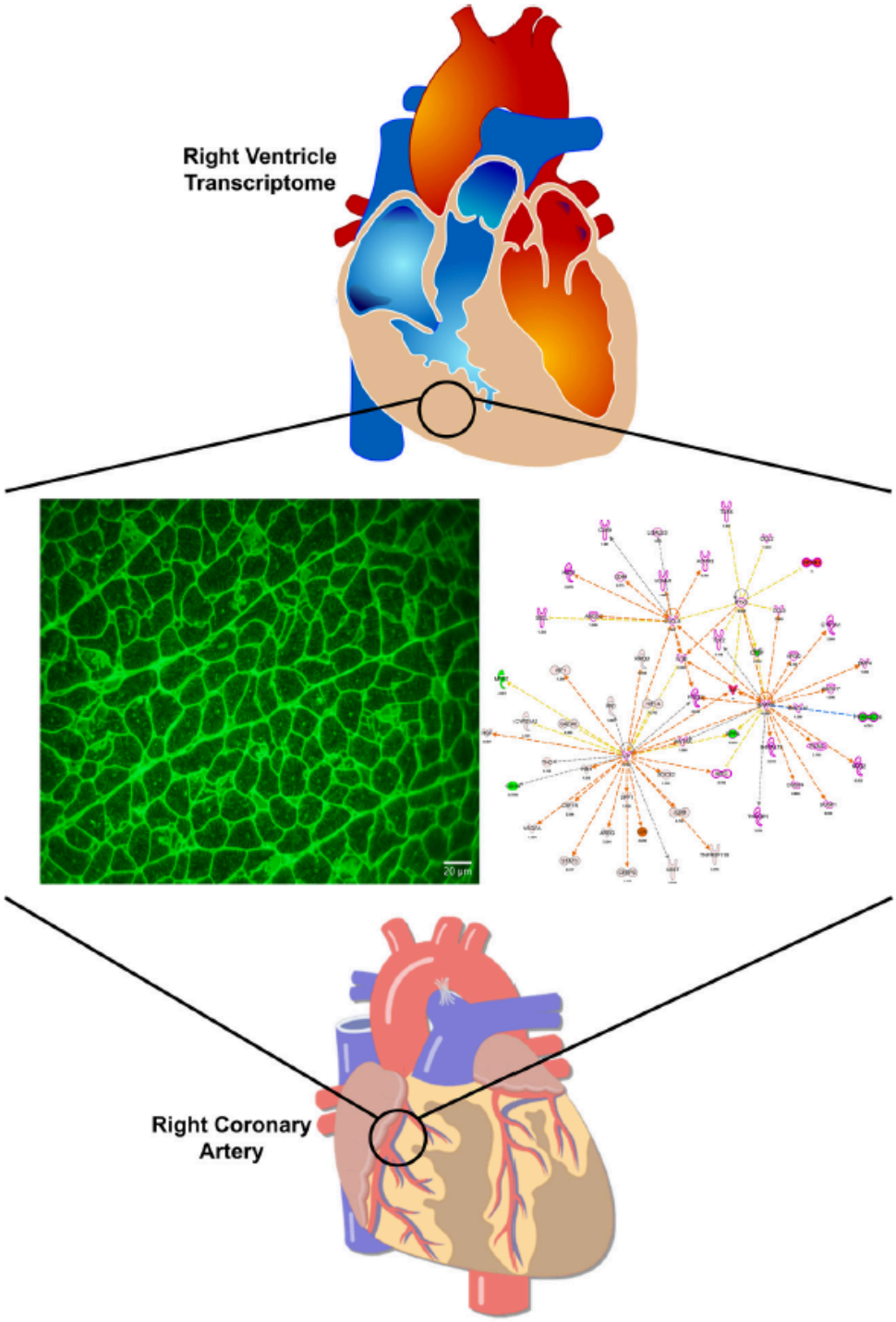
Right Ventricle
Transcriptome
20 µm
Right Coronary
Artery
Synthesis
Fibronectin ↑
OUTCOMES
Degradation
Fibronectin ↓
RCA
↑ JNK total &
phosphorylated
protein
Structural:
• Fibronectin
Accumulation
Functional:
• Increased
Vascular Stiffness
↓ MMP14 protein
&
Normal TIMP2
protein
RCA

Figure 9. *Summary of ECM regulatory imbalance.* Initial findings failed to confirm the transcriptome signature in the RV at the protein level, we therefore extended our examination into the right coronary artery (RCA) where outcomes included - **Synthesis (left)** Increased total p-JNK and JNK protein levels in the RCA potentially: **OUTCOME** - increase vascular fibronectin accumulation in the RCA. **Degradation (right)** Decreased MMP14 and normal TIMP2 protein levels in the RCA may contribute to: **OUTCOME** - increased vascular fibronectin accumulation in the RCA. **Functional Outcome (center)** Dysregulation of fibronectin in the coronary vasculature may have functional consequences as demonstrated by its association with increased RCA vascular stiffness.

Indeed, our results indicate dysregulation of fibronectin may have functional ramifications as indicated by its association with increased vascular stiffness. The negative correlation between the EEM and fibronectin suggests that as protein levels increase, there is an increase in RCA stiffness in WD-AB animals (reflected as a decrease in the EEM). Elastin is a primary contributor to vascular stiffness (193), and reductions in this important ECM protein by genetic manipulation or metabolic disease has been shown to promote arterial stiffening (178, 194, 195). The findings of a parallel decrease in the EEM and elastin protein level in the RCA in the WD-AB group are consistent with an interpretation of increased coronary vascular stiffness, matching previous findings from our laboratory in a separate Yucatan mini-swine model of aortic banding-induced HF without metabolic comorbidities (164). Considered together, these results indicate that both chronic pressure overload in the presence or absence of metabolic derangement can cause remodeling of coronary conduit vessels. An increase in large elastic artery stiffness is an independent predictor of cardiovascular events, although whether this idea can be applied by extension into the smaller coronary conduit vessels (i.e., the RCA) is not completely elucidated. Increased coronary conduit stiffness could enhance energy transmission to coronary resistance vessels, potentially

increasing pulsatility and promoting cardiac damage resulting in microvascular dysfunction. Our laboratory has previously shown an increase in coronary vascular conduit stiffness that was associated with increased vascular pulsatility (148), and when combined with our recent demonstration of impaired coronary microvascular vasodilatory capacity in the LV of the same animals used in this study (146) begin to build a foundation for this well-established large elastic artery concept in the heart. In the current study, the correlation between fibronectin and vascular stiffness observed highlights a new potential mechanistic link between coronary structure and function potentially worthy of future interrogation.

Indeed, coronary vascular dysfunction is prevalent in HF patients and associated with an increased risk of adverse cardiac events (196-198). Previous studies from our laboratory have demonstrated coronary microvascular dysfunction mediated by the large conductance calcium-activated potassium (BK_{Ca}) channel in this Ossabaw and the aforementioned Yucatan models of experimental HF (150, 154). Interestingly, fibronectin has been shown to influence BK_{Ca} channel function via coordinated regulation through integrin signaling (199, 200). In this regard, β_8-integrins have been shown to interact: 1) with fibronectin independently (201); and 2) in concert with the αv-integrin to influence transforming growth factor-β (TGF-β) and extracellular signal-related kinase (ERK) signaling (202, 203). Additional gene ontology analysis of the RV transcriptome in this study showed significant enrichment of the TGF-β, ERK, and Integrin signaling pathways that further implicate DUSP, MAPK8, β_8-integrin (gene notation - ITGB8), and fibronectin (gene notation – FN1) interactions in the observed

dysregulation of ECM remodeling in the WD-AB group (**Table 4)**. These data expand upon previous basic science biophysical findings to demonstrate the potential relevance of these mechanisms to HF in a translational large animal model and while not definitive, set the foundation for further examination regarding their relationship to ECM remodeling and overall coronary vascular function.

Table 4. Gene Ontology Analyses of Induced Fibronectin-related Signaling Pathways Expressed between CON and WD-AB Right Ventricle

Gene Ontology, Signaling Pathways

Name	Matched genes (symbol)	p-value
TGF-Beta Pathway	**DUSP1**, MKNK2, SMAD9, **DUSP4**, MRAS, EIF4A1, PSMB8, PSMB9, KIT, SOCS2, EIF4E, MYC, PSMD5, **MAPK8**, FGF12, H3F3B, PTN, FGF2, IL1A, IL1B, IL4R, IL2RG, ROR1, RAN, IL1R1, IL15RA, RPS6, IRS1, HGF, JAK2, **ITGB8**, NFKB1, JAK3, SUMO1, STAT2, STAT3, TCF15, TEK, TEAD4, TNFSF10, TNFRSF1A, CXCL8, CSF1R, CTGF, CSF2RB, UBD, UBE2B, PIK3R1, AREG, VEGFA, ARHGEF10, BMP1, BMP4, CCL2, CCL5, CD4	4.34e-9
ERK Signaling	**DUSP1**, MKNK2, SMAD9, MRAS, ADCY5, KIT, PPP1R15A, MYC, **MAPK8**, FGF12, H3F3B, PTN, FGF2, SPP1, IL1A, PTGS2, IL1B, LAMA2, MYH7, IL4R, MYH7B, IL2RG, ROR1, GNAT1, IL1R1, MYL1, LIF, IL15RA, MYL6, PMAIP1, NCF2, IRS1, HIF1A, HGF, SOX12, JAK2, **ITGB8**, NFKB1, **FN1**, JAK3, RARG, NOS2, JUNB, STAT2, STAT3, TCF15, TEK, TEAD4, OSMR, TNC, TNFSF10, TMSB4X, TNFRSF1A, CXCL8, CSF1R, CX3CL1, CTGF, CSF2RB, CXCL14, CXCL16, CXCL9, TNFAIP6, TP53BP2, PIK3R1, AREG, VEGFA, WNT5A, ARHGEF10, ATF3, BMP1, BMP4, CCL2, CCL5, CCR1, CDC42EP2, CDC25B, CD3E, CDK6, CD4	1.24e-7
Integrin Pathway	MRAS, ADCY5, PLAU, MYC, **MAPK8**, SPP1, LAMA2, MYH7, MYH7B, GNAT1, MYL1, MYL6, NCF2, JAK2, **ITGB8**, NFKB1, **FN1**, JAK3, STAT2, STAT3, CGA, THBS1, CLDN5, TNC, CXCL8, CX3CL1, CXCL14, CXCL16, CXCL9, VCAM1, PIK3R1, VEGFA, VAV1, CALM1, CCL2, CCL5, CCR1	5.23e-4

In this study, a combination of transcriptome gene signatures indicative of pulmonary disease and pathological hypertrophy at the whole organ and cellular levels were observed in the RV of this pre-clinical model of cardio-metabolic HF.

Previous evidence of LV diastolic dysfunction and atrial hypertrophy was observed in these same animals (154), supporting a theory of chronic backward hemodynamic conveyance that increases RV mechanical stress resulting in activation of signaling cascades like MAPK8 that can promote pathological remodeling (184, 185). The role of MAPK8 in cardiomyocyte hypertrophy is a subject of debate with *in vitro* studies showing a hypertrophic effect while *in vivo* studies demonstrate an anti-hypertrophic effect (119, 127, 128, 204, 205). Given the high prevalence of pulmonary hypertension in HF and its association with RV disease and increased mortality (35, 144, 206), the observed interactions between the RV, lungs, and LV suggest this large animal model holds translational potential for this specific cohort of patients. Further examination of cardiopulmonary hemodynamic function to complement the structural and genetic findings of the current study is warranted.

Although the focus herein was on the confirmation of MAPK8/JNK1 signaling identified via analysis of the RV transcriptome at the protein level in the RCA, the significant hypertrophic remodeling observed at the organ and cellular level in the RV provides an opportunity to compare its genetic signature to that of the LV. Cardio-metabolic HF is often accompanied by dysfunction in both the LV and RV (10, 18), and it is currently unclear if the pathological process is similar between heart chambers. **Figure 10A** shows a Venn diagram indicating out of 13,00 genes present in our original data, 401 genes in the RV and 626 genes in the LV were differentially expressed between the CON and WD-AB groups. Of these genes, 116 were differentially expressed between groups in both chambers

($P = 1.622 \times 10^{-60}$) demonstrating core conserved genes that are affected similarly in both the LV and RV during the development of HF. A number of significant differences in gene signatures was also observed between cardiac chambers, and we explored these differences using a heat map displaying 'Disease and Biological Function' canonical pathways generated using unbiased IPA. From this analysis we identified two gene networks related to fibrosis, specifically "Differentiation of Connective Tissue Cells" and "Growth of Connective Tissue", that were significantly activated (as determined by a z-score >2) in WD-AB animals compared to CON in the RV only. The interaction of these two pathways activated in the RV are presented in **Figure 10B**. Together, these data detail a preliminary examination comparing the RV and LV transcriptomes in this pre-clinical Ossabaw swine model of cardio-metabolic HF and highlight a number of novel gene targets for future exploration that may be relevant to differences in fibrotic structural remodeling between cardiac chambers.

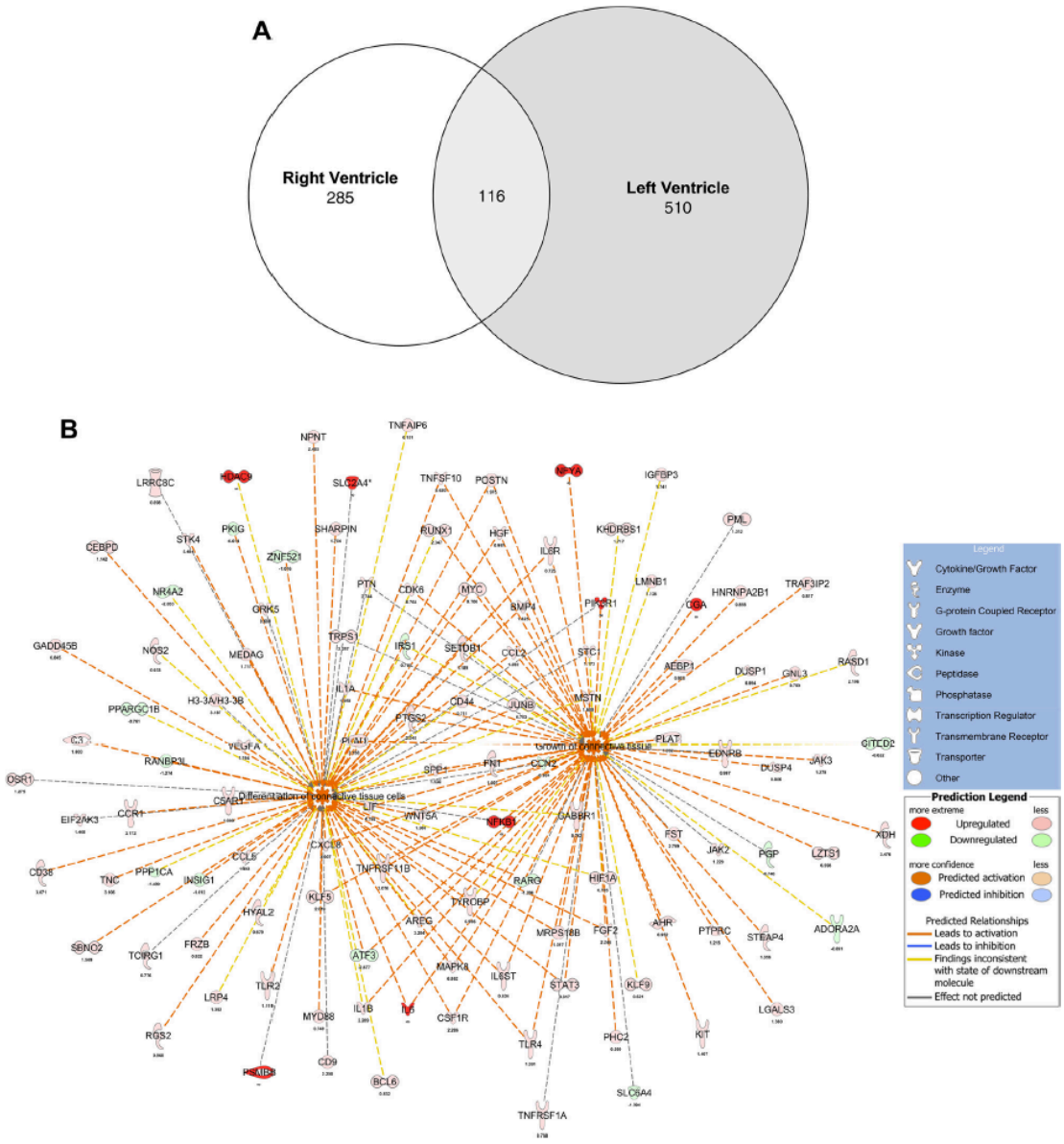

Figure 10. *Transcriptome comparison in the RV vs. LV.* **(A)** Venn diagram demonstrating out of the 401 genes in the RV and 626 genes in the LV that were differentially expressed between the CON and WD-AB groups, 285 were specific to the RV, 510 were specific to the LV, and 116 were conserved between chambers. **(B)** RV gene interactions between significantly activated 'Differentiation of Connective Tissue Cells' and 'Growth of Connective Tissue' networks revealed by Ingenuity Pathway Analysis between CON and WD-AB animals. These gene networks were not activated in the LV.

Limitations

This study examining the RV transcriptome presented a unique opportunity to evaluate molecular mechanisms in the RV and expand this assessment into the coronary vasculature. Our findings certainly warrant RNA-seq studies in the RCA and other individual cell types (cardiomyocyte, smooth muscle, endothelium, fibroblast) in the future. While currently the primary focus was on structural remodeling of the right side of the heart, the results indicate a more thorough evaluation of *in vivo* RV hemodynamics and structure is justified for subsequent evaluation. Finally, although a strength of this model is the multi-hit combination of Western diet and chronic pressure overload reminiscent of human cardio-metabolic HF, this experimental design does not allow for the determination of individual contributions by these variables to the transcriptome and provide information relevant only to this time point of disease.

Conclusions

The results of this study uncovered regulatory imbalance of the ECM based on unbiased analysis of the RV in a new pre-clinical Ossabaw swine model of cardio-metabolic HF. Initial assessment of the RV transcriptome detected molecular signatures indicative of pathological remodeling centered around MAPK8. Further verification found an imbalance in the synthesis and degradation of fibronectin in the RCA, potentially mediated by JNK1 and MMP14, that was associated with increased coronary vascular stiffness. Additional evaluation of the RV transcriptome highlighted genetic signatures supporting integration of pulmonary and RV pathology and mechanistic insight regarding the functional

implications of vascular fibronectin accumulation, providing a basis for future molecular interrogation. Overall, our findings establish a comprehensive molecular signature in the RV and uncover new insights related to the signaling mechanisms involved in coronary vascular structural remodeling in a setting of experimental HF. These outcomes suggest this unique RV transcriptome dataset may have clinical relevance for HF patients exhibiting deterioration of RV structure.

Acknowledgments

The authors would like to thank Jan Ivey for her considerable technical contributions, which were essential to the successful completion of the study, and Gore for their generous gift of vascular Gore-Tex sleeves used for aortic-banding. This work was supported with resources and the use of facilities at the Harry S. Truman Memorial Veterans Hospital in Columbia, MO.

Funding

This study was supported by a University of Missouri Research Board Grant (PI's: Emter and Rector); NIH RO1 HL112998 (PI: Emter); VA-Merit Grant I01BX003271-01 (PI: Rector); NIH K01 HL125503 (PI: Padilla); NIH K01 AG041208 and R01 HL136292 (PI: Domeier); American Heart Association postdoctoral fellowship 16POST27760052 (PI: Olver); NIH K99 HL138301 (PI: Rau); NIH R01 HL122737, NIH R01 HL123295, and NIH HL129639 (PI: Wang).

Disclosures

none

CHAPTER 3: CHRONIC PRESSURE OVERLOAD AND THE LOSS OF FEMALE SEX HORMONES ALTERS THE REGULATION OF CARDIAC FIBROSIS IN A CHAMBER-SPECIFIC MANNER

Abstract

Heart failure with preserved ejection fraction (HFpEF) disproportionality affects postmenopausal women compared with premenopausal women. The pathogenesis of HFpEF, previously known as diastolic heart failure, is not well defined. Cardiac fibrosis is a hallmark feature of HFpEF that has increased prevalence in postmenopausal women and is hypothesized to contribute to the pathogenesis of this disease. Therefore, the goal of this study was to evaluate the effect of the loss of sex hormones via ovariectomy (OVX) on the regulation of cardiac fibrosis during the development of aortic-banding (AB) induced heart failure in four groups of female Yucatan mini-swine: control, intact (CON-INT; N=7); control, ovariectomized (CON-OVX; N=6); aortic-banded, intact (AB-INT; N=7); and aortic-banded, ovariectomized (AB-OVX; N=7). Biochemical evaluation of total collagen protein demonstrated an increase in total collagen due to OVX (main effect) in the left ventricle (LV) independent of AB. In contrast, total collagen was increased due to AB (main effect) in the right ventricle (RV) independent of OVX. These results led to the hypothesis that collagen is differentially regulated in a chamber-specific manner due to imbalances in its synthesis and degradation. To determine alterations in the synthesis and degradation of collagen, mRNA and protein levels of extracellular matrix proteins and regulators were evaluated including: collagen I, collagen III, fibronectin, myofibroblasts, sex hormone receptors, the JNK pathway, the ERK1/2 pathway, matrix metalloproteinases

(MMPs) and tissue inhibitors of matrix metalloproteinases (TIMPs). In the RV, there was increased JNK activation and myofibroblasts due to chronic pressure overload. Additionally, collagen I mRNA levels were positively correlated to total collagen protein. These results point to an increase in collagen synthesis in the RV. Conversely, in the LV, these synthesis pathways were unaltered due to the loss of sex hormones suggesting that cardiac fibrosis in the LV is not due to an increase in synthesis. As for degradation, there was an increase in TIMP-3 protein levels which could suggest an increase in the inhibition of collagen degradation in the RV. In the LV, multiple MMP and TIMP isoforms were altered due to both OVX and AB suggesting an imbalance in the regulation of extracellular matrix degradation which could ultimately result in the accumulation of collagen. In conclusion, these findings demonstrate important differences in the regulation of fibrosis due to the loss of sex hormones and chronic pressure overload between the LV and RV that may be critical to understanding the pathophysiology of HFpEF.

Introduction

Heart failure (HF) is an epidemic that disproportionality affects postmenopausal women compared with premenopausal women, especially in heart failure with preserved ejection fraction (HFpEF) (3, 4, 15, 41, 43, 198). Additionally, cardiac fibrosis and diastolic dysfunction have increased prevalence in postmenopausal women compared with premenopausal women and these two characteristics are hallmark features of HFpEF that are shown to increase mortality rates (2, 38, 39, 41, 42, 44, 207, 208). These differences in disease and comorbidity prevalence between postmenopausal women and premenopausal women is often attributed to the loss of female sex hormones (i.e., estrogen and progesterone). While progesterone has not been as heavily evaluated as estrogen, both female sex hormones are shown to have cardioprotective effects. Estrogen and progesterone are anti-inflammatory, anti-hypertrophic, anti-arrhythmic, vasodilators, and anti-apoptotic (85, 89, 93, 94, 101, 102). Estrogen has also been shown to reduce cardiac fibrosis and inhibit collagen synthesis, while both processes are enhanced in the presence of progesterone (90). Although both estrogen and progesterone have been shown to reduce cardiac fibrosis, the alterations in molecular signaling pathways upstream of collagen synthesis are unknown. Additionally, changes to other extracellular matrix (ECM) regulatory pathways by sex hormones have not been heavily evaluated.

Cardiac fibrosis occurs where there is an accumulation of ECM proteins, primarily collagen, which can lead to ventricular impairments and diastolic dysfunction (55, 56). This accumulation of ECM proteins can occur when there is

an imbalance in its synthesis and degradation. It has been hypothesized in postmenopausal women that cardiac fibrosis occurs through an increase in the inhibition of collagen degradation while cardiac fibrosis in individuals with HFpEF occurs through increases in collagen synthesis as well as decreases in degradation (42, 68). Therefore, the goal of this study was to evaluate the effect of the loss of sex hormones via ovariectomy (OVX) on the development of cardiac fibrosis in female Yucatan swine with aortic-banding (AB) induced HF, a model previously developed in our lab (151, 161, 163). Unpublished results in this animal model have shown that diastolic dysfunction, as determined through the end-diastolic pressure volume relationship (EDPVR), and cardiac fibrosis in the left ventricle (LV) were increased due to the loss of sex hormones and independent of chronic pressure overload, similarly to postmenopausal women (**EDPVR**: CON-INT = 0.010 $\pm$ 0.002; AB-INT = 0.012 $\pm$ 0.002; CON-OVX = 0.19 $\pm$ 0.002; AB-OVX = 0.015 $\pm$ 0.002; main effect of OVX $p < 0.05$; **LV total collagen protein**: CON-INT = 8.27 $\pm$ 1.88; AB-INT = 8.57 $\pm$ 0.75; CON-OVX = 12.59 $\pm$ 1.97; AB-OVX = 11.38 $\pm$ 1.07; main effect of OVX $p < 0.05$). These results led to the hypothesis that the loss of sex hormones through OVX leads to an accumulation of collagen in the LV due to an imbalance in its synthesis and degradation.

Another goal of this study was to evaluate whether alterations in the synthesis and degradation of collagen in the LV are translated to the right ventricle (RV). Right ventricular dysfunction (RVD) in individuals with HFpEF is associated with increased risk of hospitalizations and up to an 80% increased risk of death (27, 28, 34). However, little research, especially from a molecular perspective, has

been conducted on the RV. A recent study from our lab evaluating transcriptome signatures between the LV and RV in a swine model of cardiometabolic HF demonstrated only 13% of the genes differentially expressed were altered in both ventricles establishing ventricle-dependent gene signatures in the progression of HF (209). Therefore, I hypothesized that chamber-specific differences in collagen regulation exist between the two ventricles. Results of this study indicate that there are ventricular dependent alterations at the mRNA, protein, and activity level in multiple regulators of both ECM synthesis and degradation. These results highlight important differences in the regulation of fibrosis due to the loss of sex hormones and chronic pressure overload between the LV and RV, emphasizing the need to evaluate the whole heart, as one system and as individual chambers, in order to fully understand the development of this disease.

Methods

Experimental Design

This is an analysis on total LV and RV homogenates (cardiomyocytes, fibroblasts, coronary blood vessels) harvested from animals previously published by our laboratory (151, 161, 163, 210). Briefly, twenty-eight intact, female Yucatan swine (7 months old) were divided into four groups: control intact (CON-INT), aortic-banded intact (AB-INT), control ovariectomy (CON-OVX), and aortic-banded ovariectomy (AB-OVX). A bilateral ovariectomy was performed at 7 months of age to surgically induce menopause and was confirmed by reduced uterus weight at the time of euthanasia as previously described (151, 163, 210). At 8 months of age, an aortic band was placed on the ascending aorta proximal to the brachiocephalic artery as previously described (5, 146, 149-152, 160, 161, 163, 210). Prior to placing the band, the peripheral mean arterial pressure was set to ~90 mmHg (AB-INT = 90 $\pm$ 1; AB-OVX = 89 $\pm$ 1) under anesthesia using phenylephrine (iv 1-3 μg/kg/min) and heart rate intrinsically set itself to ~100 bpm (AB-INT = 99 $\pm$ 5; AB-OVX = 100 $\pm$ 4). Following hemodynamic stabilization, the trans-stenotic systolic pressure gradient was set to ~70 mmHg (AB-INT = 73 $\pm$ 3; AB-OVX = 72 $\pm$ 3). One month prior to terminal studies, intact swine were orally dosed with altrenogest (4.5 mL, 0.22% solution; MATRIX®, Merck, New Jersey) to ensure that intact swine were not in estrus at the time of sacrifice (151, 163, 210). Dosing was performed for 14 days followed by 12-15 days of non-treatment. To confirm animals were not in estrus, concentrations of serum progesterone were measured with a chemiluminescent enzyme immunoassay (IMMULITE 1000,

Siemens Healthineers, PA) and serum estrogen levels were measured through radioimmunoassay at the University of Pennsylvania Radioimmunoassay and Biomarkers Core (University of Pennsylvania, Philadelphia, PA). Anestrus was confirmed in these animals as estrogen levels in 23 out of 27 animals were below the level of detection and progesterone levels were greater than 0.5 ng/ml in intact animals (CON-INT = 6 ± 4 ng/mL; AB-INT = 16 ± 4 ng/mL; CON-OVX = undetectable; AB-OVX = undetectable) (151). Terminal studies were then performed at 14 months of age in which animals were anesthetized with telazol (5 mg/kg)/xylazine (2.25 mg/kg). The animals were maintained on Propofol (6-10 mg/kg/min) for in vivo hemodynamic experiments. LV and RV tissue were harvested, flash-frozen in liquid nitrogen, and stored at -80°C for future analyses as previously described (151, 163).

Cardiac Fibrosis

Whole homogenates of LV and RV tissue were utilized to biochemically evaluate total collagen through the commercially available collagen-specific hydroxyproline assay kit per manufacturer's instructions (Cedarlane, QuickZyme Total Protein and Collagen, Leiden, The Netherlands). Briefly, LV and RV tissue were hydrolyzed in hydrochloric acid then a colorimetric assay was utilized to quantify collagen-specific hydroxyproline. Results are reported as the ratio of total collagen: total protein (146). Masson's trichrome stain and picrosirius red stain were utilized to visually assess fibrosis in the LV and RV (146, 149, 176, 177, 209).

Quantitative RT-PCR

Quantitative real-time PCR was performed as previously described (146, 149). Briefly, TRIzol was utilized to extract RNA from LV and RV homogenate per manufacturer's instructions (Applied Biosystems). RNA was then transcribed to cDNA using the High-Capacity cDNA Reverse Transcription kit (Applied Biosystems). qPCR was performed in conditions optimized for each primer and normalized to 18S ribosomal RNA using the $2^{-\Delta\Delta Ct}$ method (149, 174, 175). Primer sequences for 18S, collagen I, collagen III, fibronectin, matrix metalloproteinases-2 (MMP-2), MMP-9, MMP-14, tissue inhibitor of matrix metalloproteinase-1 (TIMP-1), TIMP-2, TIMP-4, mitogen activated protein kinase-8 (MAPK8), dual specificity phosphatase-1 (DUSP1), DUSP4, and DUSP10 have been previously published (149, 209). Sequences for primers utilized for progesterone receptor (PGR), progesterone receptor membrane component 1 (PGRMC1), estrogen receptor 1 (ESR1), ESR2, MMP-1, MMP-3, MMP-13, TIMP-3, MAPK1, MAPK3, MAPK9, DUSP6, and DUSP9 can be found in **Table 1**.

Table 1. Primer Sequences for qPCR Analysis (5' to 3')

Target Gene	Forward Primer	Reverse Primer
PGR	CCCTAGCTCACAGCGTTTCT	GTGCCCGGGACTGGATAAAT
PGRMC1	TACCATCACGTGGGCAAACT	ATATGCTTCCACCGAACGCT
ESR1	CAAGTGTGTCGAGGGAATG	ACGTGTACACTCCAGAATTAAG
ESR2	GCTACAAACCAGTGTACGATAG	GAGCCACACTTCACCATTC
MMP-1	GGTCAAGTTCATGGCTTACA	TGAGACTGCTCTCCACTATC
MMP-3	CCAGTCTACAACCCACTTAC	GATTGCATCGAAGGACAAAG
MMP-13	CGCCTGATTTGACTCATTCT	GTCAGCAGTACCATTGTGAA
TIMP-3	CCTCAGCATCCCTCTAATTG	ACTAACTCTCATCTCCCATCT
MAPK1	ATTTGTCAGGACACGGGCTC	GCTCAAAGGAGTCAAGGTGGA
MAPK3	TTACGACCATGTGCGCAAGA	TGCGATGCCAATGACGTTCT
MAPK9	GATGATTGCAGCCACTTACT	GTGTTGGAAGAGGGAAACTC
DUSP6	GTTGGAAGAACAGGCCATGC	GGCCCTAAAGAGCTCATGCT
DUSP9	CTACCTGCAGGGTGGCTTC	AGTCGGAGCCCAGACACA

Western Blot

LV and RV protein levels were evaluated through western blot as previously described (149, 160, 176, 177, 209). To begin, LV and RV tissue were homogenized in TissueLyser (Qiagen) with stainless steel beads (Next Advance) using Pierce RIPA buffer (Thermo Scientific) and protease/phosphatase inhibitors (HALT, Thermo Scientific). A Bradford assay (Bio-Rad) was utilized to determine protein concentrations per manufacturer's instructions. Western blot conditions were optimized for each protein. 10-40 μg of protein was resolved on 4-12% or 8% SDS/PAGE acrylamide gels (GenScript) followed by transfer to PVDF membranes (GE Life Sciences). Membranes were blocked in 2.5-5% milk followed by incubation in primary antibodies overnight at 4°C. Primary antibodies are listed in **Table 2**. After primary incubation, membranes were incubated in appropriate horseradish peroxidase-linked secondary antibodies (Cell Signaling, 1:2500). Membranes were then imaged using Immobilon® Forte Western HRP substrate reagent (EMD Millipore) or SuperSignal West Femto Maximum Sensitivity Substrate (Thermo Scientific) on a Kodak image station (4000R) or Bio-Rad ChemiDoc XRS+. Membranes were stained with Coomassie blue as a loading control. No differences were seen in loading controls between groups (**LV**: CON-INT = 1.0 ± 0.05; AB-INT = 1.0 ± 0.03; CON-OVX = 0.99 ± 0.04; AB-OVX = 1.02 ± 0.03; p = 0.66; **RV**: CON-INT = 1.0 ± 0.07; AB-INT = 0.98 ± 0.10; CON-OVX = 1.05± 0.05; AB-OVX = 0.97 ± 0.08; p = 0.65). Therefore, protein levels were normalized to CON-INT groups.

Table 2. Primary Antibodies for Western Blot Analysis

Protein	Protein Concentration	Molecular Weight	Company	ID	Dilution
Collagen I	10ug	95 kDa	Proteintech	14695-1-AP	1:1000
Collagen III	20ug	139 kDa	Proteintech	22734-1-AP	1:1000
Fn	40ug	262 kDa	Sigma-Aldrich	AB1954	1:5000
ERα	40ug	68 kDa	ABCAM	ab75635	1:500
ERβ	20ug	59 kDa	DSHB	CWK-F12	1:100
PGR	40ug	120, 94 kDa	ThermoFisher	MA1-12626	1:500
PGRMC1	20ug	22 kDa	ABCAM	ab224054	1:500
MMP-1	20ug	62 kDa	ABCAM	ab137332	1:500
MMP-3	20ug	60 kDa	Cell Signaling	D7F5B	1:500
MMP-13	20ug	54 kDa	ABCAM	ab39012	1:1000
MMP-14	40ug	65 kDa	Invitrogen	PA5-13183	1:1000
TIMP-1	20ug	26 kDa	Cell Signaling	D10E6	1:500
TIMP-2	40ug	24 kDa	Abcam	ab180630	1:1000
TIMP-3	20ug	25 kDa	Cell Signaling	D74B10	1:500
TIMP-4	10ug	26 kDa	ABCAM	ab58425	1:10000
p-ERK	40ug	44, 42 kDa	Cell Signaling	9101S	1:1000
ERK	40ug	44, 42 kDa	Cell Signaling	9102S	1:1000
p-SAPK/JNK	40ug	54 kDa	Cell Signaling	9255S	1:1000
SAPK/JNK	40ug	54, 46 kDa	Cell Signaling	9252S	1:1000

Zymography

Gelatin zymography was utilized to determine activity/abundance of MMP-2 and MMP-9 as previously described (179, 209). LV and RV tissue were homogenized in TissueLyser (Qiagen) with stainless steel beads (Next Advance) using lysis buffer containing 100 mM NaCl, 25 mM Tris-HCl, pH 7.5, 1% Triston X-100, and protease/phosphatase inhibitors (HALT, Thermo Scientific). Protein concentrations were determined using a Bradford Assay (Bio-Rad). 100 μg of protein was prepared in 4x loading buffer containing 250 mM Tris-HCl, pH 6.8, 40% v/v glycerol, 8% w/v SDS, 0.01% w/v bromophenol blue. Protein was resolved on 10% zymography gels (Invitrogen) prior to incubation in zymography renaturing

buffer for 30 minutes at room temperature (Invitrogen). Gels were then incubated in zymography developing buffer (Invitrogen) for 30 minutes at room temperature followed by 36 h incubation in fresh developing buffer at 37°C. Coomassie blue (0.5% w/v Coomassie, 5% v/v methanol, and 10% v/v acetic acid) was then utilized to stain the gel for one hour prior to destaining with buffer containing 10% v/v methanol and 5% v/v acetic acid until visualization of clear band with Azure Biosystems c600 Imager. Gels were further destained with buffer containing 50% v/v methanol and 10% v/v acetic acid for visualization of total protein. Image was quantified by normalizing the MMP band intensity to total lane intensity using ImageJ.

MMP-14 Activity Assay

MMP-14 activity was determined using a MMP-14 fluorogenic substrate (211, 212). LV and RV protein prepared for zymography analysis was utilized for this assay. 50 μg of protein was incubated with or without 7.5 μM of MMP-14 fluorogenic substrate (Calbiochem) for 2 hours at 37°C prior to measuring the excitation/emission (328/400; Tecan Safire).

Electrophoretic Mobility Shift Assay (EMSA)

The transcription binding of SP1 to the collagen I promoter was evaluated through EMSA with protocol adapted for infrared oligonucleotide probes from ThermoScientific's LightShift Chemiluminescent EMSA kit instructions. To begin, nuclear fractions of LV and RV tissue was extracted as previously described (213). Briefly, LV and RV tissue were homogenized in lysis buffer containing 25 mM Tris, pH 7.4, 5 mM EDTA, and protease/phosphatase inhibitors (HALT, Thermo

Scientific) with stainless steel beads (Next Advance) and TissueLyser (Qiagen). After centrifugation at 2000 rpm for 5 minutes at 4°C, the pellet containing the nuclear fraction was washed five times with hypotonic lysis buffer containing 10 mM HEPES, pH 7.5, 10 mM KCl, 3 mM $MgCl_2$, 0.05% NP-40, 1 mM EDTA, and protease/phosphatase inhibitors (HALT, Thermo Scientific) and centrifugation at 3000 rpm at 4°C. After washes, the remaining pellet was suspended in Gel Shift Lysis Buffer containing 50 mM HEPES, pH 7.9, 250 mM KCl, 0.1% NP-40, 0.1 mM EDTA, 0.1 mM EGTA, 10% glycerol and protease/phosphatase inhibitors (HALT, Thermo Scientific) and let sit on ice for 30 minutes prior to centrifugation at 13300 rpm. Protein concentrations of nuclear fractions were determined through Bradford Assay (Bio-Rad). EMSAs were completed through incubation of 20 μg nuclear extract with 10X binding buffer (100 mM Tris, pH 7.5, 500 mM KCl, 10 mM DTT), 2.5% glycerol, 5 mM $MgCl_2$, 50 ng/μL Poly (dI•dC) (Thermo Scientific), 0.05% NP-40, and 5 nM IR-700 tagged SP1 probe (F: 5'/5IR700/AGG ATA TCG GGC GGG TAA AGG A-3; R: 5'-/5IRD700/TCC TTT ACC CGC CCG ATA TCC T-3'; Integrated DNA Technologies, Inc.) for 30 minutes at 4°C. After reaction is complete, 10X orange loading dye (65% sucrose, 10 mM Tris-HCl, pH 7.5, 10 mM EDTA, and 0.3% orange G) was added to reaction. Competition experiments were completed with 200-fold excess of unlabeled SP1 probe incubated with nuclear extract 20 min prior to addition of labeled SP1 probe. Samples were resolved with 5% polyacrylamide gel followed by imaging of gels with Azure Biosystems c600 Imager. Image was quantified by normalizing the shifted band intensity to total lane intensity using ImageJ.

Histology

Immunofluorescence was performed on LV and RV tissue slices that were formalin fixed and embedded in paraffin. After paraffin was removed, antigen retrieval was performed using 10 mM citrate buffer with 0.05% Tween-20. Slides were then blocked with 10% FBS followed by incubation overnight at 4°C in primary antibodies: α-smooth muscle actin (α-SMA; Sigma-Aldrich, 1:1000) and troponin I (Cell Signaling, 1:100). Alexa-488 and Alexa-568 linked-secondary antibodies (1:250) were applied to slides followed by incubation in 5 μg/ml DAPI. Prolong gold antifade mounting media (Thermo Scientific) was used to mount slides prior to imaging using Nikon Eclipse E600 fluorescence microscope with Olympus DP72 camera at 20x objective. A minimum of 10 random fields/animal were analyzed for α-SMA positive counts which were then normalized to tissue area (214).

Statistical Analysis

Statistical analysis was performed using GraphPad Prism (Version 9.3.1, San Diego, CA). Group comparisons were completed using a two-way ANOVA (AB x OVX) and between group differences were determined using Fisher's least significant difference (LSD) posthoc test. Relationships between total collagen protein and collagen mRNA levels were determine using linear regression. Data is presented as mean ± SEM and significance is reported at the $P < 0.10$ and $P < 0.05$ levels (183, 215).

Results

Left Ventricle Fibrosis

Total collagen levels were biochemically evaluated in the LV and demonstrated a main effect of OVX, indicating an increase in total collagen levels in the LV due to the loss of sex hormones and independent of AB (**Figure 1A**). Collagen I mRNA levels were increased due to AB (**Figure 1B**) while there was a trend for an interaction for collagen III mRNA levels to be altered due to both AB and OVX (**Figure 1C**). The relationship between collagen I or III mRNA levels and total collagen was evaluated through linear regression. There was no significant relationship between collagen I mRNA levels and total collagen levels (**Figure 1D**). Additionally, there was no linear relationship between collagen III mRNA levels and total collagen levels (**Figure 1E**) indicating a disconnect between mRNA and protein. Fibrosis was visually assessed through picrosirius red (PSR) and Masson's trichrome stain (**Figure 1F**). Fibrosis deposition was diffuse within the interstitial space, consistent with HFpEF (10, 50). Cardiac fibrosis is often assessed via specific changes in collagen deposition, but fibronectin is another ECM protein that can increase ventricle and vascular stiffness as well as aid in the process of collagen matrix assembly (209, 216-218). Fibronectin mRNA levels did not show any significant differences due to OVX or AB; however, a significant decrease in fibronectin protein levels due to AB and independent of OVX was observed (**Figure 2A-C**).

Figure 1.

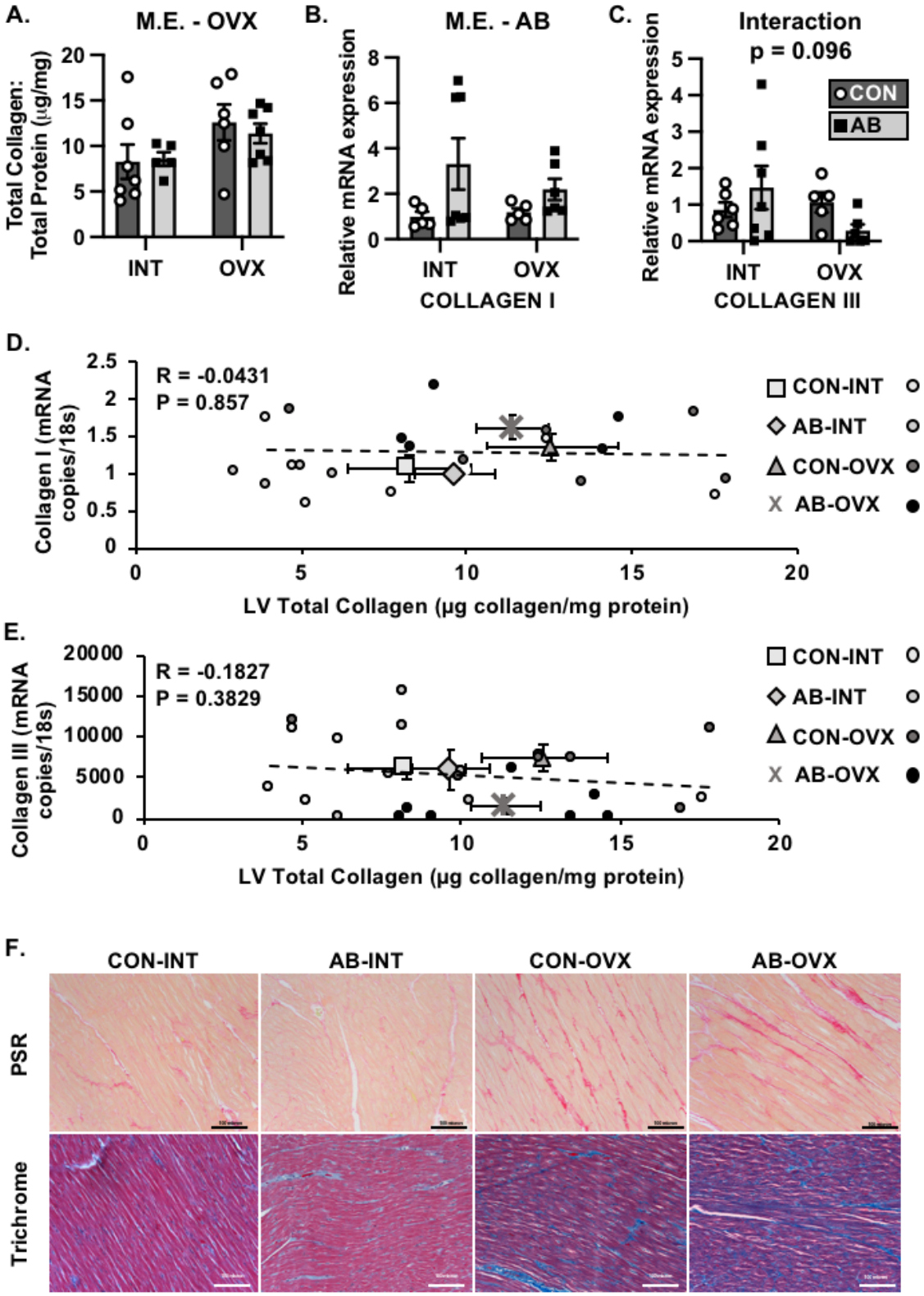
A.
M.E. - OVX
Total Collagen: Total Protein (µg/mg)
INT
OVX
B.
M.E. - AB
Relative mRNA expression
COLLAGEN I
C.
Interaction
p = 0.096
CON
AB
Relative mRNA expression
COLLAGEN III
D.
R = -0.0431
P = 0.857
Collagen I (mRNA copies/18s)
LV Total Collagen (µg collagen/mg protein)
CON-INT
AB-INT
CON-OVX
AB-OVX
E.
R = -0.1827
P = 0.3829
Collagen III (mRNA copies/18s)
LV Total Collagen (µg collagen/mg protein)
F.
CON-INT
AB-INT
CON-OVX
AB-OVX
PSR
Trichrome

Figure 1: *Myocardial collagen levels are increased due to the loss of sex hormones and independent of chronic pressure overload in the left ventricle.* **(A)** Total collagen protein levels were increased due to OVX (main effect). **(B)** Collagen I mRNA levels were increased due to AB (main effect). **(C)** There was a trend towards an interaction effect with collagen III mRNA levels. There was no linear relationship between total collagen protein levels and collagen I mRNA levels **(D)** and collagen III mRNA levels **(E)**. **(F)** Representative images of picrosirius red (PSR) demonstrate collagen deposition in red and Masson's trichrome stain demonstrates fibrosis in blue (scale bar = 100 microns). $p < 0.05$; INT, intact; OVX, ovariectomy; AB, aortic-banded; CON, control.

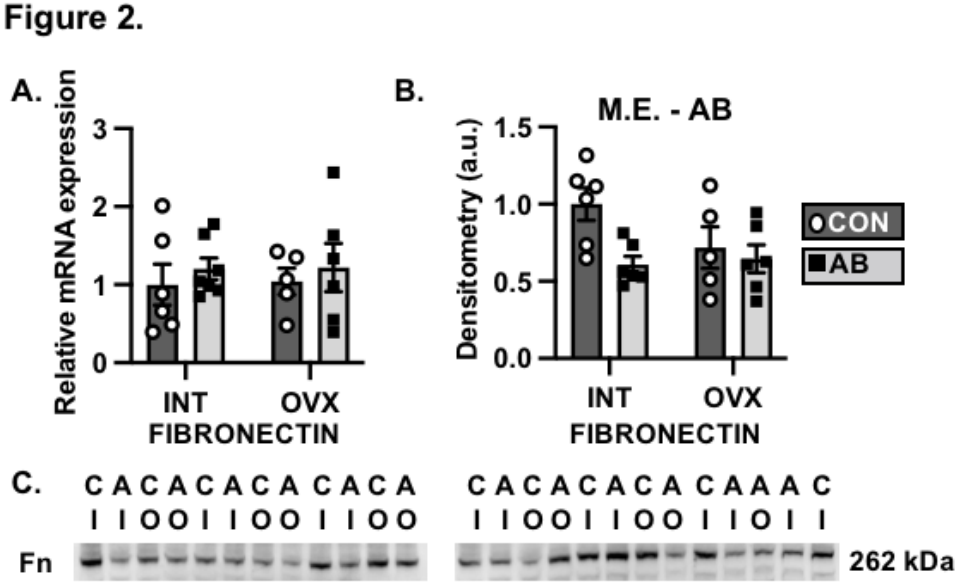

Figure 2: *Fibronectin protein levels are decreased due to the loss of sex hormones and independent of chronic pressure overload in the left ventricle.* **(A)** Fibronectin mRNA levels were not significantly different between groups while **(B)** Fibronectin protein levels were decreased due to AB (main effect). **(C)** Western blot images of fibronectin (Fn). $p < 0.05$; INT, intact; OVX, ovariectomy; AB, aortic-banded; CON, control; CI, control intact; AI, aortic-banded intact; CO, control ovariectomy; AO, aortic-banded ovariectomy; a.u., arbitrary units.

Left Ventricle Fibrosis – Synthesis

To evaluate the synthesis of cardiac fibrosis, sex hormone receptor levels were examined to determine if alterations in hormone receptor levels could lead to increases in collagen due to OVX as alterations in circulating hormones and their receptor levels can alter signal transduction pathways (99). Estrogen receptors

and progesterone receptors were evaluated both at the mRNA and protein levels. Estrogen receptor 1 (ESR1/ERα) mRNA levels were increased due to AB (**Figure 3A**), but protein levels were not significantly different between groups (**Figure 3B**). Similar to ESR1/ERα, estrogen receptor 2 (ESR2/ERβ) mRNA levels trended to be increased due to aortic banding (**Figure 3C**), but ERβ protein levels were not significantly altered (**Figure 3D**). These results suggest that increases seen in total collagen levels were not due to alterations in estrogen receptor protein levels. There are two progesterone receptors (PGR A and PGR B) transcribed from the same PGR transcript (132). There were no significant differences in PGR mRNA levels between groups (**Figure 3E**). However, there was a significant decrease in PGR B protein levels due to AB and a trend for PGR A and PGR B protein levels to be increased due to OVX (**Figure 3F-G**); therefore, alterations in PGR A and PGR B due to OVX are directionally consistent with the increase in total collagen levels. Progesterone receptor membrane component 1 (PGRMC1) has also been hypothesized to be involved with cardiac fibrosis (100). PGRMC1 mRNA levels were increased due to OVX (**Figure 3H**), but there were no significant differences in PGRMC1 protein levels (**Figure 3I**). Images from western blots are shown in **Figure 3J**.

Figure 3.

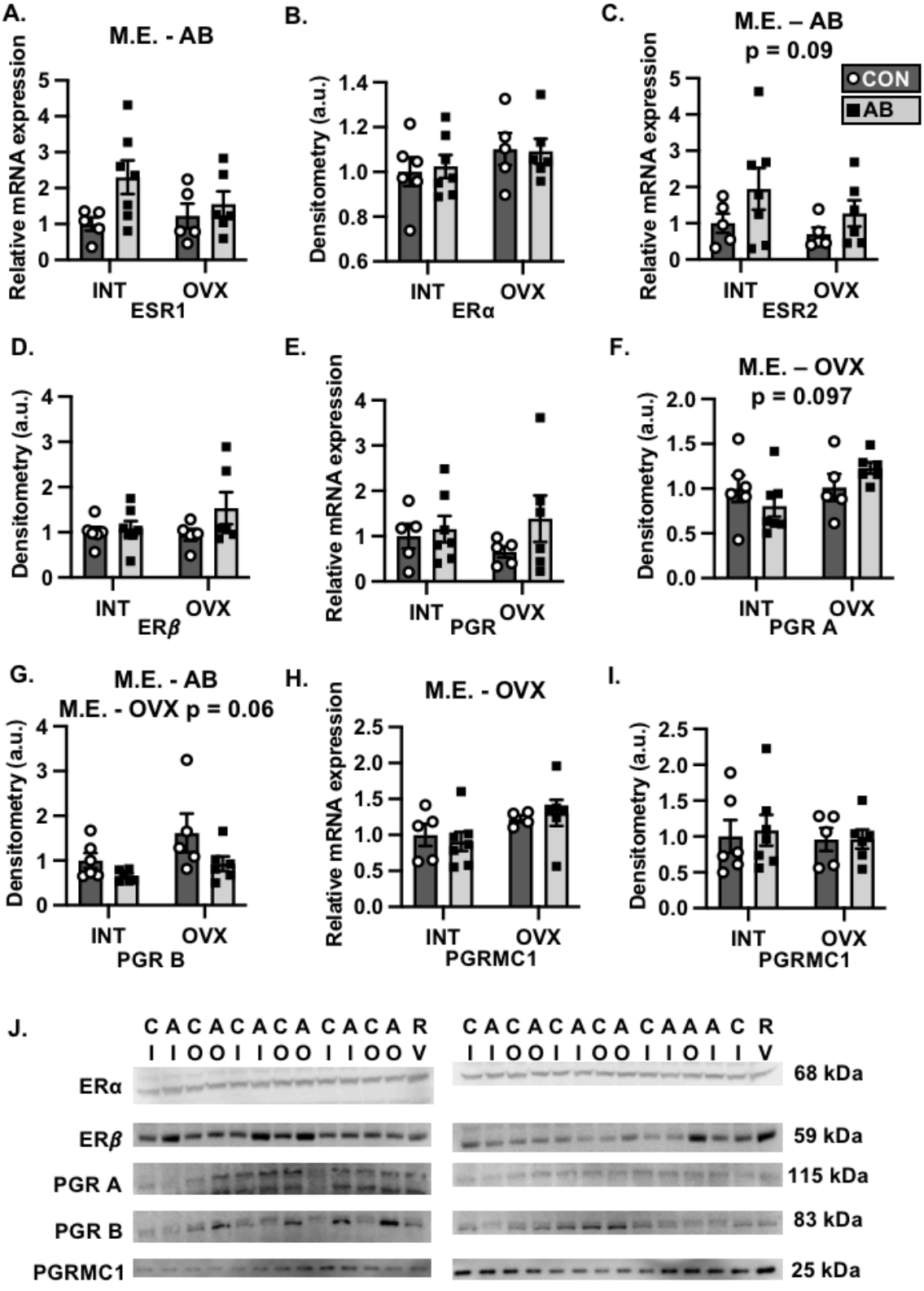
A.
M.E. - AB
Relative mRNA expression
INT
OVX
ESR1
B.
Densitometry (a.u.)
INT
OVX
ERα
C.
M.E. – AB
p = 0.09
CON
AB
Relative mRNA expression
INT
OVX
ESR2
D.
Densitometry (a.u.)
INT
OVX
ERβ
E.
Relative mRNA expression
INT
OVX
PGR
F.
M.E. – OVX
p = 0.097
Densitometry (a.u.)
INT
OVX
PGR A
G.
M.E. - AB
M.E. - OVX p = 0.06
Densitometry (a.u.)
INT
OVX
PGR B
H.
M.E. - OVX
Relative mRNA expression
INT
OVX
PGRMC1
I.
Densitometry (a.u.)
INT
OVX
PGRMC1
J.
C A C A C A C A C A C A R
I I O O I I O O I I O O V
C A C A C A C A C A A A C R
I I O O I I O O I I O I I V
ERα
ERβ
PGR A
PGR B
PGRMC1
68 kDa
59 kDa
115 kDa
83 kDa
25 kDa

Figure 3: *Progesterone receptor protein levels trended to be increased due to the loss of sex hormones in the left ventricle.* **(A)** Estrogen receptor 1/ERα mRNA levels were increased due to AB (main effect) while **(B)** no significant differences were seen at the protein level. **(C)** Estrogen receptor 2/ERβ mRNA levels trended to be increased due to AB (main effect) while **(D)** no significant differences were seen at the protein level. **(E)** There were no differences seen in progesterone receptor (PGR) mRNA levels but **(F)** PGR A protein levels trended to be increased due to OVX (main effect) and **(G)** PGR B protein levels trended to be increased due to OVX (main effect) as well as significantly decreased due to AB (main effect). **(H)** Progesterone receptor membrane component 1 (PGRMC1) mRNA levels were increased due to OVX (main effect) while **(I)** no significant differences were seen at the protein level. **(J)** Western blot images of ERα, ERβ, PGR A, PGR B, and PGRMC1. $p < 0.05$; INT, intact; OVX, ovariectomy; AB, aortic-banded; CON, control; CI, control intact; AI, aortic-banded intact; CO, control ovariectomy; AO, aortic-banded ovariectomy; a.u., arbitrary units.

Both estrogen and progesterone receptors lie upstream of the MAPK pathways ERK1/2 and JNK (40, 93, 132, 134-136). MAPK8/JNK1 mRNA levels were not significantly altered between groups (**Figure 4A**) while MAPK9/JNK2 mRNA levels trended to be increased due to AB (**Figure 4B**). The activation of JNK was evaluated by examining the ratio of phosphorylated JNK to total JNK levels. Phosphorylated JNK (pJNK) levels were significantly increased due to AB while total JNK protein levels were decreased due to OVX (**Figure 4C-D**). However, the activation of JNK was not significantly altered between groups (**Figure 4E**). Western blot images of pJNK and JNK are shown in **Figure 4F**. To determine if activation of JNK is unaltered due to an increase in phosphatase levels, DUSP-1, -4 and -10 were evaluated at the mRNA level (119). There were no significant differences in DUSP-1, DUSP-4, or DUSP-10 suggesting that DUSPs are not playing a role in the unaltered activation of JNK (**Figure 4G-I**).

Figure 4.

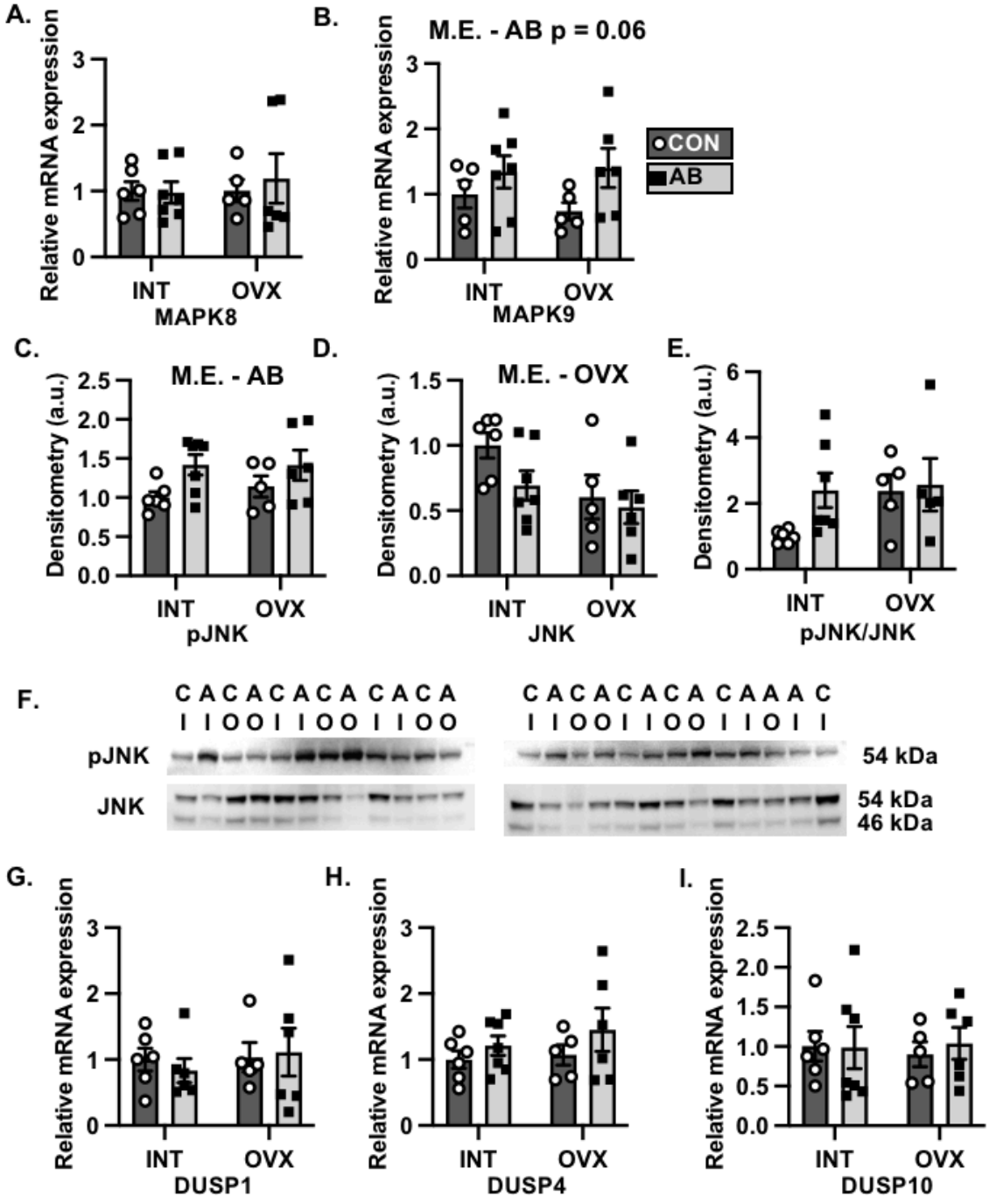
A.
Relative mRNA expression
INT
OVX
MAPK8
B.
M.E. - AB p = 0.06
CON
AB
MAPK9
C.
M.E. - AB
Densitometry (a.u.)
pJNK
D.
M.E. - OVX
JNK
E.
pJNK/JNK
F.
C A C A C A C A C A C A
I I O O I I O O I I O O
C A C A C A C A C A A A C
I I O O I I O O I I O I I
pJNK
JNK
54 kDa
54 kDa
46 kDa
G.
DUSP1
H.
DUSP4
I.
DUSP10

Figure 4. *Activation of JNK is not altered in the left ventricle due to the loss of sex hormones or chronic pressure overload.* **(A)** MAPK8/JNK1 mRNA levels were not significantly different between groups. **(B)** MAPK9/JNK2 mRNA levels trended to be increased due to AB (main effect). **(C)** pJNK was increased due to AB (main effect) while **(D)** total JNK protein was decreased due to OVX (main effect). **(E)** Activation of JNK as determined by the ratio of pJNK to JNK was not significantly different between groups. **(F)** Western blot images of pJNK and JNK. mRNA levels of DUSP1 **(G)**, DUSP4 **(H)**, and DUSP10 **(I)** were not altered between groups. $p < 0.05$; INT, intact; OVX, ovariectomy; AB, aortic-banded; CON, control; CI, control intact; AI, aortic-banded intact; CO, control ovariectomy; AO, aortic-banded ovariectomy; DUSP, dual specificity phosphatases; a.u., arbitrary units.

ERK1/2 is also downstream of sex hormone receptors. At the transcript level, ERK2 (MAPK1) and ERK1 (MAPK3) were trending to be increased due to aortic banding (**Figure 5A-B**). The phosphorylation of ERK1/2 (pERK1/2), total ERK1/2 protein levels and the activation of ERK1/2 (ratio of phosphorylated protein to total protein) were not significantly different between groups (**Figure 5C-E**). ERK1 and ERK2 activation were also evaluated separately and no significant differences were seen (**ERK1**: CON-INT = 1.0 ± 0.14; AB-INT = 1.30 ± 0.23; CON-OVX = 1.05 ± 0.29; AB-OVX = 1.29 ± 0.31; $p = 0.91$; **ERK2**: CON-INT = 1.0 ± 0.20; AB-INT = 1.36 ± 0.30; CON-OVX = 0.95 ± 0.32; AB-OVX = 1.70 ± 0.71; $p = 0.66$). Western blot images can be seen in **Figure 5F**. Phosphatases that dephosphorylate ERK1/2 are DUSP-1, -6, and -9 (119). DUSP-1 was shown in **Figure 4G** to be unaltered between groups. DUSP-6 and DUSP-9 were also not significantly between groups (**Figure 5G-H**). Overall, these results indicate no differences in these MAPK pathways in the LV due to the loss of sex hormones or chronic pressure overload.

Figure 5.

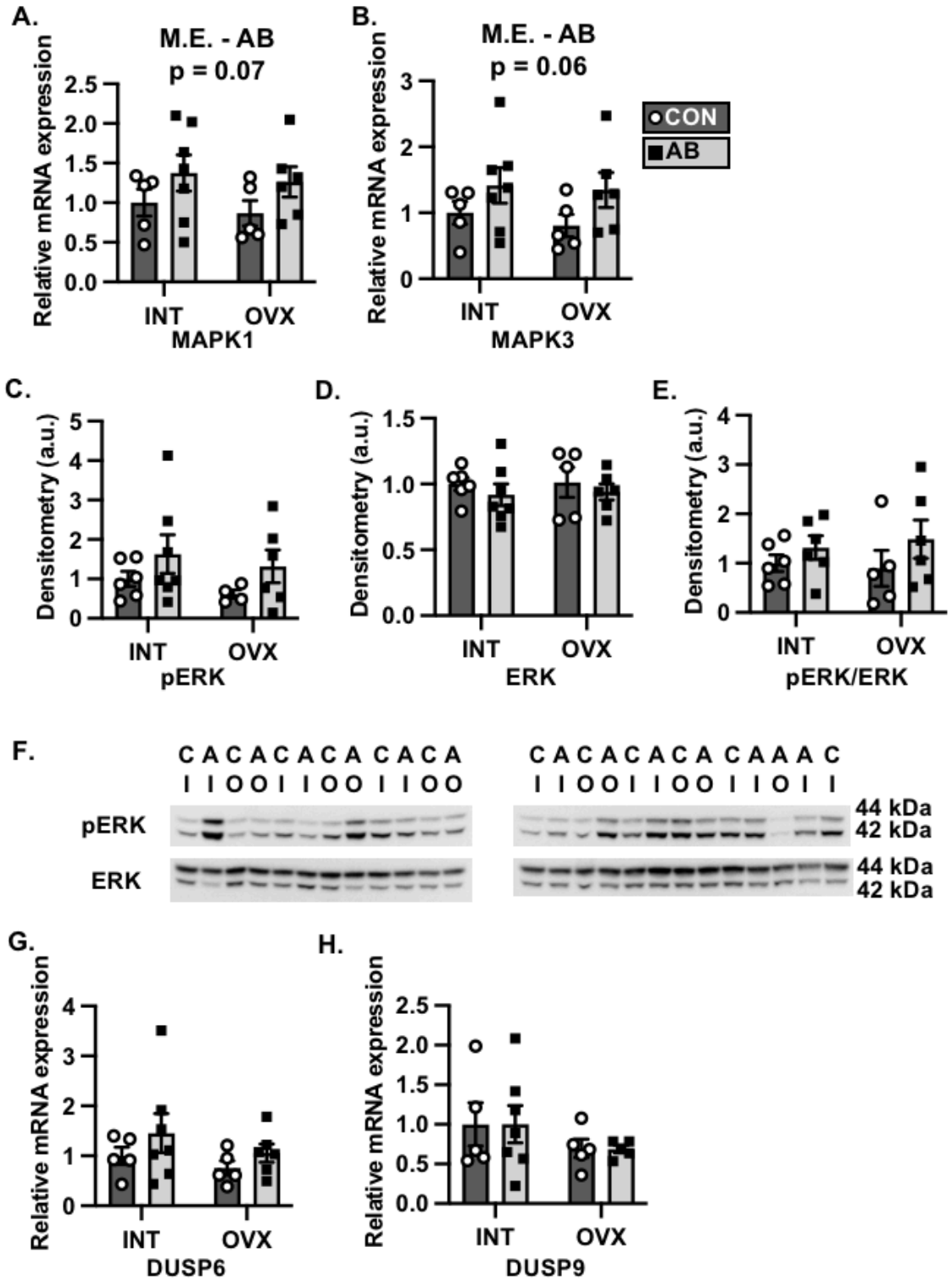
A.
M.E. - AB
p = 0.07
Relative mRNA expression
INT
OVX
MAPK1
B.
M.E. - AB
p = 0.06
Relative mRNA expression
CON
AB
INT
OVX
MAPK3
C.
Densitometry (a.u.)
INT
OVX
pERK
D.
Densitometry (a.u.)
INT
OVX
ERK
E.
Densitometry (a.u.)
INT
OVX
pERK/ERK
F.
C A C A C A C A C A C A
I I O O I I O O I I O O
C A C A C A C A C A A A C
I I O O I I O O I I O I I
pERK
ERK
44 kDa
42 kDa
44 kDa
42 kDa
G.
Relative mRNA expression
INT
OVX
DUSP6
H.
Relative mRNA expression
INT
OVX
DUSP9

Figure 5. *Activation of ERK1/2 is not altered in the left ventricle due to the loss of sex hormones or chronic pressure overload.* **(A)** MAPK1/ERK2 mRNA levels and **(B)** MAPK3/ERK1 mRNA levels trended to be increased due to AB (main effect). **(C)** pERK, **(D)** total ERK protein and **(E)** activation of ERK as determined by the ratio of pERK to ERK was not significantly different between groups. **(F)** Western blot images of pERK and ERK. **(G)** mRNA levels of DUSP6 and DUSP9 **(H)** were not altered between groups. INT, intact; OVX, ovariectomy; AB, aortic-banded; CON, control; CI, control intact; AI, aortic-banded intact; CO, control ovariectomy; AO, aortic-banded ovariectomy; DUSP, dual specificity phosphatases; a.u., arbitrary units.

Sex hormone receptors and the MAPK pathways lie upstream of transcription factors in the promoter regions of ECM protein and regulators, including the transcription factor SP1 found in the promoter region of collagen I (65, 70, 93, 139, 140, 219). SP1 transcription factor activity in the collagen I promoter region were evaluated through electromobility shift assay (EMSA). No significant differences in transcription factor binding were observed suggesting that SP1 is not playing a role in the increase in collagen I mRNA levels seen in the LV (**Figure 6A**). EMSA images are seen in **Figure 6B-C**. MAPK pathways also lie within the noncanonical pathway that activates fibroblast differentiation into myofibroblasts which can secrete ECM proteins (55). To further investigate the synthesis pathway of cardiac fibrosis, immunofluorescent staining was performed to evaluate the number of percent positive α-smooth muscle actin (α-SMA) cells, a marker of myofibroblasts. Representative images for four groups as well as the negative controls are seen in **Figures 7A-B**. Quantification of the percent positive α-SMA cells showed a trend for there to be a decrease in myofibroblasts due to OVX (**Figure 7C**). While this decrease in myofibroblasts due to OVX may not be consistent with the increase in total collagen levels due to OVX from a synthesis

perspective, this could suggest a possible compensatory mechanism to counter-balance the increase in collagen protein levels seen in this study.

Figure 6.

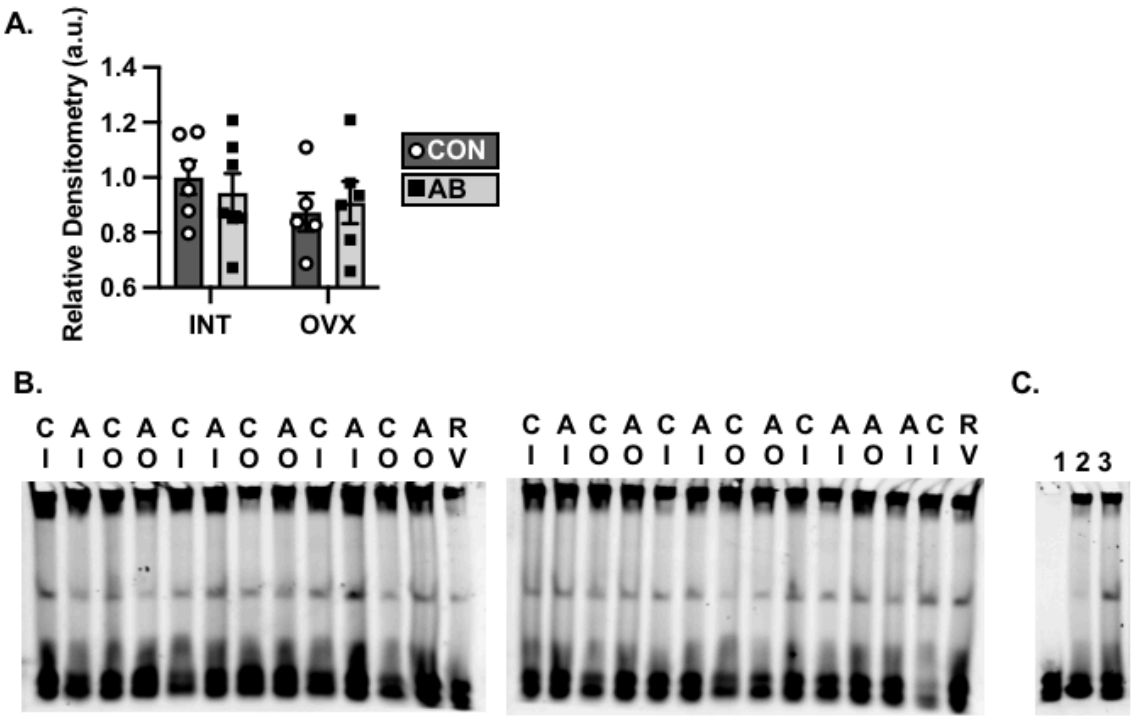

Figure 6. *SP1 transcription factor activity is not altered in the left ventricle.* **(A)** Quantification of SP1 EMSA showed no significant differences between groups. **(B)** EMSA images of the left ventricle. **(C)** EMSA control images that show (1) tagged-SP1 probe only, (2) competitive inhibition with excess unlabeled SP1 probe, and (3) tagged-SP1 probe with protein. INT, intact; OVX, ovariectomy; AB, aortic-banded; CON, control; CI, control intact; AI, aortic-banded intact; CO, control ovariectomy; AO, aortic-banded ovariectomy; a.u., arbitrary units.

Figure 7.

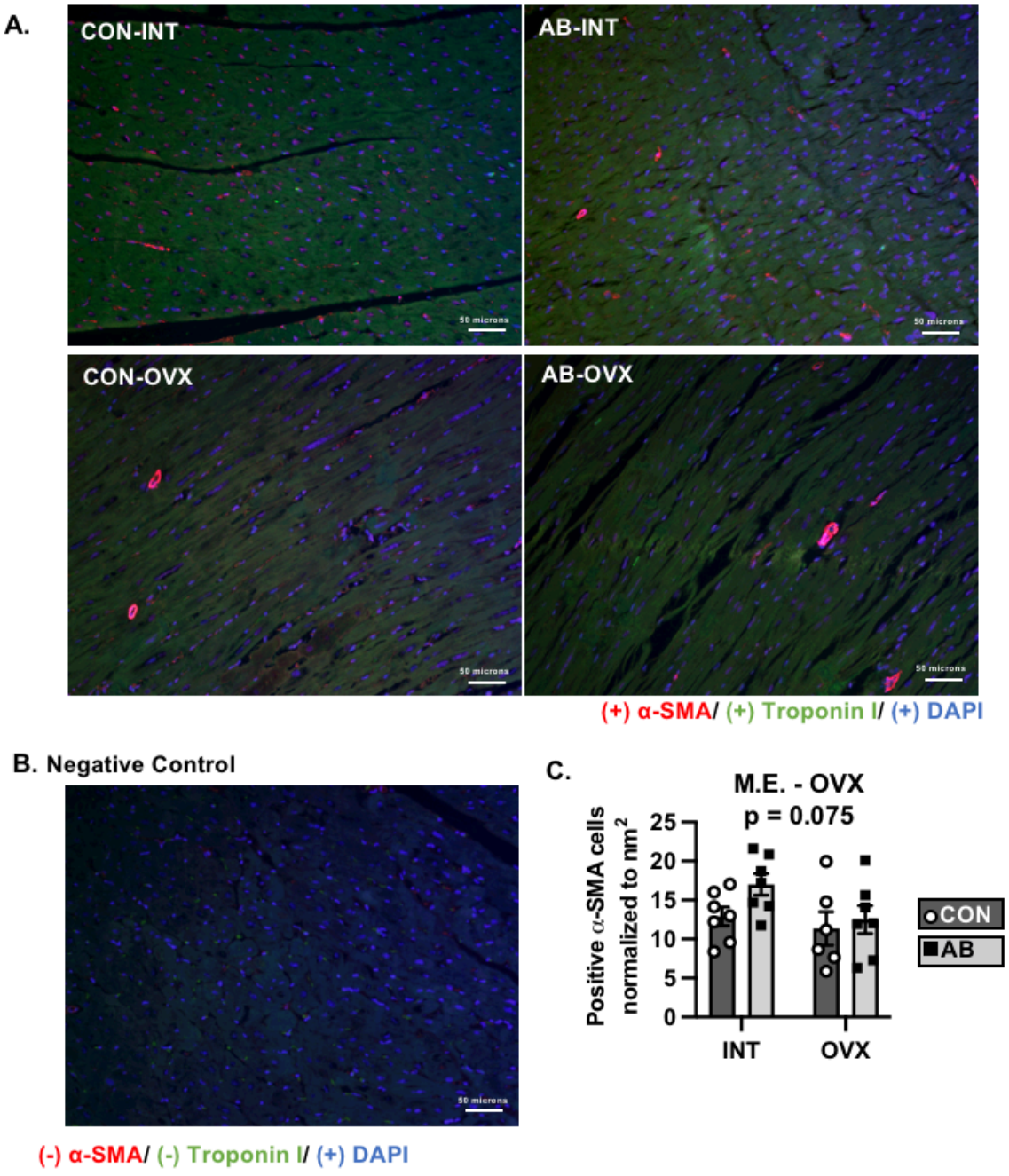

Figure 7. *α-SMA positive cells trend to be decreased due to OVX in the left ventricle.* **(A)** Representative images with stains for α-SMA (red), troponin I (green), and DAPI (blue) (scale bar = 50 microns). **(B)** Negative control image without α-SMA (red) or troponin I (green). **(C)** Quantification of α-SMA cells demonstrated a trend to be decreased due to OVX (main effect). INT, intact; OVX, ovariectomy; AB, aortic-banded; CON, control; α-SMA, α-smooth muscle actin.

Left Ventricle Fibrosis – Degradation

Excess accumulation of ECM proteins that leads to cardiac fibrosis can also occur through changes in degradation. ECM proteins are degraded through MMPs. ECM degradation is also regulated through TIMPs, which inhibit MMPs (63, 190). In the heart, MMP-1, -2, -3, -9, -13 and -14 are found to degrade collagen I and/or collagen III (64-66). At the transcript level, there was an increase in MMP-1 levels due to AB (**Figure 8A**) while there were no differences seen with MMP-2 (**Figure 8B**). MMP -3 was also increased due to AB (**Figure 8C**). MMP-9 was not significantly altered due to AB or OVX (**Figure 8D**). Additionally, there was a trend for MMP-13 to be increased due to AB (**Figure 8E**), while levels of MMP-14 were not significantly different between groups (**Figure 8F**). TIMPs were also evaluated as an increase in fibrosis in postmenopausal women is hypothesized to be due to an increase in the inhibition of collagen degradation (42). At the mRNA level, there was a trend for an interaction effect with TIMP-1 (**Figure 8G**), while there were no significant differences in TIMP-2, TIMP-3, or TIMP-4 levels (**Figure 8H-J**). From an mRNA perspective, these results suggest an increase in degradation due to MMP-1, -3, and -13 due to AB which is not directionally consistent with the increase in total collagen seen due to OVX.

Figure 8.

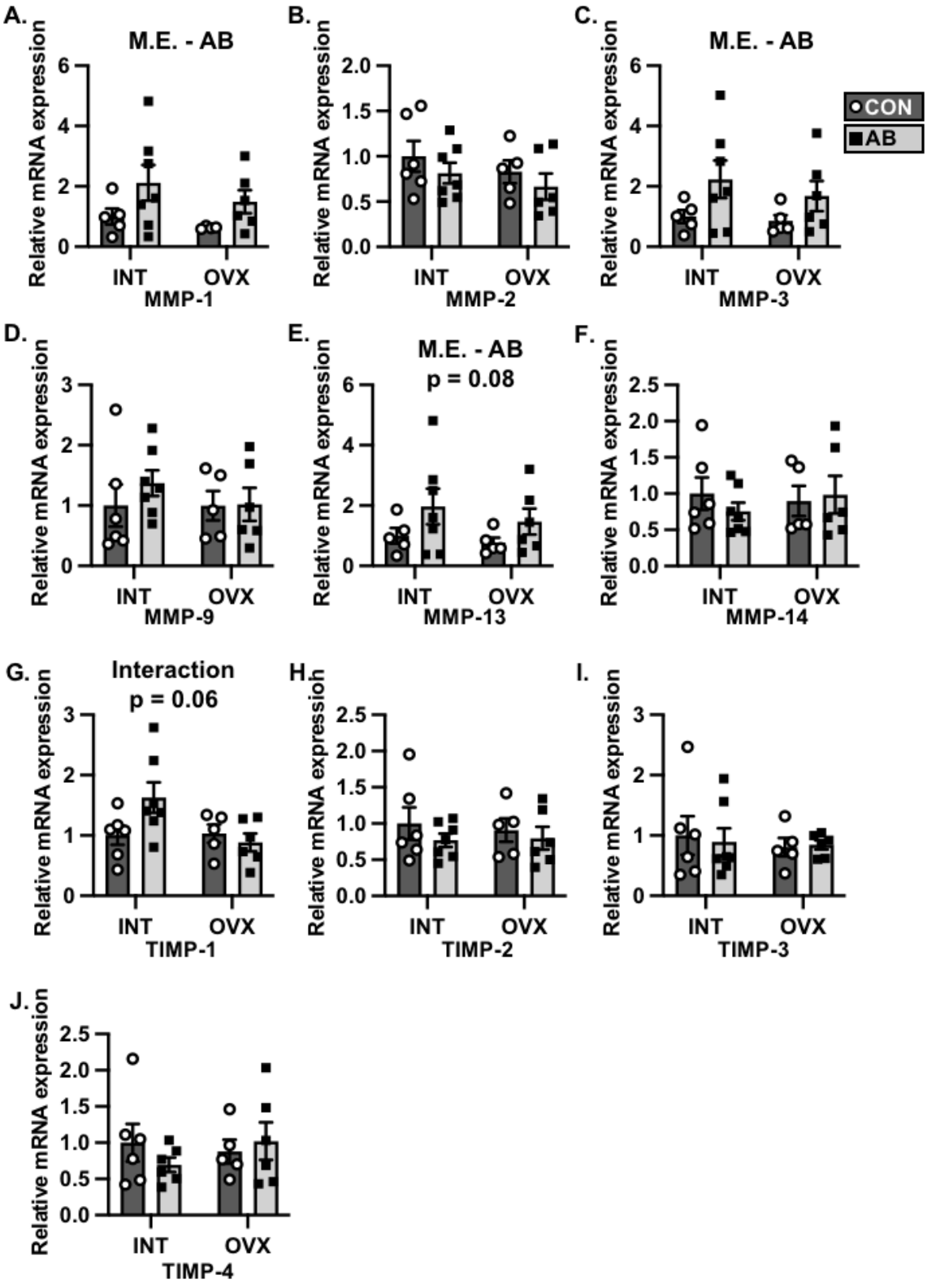
A.
M.E. - AB
Relative mRNA expression
INT
OVX
MMP-1
B.
MMP-2
C.
MMP-3
CON
AB
D.
MMP-9
E.
M.E. - AB
p = 0.08
MMP-13
F.
MMP-14
G.
Interaction
p = 0.06
TIMP-1
H.
TIMP-2
I.
TIMP-3
J.
TIMP-4

Figure 8. *MMP-1, -3, and -13 mRNA levels are increased due to chronic pressure overload in the left ventricle.* **(A)** MMP-1 mRNA levels were significantly increased due to AB (main effect). **(B)** MMP-2 mRNA levels were not significantly different between groups. **(C)** MMP-3 mRNA levels were significantly increased due to AB (main effect). **(D)** MMP-9 mRNA levels were not significantly different between groups. **(E)** MMP-13 mRNA levels trended to be increased due to AB (main effect). **(F)** MMP-14 mRNA levels were not significantly different between groups. **(G)** There was a trend towards an interaction effect with TIMP-1 mRNA levels. mRNA levels of TIMP-2 **(H)**, TIMP-3 **(I)**, TIMP-4 **(J)** were not altered due to OVX or AB. $p < 0.05$; INT, intact; OVX, ovariectomy; AB, aortic-banded; CON, control.

Protein and/or activity levels of MMPs and TIMPs were also evaluated. MMP-1 protein levels were decreased due to OVX which would suggest a decrease in collagen degradation due to the loss of sex hormones (**Figure 9A**). While MMP-3, MMP-13 mRNA levels were increased due to AB, there were no significant differences between groups at the protein level (**Figure 9B-C**). MMP-14 protein levels were not significantly altered between groups, but MMP-14 activity levels were decreased due to AB (**Figure 9D-E**). MMP-2 and MMP-9 activity and/or abundance was determined through zymography. The activity and/or abundance for MMP-2 and MMP-9 due to AB was dependent upon the presence of sex hormones (interaction). Specifically, MMP-2 activity/abundance was increased in AB-INT animals compared with AB-OVX animals (**Figure 9F**) while MMP-9 activity/abundance was decreased in the CON-INT group compared with the AB-INT and CON-OVX groups (**Figure 9G**). Western blot and zymography images are seen in **Figure 9H-I**. Overall, MMP protein and activity levels are altered due to both AB and OVX in the LV.

Figure 9.

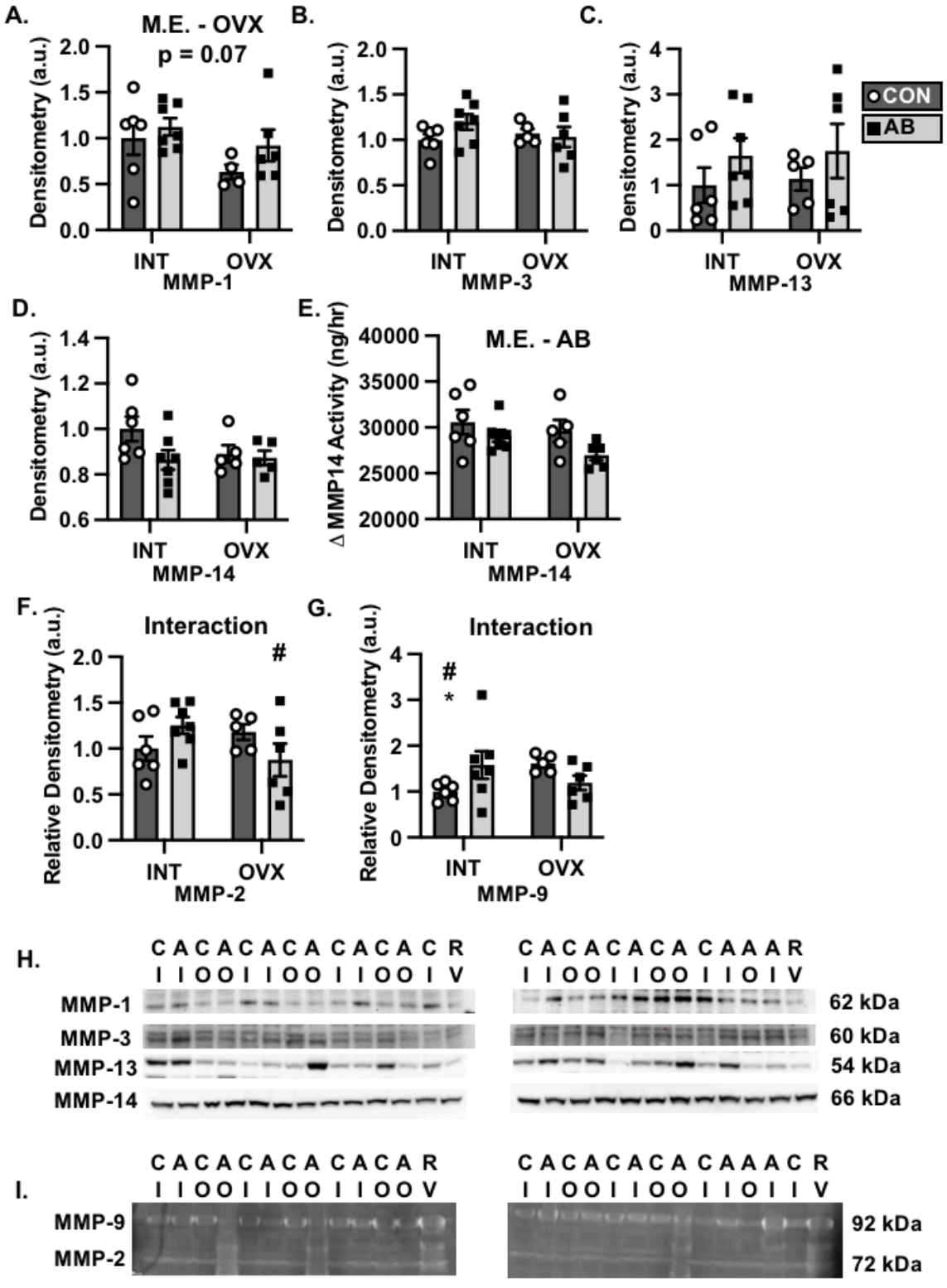
A.
M.E. - OVX
p = 0.07
Densitometry (a.u.)
INT
OVX
MMP-1
B.
MMP-3
C.
MMP-13
CON
AB
D.
MMP-14
E.
M.E. - AB
Δ MMP14 Activity (ng/hr)
F.
Interaction
Relative Densitometry (a.u.)
MMP-2
G.
MMP-9
H.
C A C A C A C A C A C A C R
I I O O I I O O I I O O I V
C A C A C A C A C A A A R
I I O O I I O O I I O I V
MMP-1
MMP-3
MMP-13
MMP-14
62 kDa
60 kDa
54 kDa
66 kDa
I.
C A C A C A C A C A C A R
I I O O I I O O I I O O V
C A C A C A C A C A A A C R
I I O O I I O O I I O I I V
MMP-9
MMP-2
92 kDa
72 kDa

Figure 9. *MMP-1, -2, -9 and -14 protein or activity levels were altered by both AB and/or OVX in the left ventricle.* **(A)** MMP-1 protein levels trended to be decreased due to OVX (main effect). MMP-3 **(B)**, MMP-13 **(C)**, and MMP-14 **(D)** protein levels were not significantly different between groups. **(E)** MMP-14 activity was significantly decreased due to AB (main effect). **(F)** There was a significant interaction effect with MMP-2 activity/abundance consisting of an increase in activity/abundance in AB-INT animals compared with AB-OVX animals. **(G)** There was a significant interaction effect for MMP-9 activity/abundance with decreased MMP-9 activity/abundance in CON-INT animals compared AB-INT and CON-OVX animals. **(H)** Western blot images of MMP-1, -3, -13, and -14. **(I)** Zymography images of MMP-2 and -9. # Post hoc vs AB-INT, * Post hoc vs CON-OVX, $p < 0.05$; INT, intact; OVX, ovariectomy; AB, aortic-banded; CON, control; CI, control intact; AI, aortic-banded intact; CO, control ovariectomy; AO, aortic-banded ovariectomy; a.u., arbitrary units.

TIMP-1 protein levels were not significantly altered between groups (**Figure 10A**). TIMP-2 protein levels were trending to be decreased due to OVX suggesting that there is a decrease in inhibition of collagen degradation due to the loss of sex hormones (**Figure 10B**). TIMP-3 protein levels were significantly increased due to AB (**Figure 10C**), while there was a trend for an interaction effect with TIMP-4 protein levels (**Figure 10D**). Western blot images can be seen in **Figure 10E**. Similar to MMP protein/activity results, TIMP protein levels are altered due to both AB and OVX in the LV.

Figure 10.

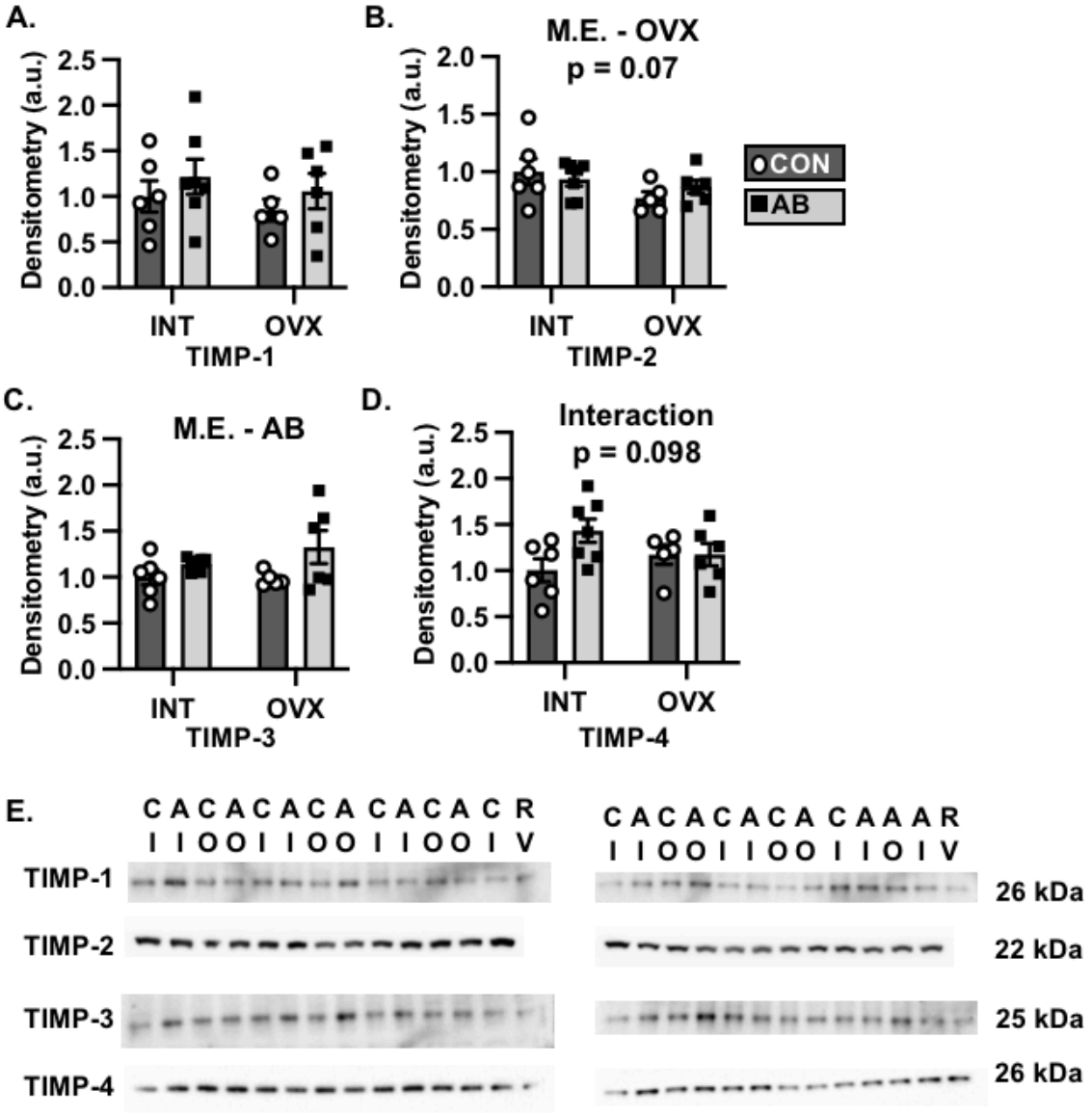

Figure 10. *TIMP-2, -3, and -4 protein levels were altered by AB and/or OVX in the left ventricle.* **(A)** TIMP-1 protein levels were not altered between groups. **(B)** TIMP-2 protein levels trended to be decreased due to OVX (main effect). **(C)** TIMP-3 protein levels were increased due to AB (main effect). **(D)** There was a trend for an interaction effect with TIMP-4 protein levels. **(E)** Western blot images of TIMP-1, -2, -3 and -4. $p < 0.05$; INT, intact; OVX, ovariectomy; AB, aortic-banded; CON, control; CI, control intact; AI, aortic-banded intact; CO, control ovariectomy; AO, aortic-banded ovariectomy; a.u., arbitrary units.

Right Ventricle Fibrosis

Often, alterations in the LV are hypothesized to be translated to the RV. Therefore, this study also sought to determine how molecular pathways are altered due to AB and/or OVX in the RV. Total collagen was biochemically evaluated and a significant main effect of AB was observed (**Figure 11A**). These results indicate an increase in cardiac fibrosis in the RV due to chronic pressure overload and independent of the loss of female sex hormones that contrasts the results seen in the LV. These data suggest that the regulation of cardiac fibrosis due to AB and OVX occurs in a chamber-specific manner. Evaluation of mRNA levels showed an increase in collagen I due to AB (**Figure 11B**) and a trend for collagen III to be increased due to AB (**Figure 11C**). Additionally, collagen III mRNA levels were decreased due to OVX. Linear regression indicated a significant positive correlation between collagen I mRNA levels and total collagen protein suggesting that increases in mRNA are associated with increases in total protein (**Figure 11D**). This linear relationship was not seen with collagen III mRNA and total collagen protein (**Figure 11E**). Fibrosis was also visually assessed through PSR and Masson's trichrome and similar to the LV, fibrosis in the RV was observed to be diffuse in the interstitial space (**Figure 11F**). In the RV, fibronectin mRNA levels were increased due to AB (**Figure 12A**), but this did not translate to alterations at the protein level as there were no significant differences between groups (**Figure 12B**; representative western blot images are shown in **Figure 12C**).

Figure 11.

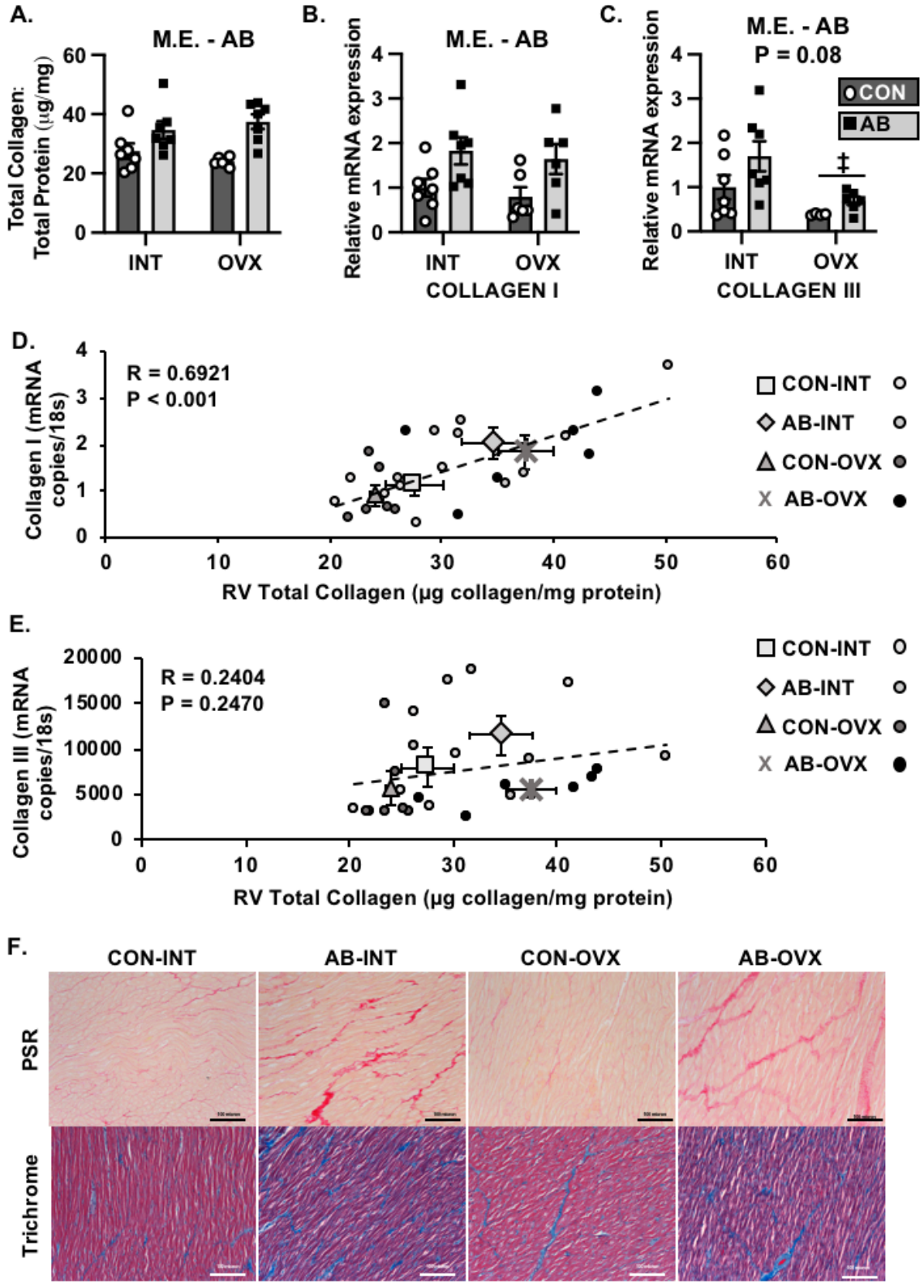
A.
M.E. - AB
Total Collagen: Total Protein (µg/mg)
INT
OVX
B.
M.E. - AB
Relative mRNA expression
INT
OVX
COLLAGEN I
C.
M.E. - AB
P = 0.08
CON
AB
‡
Relative mRNA expression
INT
OVX
COLLAGEN III
D.
R = 0.6921
P < 0.001
Collagen I (mRNA copies/18s)
RV Total Collagen (µg collagen/mg protein)
CON-INT
AB-INT
CON-OVX
AB-OVX
E.
R = 0.2404
P = 0.2470
Collagen III (mRNA copies/18s)
RV Total Collagen (µg collagen/mg protein)
CON-INT
AB-INT
CON-OVX
AB-OVX
F.
CON-INT
AB-INT
CON-OVX
AB-OVX
PSR
Trichrome

Figure 11: *Myocardial collagen levels are increased due to chronic pressure overload and independent of the loss of sex hormones in the right ventricle.* **(A)** Total collagen protein levels were increased due to AB (main effect). **(B)** Collagen I mRNA levels were increased due to AB (main effect). **(C)** Collagen III mRNA levels were decreased due to OVX (main effect) and trended to be increased due to AB (main effect). **(D)** There is a positive correlation between collagen I mRNA levels and total collagen protein in the right ventricle. **(E)** There is no linear relationship between total collagen protein levels and collagen III mRNA levels. **(F)** Representative images of picrosirius red (PSR) and Masson's trichrome stains (scale bar = 100 microns). $p < 0.05$; INT, intact; OVX, ovariectomy; AB, aortic-banded; CON, control.

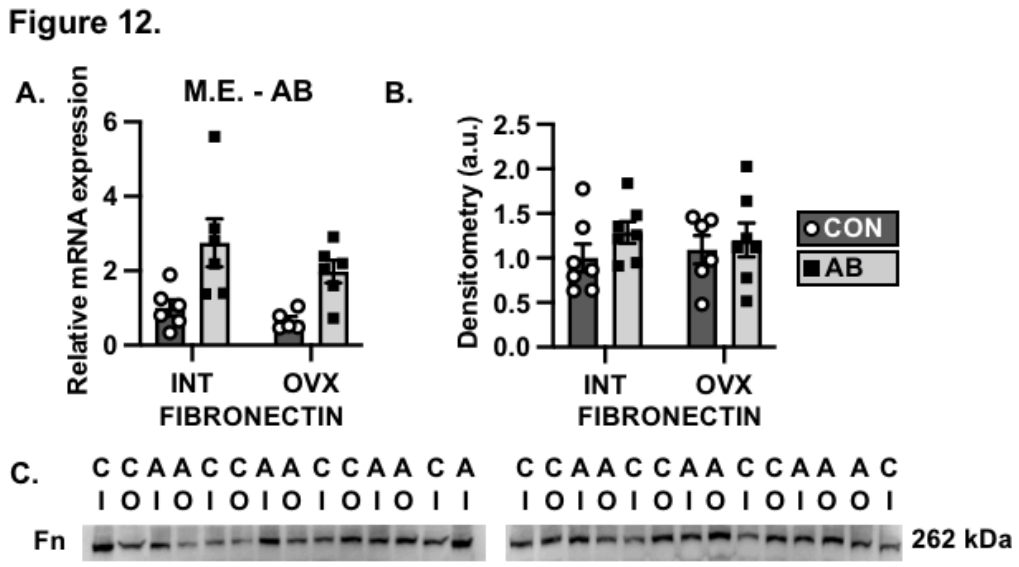

Figure 12: *Fibronectin mRNA is increased due to chronic pressure overload in the right ventricle.* **(A)** Fibronectin mRNA levels were increased due to AB (main effect) while **(B)** fibronectin protein levels were not significantly different between groups. **(C)** Western blot images of fibronectin (Fn). $p < 0.05$; INT, intact; OVX, ovariectomy; AB, aortic-banded; CON, control; CI, control intact; AI, aortic-banded intact; CO, control ovariectomy; AO, aortic-banded ovariectomy; a.u., arbitrary units.

Right Ventricle Fibrosis – Synthesis

While there was not an alteration in total collagen content due to OVX, sex hormone receptors levels, specifically estrogen receptors, have been shown to be increased due to pressure overload as well as play a role in the regulation of

fibrosis (93, 94). ESR1/ERα mRNA and protein levels were not altered due to AB or OVX (**Figure 13A-B**). ESR2 mRNA levels were increased due to AB (**Figure 13C**) while alterations in ERβ protein levels due to AB were dependent upon the presence of sex hormones (**Figure 13D**; interaction). Specifically, ERβ protein levels were increased in AB-OVX animals compared with AB-INT and CON-OVX. Differences in PGR mRNA levels due to AB were also dependent upon the presence of female sex hormones (**Figure 13E**; interaction). PGR mRNA levels were increased due to AB-OVX compared with CON-OVX and trended to be increased compared to AB-INT. However, PGR A and PGR B protein levels were not significantly different between groups (**Figure 13F-G**). Finally, PGRMC1 mRNA levels trended to be decreased due to AB (**Figure 13H**) while no significant differences were seen at the protein level (**Figure 13I**). Western blot images can be seen in **Figure 13J**.

Figure 13.

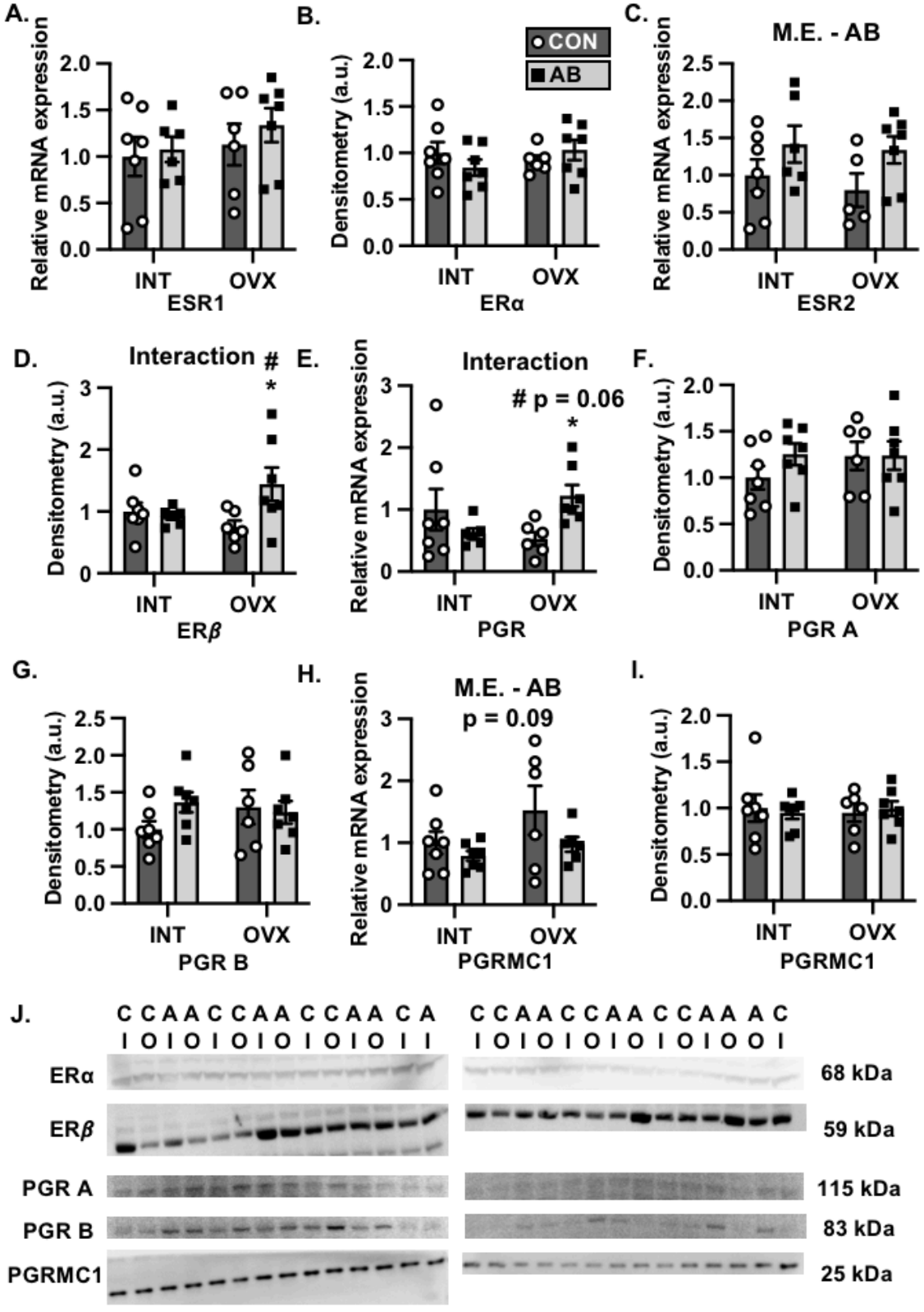
A.
Relative mRNA expression
2.0
1.5
1.0
0.5
0.0
INT
OVX
ESR1
B.
CON
AB
Densitometry (a.u.)
INT
OVX
ERα
C.
M.E. - AB
Relative mRNA expression
INT
OVX
ESR2
D.
Interaction
#
*
Densitometry (a.u.)
3
2
1
0
INT
OVX
ERβ
E.
Interaction
p = 0.06
*
Relative mRNA expression
INT
OVX
PGR
F.
Densitometry (a.u.)
INT
OVX
PGR A
G.
Densitometry (a.u.)
2.5
INT
OVX
PGR B
H.
M.E. - AB
p = 0.09
Relative mRNA expression
INT
OVX
PGRMC1
I.
Densitometry (a.u.)
INT
OVX
PGRMC1
J.
C C A A C C A A C C A A C A
I O I O I O I O I O I O I I
C C A A C C A A C C A A A C
I O I O I O I O I O I O O I
ERα
ERβ
PGR A
PGR B
PGRMC1
68 kDa
59 kDa
115 kDa
83 kDa
25 kDa

Figure 13: *Estrogen receptor β protein levels were increased in AB-OVX animals in the right ventricle.* **(A)** Estrogen receptor 1/ERα mRNA levels **(B)** and protein levels were not significantly different between groups. **(C)** Estrogen receptor 2/ERβ mRNA levels were increased due to AB (main effect) while **(D)** there was a significant interaction effect for ERβ protein levels consisting of increased ERβ protein in AB-OVX animals compared to CON-OVX animals and AB-INT animals. **(E)** There was a significant interaction effect for progesterone receptor (PGR) mRNA levels in which PGR mRNA levels were increased in AB-OVX animals compared to CON-OVX animals and trended to be increased in AB-OVX animals compared to AB-INT animals. **(F)** PGR A protein levels and **(G)** PGR B protein levels were not significantly different between groups. **(H)** Progesterone receptor membrane component 1 (PGRMC1) mRNA levels trended to be increased due to AB (main effect) while **(I)** no significant differences were seen at the protein level. **(J)** Western blot images of ERα, ERβ, PGR A, PGR B, and PGRMC1. # Post hoc vs AB-INT, * Post hoc vs CON-OVX, $p < 0.05$; INT, intact; OVX, ovariectomy; AB, aortic-banded; CON, control; CI, control intact; AI, aortic-banded intact; CO, control ovariectomy; AO, aortic-banded ovariectomy; a.u., arbitrary units.

To determine if there are differences in sex hormone receptor levels between ventricles, a three-way ANOVA was utilized. As a result, ESR1 mRNA levels were increased in the LV compared to the RV and due to AB (**Figure 14A**) while alterations in ERα protein levels due to AB were dependent upon the presence of sex hormones as well as the ventricle (**Figure 14B**, interaction). Specifically, ERα protein levels in LV CON-INT animals were trending to be increased compared to RV CON-INT animals ($p = 0.09$) and were significantly increased compared to RV AB-INT, and RV CON-OVX animals. ERα protein levels in LV AB-INT animals were significantly increased compared with RV CON-INT and RV AB-INT, as well as trending to be increased compared to RV AB-OVX animals ($p = 0.06$). LV CON-OVX ERα protein levels were significantly increased compared to RV CON-INT and RV CON-OVX levels, as well as trending to be increased compared to RV AB-OVX levels ($p = 0.07$). Lastly, LV AB-OVX ERα

protein levels were significantly increased compared to RV AB-INT and RV CON-OVX levels, as well as trending to be increased compared to RV AB-OVX levels ($p = 0.052$). ESR2 mRNA levels were increased in the LV compared to the RV as well as trending to be increased due to AB and trending to be decreased due to OVX (**Figure 14C**). ERβ protein levels were not significantly different between the two ventricles but were trending to be increased due to AB (**Figure 14D**). When PGR mRNA levels were evaluated, alterations due to AB were dependent upon the presence of sex hormones (**Figure 14E**, interaction). Specifically, PGR mRNA levels in RV AB-OVX animals were trending to be increased compared to LV CON-OVX, RV AB-INT, and RV CON-OVX animals (RV AB-OVX vs LV CON-OVX $p = 0.07$, RV AB-OVX vs RV AB-INT $p = 0.07$, RV AB-OVX vs RV CON-OVX $p = 0.098$). Additionally, PGR mRNA levels were trending to be increased in LV AB-OVX animals compared with RV CON-OVX animals ($p = 0.07$). PGRMC1 mRNA levels were decreased in the LV compared to the RV as well as trending to be increased due to OVX (**Figure 14F**). PGRMC1 protein levels were not significantly different between groups (**Figure 14G**). Overall, there were significant differences in sex hormone receptor mRNA and protein levels between ventricles.

Figure 14.

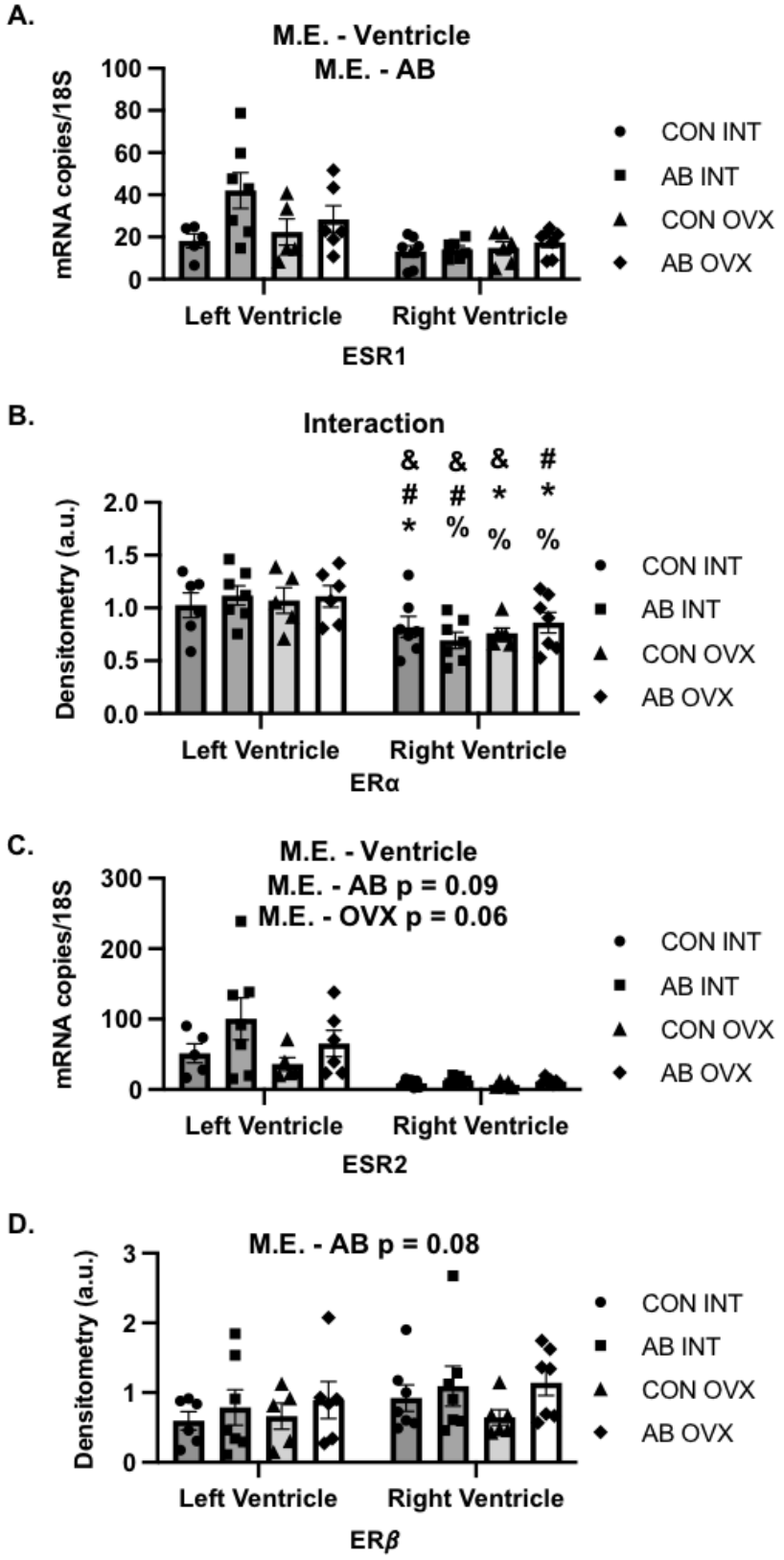
A.
M.E. - Ventricle
M.E. - AB
mRNA copies/18S
100
80
60
40
20
0
Left Ventricle
Right Ventricle
ESR1
CON INT
AB INT
CON OVX
AB OVX
B.
Interaction
& & & #
# # * *
* % % %
Densitometry (a.u.)
2.0
1.5
1.0
0.5
0.0
Left Ventricle
Right Ventricle
ERα
CON INT
AB INT
CON OVX
AB OVX
C.
M.E. - Ventricle
M.E. - AB p = 0.09
M.E. - OVX p = 0.06
mRNA copies/18S
300
200
100
0
Left Ventricle
Right Ventricle
ESR2
CON INT
AB INT
CON OVX
AB OVX
D.
M.E. - AB p = 0.08
Densitometry (a.u.)
3
2
1
0
Left Ventricle
Right Ventricle
ERβ
CON INT
AB INT
CON OVX
AB OVX

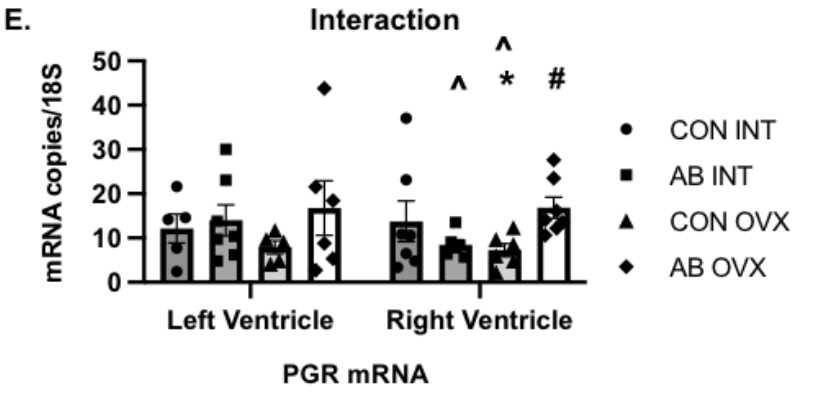
E.
Interaction
mRNA copies/18S
50
40
30
20
10
0
^
^
*
#
Left Ventricle
Right Ventricle
CON INT
AB INT
CON OVX
AB OVX
PGR mRNA

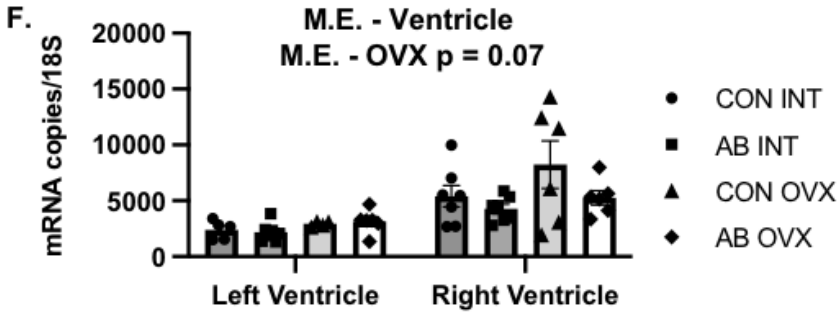
F.
M.E. - Ventricle
M.E. - OVX p = 0.07
mRNA copies/18S
20000
15000
10000
5000
0
Left Ventricle
Right Ventricle
CON INT
AB INT
CON OVX
AB OVX
PGRMC1 mRNA

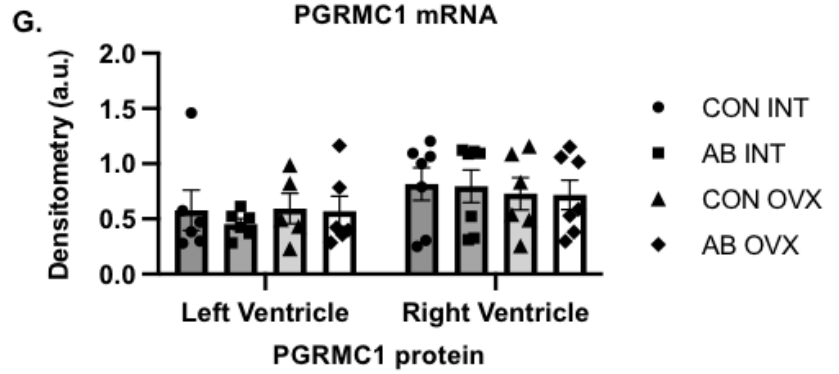
G.
Densitometry (a.u.)
2.0
1.5
1.0
0.5
0.0
Left Ventricle
Right Ventricle
CON INT
AB INT
CON OVX
AB OVX
PGRMC1 protein

Figure 14: *ESR1 mRNA, ERα protein, and ESR2 mRNA levels are increased in the left ventricle while PGRMC1 mRNA levels are increased in the right ventricle.* **(A)** Estrogen receptor 1 (ESR1) mRNA levels are increased in the left ventricle and due to AB (main effect). **(B)** There is a significant interaction affect in ERα protein levels due to the ventricle, AB, and OVX. Specifically, ERα protein levels in LV CON-INT were increased compared with RV CON-INT, RV AB-INT, and RV CON-OVX. ERα protein levels in LV AB-INT were increased compared with RV CON-INT, RV AB-INT, and RV AB-OVX. LV CON-OVX ERα protein levels were increased compared to RV CON-INT, RV CON-OVX, and RV AB-OVX. LV AB-OVX ERα protein levels were increased compared to RV AB-INT, RV CON-OVX, and RV AB-OVX. **(C)** Estrogen receptor 2 (ESR2) mRNA levels were increased in the LV compared to the RV as well as increased due to AB and decreased due to OVX (main effect). **(D)** ERβ protein levels were increased due to AB (main effect). **(E)** There was a significant interaction effect for progesterone receptor (PGR) mRNA levels due to AB and OVX in which PGR mRNA levels were increased in RV AB-OVX animals compared to LV CON-OVX, RV AB-INT, and RV CON-OVX animals and LV AB-OVX animals compared to RV CON-OVX animals. **(F)** Progesterone receptor membrane component 1 (PGRMC1) mRNA levels were increased in the RV and due to OVX (main effects) while **(G)** no significant differences were seen at the protein level. & Posthoc vs LV CON-INT, # Posthoc vs LV AB-INT, * Posthoc vs LV CON-OVX, % Posthoc vs LV AB-OVX, ^ Posthoc vs RV AB-OVX, $p < 0.1$; INT, intact; OVX, ovariectomy; AB, aortic-banded; CON, control; a.u., arbitrary units.

The MAPK pathways of JNK and ERK1/2 were evaluated as they are both activated by sex hormone receptors. At the transcript level, MAPK8/JNK1 was significantly increased due to AB (**Figure 15A**) while there was a trend for an interaction with MAPK9/JNK2 (**Figure 15B**). The phosphorylation of JNK and total JNK were not significantly different between groups (**Figure 15C-D**), but when the ratio of pJNK/JNK was utilized to evaluate the activation of JNK, there was a trend for increased activation due to AB (**Figure 15E**). Images of these western blots can be seen in **Figure 15F**. Phosphatases of JNK were evaluated to determine if alterations could be affecting activation of pJNK. DUSP1 mRNA levels were significantly increased due to AB which could suggest an increase in the dephosphorylation of JNK (**Figure 15G**). DUSP4 mRNA levels were not

significantly different between groups (**Figure 15H**) while there was a trend towards an interaction effect with DUSP10 (**Figure 15I**). Overall, we see a trend towards an increase in JNK activation with an increase in DUSP1 levels suggesting a compensatory regulatory response regarding increased activation of synthesis pathways known to increase ECM protein levels.

Figure 15.

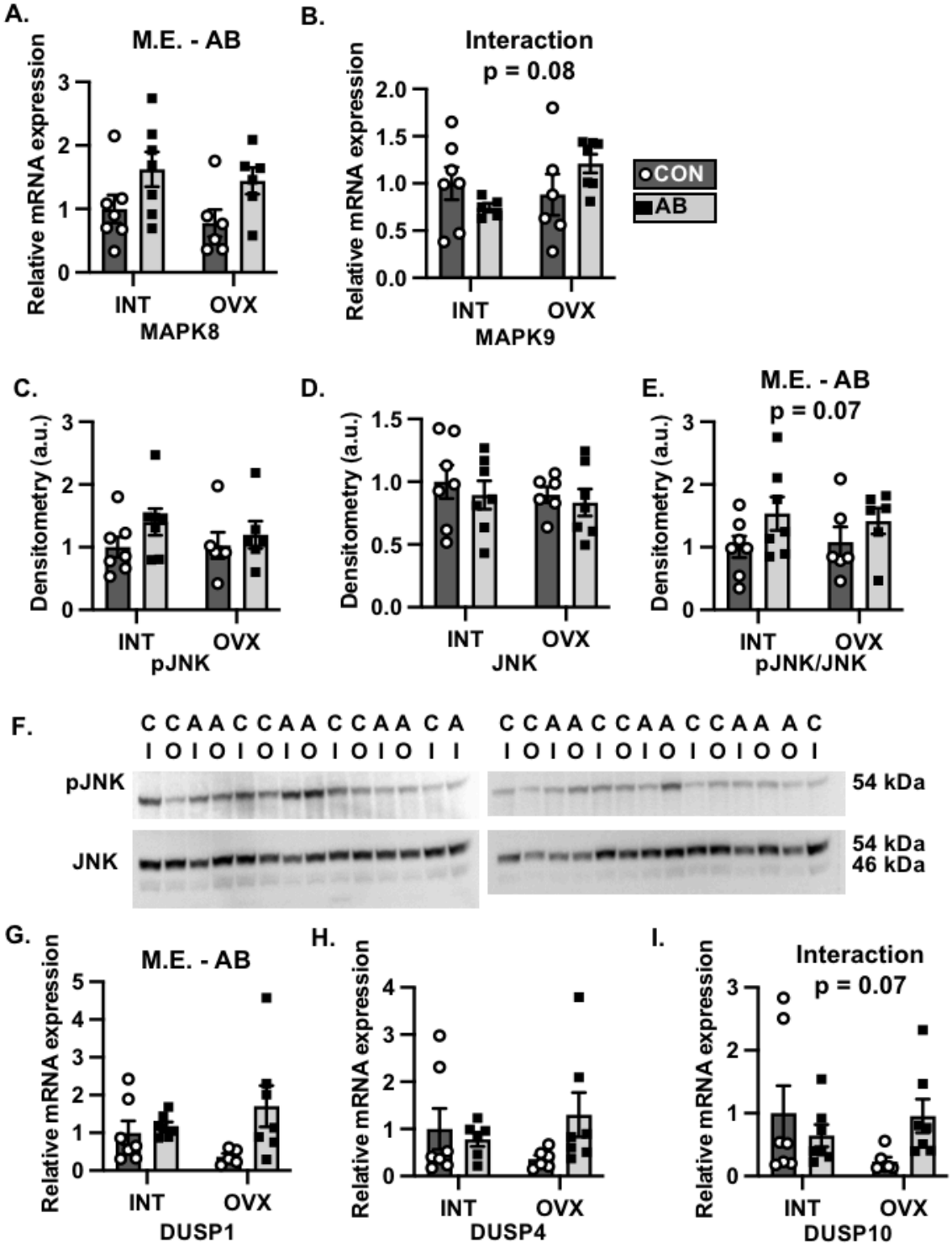
A.
M.E. - AB
Relative mRNA expression
INT
OVX
MAPK8
B.
Interaction
p = 0.08
CON
AB
MAPK9
C.
Densitometry (a.u.)
pJNK
D.
JNK
E.
M.E. - AB
p = 0.07
pJNK/JNK
F.
C C A A C C A A C C A A C A
I O I O I O I O I O I O I I
C C A A C C A A C C A A A C
I O I O I O I O I O I O O I
pJNK
JNK
54 kDa
54 kDa
46 kDa
G.
DUSP1
H.
DUSP4
I.
Interaction
p = 0.07
DUSP10

Figure 15. *Activation of JNK trended to be increased in the right ventricle due to chronic pressure overload.* **(A)** MAPK8/JNK1 mRNA levels increased due to AB (main effect). **(B)** There was a trend towards an interaction effect with MAPK9/JNK2 mRNA levels. **(C)** pJNK protein levels and **(D)** total JNK protein levels were not significantly different between groups. **(E)** Activation of JNK as determined by the ratio of pJNK to JNK trended to be increased due to AB (main effect). **(F)** Western blot images of pJNK and JNK. **(G)** mRNA levels of DUSP1 were increased due to AB (main effect). **(H)** DUSP4 mRNA levels were not significantly altered between groups. **(I)** There was a trend towards an interaction effect with DUSP10 mRNA levels. $p < 0.05$; INT, intact; OVX, ovariectomy; AB, aortic-banded; CON, control; CI, control intact; AI, aortic-banded intact; CO, control ovariectomy; AO, aortic-banded ovariectomy; DUSP, dual specificity phosphatases; a.u., arbitrary units.

Examination of ERK1/2 at the mRNA level showed a trend towards an interaction effect for both MAPK1/ERK2 and MAPK3/ERK1 in which alterations at the mRNA levels due to AB were dependent upon the presence of sex hormones (**Figure 16A-B**; interaction). Phosphorylated ERK1/2, total ERK1/2 protein, and activation of ERK1/2 were not significantly different between groups (**Figure 16C-E**). When evaluated at the protein level, no significant differences were seen in ERK1 activation (**ERK1**: CON-INT = 1.0 ± 0.19; AB-INT = 1.14 ± 0.36; CON-OVX = 0.57 ± 0.13; AB-OVX = 1.23 ± 0.33; $p = 0.36$) while there was a trend for an interaction effect with ERK2 activation (**ERK2**: CON-INT = 1.0 ± 0.28; AB-INT = 1.72 ± 0.93; CON-OVX = 0.38 ± 0.09; AB-OVX = 1.31 ± 0.42; $p = 0.086$). These results could suggest specific isoform differences with ERK1/2 activation in the RV. Western blot images of pERK, ERK, and ERK activation are shown in **Figure 16F**. Evaluation of DUSP6 and DUSP9 mRNA showed no significant differences between groups suggesting that unaltered activation in ERK1/2 is not due to alterations in phosphatases (**Figure 16G-H**).

Figure 16.

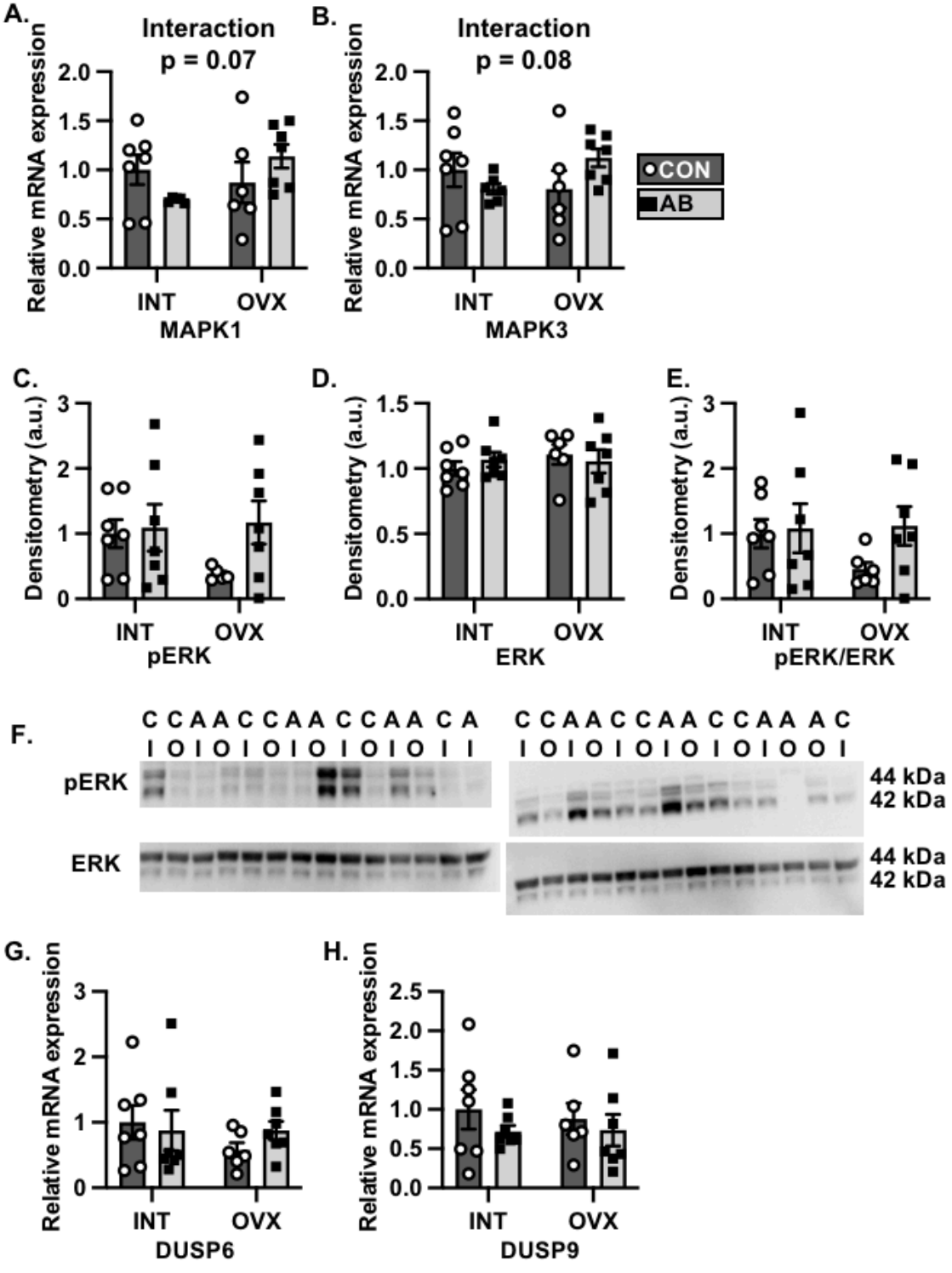
A.
Interaction
p = 0.07
Relative mRNA expression
2.0
1.5
1.0
0.5
0.0
INT
OVX
MAPK1
B.
Interaction
p = 0.08
Relative mRNA expression
2.0
1.5
1.0
0.5
0.0
INT
OVX
MAPK3
CON
AB
C.
Densitometry (a.u.)
3
2
1
0
INT
OVX
pERK
D.
Densitometry (a.u.)
1.5
1.0
0.5
0.0
INT
OVX
ERK
E.
Densitometry (a.u.)
3
2
1
0
INT
OVX
pERK/ERK
F.
C C A A C C A A C C A A C A
I O I O I O I O I O I O I I
C C A A C C A A C C A A A C
I O I O I O I O I O I O O I
pERK
ERK
44 kDa
42 kDa
44 kDa
42 kDa
G.
Relative mRNA expression
3
2
1
0
INT
OVX
DUSP6
H.
Relative mRNA expression
2.5
2.0
1.5
1.0
0.5
0.0
INT
OVX
DUSP9

Figure 16. *Activation of ERK1/2 is not altered in the right ventricle due to the loss of sex hormones or chronic pressure overload.* **(A)** There is a trend in an interaction effect with MAPK1/ERK2 and **(B)** MAPK3/ERK1 mRNA levels. **(C)** pERK, **(D)** total ERK protein and **(E)** activation of ERK as determined by the ratio of pERK to ERK were not significantly different between groups. **(F)** Western blot images of pERK and ERK. **(G)** mRNA levels of DUSP6 and DUSP9 **(H)** were not altered between groups. INT, intact; OVX, ovariectomy; AB, aortic-banded; CON, control; CI, control intact; AI, aortic-banded intact; CO, control ovariectomy; AO, aortic-banded ovariectomy; DUSP, dual specificity phosphatases; a.u., arbitrary units.

JNK activation can lead to activation of multiple transcription factors in the collagen promoter regions, such as SP1. Therefore, SP1 transcription factor activity was evaluated through EMSA. There were no significant differences between groups in the binding of SP1 suggesting that the increases seen in collagen I mRNA are not due to alterations in SP1 transcription factor binding (**Figure 17A-B**). As mentioned previously, JNK is involved in the noncanonical pathway for myofibroblast differentiation (55). Representative images of α-SMA staining, a marker of myofibroblasts, are shown in **Figures 18A** (negative control image is presented in **Figure 18B**). Quantification of these images show a trend towards an increase in the percent of α-SMA cells due to AB (**Figure 18C**). Overall, these results suggest that there is an increase in collagen synthesis due to AB in the RV.

Figure 17.

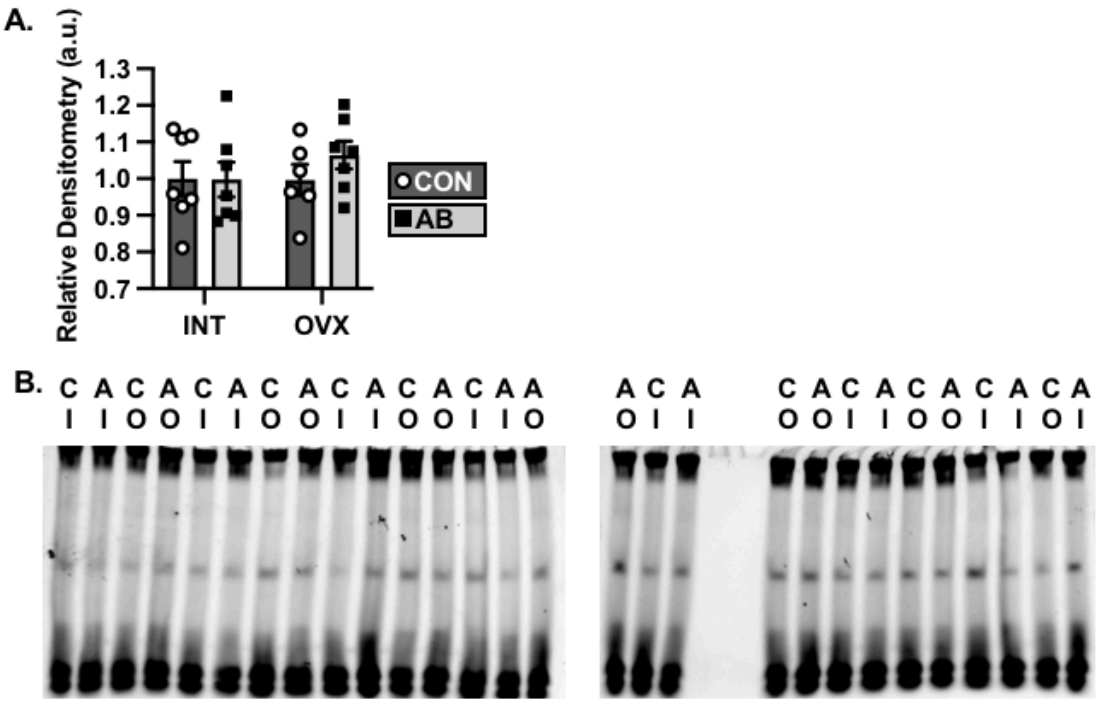

Figure 17. *SP1 transcription factor activity is not altered in the right ventricle.* **(A)** Quantification of SP1 EMSA showed no significant differences between groups. **(B)** EMSA images of the right ventricle. INT, intact; OVX, ovariectomy; AB, aortic-banded; CON, control; CI, control intact; AI, aortic-banded intact; CO, control ovariectomy; AO, aortic-banded ovariectomy; a.u., arbitrary units.

Figure 18.

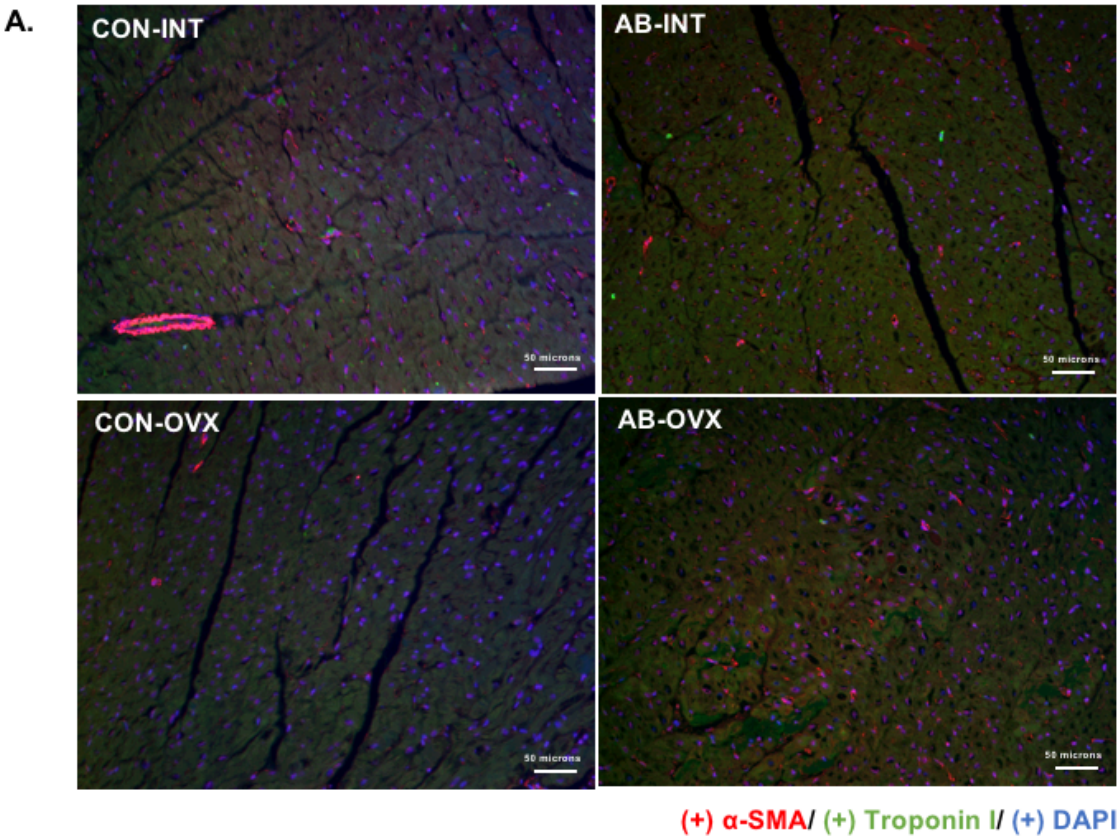
A.
CON-INT
AB-INT
CON-OVX
AB-OVX
50 microns
(+) α-SMA/ (+) Troponin I/ (+) DAPI
B. Negative Control
(-) α-SMA/ (-) Troponin I/ (+) DAPI
C.
M.E. - AB
p = 0.08
Positive α-SMA cells normalized to nm²
30
20
10
0
INT
OVX
CON
AB

Figure 18. *α-SMA positive cells trend to be increased due to chronic pressure overload in the right ventricle.* **(A)** Representative images with stains for α-SMA (red), troponin I (green), and DAPI (blue) (scale bar = 50 microns). **(B)** Negative control image without α-SMA (red) or troponin I (green). **(C)** Quantification of α-SMA cells demonstrated a trend to be increased due to AB (main effect). INT, intact; OVX, ovariectomy; AB, aortic-banded; CON, control; α-SMA, α-smooth muscle actin.

Right Ventricle Fibrosis – Degradation

The potential role of degradation in the increased collagen deposition observed in the RV was also examined. At the mRNA level, MMP-1 was not significantly different between groups (**Figure 19A**). MMP-2 levels were significantly increased due to AB and decreased due to OVX (**Figure 19B**). There were no significant differences in MMP-3 levels (**Figure 19C**) while MMP-9 levels were increased due to AB and trended to be decreased due to OVX (**Figure 19D**). MMP-13 was not altered between groups (**Figure 19E**). Lastly, MMP-14 was significantly increased due to AB (**Figure 19F**). This is different from the mRNA results seen in the LV as there was an increase in MMP-1, MMP-3, and MMP-13 due to AB in the LV but no significant differences in the RV. While MMP-2, -9, and -14 were not significantly different in the LV but demonstrated a main effect of AB in the RV. TIMP mRNA levels demonstrate TIMP-1 was significantly decreased due to OVX (**Figure 19G**) while TIMP-2 and TIMP-4 were significantly increased due to AB (**Figure 19H and J**) with no significant differences seen for TIMP-3 (**Figure 19I**). Overall, these results suggest that there are increases in ECM degradation as well as increases in the inhibition of ECM degradation in the RV.

Figure 19.

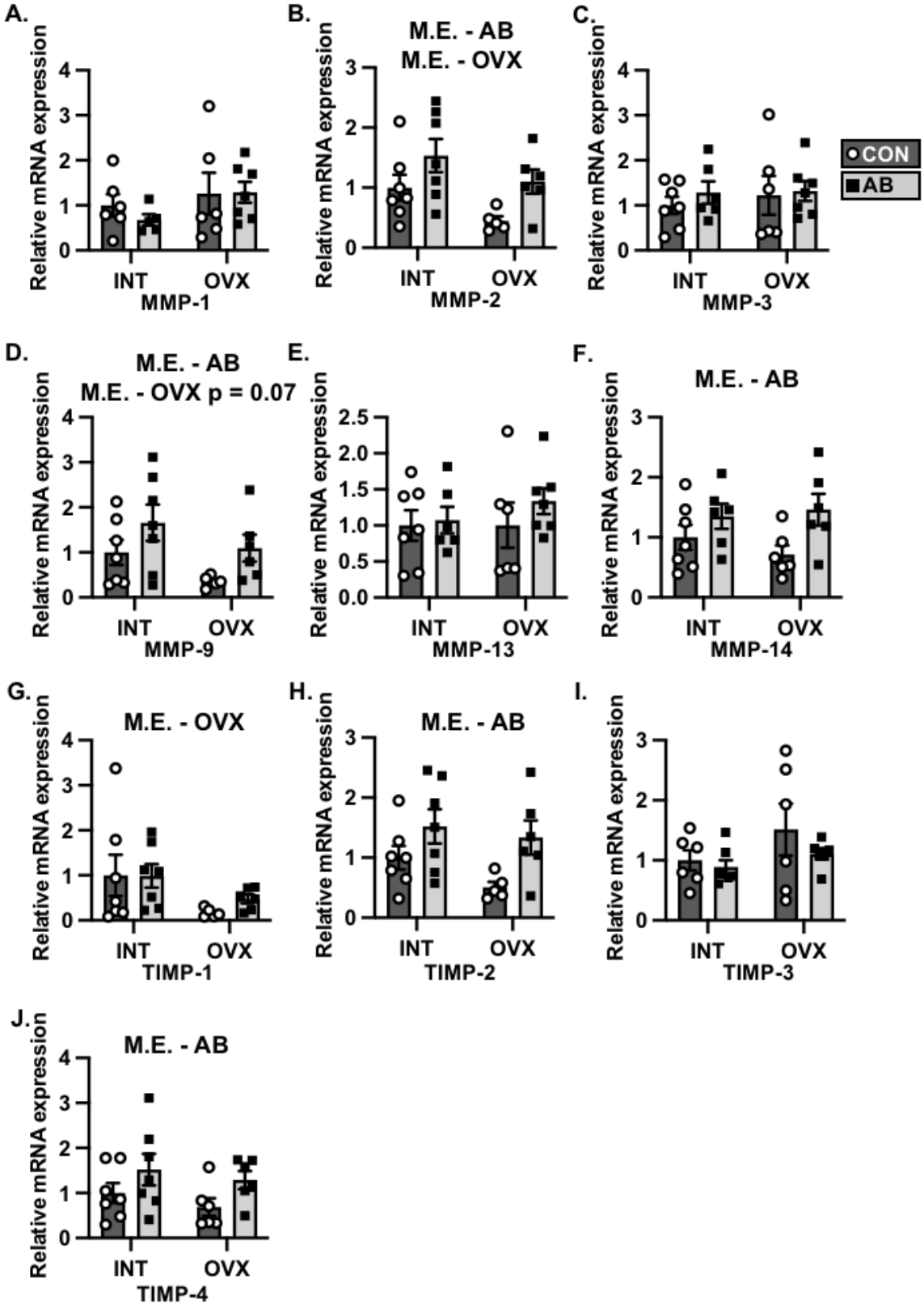
A.
Relative mRNA expression
INT
OVX
MMP-1
B.
M.E. - AB
M.E. - OVX
MMP-2
C.
CON
AB
MMP-3
D.
M.E. - AB
M.E. - OVX p = 0.07
MMP-9
E.
MMP-13
F.
M.E. - AB
MMP-14
G.
M.E. - OVX
TIMP-1
H.
M.E. - AB
TIMP-2
I.
TIMP-3
J.
M.E. - AB
TIMP-4

Figure 19. *MMP-2, -9, and -14 and TIMP-2 and -4 mRNA levels are increased due to chronic pressure overload in the right ventricle.* **(A)** MMP-1 mRNA levels were not significantly different between groups. **(B)** MMP-2 mRNA levels were significantly increased due to AB (main effect) and decreased due to OVX (main effect). **(C)** MMP-3 mRNA levels were not significantly different between groups. **(D)** MMP-9 mRNA levels were significantly increased due to AB (main effect) and trended to be decreased due to OVX (main effect). **(E)** MMP-13 mRNA levels were not significantly different between groups. **(F)** MMP-14 mRNA levels were significantly increased due to AB (main effect). **(G)** TIMP-1 mRNA levels were significantly decreased due to OVX (main effect). **(H)** TIMP-2 mRNA levels of were increased due to AB (main effect). **(I)** TIMP-3 mRNA levels were not significantly decreased between groups. **(J)** TIMP-4 mRNA levels of were increased due to AB (main effect). $p < 0.05$; INT, intact; OVX, ovariectomy; AB, aortic-banded; CON, control; a.u., arbitrary units.

Evaluation at the protein and/or activity level indicated MMP-1 protein levels and MMP-2 activity/abundance were significantly decreased due to OVX (**Figure 20A and F**). Alternately, MMP-3, -13, and -14 protein levels, MMP-14 activity, and MMP-9 activity/abundance were not significantly different between groups (**Figure 20B-E, G**). Images from these western blots and zymography assays can be seen in Figure **20H-I**. Overall, these results suggest that an alteration in degradation is seen in the RV due to the loss of sex hormones which is not directionally consistent with the increase in total collagen protein levels due to AB in the RV. Regarding TIMP protein levels, TIMP-1, -2, and -4 levels were not significantly altered between groups in the RV (**Figure 21A, B, D**). However, TIMP-3 protein levels trended to be increased due to AB suggesting an increase in the inhibition of collagen degradation due to AB (**Figure 21C**). Western blot images can be seen in Figure **21E**.

Figure 20.

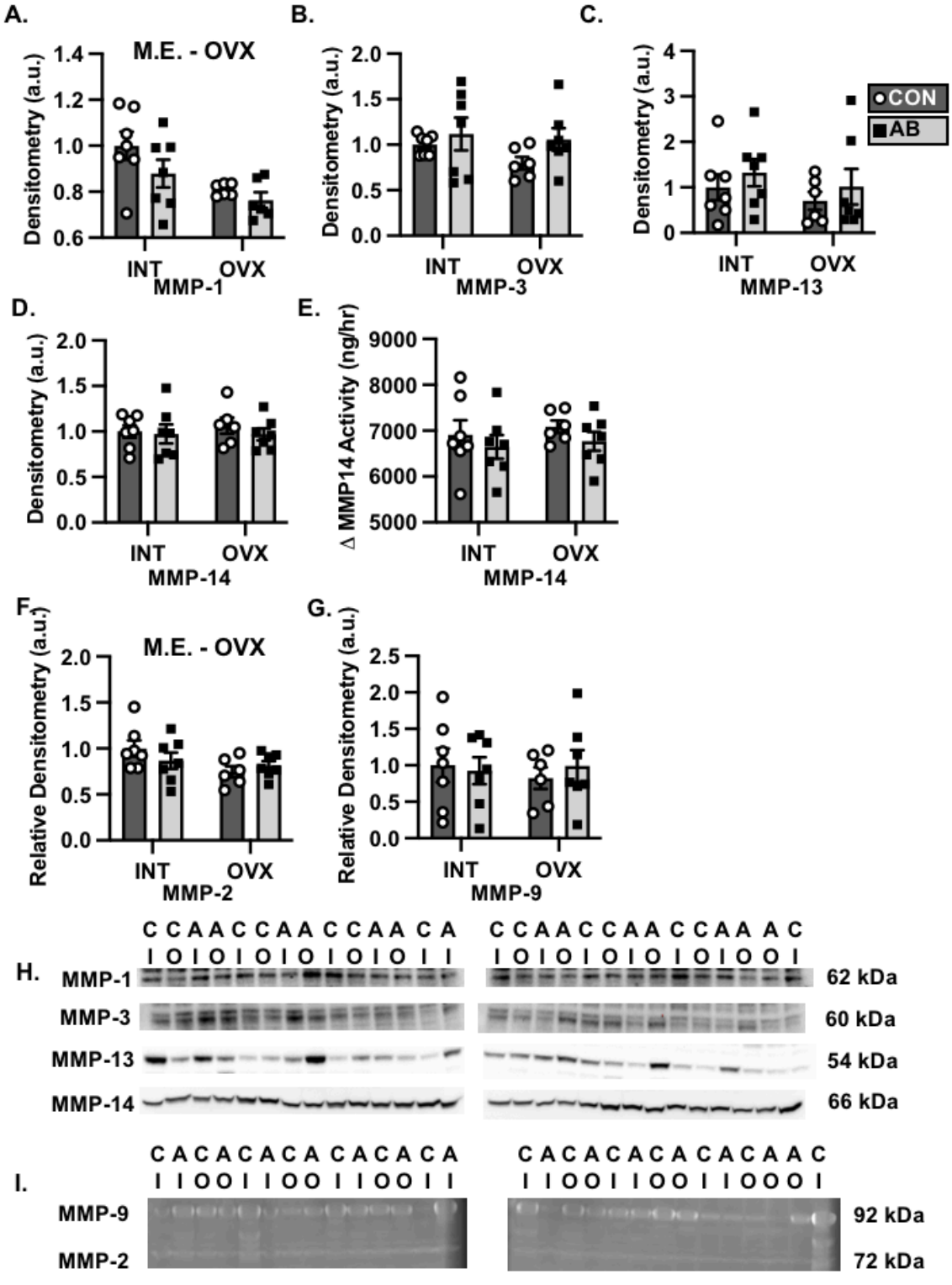
A.
M.E. - OVX
Densitometry (a.u.)
INT
OVX
MMP-1
B.
MMP-3
C.
MMP-13
CON
AB
D.
MMP-14
E.
Δ MMP14 Activity (ng/hr)
MMP-14
F.
Relative Densitometry (a.u.)
MMP-2
G.
MMP-9
H.
MMP-1
MMP-3
MMP-13
MMP-14
62 kDa
60 kDa
54 kDa
66 kDa
I.
MMP-9
MMP-2
92 kDa
72 kDa

Figure 20. *MMP-1 protein level and MMP-2 activity/abundance are decreased by ovariectomy in the right ventricle.* **(A)** MMP-1 protein levels were decreased due to OVX (main effect). MMP-3 protein **(B)**, MMP-13 protein **(C)**, MMP-14 protein **(D)**, and MMP-14 activity **(E)** levels were not significantly different between groups. **(F)** MMP-2 activity/abundance was decreased due to OVX (main effect). **(G)** MMP-9 activity/abundance was not significantly different between groups. **(H)** Western blot images of MMP-1, -3, -13, and -14. **(I)** Zymography images of MMP-2 and -9. $p < 0.05$; INT, intact; OVX, ovariectomy; AB, aortic-banded; CON, control; CI, control intact; AI, aortic-banded intact; CO, control ovariectomy; AO, aortic-banded ovariectomy; a.u., arbitrary units.

Figure 21.

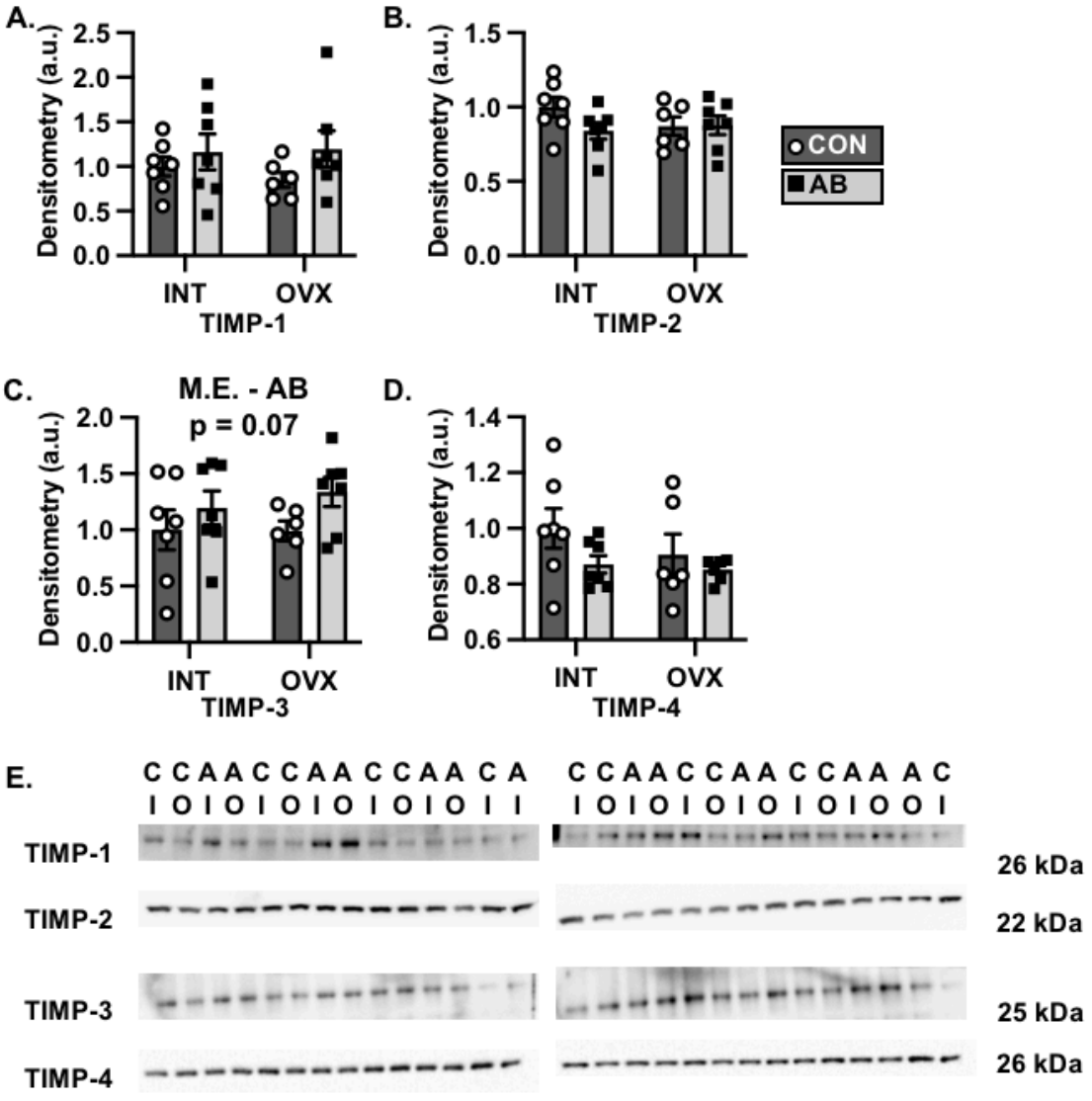

Figure 21. *TIMP-3 protein levels were increased due to AB in the right ventricle.* TIMP-1 **(A)** and TIMP-2 **(B)** protein levels were not altered between groups. **(C)** TIMP-3 protein levels trended to be increased due to AB (main effect). **(D)** TIMP-4 protein levels were not significantly different between groups. **(E)** Western blot images of TIMP-1, -2, -3 and -4. INT, intact; OVX, ovariectomy; AB, aortic-banded; CON, control; CI, control intact; AI, aortic-banded intact; CO, control ovariectomy; AO, aortic-banded ovariectomy; a.u., arbitrary units.

Discussion

As the pathogenesis of HFpEF is not well defined, a great emphasis has been placed on evaluating molecular mechanisms behind the development of this disease (10). One hallmark feature of HFpEF that is hypothesized to contribute to the disease and increase the risk of death is cardiac fibrosis (36, 51). Cardiac fibrosis occurs when there are imbalances in synthesis and degradation resulting in the accumulation of ECM components. How these two pathways are altered to increase collagen deposition due to the loss of female sex hormones during the development of HF is unknown. Therefore, the purpose of this study was to evaluate these pathways in a swine model subject to chronic pressure overload and/or the loss of sex hormones in order to elucidate the mechanism behind the development of fibrosis. Overall, this study demonstrates how the influence of the loss of sex hormones on the progression of aortic-banded induced heart failure can affect the heart in a chamber-specific manner as well as alter regulation of both the synthesis and degradation of cardiac fibrosis.

Left Ventricle

There is an increase in collagen deposition due to the loss of sex hormones which is in line with previous research conducted demonstrating an increase in fibrosis in post-menopausal women and animals subject to OVX (42, 86, 88, 112). However, this increase in total collagen levels due to the loss of sex hormones was not associated with an increase in collagen synthesis. This includes no significant increases due to the loss of sex hormones in activation of MAPK signaling, SP1 transcription or myofibroblast activation. Additionally, the relationship between

collagen mRNA and protein is no longer intact. It is a common misconception that alterations at the mRNA levels are translated to similar alterations at the protein level. In reality, it has been reported that ~40% of variation in protein expression can be explained by changes in mRNA levels implying that other cellular mechanisms involved in protein regulation such as protein stability and degradation are also heavily involved in determining total protein concentrations (220). This is seen in the present study in which ~15% of alterations at the mRNA level are translated to the protein level. Therefore, other mechanisms such as protein degradation could be leading to this increase in collagen protein in the LV. The results of this study demonstrating no alterations in LV collagen synthesis due to the loss of sex hormones is similar to clinical studies that have evaluated markers of collagen synthesis in premenopausal and postmenopausal women. It has previously been reported that biomarkers of collagen synthesis, specifically carboxy-terminal pro-peptide of procollagen I (PICP) and amino-terminal pro-peptide type I (PINP) serum levels, are not significantly altered after menopause (221-223). These results demonstrate that the increase in collagen seen in postmenopausal women is not attributed to an increase in synthesis, similar to the LV results seen in our animal model. Alternatively, these results from our pre-clinical swine model on collagen synthesis differ from previous studies in individuals with HFpEF. It was reported that collagen synthesis is increased in individuals with HFpEF; however, these studies have focused on identifying biomarkers found in the blood rather than evaluating myocardial tissue as human biopsy samples are not readily available (12, 18). These studies have shown

elevated serum levels of PICP and amino-terminal pro-peptide type III (PIIINP), both of which are cleaved during collagen synthesis (68, 69, 224), and are indicative of an overall increase in systemic collagen synthesis rather than cardiac-specific fibrosis.

There are other processes involved in the regulation of protein expression besides the rate of synthesis including the rate of protein degradation. Regarding degradation of collagen in the LV, there is a decrease in MMP-1 protein due to the loss of sex hormones which is directionally consistent with the increase in collagen due to the loss of sex hormones as well as decreases in MMP-2 activity/abundance in AB-OVX animals compared with AB-INT animals leading to a decrease in degradation. However, increases in MMP-9 activity/abundance in CON-INT animals compared with CON-OVX animals were also observed suggesting an increase in degradation in CON-OVX animals. There are also decreases in TIMP-2 protein levels due to the loss of sex hormones which would indicate a decrease in the inhibition of collagen degradation thus a decrease in collagen, which is not directionally consistent with the total collagen protein results. Interestingly, lower concentrations of TIMP-2 protein act in combination with MMP-14 to activate MMP-2 (190, 191). Therefore, this could suggest a decrease in MMP-2 activation, but this decrease in activation is only seen in the AB-OVX groups compared with AB-INT groups and not in the CON-OVX groups compared with the CON-INT groups. Overall, we see that degradation of collagen in the ECM is difficult to sort through as the results are not necessarily consistent with an increase in collagen due to the loss of sex hormones. Therefore, these results indicate that the accumulation

of cardiac fibrosis in the LV due to the loss of sex hormones is not due to the alteration of synthesis and there is a dysregulation of MMPs and TIMPs which degrade ECM proteins. Previous studies suggest the increase in collagen in individuals with HFpEF as well as postmenopausal women is due a decrease in collagen degradation either through decreases in MMPs and/or increases in TIMPs (42, 62, 75, 77). In individuals with HFpEF, serum biomarkers of collagen degradation including increases in carboxy-terminal telopeptide of collagen type I (CITP), MMP-2, MMP-3, and MMP-9 suggesting an increase in degradation and increases in collagen turnover (68, 224). TIMP-1, TIMP-2, and TIMP-4 levels were also increased in the serum of individuals with HFpEF which would suggest a decrease in collagen degradation through increases in its inhibition. Thus, in many studies there are increases in both MMPs and TIMPs so it is difficult to determine exactly how collagen degradation is altered, similar to the results presented in this present study. Overall, the results of this study indicate a collective imbalance in regulation of the ECM system that ultimately results in collagen accumulation, despite the inability to identify a clear linear path of molecular dysfunction (**Figure 22A**).

Another aspect of collagen regulation occurs in collagen matrix assembly, which can be aided by the presence of fibronectin (216-218). Previous studies have demonstrated that an initial deposition of fibronectin allows for collagen matrix assembly; therefore, there is a positive relationship between these two ECM proteins (216-218). In the present study, fibronectin protein levels were decreased in aortic-banding animals which could suggest an impairment in the normal

assembly of the collagen matrix. This may aid in the dysregulation of collagen in animals subject to chronic pressure overload thus attenuating an increase in collagen in the animals. However, aspects of collagen matrix assembly and cross-linking were not evaluated in this study. Further research needs to be conducted to explore the relationship between fibronectin and collagen matrix assembly and determine whether these changes alter collagen cross-linking, matrix assembly, and ultimately normal regulation.

Overall, in the LV there is an increase in collagen due to the loss of sex hormones; however, from these results there is not a clear connection linking the loss of sex hormones mechanistically to this increase in fibrosis. In these animals, it has been previously reported that serum progesterone levels were undetected in OVX animals while no differences were seen in the intact animals (CON-INT = 16 $\pm$ 4 ng/mL; AB-INT = 16 $\pm$ 4 ng/mL; $p > 0.99$) (151). Progesterone has been shown to be involved in other signal transduction pathways including the nitric oxide and protein kinase G (PKG) pathway, which have been shown to be anti-fibrotic (18, 138, 225); therefore, there could be other pathways involved in this increase in fibrosis that we have yet to explore. Future directions would consist of exploring other pathways linking sex hormones and cardiac fibrosis as well as other regulators of the ECM such as a disintegrin and metalloproteinase (ADAMs) or ADAM with thrombospondin motifs (ADAMTS) which are also shown to degrade the ECM (184). Lastly, the accumulation of collagen leading to cardiac fibrosis is often thought of as this balance between synthesis and degradation, but the regulation of protein expression in a cell also involves rate of translation and the

stability of both the mRNA transcript and protein, all of which have yet to be evaluated and would provide more clues as to why there is an increase in collagen due to the loss of sex hormones in the LV.

Right Ventricle

Overall, in the RV chronic pressure overload leads to an increase in collagen deposition due to an imbalance between synthesis and degradation consisting of an increase in synthesis as well as an increase in the inhibition of collagen degradation. This is demonstrated in our results by the increase in activation of JNK due to AB which can influence the transition of fibroblasts to myofibroblasts as well as stimulate collagen production in cardiomyocytes (70, 226). This transition to myofibroblasts from fibroblasts leads to a pro-fibrotic environment and an increase in the synthesis of ECM components including collagen mRNA levels (4, 59). There was a significant positive correlation between collagen I mRNA levels and total collagen protein levels indicating that an increase in collagen mRNA was associated with an increase in collagen protein, once again suggesting an increase in collagen synthesis. However, this was not shown with collagen III mRNA levels suggesting that collagen I is playing a more prominent role in the accumulation of cardiac fibrosis in the RV. In addition to this increase in synthesis, there is a potential increase in the inhibition of collagen degradation through increases in TIMP-3 protein levels.

JNK activation and its role in cardiac fibrosis is debated. JNK, a member of the stress-activated protein kinase (SAPK) family, is activated by physical, chemical, and physiological stressors (119). Previous studies have demonstrated

that activation of JNK can lead to selective ECM remodeling with increases in fibronectin but not collagen (119, 127). In contrast, JNK inhibition has also been shown to be cardioprotective against fibrosis or induce cardiac fibrosis depending on the disease state as well as timing of inhibition (125, 128-130). However, cardiac specific JNK activation and subsequent microarray analysis did demonstrate an increase in collagen 1, fibronectin, TIMP-1 and MMP-2 gene expression (131). In the current study, the trend for JNK activation to be increased due to AB is consistent with the increase in collagen I mRNA levels and total collagen protein levels due to AB which could suggest a mechanistic relationship. JNK is upstream of multiple transcription factors, including SP1, which is located in the promoter region of the collagen I transcript (219); however, EMSA results demonstrated no significant differences in transcription factor binding that would suggest an increase in collagen I transcription due to SP1. There are multiple transcription factors involved in the transcription of collagen I; therefore, other transcription factors could be involved in this increase in transcription. One of these transcription factors increased due to JNK activation is the basic transcription element binding protein (BTEB) which could be further explored in the future as well as other pathways altered by the TGFβ and SMAD pathways which are prominent regulators of fibrosis (219). While JNK activation might not directly activate transcription the SP1 factor in the collagen I promoter region, JNK is also involved in the differentiation of fibroblasts to myofibroblasts (70). Therefore, this increase in collagen synthesis due to chronic pressure overload could be due to

the pro-fibrotic environment of the myofibroblasts in AB animals which is aided by the activation of JNK.

Besides the increase in synthesis, there are also alterations seen in degradation in the RV, specifically a trend towards an increase in the inhibition of collagen degradation via TIMP-3 due to aortic-banding. This data would suggest a decrease in degradation due to chronic pressure overload which is directionally consistent with the increase in total collagen content seen in the RV. However, TIMP-3 is just one of ten ECM regulators evaluated in these animals. While a majority of these ECM regulators were unaltered due to AB or OVX at the protein or activity level in the RV, MMP-1 protein and MMP-2 activity/abundance were decreased due to OVX which would indicate a decrease in degradation; however, this is not directionally consistent with an increase in collagen protein levels due to chronic pressure overload. This once again suggests an imbalance in the regulation of collagen degradation that may be leading to an increase in collagen due to chronic pressure overload in the RV, specifically through an increase in the inhibition of collagen degradation (**Figure 22B**).

Figure 22.

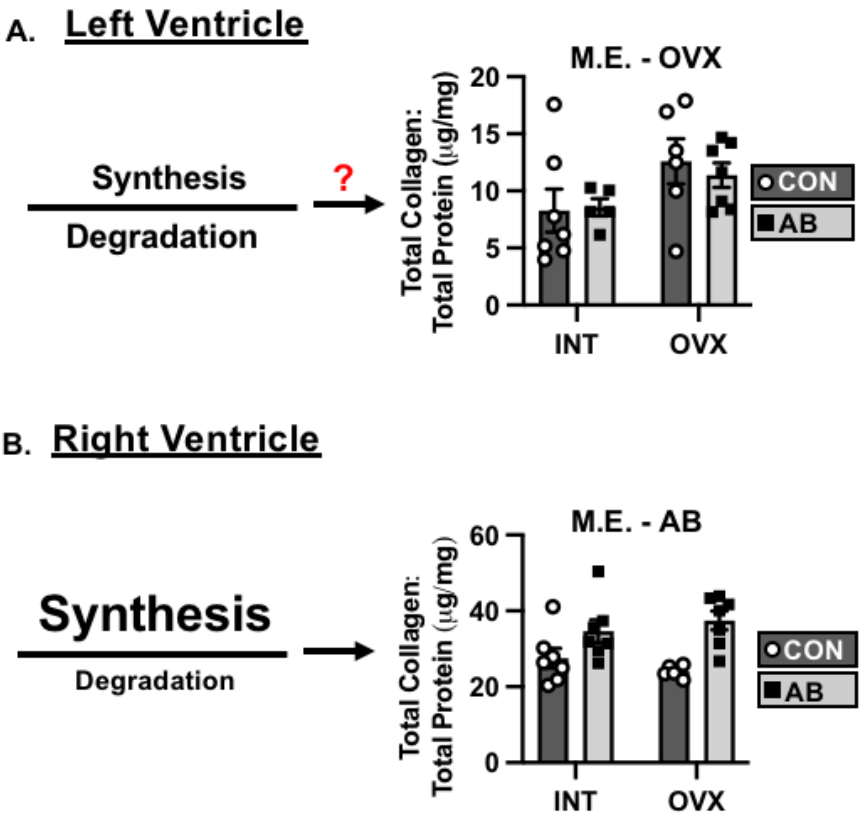

Figure 22. *Summary of results evaluating the balance between synthesis and degradation in the left and right ventricles.* **(A)** Total collagen levels were increased due to the loss of sex hormones in the LV with a dysregulation of ECM components due to both AB and OVX, making it difficult to identify a clear linear path for this accumulation. **(B)** The increase in total collagen due to chronic pressure overload in the RV was due to an increase in synthesis of collagen and an inhibition of collagen degradation suggesting a decrease in degradation. $p < 0.05$; INT, intact; OVX, ovariectomy; AB, aortic-banded; CON, control

Little research has been conducted from a molecular perspective on the RV in individuals with HFpEF and postmenopausal women, even though individuals with HFpEF demonstrate RV fibrosis in addition to LV fibrosis and estrogen has been shown to reduce fibrosis in the RV (60, 81, 118). One recently published study from our lab evaluated RV remodeling at a molecular level in a swine model

of cardiometabolic heart failure. This study demonstrated an increase in MMP-2 activity/abundance due to chronic pressure overload and western-diet with no change in protein levels of RV collagen, fibronectin, MMP-14, TIMP-2, or JNK activation (209). These results are comparable to the current study as they both see no differences in fibronectin protein, MMP-14 protein, or TIMP-2 protein; however, they differ in that this current study demonstrated an increase in RV collagen and JNK activation due to chronic pressure overload which could be due to the increase in sample size or absence of metabolic derangement in the animals of the current study. Overall, this is the first study to evaluate how RV fibrosis turnover is altered due to both the loss of sex hormones and chronic pressure overload and demonstrates cardiac fibrosis is increased due to chronic pressure overload, independent of sex hormones which most likely occurs through an increase in the synthesis of collagen.

Left and Right Ventricle Differences

Most research investigating the molecular pathogenesis of HFpEF focuses on the LV, and over the past few decades the results seen in the LV are assumed to translate to the RV. In a recently completed study from our lab, it was established that alterations in the LV rarely translate to alterations in the RV as only 13% of genes altered in the progression of heart failure are similarly altered in both ventricles (209). This highlights the need to evaluate both ventricles in the progression of heart failure. Likewise, in the current study there were profound differences seen between the left and right ventricles as only 34% of the targets evaluated were similarly altered (or unaltered) between the two ventricles.

Therefore, two-thirds of the targets evaluated regarding the regulation of cardiac fibrosis are not altered in a similar fashion between the two ventricles, once again highlighting the differences in the ventricles and providing evidence against long-held assumptions that changes in the LV translate to the RV.

One of the main differences seen between the two ventricles is with cardiac fibrosis. First, there are differences in the total amount of collagen between the two ventricles. A previous review has reported that the RV contains about 30% more collagen than the LV (26), but our results demonstrate that the RV has ~three times more collagen than the LV (LV = 10.24 $\pm$ 0.83; RV = 31.17 $\pm$ 1.55). This could be indicative of an increase in the stiffness of the RV compared to the LV, but little research has been conducted on the molecular differences between the LV and RV that could lead to this baseline increase of collagen. The results of this study, though, demonstrated differences between the LV and RV with ERα protein levels. ERα protein levels were increased in the LV compared to the RV for each of the four groups. Since tissues responsiveness to a hormone is dependent upon the number of receptors as well as the amount of circulating hormones, these results may be indicative of a greater hormone response in the LV compared to the RV (99). As sex hormones and their receptors have been shown to play a cardioprotective role against the development of fibrosis, this increase in receptor levels in the LV may suggest a reduction in fibrosis in the LV compared to the RV, which is seen in this study.

Additionally, the increase in collagen protein levels in the LV occurs due to the loss of sex hormones and is independent of chronic pressure overload but in

the RV, total collagen protein levels were increased due to chronic pressure overload and independent of the loss of sex hormones. There are fundamental differences seen between the LV and RV which would lead to the hypothesis that alterations in one ventricle may not translate to the other ventricle. These differences include wall thickness, ventricle shape, cardiomyocyte size, collagen content, pressures, and compliance (26, 133). Due to the thinner wall that is present in the RV, it is more susceptible to changes in pressure than the LV thus smaller changes in pressure or afterload could activate a stress response, such as through the stress-activated protein kinase, JNK. However, this is speculation as differences in afterload or the pressure gradients in the RV were not determined in this analysis. Therefore, a conclusion about stress responses to stretch or pressure changes cannot be made. However, there is an increase in activation of the stress-activated protein kinase JNK in the RV but not the LV which would suggest differences in stress placed on each ventricle in this animal model. JNK can also be activated through inflammatory or oxidative stress; thus, the increase in synthesis seen in the RV (but not the LV) could be further evaluated though other upstream molecular stressors.

Another interesting finding when evaluating differences between the LV and RV is regarding MMP transcription. In the LV, MMP-1, -3 and -13 were all increased due to AB while MMP-2, -9, and -14 were unaltered due to AB or OVX. In the RV, though, the mRNA levels of these MMPs produced the reverse results consisting of MMP-1, -3, and -13 levels that were unaltered due to AB or OVX and MMP-2, -9, and -14 were increased due to AB. This prompted further research into

the transcriptional regulation of these MMPs. MMP-1, -3, -13 are under transcriptional regulation through the AP-1 transcription factor while MMP-2 and MMP-14 are not under AP-1 transcriptional regulation. MMP-2, -9, and -14 are under transcriptional regulation through SP1 transcription factor while MMP-1, -3, and -13 lack SP1 binding sites (58, 65). The differences presented here highlight chamber-specific mechanisms in the regulation of cardiac fibrosis biomarkers. Both AP-1 and SP1 are common transcription factors involved in the regulation of many genes and cellular processes. AP-1 is mainly activated through MAPK pathways including JNK, ERK1/2 and p38 while SP1 is activated by multiple pathways in addition to the MAPKs including A-cyclin dependent kinase (CDK), phosphatidylinositol 3-kinase (PI3K), casein kinase II (CKII), and protein kinase C (PKC) (142, 227). These results provide insight into other potential pathways that are activated in the LV versus the RV that could be contributing to chamber-specific differences.

One unique aspect of this study is the evaluation of sex hormone receptor levels in the heart and whether they are altered after the loss of sex hormones through surgically induced menopause. This is the first study to report how protein levels of sex hormone receptors are altered after OVX in the heart of a large animal model. Previous studies have shown that ERα and ERβ protein levels in the heart decline after OVX in rats but they have not been evaluated in a larger animal model or in postmenopausal women (86-88). Additionally, progesterone receptor levels have not been evaluated in the heart of postmenopausal women or in animals subject to OVX. Interestingly, the results differ from previous reported studies in

other tissues which demonstrate a decrease in sex hormone receptor levels after the loss of sex hormones (83, 97-99). ERα and ERβ protein levels were not altered due to OVX in either the LV or the RV. Progesterone receptor levels in the RV were also unaltered due to OVX, but there were trends for increased PGR A and B protein levels due to OVX in the LV. Serum progesterone levels were previously shown to be undetected in these OVX animals which could lead to the idea of a possible compensation mechanism to increase PGR levels in the heart due to the loss of serum progesterone levels but this needs to be further explored (151). There were also ventricle-dependent sex hormone receptor differences due to chronic pressure overload which little research has been conducted on how these receptor levels change in the progression of heart failure. One previous study has demonstrated that individuals with aortic stenosis have increased mRNA levels of ERα and ERβ (93). While our results are in line with this previous study given the observed increases in both ESR1 and ESR2 mRNA due to AB in the LV and increases in ESR2 mRNA due to AB in the RV, these results did not translate to the protein level. In the LV, there were no significant differences in ER protein levels, but PGR B was decreased due to AB while in the RV there was an increase in ERβ in AB-OVX animals. While alterations in sex hormone receptor levels can provide clues into the signaling pathways of these proteins, the proteins themselves can also act as transcription factors by dimerizing and translocating to the nucleus (132, 133). Therefore, the transcriptional activity of these receptors should further be evaluated to determine if they have a direct effect on any genes involved in the regulation of fibrosis.

ERα and ERβ are known as the nuclear estrogen receptors; however, the G protein-coupled receptor 30 (GPR30; also known as G protein-coupled estrogen receptor 1, or GPER1) is another receptor activated by estrogen and has been shown to activate multiple signaling pathways including PI3K and MAPKs (92, 207). Additionally, GPR30 activation has been shown to have beneficial effects on the cardiovascular system, similar to estrogen's nuclear receptors. These cardioprotective effects include: decreased cardiac fibrosis, suppression of fibroblast differentiation into myofibroblasts, vasodilation and reduction in myocardial infarction severity (41, 92, 207). Therefore, a limitation of this study is that only nuclear estrogen receptors were evaluated and future directions would include investigation into GPR30 to determine if this receptor could be playing a role in the development of fibrosis in the progression of HF. Overall, these results demonstrate different responses of sex hormone receptors in each ventricle due to the loss of sex hormones and chronic pressure overload.

Limitations

While this study provided a unique opportunity to determine how the loss of sex hormones alters the regulation of fibrosis in animals subject to chronic pressure overload in both the left and right ventricles, there were some limitations that were presented during this analysis. As this study has focused on the molecular alterations seen between the two chambers of the heart, it is difficult to link these alterations at the molecular level to functional changes as evaluation of RV structure and function was not completed at the time of sacrifice. Also, this study was designed for intact animals to be in anestrus during the time of sacrifice

at a time in the estrus cycle where estrogen levels are low. Indeed, estrogen levels were undetectable in all four groups of animals assessed by radioimmunoassay. If the intact animals were sacrificed during estrus when estrogen levels are high, there may be more pronounced signaling differences between intact and OVX animals that might provide more clues to the increase in collagen in the LV due to the loss of sex hormones. In addition to the timing of the estrus cycle, some of the targets evaluated such as ERK1/2 and JNK are transient therefore it is difficult to determine if the inactivation of ERK1/2 in the LV and RV or inactivation of JNK in the LV is due to the protein not being activated or simply missing the time frame when it is activated. Lastly, the focus of this study has been on the balance between synthesis and degradation where an imbalance between these two factors has been shown to lead to cardiac fibrosis; however, there are other factors in the regulation of collagen that should be evaluated to determine why there is an increase in collagen in the LV due to the loss of sex hormones. Those other factors include evaluating the rate of translation of collagen as well as alterations in the stability of the protein.

Conclusions

The results of this study revealed chamber-specific differences in the regulation of cardiac fibrosis due to the loss of sex hormones and chronic pressure overload in a pre-clinical swine model with relevance to HFpEF. These chamber specific differences consist of an increase in total collagen levels in the LV due to the loss of sex hormones but an increase in total collagen levels in the RV due to chronic pressure overload. In the RV, this increase in total collagen was due to an

increase in synthesis through activation of JNK and an increase in myofibroblasts. In the LV, the data did not elucidate a clear linear path supporting increases in collagen but rather, an imbalance in the entire regulatory system. Overall, these results highlight the need to evaluate both ventricles of the heart in order fully understand the pathogenesis of HFpEF and develop possible therapeutics for the disease. The stark chamber-specific differences in fibrosis between the two ventricles emphasizes a need to focus on the components of the heart in addition to the heart as a whole when evaluating fibrosis.

CHAPTER 4: CONCLUSIONS

The focus of this dissertation was to evaluate cardiac remodeling in the right ventricle in two swine models of HFpEF. The first model consisted of Ossabaw swine subject to western-diet and aortic-banding to replicate a “multi-hit” model of HFpEF focused on two common comorbidities including metabolic syndrome and hypertension (Chapter 2). The second model consisted of Yucatan mini-swine subject to surgically induced menopause through ovariectomy and/or aortic-banding to investigate the influence of sex hormones and chronic pressure-overload on the progression of HFpEF (Chapter 3). The second focus of this dissertation was to investigate the differences in cardiac remodeling between the left and right ventricles of the latter Yucatan mini-swine model.

The incidence of HF is expected to increase exponentially by 46% over the next decade while the cost of HF is expected to increase by more than 127% (1). Despite these projections, the pathogenesis of HFpEF, currently the most prominent form of HF, is not well defined and lacks effective treatment options (6, 8, 10). HFpEF, formerly known as diastolic HF, occurs when the heart is not able to relax due to a stiffening of the ventricular wall (7, 10, 11). This increase in stiffness of the ventricular wall is hypothesized to be due in part to an increase in myocardial fibrosis through the accumulation of extracellular matrix proteins, as end-diastolic pressures have been shown to correlate with collagen-based stiffness (4, 12, 13, 19). While individuals with HFpEF have been shown to have increased collagen synthesis and well as decreased collagen degradation through serum biomarkers, these alterations reflect systemic changes in the regulation of

fibrosis and the myocardium has yet to be evaluated (12, 68, 69, 224). Therefore, the purpose of these studies was to determine how the regulation of fibrosis is altered in the myocardium of previously completed swine models from our lab in hopes to provide insight into the pathogenesis of HFpEF.

Swine represent a translational model for cardiovascular disease studies as humans and swine share similar physiological characteristics compared with other laboratory animal species, such as heart size, coronary anatomy, and heart rate (5, 228, 229). Therefore, our lab has focused on the use of large animal models to study the development of heart failure induced by aortic-banding. The first animal model of HFpEF replicates a cardiometabolic HF phenotype utilizing female, intact, Ossabaw swine with characteristics including: an ejection fraction greater than 50%, global cardiac hypertrophy, concentric hypertrophy, diastolic dysfunction, increased wet lung weight, increased LV brain natriuretic peptide mRNA levels, obesity, inactivity, insulin resistance and dyslipidemia (146, 209). The second animal model of HFpEF in Yucatan mini-swine focused on a postmenopausal phenotype as HFpEF incidence greatly increases after menopause and more predominantly affects females over males (15, 151). This model developed characteristics replicative of a HFpEF phenotype including: an ejection fraction greater than 50%, global cardiac hypertrophy, concentric hypertrophy, and increased LV BNP mRNA levels (151). However, diastolic dysfunction and cardiac fibrosis were only seen in those animals that underwent surgically induced menopause through OVX and not due to chronic pressure overload via aortic-banding. While both animal models demonstrate characteristics of HFpEF, the

Ossabaw model also had classic comorbidities found with HFpEF, such as metabolic syndrome while the Yucatan mini-swine lack these comorbidities. This is due to the Ossabaw swine being genetically predisposed to develop metabolic syndrome when fed a high-fat diet (230, 231). Additionally, the Ossabaw swine subject to aortic-banding developed diastolic dysfunction that was independent of increases in cardiac fibrosis while the Yucatan swine did not develop diastolic dysfunction or cardiac fibrosis due to AB, but instead these characteristics were developed due to the loss of female sex hormones (146). Overall, these two animal models provide the opportunity to explore the development of cardiac fibrosis and how it is affected by chronic pressure overload, the loss of sex hormones, and Western diet induced metabolic comorbidities.

The first steps in evaluating RV remodeling in these swine models consisted of transcriptome analysis of the right ventricular tissue in the Ossabaw swine. This led to further exploration of the molecular target MAPK8/JNK1 and its role in ventricular remodeling as JNK was shown to be upstream of ECM remodeling consisting of an increase in fibronectin accumulation (119, 127). However, one limitation of this study was that we were unable to decipher whether alterations seen in the WD-AB animals were due to diet, chronic pressure overload, or a combination of these two variables. By comparing these results from the Ossabaw study to those in the Yucatan study, we do see that there are similar alterations due to chronic pressure overload thus suggesting that these alterations where not due to the influence of diet or metabolic comorbidities. There alterations at the mRNA level include increases in MAPK8, fibronectin, MMP-2, MMP-9, MMP-14,

TIMP-2, TIMP-4 and DUSP1 levels. These changes at the mRNA level in the RV of these animals due to AB did not translate to protein as there were no significant differences seen in pJNK, total JNK protein, fibronectin, MMP-9, MMP-14, or TIMP-2 protein levels. Even though some of the genes identified were not associated with a commensurate increase in protein expression, the transcript changes identified provide insight into the development of this disease. The differentially expressed genes and pathways are altered in response to stressors such as aortic-banding; therefore, this analysis allows for the identification of which particular pathways are first altered in response to these stressors and provides insights into potential upstream pathways that are initially activated or suppressed in the progression of aortic-banding induced HF (232, 233).

One of the most profound differences between these two animal models occurs when comparing the differences in total collagen protein in the RV. Total collagen levels in the RV of the Ossabaw swine model of cardiometabolic HF were not significantly altered in the WD-AB group; however, total collagen levels in the Yucatan model without comorbidities demonstrated an increase in RV total collagen levels due to AB. In the Yucatan model, collagen protein levels were also strongly correlated to collagen I mRNA levels which were similarly increased due to AB. Neither collagen I nor collagen III mRNA levels were increased due to WD-AB nor were they correlated with total collagen protein levels (Collagen I: $r = 0.3652$, $p = 0.33$; Collagen III: $r = -0.051$, $p = 0.89$). These results suggest differences in collagen regulation between these two sets of animals. Both models were subject to chronic pressure overload for 6 months with a trans-stenotic

systolic pressure gradient of ~70 mmHg; however, the Ossabaws were banded at 6 months of age, the onset of sexual maturity in a swine, before terminal studies at 12 months of age while the Yucatan swine were banded at 8 months of age before terminal studies at 14 months of age (146, 151). Therefore, while it is difficult to draw solid conclusions given differences in multiple experimental variables between groups such as age, species, and metabolic comorbidities induced by western diet, it does raise the question as to whether western diet could be altering the development of cardiac fibrosis in the RV as a potential compensatory mechanism against the development of fibrosis after chronic pressure overload. This idea contradicts previous research, though. Metabolic syndrome has been shown to increase the incidence of cardiac fibrosis both in the left and right ventricles as well as increase the risk of developing HF (9, 234-238). Metabolic syndrome has also been shown to increase RV diastolic dysfunction, RV systolic function, RV EDV, RV ESV and RV hypertrophy as well as reduce RV ejection fraction (239-241). Thus, it is more likely that metabolic syndrome is detrimental to cardiac structure and function. However, the results presented in Chapter 2 do challenge this idea as there was no increase in cardiac fibrosis in aortic-banded Ossabaw swine fed a western-diet. Whether these results in collagen deposition would be similar after 8 months, 1 year or 2 years of chronic pressure overload shall be considered as a future question to explore in order to determine if diet alters fibrosis as this disease progresses. Additionally, it would be valuable to determine if the progression of fibrosis differs based on the comorbidities present as this has potential relevance to differences in HFpEF phenotypes.

While these results are perplexing, there are multiple regulatory steps involved in the development of fibrosis. One of these regulators evaluated in these models is stress-activated protein kinase, or JNK. The focus of these studies on JNK began when MAPK8/JNK1 was identified as a hub gene involved in RV remodeling from the transcriptome analysis in the cardio-metabolic swine model of HF. Previous studies have demonstrated that an increase in cardiac-specific activation of JNK lead to the increase in ECM mRNA levels including fibronectin, collagen, MMP-2, and TIMP-1 while additional studies have shown cardiac-specific activation of JNK lead to increases in fibronectin, but not collagen protein levels (119, 127, 131). Therefore, JNK was investigated in the cardio-metabolic swine model. Evaluating the JNK pathway was then pursued in the Yucatan swine model as JNK has been shown to be altered due to sex hormone receptors and activated in HF models (40, 93, 136, 242-244). Therefore, JNK was evaluated to determine if these pathways are similarly altered in two swine models with relevance to two HFpEF phenotypes. In the Yucatan mini-swine model without comorbidities, there is a trend for an increase in the activation of JNK in the RV. In contrast, Ossabaw swine with metabolic comorbidities did not see a significant increase in JNK activation or total JNK protein levels in the RV whole homogenate. JNK's role in the development of fibrosis is the subject of debate as it has been shown to both increase and decrease collagen levels depending on timing of activation or inhibition as well as the disease state (119, 125, 127, 128, 130, 131). Therefore, the increase in JNK could be leading to the increase in collagen I mRNA levels that is strongly correlated to total collagen in the Yucatan mini-swine but not

in the Ossabaw swine. Once again though, this contradicts previous research that demonstrates increases in JNK activation with metabolic syndrome and HF raising the question as to how metabolic syndrome is not associated with an increase in collagen due to aortic-banding (242-244). Mechanistically, there is an increase in DUSP4 mRNA levels due to WD-AB in the Ossabaws that is not altered in Yucatan mini-swine, suggesting a potential compensatory increase in phosphatase activity to offset an increase in JNK activation. Therefore, there are differences in upstream regulators of collagen synthesis that may be leading to these differences in total collagen protein levels seen in the RV of the Ossabaw and Yucatan mini-swine.

In the WD-AB Ossabaws, there are also alterations in the degradation of collagen that were not seen in the Yucatan mini-swine model. There was an increase in MMP-2 activity in the Ossabaws whereas in the Yucatan's, there is no difference in MMP-2 activity due to AB. This could suggest that the increase in degradation of collagen through MMP-2 is helping to attenuate a potential increase in collagen levels due to chronic pressure overload as collagen levels are similar in WD-AB animals compared to controls. This is in line with previous studies that demonstrate an increase in serum MMP-2 levels with metabolic syndrome (245, 246). Overall, when evaluating collagen regulation in the RV of these two animal models, there is an increase in collagen protein that correlates with collagen I mRNA levels in Yucatan mini-swine subject to AB as well as increases in upstream regulator JNK while Ossabaw swine subject to western-diet and AB do not have increases in collagen protein or mRNA, possibly due to normal JNK signaling

attenuated by increased DUSP4 and/or increases in MMP-2 activity/abundance (**Figure 1**).

Figure 1.

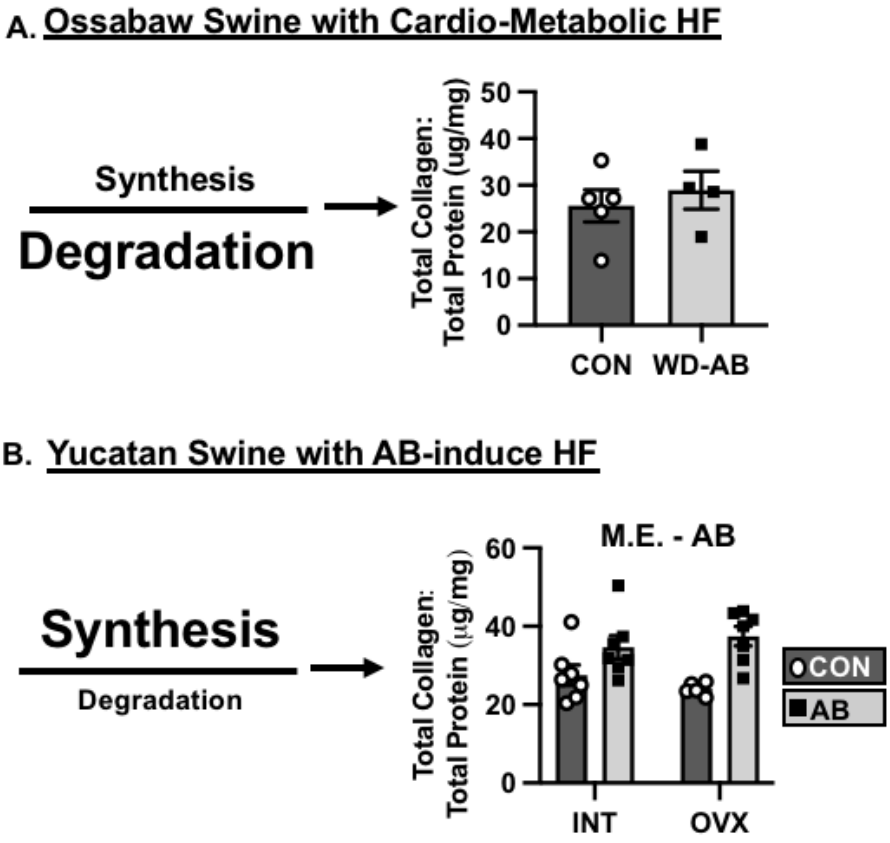

Figure 1. *Summary of results evaluating the balance between synthesis and degradation of cardiac fibrosis in the right ventricle of two swine models of heart failure (HF).* **(A)** An increase in degradation in western diet-fed, aortic-banded animals could lead to collagen levels similar to that of controls in the RV. **(B)** The increase in total collagen due to chronic pressure overload in the RV might be the result of increased synthesis as evident by an increase in activated JNK. $p < 0.05$; CON, control; WD-AB, western-diet, aortic-banded; INT, intact; OVX, ovariectomy; AB, aortic-banded; CON, control

There were also differences in ECM proteins in the LV of these two animal models. In the Ossabaw swine model, there were no differences in total collagen level but there were increases in total collagen levels in the Yucatan swine due to

the loss of sex hormones via OVX (146). The Ossabaw swine were intact females and when this is compared to the intact Yucatan swine, there were no differences seen between the CON-INT and AB-INT groups. Therefore, the results in the Ossabaws are in line with the results seen with the Yucatan model. This is also in line with previous research conducted in animal models that have demonstrated the cardioprotective effects of sex hormones against the development of cardiac fibrosis (86, 87, 94). This could suggest that if the Ossabaw swine that were western-diet fed and aortic-banded underwent OVX, then there could be an increase in fibrosis due to the loss of sex hormones. This work is currently being investigated in our lab.

Therapeutic potential

The results of these studies identify multiple targets that are altered in the development of cardiac fibrosis; however, whether these genes or proteins would present possible therapeutic targets is questionable. First, there are multiple differences shown here in the development of fibrosis between the left and right ventricles; therefore, targeting one protein, such as JNK, may be beneficial for one ventricle but not the other. This would increase the need for drug-specificity that goes beyond just targeting the heart, but targeting each ventricle. Second, many of the proteins evaluated in this study are involved in multiple cell processes. For example, JNK is not only involved in cardiac fibrosis. It has also been shown to aid in cell proliferation, differentiation, metabolism, survival, and signal transduction as JNK cross-talk is implicated with many other signaling pathways (119, 247). Therefore, there may be multiple off-target effects that could be harmful to other

cellular processes. There has been research into the study of JNK inhibitors in the treatment of disease such as cancer and heart failure *in vitro* or in small animal models; however, most treatment options developed lack isoform specificity or present cellular toxicity (247, 248). ECM regulation through MMPs and TIMPs also present another possible therapeutic target, but previous studies have found that MMP inhibitors are not efficacious and resulted in an increase in musculoskeletal pain and inflammation (58, 140). While MMPs and TIMPs do provide a target for degradation of ECM proteins, it is difficult to specifically target one MMP or TIMP as they are under similar transcriptional regulation and there is cross-talk between isoforms (65, 140). Additionally, there is a fine balance between targeting pathological remodeling and physiological remodeling that occurs as a compensatory mechanism which also makes these enzymes a difficult target for therapeutics.

While no effective pharmacological therapies have been developed targeting the proteins identified in this study, exercise has been shown to have beneficial effects on cardiac function in individuals with HFpEF (21-24). Additionally, a previous study from our lab in male swine subject to 6 month of chronic pressure overload via aortic-banding has demonstrated chronic low-intensity interval exercise training reduced pathological LV remodeling, attenuated LV diastolic dysfunction, and improved cardiac efficiency (149, 177). Additionally, exercise training reduced fibrotic remodeling and preserved normal ECM regulatory biomarkers mRNA levels including MMP-2, MMP-9, TIMP-1 and TIMP-4 (149). However, this research was completed on the LV and has not been further

investigated in the RV. While research still needs to be done to find appropriate pharmacological interventions for treatment of HFpEF and targeting potential biomarkers identified by these studies, exercise intervention may be a possible first step towards improvements of ECM regulation in individuals with HF.

The genes and proteins identified in regulating cardiac fibrosis in the progression of AB-induced HF may not represent the most effective therapeutic targets due to their lack of specificity and potential off target effects; however, they do represent potential biomarkers for risk assessments to determine the severity of disease. Previous research has demonstrated that MMPs, TIMPs, and cleaved products of collagen synthesis and degradation can be measured in the blood and these products have potential to predict the presence of diastolic dysfunction and HFpEF (68, 69, 224). In a recent study, it was demonstrated that biomarkers of fibrosis ranked higher than traditional biomarkers such as BNP in predictive capabilities (69). Importantly, the use of biomarkers from the blood represents systemic changes rather than cardiac-specific changes. Thus, these biomarkers may be useful for diagnostic purposes but caution should be taken when utilizing these biomarkers in the blood to determine the molecular mechanisms involved in the pathogenesis of HFpEF as one cannot decipher what is altered within each ventricle.

Limitations and Future Directions

While both studies evaluated swine subject to chronic pressure overload for 6 months with a trans-stenotic systolic pressure gradient of ~70 mmHg, there are inherent differences between the groups due to swine species such as Ossabaws

having a lower heart rate (Ossabaw = 84 ± 3 bpm; Yucatan = 104 ± 4 bpm; $p < 0.05$) as well as Ossabaws having more collagen in the heart in both the LV and RV compared to Yucatan mini-swine LV (Ossabaw LV = 33.61 ± 2.1 μg/mg; Ossabaw RV = 27.08 ± 2.53 μg/mg; Yucatan LV = 10.24 ± 0.83 μg/mg; Yucatan RV = 31.17 ± 1.55 μg/mg; Interaction $p < 0.0001$). Therefore, results comparing differences between these two models should be completed with caution as it is difficult to determine if the differences seen are due to induction of western diet or inherent differences between species. Additionally, with the Ossabaw study, female animals were intact at the time of terminal studies, but their estrus cycles were not synchronized and estrogen or progesterone serum levels were not analyzed making it difficult to determine which stage of the estrus cycle they are in when tissue samples were taken. As estrogen and progesterone have been shown to alter the signaling of many targets and signaling pathways, it also makes it difficult to compare the intact Yucatan mini-swine with the intact Ossabaws as the stage of the estrus cycle could affect signaling pathways. Additionally, the Yucatan mini-swine were sacrificed during anestrus, a time where estrogen levels are low, which could attenuate estrogens effect on signal transduction pathways. Therefore, evaluating animals during peak estrus when estrogen levels are high may provide insight that we are unable to see due to the undetectable levels of estrogen. As a note, OVX removes the ovarian source of sex hormones, but these hormones are also produced by other sources including the adrenal gland. Estrogen is also produced through aromatization of testosterone in tissues such as adipose tissue, bone, and aortic smooth muscle cells (83, 249). Therefore, while

estrogen levels are reduced in the OVX animals and sex hormone levels were below the detectable threshold level of assays performed (10ng/ml), there could be circulating estrogen levels still present in the OVX animals that could be affecting multiple signaling pathways, particularly in the RV of AB-OVX animals as we see a significant increase in ERβ receptor levels. Furthermore, providing animals that underwent OVX with hormone therapy to determine if further addition of hormones could reduce fibrosis or diastolic dysfunction in these animals which would provide insight into new therapeutic options for post-menopausal women.

While differences in molecular signaling pathways have been proposed based on these studies, how these molecular changes affect the function of each ventricle is unknown as functional studies in the RV were not analyzed at the time of sacrifice. However, moving forward with new animal models RV functional data through echocardiography and pressure analysis is being completed in hopes to link functional changes and molecular changes in the future. Lastly, tissue samples in these animals were derived from powdered samples that contained multiple cell types including cardiomyocytes, fibroblasts, and coronary blood vessels; therefore, it is difficult to determine cell specific changes in these animals and whether these changes in the ECM stem from cardiomyocytes or fibroblasts. Future directions would consist of isolating specific cell types and performing analyses on these separate cell types to localize these changes observed from a combined tissue homogenate. Other future directions for these studies would consist of evaluating the Ossabaw LV to determine how the Ossabaw LV differs from the RV and if there are similar ventricle-dependent gene signatures as seen in the Yucatan study.

Also, vascular stiffness and function were not analyzed in the right coronary arteries in the Yucatan swine nor the left anterior descending artery or the left circumflex artery; therefore, a future direction would be to continue the vascular studies in future swine models to determine if the results found in the Ossabaws translate to other animal models or arteries.

Conclusions

The current studies presented here investigated the molecular regulation of fibrotic remodeling in the heart due to chronic pressure overload, with the focus on the balance between the synthesis and degradation of ECM proteins. The main focus of these studies was on the RV as dysfunction on the right side of the heart can significantly increase mortality rates in individuals with HFpEF. Analysis of the RV in a cardiometabolic swine model of HF lead us to an increase in fibronectin in the RCA due to an increase in synthesis through JNK pathway as well as a decrease in degradation through MMP14. This increase in fibronectin was also associated with an increase in vascular stiffness. The second study analyzed the RV of swine subject to chronic pressure overload and/or the loss of sex hormones. There was an increase in cardiac fibrosis due to chronic pressure overload and independent loss of sex hormones through pathways related to collagen synthesis. Interestingly, in the LV the increase in cardiac fibrosis was due to the loss of sex hormones and independent of chronic pressure overload. This increase in collagen in the LV was not due to linear alterations in synthesis or degradation.

Overall, these results highlight the differences between the LV, RV, and vasculature in the regulation of ECM proteins, and that alterations seen in one

tissue type may not necessarily translate to the other tissues even though they are all within the same organ system. Thus, these studies highlight the need to evaluate multiple components of one system to understand the development of a disease. Additionally, these results provide molecular insight into the pathogenesis of cardiac fibrosis in individuals with HFpEF. While these results may not present a straight-forward answer to the increase in deposition of fibrosis in the heart, the results do provide possible diagnostic markers as well as potential targets for pharmacological intervention and lifestyle interventions, such as exercise, for treatment of HFpEF.

REFERENCES

1. Tsao CW, Aday AW, Almarzooq ZI, Alonso A, Beaton AZ, Bittencourt MS, Boehme AK, Buxton AE, Carson AP, Commodore-Mensah Y, Elkind MSV, Evenson KR, Eze-Nliam C, Ferguson JF, Generoso G, Ho JE, Kalani R, Khan SS, Kissela BM, Knutson KL, Levine DA, Lewis TT, Liu J, Loop MS, Ma J, Mussolino ME, Navaneethan SD, Perak AM, Poudel R, Rezk-Hanna M, Roth GA, Schroeder EB, Shah SH, Thacker EL, VanWagner LB, Virani SS, Voecks JH, Wang NY, Yaffe K, Martin SS. Heart Disease and Stroke Statistics-2022 Update: A Report From the American Heart Association. Circulation. 2022;145(8):e153-e639. Epub 2022/01/27. doi: 10.1161/CIR.0000000000001052. PubMed PMID: 35078371.
2. Virani SS, Alonso A, Aparicio HJ, Benjamin EJ, Bittencourt MS, Callaway CW, Carson AP, Chamberlain AM, Cheng S, Delling FN, Elkind MSV, Evenson KR, Ferguson JF, Gupta DK, Khan SS, Kissela BM, Knutson KL, Lee CD, Lewis TT, Liu J, Loop MS, Lutsey PL, Ma J, Mackey J, Martin SS, Matchar DB, Mussolino ME, Navaneethan SD, Perak AM, Roth GA, Samad Z, Satou GM, Schroeder EB, Shah SH, Shay CM, Stokes A, VanWagner LB, Wang NY, Tsao CW, American Heart Association Council on E, Prevention Statistics C, Stroke Statistics S. Heart Disease and Stroke Statistics-2021 Update: A Report From the American Heart Association. Circulation. 2021;143(8):e254-e743. Epub 2021/01/28. doi: 10.1161/CIR.0000000000000950. PubMed PMID: 33501848.
3. Borlaug BA, Redfield MM. Diastolic and systolic heart failure are distinct phenotypes within the heart failure spectrum. Circulation. 2011;123(18):2006-13; discussion 14. Epub 2011/05/11. doi: 10.1161/CIRCULATIONAHA.110.954388. PubMed PMID: 21555723; PMCID: PMC3420141.
4. Gevaert AB, Boen JRA, Segers VF, Van Craenenbroeck EM. Heart Failure With Preserved Ejection Fraction: A Review of Cardiac and Noncardiac Pathophysiology. Front Physiol. 2019;10:638. Epub 2019/06/14. doi: 10.3389/fphys.2019.00638. PubMed PMID: 31191343; PMCID: PMC6548802.
5. Andronic AA, Mihaila S, Cinteza M. Heart Failure with Mid-Range Ejection Fraction - a New Category of Heart Failure or Still a Gray Zone. Maedica (Bucur). 2016;11(4):320-4. Epub 2017/08/23. PubMed PMID: 28828050; PMCID: PMC5543525.
6. Roger VL. Epidemiology of Heart Failure: A Contemporary Perspective. Circ Res. 2021;128(10):1421-34. Epub 2021/05/14. doi: 10.1161/CIRCRESAHA.121.318172. PubMed PMID: 33983838.
7. Savarese G, D'Amario D. Sex Differences in Heart Failure. Adv Exp Med Biol. 2018;1065:529-44. Epub 2018/07/28. doi: 10.1007/978-3-319-77932-4_32. PubMed PMID: 30051405.
8. Paulus WJ, Zile MR. From Systemic Inflammation to Myocardial Fibrosis: The Heart Failure With Preserved Ejection Fraction Paradigm Revisited. Circ Res. 2021;128(10):1451-67. Epub 2021/05/14. doi: 10.1161/CIRCRESAHA.121.318159. PubMed PMID: 33983831; PMCID: PMC8351796.

9. Oktay AA, Rich JD, Shah SJ. The emerging epidemic of heart failure with preserved ejection fraction. Curr Heart Fail Rep. 2013;10(4):401-10. Epub 2013/10/01. doi: 10.1007/s11897-013-0155-7. PubMed PMID: 24078336; PMCID: PMC3870014.
10. Shah SJ, Borlaug BA, Kitzman DW, McCulloch AD, Blaxall BC, Agarwal R, Chirinos JA, Collins S, Deo RC, Gladwin MT, Granzier H, Hummel SL, Kass DA, Redfield MM, Sam F, Wang TJ, Desvigne-Nickens P, Adhikari BB. Research Priorities for Heart Failure With Preserved Ejection Fraction: National Heart, Lung, and Blood Institute Working Group Summary. Circulation. 2020;141(12):1001-26. Epub 2020/03/24. doi: 10.1161/CIRCULATIONAHA.119.041886. PubMed PMID: 32202936; PMCID: PMC7101072.
11. Paulus WJ, Tschope C. A novel paradigm for heart failure with preserved ejection fraction: comorbidities drive myocardial dysfunction and remodeling through coronary microvascular endothelial inflammation. J Am Coll Cardiol. 2013;62(4):263-71. Epub 2013/05/21. doi: 10.1016/j.jacc.2013.02.092. PubMed PMID: 23684677.
12. D'Elia E, Vaduganathan M, Gori M, Gavazzi A, Butler J, Senni M. Role of biomarkers in cardiac structure phenotyping in heart failure with preserved ejection fraction: critical appraisal and practical use. Eur J Heart Fail. 2015;17(12):1231-9. Epub 2015/10/24. doi: 10.1002/ejhf.430. PubMed PMID: 26493383.
13. Lyle MA, Brozovich FV. HFpEF, a Disease of the Vasculature: A Closer Look at the Other Half. Mayo Clin Proc. 2018;93(9):1305-14. Epub 2018/08/02. doi: 10.1016/j.mayocp.2018.05.001. PubMed PMID: 30064827.
14. Shah SJ. Precision Medicine for Heart Failure with Preserved Ejection Fraction: An Overview. J Cardiovasc Transl Res. 2017;10(3):233-44. Epub 2017/06/07. doi: 10.1007/s12265-017-9756-y. PubMed PMID: 28585183; PMCID: PMC5540576.
15. Dunlay SM, Roger VL, Redfield MM. Epidemiology of heart failure with preserved ejection fraction. Nat Rev Cardiol. 2017;14(10):591-602. Epub 2017/05/12. doi: 10.1038/nrcardio.2017.65. PubMed PMID: 28492288.
16. Lam CSP, Arnott C, Beale AL, Chandramouli C, Hilfiker-Kleiner D, Kaye DM, Ky B, Santema BT, Sliwa K, Voors AA. Sex differences in heart failure. Eur Heart J. 2019;40(47):3859-68c. Epub 2019/12/05. doi: 10.1093/eurheartj/ehz835. PubMed PMID: 31800034.
17. Owan TE, Hodge DO, Herges RM, Jacobsen SJ, Roger VL, Redfield MM. Trends in prevalence and outcome of heart failure with preserved ejection fraction. N Engl J Med. 2006;355(3):251-9. Epub 2006/07/21. doi: 10.1056/NEJMoa052256. PubMed PMID: 16855265.
18. Shah SJ, Kitzman DW, Borlaug BA, van Heerebeek L, Zile MR, Kass DA, Paulus WJ. Phenotype-Specific Treatment of Heart Failure With Preserved Ejection Fraction: A Multiorgan Roadmap. Circulation. 2016;134(1):73-90. Epub 2016/07/01. doi: 10.1161/CIRCULATIONAHA.116.021884. PubMed PMID: 27358439; PMCID: PMC4930115.

19. Zile MR, Baicu CF, Ikonomidis JS, Stroud RE, Nietert PJ, Bradshaw AD, Slater R, Palmer BM, Van Buren P, Meyer M, Redfield MM, Bull DA, Granzier HL, LeWinter MM. Myocardial stiffness in patients with heart failure and a preserved ejection fraction: contributions of collagen and titin. Circulation. 2015;131(14):1247-59. Epub 2015/02/01. doi: 10.1161/CIRCULATIONAHA.114.013215. PubMed PMID: 25637629; PMCID: PMC4390480.
20. Juilliere Y, Venner C, Filippetti L, Popovic B, Huttin O, Selton-Suty C. Heart failure with preserved ejection fraction: A systemic disease linked to multiple comorbidities, targeting new therapeutic options. Arch Cardiovasc Dis. 2018;111(12):766-81. Epub 2018/07/02. doi: 10.1016/j.acvd.2018.04.007. PubMed PMID: 29960837.
21. Pandey A, Parashar A, Kumbhani D, Agarwal S, Garg J, Kitzman D, Levine B, Drazner M, Berry J. Exercise training in patients with heart failure and preserved ejection fraction: meta-analysis of randomized control trials. Circ Heart Fail. 2015;8(1):33-40. Epub 2014/11/18. doi: 10.1161/CIRCHEARTFAILURE.114.001615. PubMed PMID: 25399909; PMCID: PMC4792111.
22. Kitzman DW, Brubaker PH, Morgan TM, Stewart KP, Little WC. Exercise training in older patients with heart failure and preserved ejection fraction: a randomized, controlled, single-blind trial. Circ Heart Fail. 2010;3(6):659-67. Epub 2010/09/21. doi: 10.1161/CIRCHEARTFAILURE.110.958785. PubMed PMID: 20852060; PMCID: PMC3065299.
23. Kitzman DW, Brubaker P, Morgan T, Haykowsky M, Hundley G, Kraus WE, Eggebeen J, Nicklas BJ. Effect of Caloric Restriction or Aerobic Exercise Training on Peak Oxygen Consumption and Quality of Life in Obese Older Patients With Heart Failure With Preserved Ejection Fraction: A Randomized Clinical Trial. JAMA. 2016;315(1):36-46. Epub 2016/01/10. doi: 10.1001/jama.2015.17346. PubMed PMID: 26746456; PMCID: PMC4787295.
24. Dieberg G, Ismail H, Giallauria F, Smart NA. Clinical outcomes and cardiovascular responses to exercise training in heart failure patients with preserved ejection fraction: a systematic review and meta-analysis. J Appl Physiol (1985). 2015;119(6):726-33. Epub 2015/03/10. doi: 10.1152/japplphysiol.00904.2014. PubMed PMID: 25749444.
25. Angadi SS, Jarrett CL, Sherif M, Gaesser GA, Mookadam F. The effect of exercise training on biventricular myocardial strain in heart failure with preserved ejection fraction. ESC Heart Fail. 2017;4(3):356-9. Epub 2017/08/05. doi: 10.1002/ehf2.12149. PubMed PMID: 28772048; PMCID: PMC5542728.
26. Sanz J, Sanchez-Quintana D, Bossone E, Bogaard HJ, Naeije R. Anatomy, Function, and Dysfunction of the Right Ventricle: JACC State-of-the-Art Review. J Am Coll Cardiol. 2019;73(12):1463-82. Epub 2019/03/30. doi: 10.1016/j.jacc.2018.12.076. PubMed PMID: 30922478.
27. Bellofiore A, Chesler NC. Methods for measuring right ventricular function and hemodynamic coupling with the pulmonary vasculature. Ann Biomed Eng. 2013;41(7):1384-98. Epub 2013/02/21. doi: 10.1007/s10439-013-0752-3. PubMed PMID: 23423705; PMCID: PMC3679286.

28. Raina A, Meeran T. Right Ventricular Dysfunction and Its Contribution to Morbidity and Mortality in Left Ventricular Heart Failure. Curr Heart Fail Rep. 2018;15(2):94-105. Epub 2018/02/23. doi: 10.1007/s11897-018-0378-8. PubMed PMID: 29468529.
29. Gorter TM, van Veldhuisen DJ, Bauersachs J, Borlaug BA, Celutkiene J, Coats AJS, Crespo-Leiro MG, Guazzi M, Harjola VP, Heymans S, Hill L, Lainscak M, Lam CSP, Lund LH, Lyon AR, Mebazaa A, Mueller C, Paulus WJ, Pieske B, Piepoli MF, Ruschitzka F, Rutten FH, Seferovic PM, Solomon SD, Shah SJ, Triposkiadis F, Wachter R, Tschope C, de Boer RA. Right heart dysfunction and failure in heart failure with preserved ejection fraction: mechanisms and management. Position statement on behalf of the Heart Failure Association of the European Society of Cardiology. Eur J Heart Fail. 2018;20(1):16-37. Epub 2017/10/19. doi: 10.1002/ejhf.1029. PubMed PMID: 29044932.
30. Berglund F, Pina P, Herrera CJ. Right ventricle in heart failure with preserved ejection fraction. Heart. 2020;106(23):1798-804. Epub 2020/09/09. doi: 10.1136/heartjnl-2020-317342. PubMed PMID: 32895314.
31. Gorter TM, Hoendermis ES, van Veldhuisen DJ, Voors AA, Lam CS, Geelhoed B, Willems TP, van Melle JP. Right ventricular dysfunction in heart failure with preserved ejection fraction: a systematic review and meta-analysis. Eur J Heart Fail. 2016;18(12):1472-87. Epub 2016/09/22. doi: 10.1002/ejhf.630. PubMed PMID: 27650220.
32. Melenovsky V, Hwang SJ, Lin G, Redfield MM, Borlaug BA. Right heart dysfunction in heart failure with preserved ejection fraction. Eur Heart J. 2014;35(48):3452-62. Epub 2014/05/31. doi: 10.1093/eurheartj/ehu193. PubMed PMID: 24875795; PMCID: PMC4425842.
33. Mohammed SF, Hussain I, AbouEzzeddine OF, Takahama H, Kwon SH, Forfia P, Roger VL, Redfield MM. Right ventricular function in heart failure with preserved ejection fraction: a community-based study. Circulation. 2014;130(25):2310-20. Epub 2014/11/14. doi: 10.1161/CIRCULATIONAHA.113.008461. PubMed PMID: 25391518; PMCID: PMC4276536.
34. Obokata M, Reddy YNV, Melenovsky V, Pislaru S, Borlaug BA. Deterioration in right ventricular structure and function over time in patients with heart failure and preserved ejection fraction. Eur Heart J. 2019;40(8):689-97. Epub 2018/12/14. doi: 10.1093/eurheartj/ehy809. PubMed PMID: 30544228; PMCID: PMC7963126.
35. Ghio S, Raineri C, Scelsi L, Asanin M, Polovina M, Seferovic P. Pulmonary hypertension and right ventricular remodeling in HFpEF and HFrEF. Heart Fail Rev. 2020;25(1):85-91. Epub 2019/06/15. doi: 10.1007/s10741-019-09810-4. PubMed PMID: 31197562.
36. Garg P, Assadi H, Jones R, Chan WB, Metherall P, Thomas R, van der Geest R, Swift AJ, Al-Mohammad A. Left ventricular fibrosis and hypertrophy are associated with mortality in heart failure with preserved ejection fraction. Sci Rep. 2021;11(1):617. Epub 2021/01/14. doi: 10.1038/s41598-020-79729-6. PubMed PMID: 33436786; PMCID: PMC7804435.

37. Harada D, Asanoi H, Noto T, Takagawa J. The impact of right ventricular dysfunction on the effectiveness of beta-blockers in heart failure with preserved ejection fraction. J Cardiol. 2020;76(4):325-34. Epub 2020/06/02. doi: 10.1016/j.jjcc.2020.05.001. PubMed PMID: 32475652.
38. Stein GY, Ben-Gal T, Kremer A, Bental T, Alon D, Korenfeld R, Yedidia I, Porter A, Abramson E, Sagie A, Fuchs S. Gender-related differences in hospitalized heart failure patients. Eur J Heart Fail. 2013;15(7):734-41. Epub 2013/02/20. doi: 10.1093/eurjhf/hft024. PubMed PMID: 23419512.
39. Scantlebury DC, Borlaug BA. Why are women more likely than men to develop heart failure with preserved ejection fraction? Curr Opin Cardiol. 2011;26(6):562-8. Epub 2011/10/14. doi: 10.1097/HCO.0b013e32834b7faf. PubMed PMID: 21993357.
40. Prabhavathi K, Selvi KT, Poornima KN, Sarvanan A. Role of biological sex in normal cardiac function and in its disease outcome - a review. J Clin Diagn Res. 2014;8(8):BE01-4. Epub 2014/10/11. doi: 10.7860/JCDR/2014/9635.4771. PubMed PMID: 25302188; PMCID: PMC4190707.
41. Zhao Z, Wang H, Jessup JA, Lindsey SH, Chappell MC, Groban L. Role of estrogen in diastolic dysfunction. Am J Physiol Heart Circ Physiol. 2014;306(5):H628-40. Epub 2014/01/15. doi: 10.1152/ajpheart.00859.2013. PubMed PMID: 24414072; PMCID: PMC3949059.
42. Dworatzek E, Baczko I, Kararigas G. Effects of aging on cardiac extracellular matrix in men and women. Proteomics Clin Appl. 2016;10(1):84-91. Epub 2015/08/19. doi: 10.1002/prca.201500031. PubMed PMID: 26280680.
43. Virani SS, Alonso A, Benjamin EJ, Bittencourt MS, Callaway CW, Carson AP, Chamberlain AM, Chang AR, Cheng S, Delling FN, Djousse L, Elkind MSV, Ferguson JF, Fornage M, Khan SS, Kissela BM, Knutson KL, Kwan TW, Lackland DT, Lewis TT, Lichtman JH, Longenecker CT, Loop MS, Lutsey PL, Martin SS, Matsushita K, Moran AE, Mussolino ME, Perak AM, Rosamond WD, Roth GA, Sampson UKA, Satou GM, Schroeder EB, Shah SH, Shay CM, Spartano NL, Stokes A, Tirschwell DL, VanWagner LB, Tsao CW, American Heart Association Council on E, Prevention Statistics C, Stroke Statistics S. Heart Disease and Stroke Statistics-2020 Update: A Report From the American Heart Association. Circulation. 2020;141(9):e139-e596. Epub 2020/01/30. doi: 10.1161/CIR.0000000000000757. PubMed PMID: 31992061.
44. Redfield MM, Jacobsen SJ, Burnett JC, Jr., Mahoney DW, Bailey KR, Rodeheffer RJ. Burden of systolic and diastolic ventricular dysfunction in the community: appreciating the scope of the heart failure epidemic. JAMA. 2003;289(2):194-202. Epub 2003/01/09. doi: 10.1001/jama.289.2.194. PubMed PMID: 12517230.
45. Sotomi Y, Hikoso S, Nakatani D, Mizuno H, Okada K, Dohi T, Kitamura T, Sunaga A, Kida H, Oeun B, Sato T, Komukai S, Tamaki S, Yano M, Hayashi T, Nakagawa A, Nakagawa Y, Yasumura Y, Yamada T, Sakata Y, Investigators PU-H. Sex Differences in Heart Failure With Preserved Ejection Fraction. J Am Heart Assoc. 2021;10(5):e018574. Epub 2021/02/24. doi: 10.1161/JAHA.120.018574. PubMed PMID: 33619973; PMCID: PMC8174270.

46. Diaz-Canestro C, Montero D. Female sex-specific curtailment of left ventricular volume and mass in HFpEF patients with high end-diastolic filling pressure. J Hum Hypertens. 2021;35(3):296-9. Epub 2020/08/12. doi: 10.1038/s41371-020-00394-3. PubMed PMID: 32778747.
47. Chahal H, Johnson C, Tandri H, Jain A, Hundley WG, Barr RG, Kawut SM, Lima JA, Bluemke DA. Relation of cardiovascular risk factors to right ventricular structure and function as determined by magnetic resonance imaging (results from the multi-ethnic study of atherosclerosis). Am J Cardiol. 2010;106(1):110-6. Epub 2010/07/09. doi: 10.1016/j.amjcard.2010.02.022. PubMed PMID: 20609657; PMCID: PMC2901248.
48. Kawut SM, Lima JA, Barr RG, Chahal H, Jain A, Tandri H, Praestgaard A, Bagiella E, Kizer JR, Johnson WC, Kronmal RA, Bluemke DA. Sex and race differences in right ventricular structure and function: the multi-ethnic study of atherosclerosis-right ventricle study. Circulation. 2011;123(22):2542-51. Epub 2011/06/08. doi: 10.1161/CIRCULATIONAHA.110.985515. PubMed PMID: 21646505; PMCID: PMC3111939.
49. Ventetuolo CE, Ouyang P, Bluemke DA, Tandri H, Barr RG, Bagiella E, Cappola AR, Bristow MR, Johnson C, Kronmal RA, Kizer JR, Lima JA, Kawut SM. Sex hormones are associated with right ventricular structure and function: The MESA-right ventricle study. Am J Respir Crit Care Med. 2011;183(5):659-67. Epub 2010/10/05. doi: 10.1164/rccm.201007-1027OC. PubMed PMID: 20889903; PMCID: PMC3081282.
50. Hahn VS, Yanek LR, Vaishnav J, Ying W, Vaidya D, Lee YZJ, Riley SJ, Subramanya V, Brown EE, Hopkins CD, Ononogbu S, Perzel Mandell K, Halushka MK, Steenbergen C, Jr., Rosenberg AZ, Tedford RJ, Judge DP, Shah SJ, Russell SD, Kass DA, Sharma K. Endomyocardial Biopsy Characterization of Heart Failure With Preserved Ejection Fraction and Prevalence of Cardiac Amyloidosis. JACC Heart Fail. 2020;8(9):712-24. Epub 2020/07/13. doi: 10.1016/j.jchf.2020.04.007. PubMed PMID: 32653448; PMCID: PMC7604801.
51. Spinale FG, Frangogiannis NG, Hinz B, Holmes JW, Kassiri Z, Lindsey ML. Crossing Into the Next Frontier of Cardiac Extracellular Matrix Research. Circ Res. 2016;119(10):1040-5. Epub 2016/10/30. doi: 10.1161/CIRCRESAHA.116.309916. PubMed PMID: 27789578; PMCID: PMC5123693.
52. Su MY, Lin LY, Tseng YH, Chang CC, Wu CK, Lin JL, Tseng WY. CMR-verified diffuse myocardial fibrosis is associated with diastolic dysfunction in HFpEF. JACC Cardiovasc Imaging. 2014;7(10):991-7. Epub 2014/09/23. doi: 10.1016/j.jcmg.2014.04.022. PubMed PMID: 25240451.
53. Manabe I, Shindo T, Nagai R. Gene expression in fibroblasts and fibrosis: involvement in cardiac hypertrophy. Circ Res. 2002;91(12):1103-13. Epub 2002/12/14. doi: 10.1161/01.res.0000046452.67724.b8. PubMed PMID: 12480810.
54. Hinderer S, Schenke-Layland K. Cardiac fibrosis - A short review of causes and therapeutic strategies. Adv Drug Deliv Rev. 2019;146:77-82. Epub 2019/06/04. doi: 10.1016/j.addr.2019.05.011. PubMed PMID: 31158407.

55. Travers JG, Kamal FA, Robbins J, Yutzey KE, Blaxall BC. Cardiac Fibrosis: The Fibroblast Awakens. Circ Res. 2016;118(6):1021-40. Epub 2016/03/19. doi: 10.1161/CIRCRESAHA.115.306565. PubMed PMID: 26987915; PMCID: PMC4800485.
56. Kong P, Christia P, Frangogiannis NG. The pathogenesis of cardiac fibrosis. Cell Mol Life Sci. 2014;71(4):549-74. Epub 2013/05/08. doi: 10.1007/s00018-013-1349-6. PubMed PMID: 23649149; PMCID: PMC3769482.
57. Krebber MM, van Dijk CGM, Vernooij RWM, Brandt MM, Emter CA, Rau CD, Fledderus JO, Duncker DJ, Verhaar MC, Cheng C, Joles JA. Matrix Metalloproteinases and Tissue Inhibitors of Metalloproteinases in Extracellular Matrix Remodeling during Left Ventricular Diastolic Dysfunction and Heart Failure with Preserved Ejection Fraction: A Systematic Review and Meta-Analysis. Int J Mol Sci. 2020;21(18). Epub 2020/09/18. doi: 10.3390/ijms21186742. PubMed PMID: 32937927; PMCID: PMC7555240.
58. Yan C, Boyd DD. Regulation of matrix metalloproteinase gene expression. J Cell Physiol. 2007;211(1):19-26. Epub 2006/12/15. doi: 10.1002/jcp.20948. PubMed PMID: 17167774.
59. Loffredo FS, Nikolova AP, Pancoast JR, Lee RT. Heart failure with preserved ejection fraction: molecular pathways of the aging myocardium. Circ Res. 2014;115(1):97-107. Epub 2014/06/22. doi: 10.1161/CIRCRESAHA.115.302929. PubMed PMID: 24951760; PMCID: PMC4094348.
60. Nadadur RD, Umar S, Wong G, Eghbali M, Iorga A, Matori H, Partow-Navid R, Eghbali M. Reverse right ventricular structural and extracellular matrix remodeling by estrogen in severe pulmonary hypertension. J Appl Physiol (1985). 2012;113(1):149-58. Epub 2012/05/26. doi: 10.1152/japplphysiol.01349.2011. PubMed PMID: 22628376; PMCID: PMC3404831.
61. Walker CJ, Schroeder ME, Aguado BA, Anseth KS, Leinwand LA. Matters of the heart: Cellular sex differences. J Mol Cell Cardiol. 2021;160:42-55. Epub 2021/06/25. doi: 10.1016/j.yjmcc.2021.04.010. PubMed PMID: 34166708; PMCID: PMC8571046.
62. Moore L, Fan D, Basu R, Kandalam V, Kassiri Z. Tissue inhibitor of metalloproteinases (TIMPs) in heart failure. Heart Fail Rev. 2012;17(4-5):693-706. Epub 2011/07/01. doi: 10.1007/s10741-011-9266-y. PubMed PMID: 21717224.
63. Vincenti MP. The matrix metalloproteinase (MMP) and tissue inhibitor of metalloproteinase (TIMP) genes. Transcriptional and posttranscriptional regulation, signal transduction and cell-type-specific expression. Methods Mol Biol. 2001;151:121-48. Epub 2001/02/24. doi: 10.1385/1-59259-046-2:121. PubMed PMID: 11217296.
64. Liu P, Sun M, Sader S. Matrix metalloproteinases in cardiovascular disease. Canadian Journal of Cardiology. 2006;22:25B-30B. doi: 10.1016/s0828-282x(06)70983-7.
65. Deschamps AM, Spinale FG. Pathways of matrix metalloproteinase induction in heart failure: bioactive molecules and transcriptional regulation.

Cardiovasc Res. 2006;69(3):666-76. Epub 2006/01/24. doi: 10.1016/j.cardiores.2005.10.004. PubMed PMID: 16426590.
66. Spinale FG. Matrix metalloproteinases: regulation and dysregulation in the failing heart. Circ Res. 2002;90(5):520-30. Epub 2002/03/23. doi: 10.1161/01.res.0000013290.12884.a3. PubMed PMID: 11909815.
67. DeLeon-Pennell KY, Meschiari CA, Jung M, Lindsey ML. Matrix Metalloproteinases in Myocardial Infarction and Heart Failure. Prog Mol Biol Transl Sci. 2017;147:75-100. Epub 2017/04/18. doi: 10.1016/bs.pmbts.2017.02.001. PubMed PMID: 28413032; PMCID: PMC5576003.
68. Martos R, Baugh J, Ledwidge M, O'Loughlin C, Conlon C, Patle A, Donnelly SC, McDonald K. Diastolic heart failure: evidence of increased myocardial collagen turnover linked to diastolic dysfunction. Circulation. 2007;115(7):888-95. Epub 2007/02/07. doi: 10.1161/CIRCULATIONAHA.106.638569. PubMed PMID: 17283265.
69. Ward M, Yeganegi A, Baicu CF, Bradshaw A, Spinale FG, Zile MR, Richardson WJ. Ensemble Machine Learning Model Identifies HFpEF Patients from Matrix-Related Plasma Biomarkers. Am J Physiol Heart Circ Physiol. 2022. Epub 2022/03/12. doi: 10.1152/ajpheart.00497.2021. PubMed PMID: 35275763.
70. Sweeney M, Corden B, Cook SA. Targeting cardiac fibrosis in heart failure with preserved ejection fraction: mirage or miracle? EMBO Mol Med. 2020;12(10):e10865. Epub 2020/09/22. doi: 10.15252/emmm.201910865. PubMed PMID: 32955172; PMCID: PMC7539225.
71. Glasenapp A, Derlin K, Gutberlet M, Hess A, Ross TL, Wester HJ, Bengel FM, Thackeray JT. Molecular Imaging of Inflammation and Fibrosis in Pressure Overload Heart Failure. Circ Res. 2021;129(3):369-82. Epub 2021/06/03. doi: 10.1161/CIRCRESAHA.120.318539. PubMed PMID: 34074134.
72. Bing R, Cavalcante JL, Everett RJ, Clavel MA, Newby DE, Dweck MR. Imaging and Impact of Myocardial Fibrosis in Aortic Stenosis. JACC Cardiovasc Imaging. 2019;12(2):283-96. Epub 2019/02/09. doi: 10.1016/j.jcmg.2018.11.026. PubMed PMID: 30732723; PMCID: PMC6361867.
73. Everett RJ, Tastet L, Clavel MA, Chin CWL, Capoulade R, Vassiliou VS, Kwiecinski J, Gomez M, van Beek EJR, White AC, Prasad SK, Larose E, Tuck C, Semple S, Newby DE, Pibarot P, Dweck MR. Progression of Hypertrophy and Myocardial Fibrosis in Aortic Stenosis: A Multicenter Cardiac Magnetic Resonance Study. Circ Cardiovasc Imaging. 2018;11(6):e007451. Epub 2018/06/20. doi: 10.1161/CIRCIMAGING.117.007451. PubMed PMID: 29914867; PMCID: PMC6023592.
74. Treibel TA, Kozor R, Schofield R, Benedetti G, Fontana M, Bhuva AN, Sheikh A, Lopez B, Gonzalez A, Manisty C, Lloyd G, Kellman P, Diez J, Moon JC. Reverse Myocardial Remodeling Following Valve Replacement in Patients With Aortic Stenosis. J Am Coll Cardiol. 2018;71(8):860-71. Epub 2018/02/24. doi: 10.1016/j.jacc.2017.12.035. PubMed PMID: 29471937; PMCID: PMC5821681.
75. Laviades C, Varo N, Fernandez J, Mayor G, Gil MJ, Monreal I, Diez J. Abnormalities of the extracellular degradation of collagen type I in essential

hypertension. Circulation. 1998;98(6):535-40. Epub 1998/08/26. doi: 10.1161/01.cir.98.6.535. PubMed PMID: 9714110.
76. Marchesi C, Dentali F, Nicolini E, Maresca AM, Tayebjee MH, Franz M, Guasti L, Venco A, Schiffrin EL, Lip GY, Grandi AM. Plasma levels of matrix metalloproteinases and their inhibitors in hypertension: a systematic review and meta-analysis. J Hypertens. 2012;30(1):3-16. Epub 2011/12/03. doi: 10.1097/HJH.0b013e32834d249a. PubMed PMID: 22134384.
77. Heymans S, Schroen B, Vermeersch P, Milting H, Gao F, Kassner A, Gillijns H, Herijgers P, Flameng W, Carmeliet P, Van de Werf F, Pinto YM, Janssens S. Increased cardiac expression of tissue inhibitor of metalloproteinase-1 and tissue inhibitor of metalloproteinase-2 is related to cardiac fibrosis and dysfunction in the chronic pressure-overloaded human heart. Circulation. 2005;112(8):1136-44. Epub 2005/08/17. doi: 10.1161/CIRCULATIONAHA.104.516963. PubMed PMID: 16103240.
78. Yarbrough WM, Mukherjee R, Stroud RE, Rivers WT, Oelsen JM, Dixon JA, Eckhouse SR, Ikonomidis JS, Zile MR, Spinale FG. Progressive induction of left ventricular pressure overload in a large animal model elicits myocardial remodeling and a unique matrix signature. J Thorac Cardiovasc Surg. 2012;143(1):215-23. Epub 2011/11/08. doi: 10.1016/j.jtcvs.2011.09.032. PubMed PMID: 22056365; PMCID: PMC3241904.
79. Nagatomo Y, Carabello BA, Coker ML, McDermott PJ, Nemoto S, Hamawaki M, Spinale FG. Differential effects of pressure or volume overload on myocardial MMP levels and inhibitory control. Am J Physiol Heart Circ Physiol. 2000;278(1):H151-61. Epub 2000/01/25. doi: 10.1152/ajpheart.2000.278.1.H151. PubMed PMID: 10644594.
80. Skrbic B, Bjornstad JL, Marstein HS, Carlson CR, Sjaastad I, Nygard S, Bjornstad S, Christensen G, Tonnessen T. Differential regulation of extracellular matrix constituents in myocardial remodeling with and without heart failure following pressure overload. Matrix Biol. 2013;32(2):133-42. Epub 2012/12/12. doi: 10.1016/j.matbio.2012.11.011. PubMed PMID: 23220517.
81. Patel RB, Li E, Benefield BC, Swat SA, Polsinelli VB, Carr JC, Shah SJ, Markl M, Collins JD, Freed BH. Diffuse right ventricular fibrosis in heart failure with preserved ejection fraction and pulmonary hypertension. ESC Heart Fail. 2020;7(1):253-63. Epub 2020/01/07. doi: 10.1002/ehf2.12565. PubMed PMID: 31903694; PMCID: PMC7083501.
82. Tadic M, Cuspidi C. Obesity and heart failure with preserved ejection fraction: a paradox or something else? Heart Fail Rev. 2019;24(3):379-85. Epub 2019/01/06. doi: 10.1007/s10741-018-09766-x. PubMed PMID: 30610456.
83. Salerni S, Di Francescomarino S, Cadeddu C, Acquistapace F, Maffei S, Gallina S. The different role of sex hormones on female cardiovascular physiology and function: not only oestrogens. Eur J Clin Invest. 2015;45(6):634-45. Epub 2015/04/08. doi: 10.1111/eci.12447. PubMed PMID: 25845675.
84. Grohé C, Kahlert S, Löbbert K, Stimpel M, Karas RH, Vetter H, Neyses L. Cardiac myocytes and fibroblasts contain functional estrogen receptors 1. FEBS Letters. 1997;416(1):107-12. doi: 10.1016/s0014-5793(97)01179-4.

85. Sabbatini AR, Kararigas G. Menopause-Related Estrogen Decrease and the Pathogenesis of HFpEF: JACC Review Topic of the Week. J Am Coll Cardiol. 2020;75(9):1074-82. Epub 2020/03/07. doi: 10.1016/j.jacc.2019.12.049. PubMed PMID: 32138968.
86. Lin YY, Chen JS, Wu XB, Shyu WC, Chaunchaiyakul R, Zhao XL, Kuo CH, Cheng YJ, Yang AL, Lee SD. Combined effects of 17beta-estradiol and exercise training on cardiac apoptosis in ovariectomized rats. PLoS One. 2018;13(12):e0208633. Epub 2018/12/21. doi: 10.1371/journal.pone.0208633. PubMed PMID: 30571718; PMCID: PMC6301615.
87. Lin YY, Hong Y, Zhou MC, Huang HL, Shyu WC, Chen JS, Ting H, Cheng YJ, Yang AL, Lee SD. Exercise training attenuates cardiac inflammation and fibrosis in hypertensive ovariectomized rats. J Appl Physiol (1985). 2020;128(4):1033-43. Epub 2020/03/13. doi: 10.1152/japplphysiol.00844.2019. PubMed PMID: 32163326.
88. Xu Y. Estrogen modulation of left ventricular remodeling in the aged heart. Cardiovascular Research. 2003;57(2):388-94. doi: 10.1016/s0008-6363(02)00705-8.
89. Dantas AP, Tostes RC, Fortes ZB, Costa SG, Nigro D, Carvalho MH. In vivo evidence for antioxidant potential of estrogen in microvessels of female spontaneously hypertensive rats. Hypertension. 2002;39(2 Pt 2):405-11. Epub 2002/03/08. doi: 10.1161/hy0202.102993. PubMed PMID: 11882581.
90. Dubey RK, Gillespie DG, Jackson EK, Keller PJ. 17Beta-estradiol, its metabolites, and progesterone inhibit cardiac fibroblast growth. Hypertension. 1998;31(1 Pt 2):522-8. Epub 1998/02/07. doi: 10.1161/01.hyp.31.1.522. PubMed PMID: 9453356.
91. Luczak ED, Leinwand LA. Sex-based cardiac physiology. Annu Rev Physiol. 2009;71:1-18. Epub 2008/10/03. doi: 10.1146/annurev.physiol.010908.163156. PubMed PMID: 18828746.
92. Murphy E. Estrogen signaling and cardiovascular disease. Circ Res. 2011;109(6):687-96. Epub 2011/09/03. doi: 10.1161/CIRCRESAHA.110.236687. PubMed PMID: 21885836; PMCID: PMC3398381.
93. Regitz-Zagrosek V, Kararigas G. Mechanistic Pathways of Sex Differences in Cardiovascular Disease. Physiol Rev. 2017;97(1):1-37. Epub 2016/11/04. doi: 10.1152/physrev.00021.2015. PubMed PMID: 27807199.
94. Fliegner D, Schubert C, Penkalla A, Witt H, Kararigas G, Dworatzek E, Staub E, Martus P, Ruiz Noppinger P, Kintscher U, Gustafsson JA, Regitz-Zagrosek V. Female sex and estrogen receptor-beta attenuate cardiac remodeling and apoptosis in pressure overload. Am J Physiol Regul Integr Comp Physiol. 2010;298(6):R1597-606. Epub 2010/04/09. doi: 10.1152/ajpregu.00825.2009. PubMed PMID: 20375266.
95. Westphal C, Schubert C, Prelle K, Penkalla A, Fliegner D, Petrov G, Regitz-Zagrosek V. Effects of estrogen, an ERalpha agonist and raloxifene on pressure overload induced cardiac hypertrophy. PLoS One. 2012;7(12):e50802. Epub 2012/12/12. doi: 10.1371/journal.pone.0050802. PubMed PMID: 23227210; PMCID: PMC3515519.

96. Goldstein J, Sites CK, Toth MJ. Progesterone stimulates cardiac muscle protein synthesis via receptor-dependent pathway. Fertil Steril. 2004;82(2):430-6. Epub 2004/08/11. doi: 10.1016/j.fertnstert.2004.03.018. PubMed PMID: 15302294.
97. Furuta M, Fukushima A, Chiba S, Sano A, Akema T, Kimura F, Funabashi T. Progesterone receptor immunoreactivity in the brains of ovariectomized aged rats. Neuroreport. 2010;21(11):777-81. Epub 2010/06/18. doi: 10.1097/WNR.0b013e32833c5b6f. PubMed PMID: 20555290.
98. Hosoda M, Yamamoto M, Nakano K, Hatanaka KC, Takakuwa E, Hatanaka Y, Matsuno Y, Yamashita H. Differential expression of progesterone receptor, FOXA1, GATA3, and p53 between pre- and postmenopausal women with estrogen receptor-positive breast cancer. Breast Cancer Res Treat. 2014;144(2):249-61. Epub 2014/02/20. doi: 10.1007/s10549-014-2867-0. PubMed PMID: 24549642.
99. Meza-Munoz DE, Fajardo ME, Perez-Luque EL, Malacara JM. Factors associated with estrogen receptors-alpha (ER-alpha) and -beta (ER-beta) and progesterone receptor abundance in obese and non obese pre- and post-menopausal women. Steroids. 2006;71(6):498-503. Epub 2006/03/29. doi: 10.1016/j.steroids.2006.01.011. PubMed PMID: 16566954.
100. Lee SR, Heo JH, Jo SL, Kim G, Kim SJ, Yoo HJ, Lee KP, Kwun HJ, Shin HJ, Baek IJ, Hong EJ. Progesterone receptor membrane component 1 reduces cardiac steatosis and lipotoxicity via activation of fatty acid oxidation and mitochondrial respiration. Sci Rep. 2021;11(1):8781. Epub 2021/04/24. doi: 10.1038/s41598-021-88251-2. PubMed PMID: 33888830; PMCID: PMC8062525.
101. Nakamura H, Kurokawa J, Bai CX, Asada K, Xu J, Oren RV, Zhu ZI, Clancy CE, Isobe M, Furukawa T. Progesterone regulates cardiac repolarization through a nongenomic pathway: an in vitro patch-clamp and computational modeling study. Circulation. 2007;116(25):2913-22. Epub 2007/12/07. doi: 10.1161/CIRCULATIONAHA.107.702407. PubMed PMID: 18056530.
102. Molinari C, Battaglia A, Grossini E, Mary DA, Surico N, Vacca G. Effect of progesterone on peripheral blood flow in prepubertal female anesthetized pigs. J Vasc Res. 2001;38(6):569-77. Epub 2001/12/12. doi: 10.1159/000051093. PubMed PMID: 11740156.
103. Kuebler JF, Jarrar D, Bland KI, Rue L, 3rd, Wang P, Chaudry IH. Progesterone administration after trauma and hemorrhagic shock improves cardiovascular responses. Crit Care Med. 2003;31(6):1786-93. Epub 2003/06/10. doi: 10.1097/01.CCM.0000063441.41446.23. PubMed PMID: 12794421.
104. Pecins-Thompson M, Keller-Wood M. Effects of progesterone on blood pressure, plasma volume, and responses to hypotension. Am J Physiol. 1997;272(1 Pt 2):R377-85. Epub 1997/01/01. doi: 10.1152/ajpregu.1997.272.1.R377. PubMed PMID: 9039032.
105. Drummond CA, Buddny G, Haller ST, Liu J, Yan Y, Xie Z, Malhotra D, Shapiro JI, Tian J. Gender differences in the development of uremic cardiomyopathy following partial nephrectomy: Role of progesterone. J Hypertens (Los Angel). 2013;2. Epub 2014/01/10. doi: 10.4172/2167-1095.1000109. PubMed PMID: 24404431; PMCID: PMC3880896.

106. Lim WK, Wren B, Jepson N, Roy S, Caplan G. Effect of hormone replacement therapy on left ventricular hypertrophy. The American Journal of Cardiology. 1999;83(7):1132-4. doi: 10.1016/s0002-9149(99)00029-6.
107. Hulley S, Grady D, Bush T, Furberg C, Herrington D, Riggs B, Vittinghoff E. Randomized trial of estrogen plus progestin for secondary prevention of coronary heart disease in postmenopausal women. Heart and Estrogen/progestin Replacement Study (HERS) Research Group. JAMA. 1998;280(7):605-13. Epub 1998/08/26. doi: 10.1001/jama.280.7.605. PubMed PMID: 9718051.
108. Rossouw JE, Anderson GL, Prentice RL, LaCroix AZ, Kooperberg C, Stefanick ML, Jackson RD, Beresford SA, Howard BV, Johnson KC, Kotchen JM, Ockene J, Writing Group for the Women's Health Initiative I. Risks and benefits of estrogen plus progestin in healthy postmenopausal women: principal results From the Women's Health Initiative randomized controlled trial. JAMA. 2002;288(3):321-33. Epub 2002/07/19. doi: 10.1001/jama.288.3.321. PubMed PMID: 12117397.
109. Hermsmeyer RK, Thompson TL, Pohost GM, Kaski JC. Cardiovascular effects of medroxyprogesterone acetate and progesterone: a case of mistaken identity? Nat Clin Pract Cardiovasc Med. 2008;5(7):387-95. Epub 2008/06/04. doi: 10.1038/ncpcardio1234. PubMed PMID: 18521110.
110. Arias-Loza PA, Hu K, Schafer A, Bauersachs J, Quaschning T, Galle J, Jazbutyte V, Neyses L, Ertl G, Fritzemeier KH, Hegele-Hartung C, Pelzer T. Medroxyprogesterone acetate but not drospirenone ablates the protective function of 17 beta-estradiol in aldosterone salt-treated rats. Hypertension. 2006;48(5):994-1001. Epub 2006/09/27. doi: 10.1161/01.HYP.0000242482.57186.e8. PubMed PMID: 17000933.
111. Prentice RL, Aragaki AK, Chlebowski RT, Rossouw JE, Anderson GL, Stefanick ML, Wactawski-Wende J, Kuller LH, Wallace R, Johnson KC, Shadyab AH, Gass M, Manson JE. Randomized Trial Evaluation of the Benefits and Risks of Menopausal Hormone Therapy Among Women 50-59 Years of Age. Am J Epidemiol. 2021;190(3):365-75. Epub 2020/10/08. doi: 10.1093/aje/kwaa210. PubMed PMID: 33025002; PMCID: PMC8086238.
112. Dworatzek E, Mahmoodzadeh S, Schriever C, Kusumoto K, Kramer L, Santos G, Fliegner D, Leung YK, Ho SM, Zimmermann WH, Lutz S, Regitz-Zagrosek V. Sex-specific regulation of collagen I and III expression by 17beta-Estradiol in cardiac fibroblasts: role of estrogen receptors. Cardiovasc Res. 2019;115(2):315-27. Epub 2018/07/18. doi: 10.1093/cvr/cvy185. PubMed PMID: 30016401; PMCID: PMC6933535.
113. Stienen S, Ferreira JP, Kobayashi M, Preud'homme G, Dobre D, Machu JL, Duarte K, Bresso E, Devignes MD, Andres NL, Girerd N, Aakhus S, Ambrosio G, Rocca HB, Fontes-Carvalho R, Fraser AG, van Heerebeek L, de Keulenaer G, Marino P, McDonald K, Mebazaa A, Papp Z, Raddino R, Tschope C, Paulus WJ, Zannad F, Rossignol P. Sex differences in circulating proteins in heart failure with preserved ejection fraction. Biol Sex Differ. 2020;11(1):47. Epub 2020/08/25. doi: 10.1186/s13293-020-00322-7. PubMed PMID: 32831121; PMCID: PMC7444077.
114. Mercier I, Colombo F, Mader S, Calderone A. Ovarian hormones induce TGF-β3 and fibronectin mRNAs but exhibit a disparate action on cardiac

fibroblast proliferation. Cardiovascular Research. 2002;53(3):728-39. doi: 10.1016/s0008-6363(01)00525-9.
115. Iorga A, Li J, Sharma S, Umar S, Bopassa JC, Nadadur RD, Centala A, Ren S, Saito T, Toro L, Wang Y, Stefani E, Eghbali M. Rescue of Pressure Overload-Induced Heart Failure by Estrogen Therapy. J Am Heart Assoc. 2016;5(1). Epub 2016/01/24. doi: 10.1161/JAHA.115.002482. PubMed PMID: 26802104; PMCID: PMC4859364.
116. Pedram A, Razandi M, Lubahn D, Liu J, Vannan M, Levin ER. Estrogen inhibits cardiac hypertrophy: role of estrogen receptor-beta to inhibit calcineurin. Endocrinology. 2008;149(7):3361-9. Epub 2008/03/29. doi: 10.1210/en.2008-0133. PubMed PMID: 18372323; PMCID: PMC2453079.
117. Tofovic PS, Zhang X, Petrusevska G. Progesterone inhibits vascular remodeling and attenuates monocrotaline-induced pulmonary hypertension in estrogen-deficient rats. Prilozi. 2009;30(1):25-44. Epub 2009/09/09. PubMed PMID: 19736529.
118. Umar S, Iorga A, Matori H, Nadadur RD, Li J, Maltese F, van der Laarse A, Eghbali M. Estrogen rescues preexisting severe pulmonary hypertension in rats. Am J Respir Crit Care Med. 2011;184(6):715-23. Epub 2011/06/28. doi: 10.1164/rccm.201101-0078OC. PubMed PMID: 21700911; PMCID: PMC3208600.
119. Rose BA, Force T, Wang Y. Mitogen-activated protein kinase signaling in the heart: angels versus demons in a heart-breaking tale. Physiol Rev. 2010;90(4):1507-46. Epub 2010/10/21. doi: 10.1152/physrev.00054.2009. PubMed PMID: 20959622; PMCID: PMC3808831.
120. Huang H, Petkova SB, Cohen AW, Bouzahzah B, Chan J, Zhou JN, Factor SM, Weiss LM, Krishnamachary M, Mukherjee S, Wittner M, Kitsis RN, Pestell RG, Lisanti MP, Albanese C, Tanowitz HB. Activation of transcription factors AP-1 and NF-kappa B in murine Chagasic myocarditis. Infect Immun. 2003;71(5):2859-67. Epub 2003/04/22. doi: 10.1128/iai.71.5.2859-2867.2003. PubMed PMID: 12704159; PMCID: PMC153290.
121. Zhang W, Elimban V, Nijjar MS, Gupta SK, Dhalla NS. Role of mitogen-activated protein kinase in cardiac hypertrophy and heart failure. Exp Clin Cardiol. 2003;8(4):173-83. Epub 2003/01/01. PubMed PMID: 19649217; PMCID: PMC2719157.
122. Bueno OF, De Windt LJ, Tymitz KM, Witt SA, Kimball TR, Klevitsky R, Hewett TE, Jones SP, Lefer DJ, Peng CF, Kitsis RN, Molkentin JD. The MEK1-ERK1/2 signaling pathway promotes compensated cardiac hypertrophy in transgenic mice. EMBO J. 2000;19(23):6341-50. Epub 2000/12/02. doi: 10.1093/emboj/19.23.6341. PubMed PMID: 11101507; PMCID: PMC305855.
123. Mutlak M, Schlesinger-Laufer M, Haas T, Shofti R, Ballan N, Lewis YE, Zuler M, Zohar Y, Caspi LH, Kehat I. Extracellular signal-regulated kinase (ERK) activation preserves cardiac function in pressure overload induced hypertrophy. Int J Cardiol. 2018;270:204-13. Epub 2018/06/03. doi: 10.1016/j.ijcard.2018.05.068. PubMed PMID: 29857938.
124. Li XM, Ma YT, Yang YN, Liu F, Chen BD, Han W, Zhang JF, Gao XM. Downregulation of survival signalling pathways and increased apoptosis in the

transition of pressure overload-induced cardiac hypertrophy to heart failure. Clin Exp Pharmacol Physiol. 2009;36(11):1054-61. Epub 2009/07/02. doi: 10.1111/j.1440-1681.2009.05243.x. PubMed PMID: 19566828.
125. Wu W, Muchir A, Shan J, Bonne G, Worman HJ. Mitogen-activated protein kinase inhibitors improve heart function and prevent fibrosis in cardiomyopathy caused by mutation in lamin A/C gene. Circulation. 2011;123(1):53-61. Epub 2010/12/22. doi: 10.1161/CIRCULATIONAHA.110.970673. PubMed PMID: 21173351; PMCID: PMC3061281.
126. Davis RJ. Signal transduction by the JNK group of MAP kinases. Cell. 2000;103(2):239-52. Epub 2000/11/01. doi: 10.1016/s0092-8674(00)00116-1. PubMed PMID: 11057897.
127. Petrich BG, Eloff BC, Lerner DL, Kovacs A, Saffitz JE, Rosenbaum DS, Wang Y. Targeted activation of c-Jun N-terminal kinase in vivo induces restrictive cardiomyopathy and conduction defects. J Biol Chem. 2004;279(15):15330-8. Epub 2004/01/27. doi: 10.1074/jbc.M314142200. PubMed PMID: 14742426.
128. Tachibana H, Perrino C, Takaoka H, Davis RJ, Naga Prasad SV, Rockman HA. JNK1 is required to preserve cardiac function in the early response to pressure overload. Biochem Biophys Res Commun. 2006;343(4):1060-6. Epub 2006/04/04. doi: 10.1016/j.bbrc.2006.03.065. PubMed PMID: 16579967.
129. Kyoi S, Otani H, Matsuhisa S, Akita Y, Tatsumi K, Enoki C, Fujiwara H, Imamura H, Kamihata H, Iwasaka T. Opposing effect of p38 MAP kinase and JNK inhibitors on the development of heart failure in the cardiomyopathic hamster. Cardiovasc Res. 2006;69(4):888-98. Epub 2005/12/27. doi: 10.1016/j.cardiores.2005.11.015. PubMed PMID: 16375879.
130. Pan Y, Wang Y, Zhao Y, Peng K, Li W, Wang Y, Zhang J, Zhou S, Liu Q, Li X, Cai L, Liang G. Inhibition of JNK phosphorylation by a novel curcumin analog prevents high glucose-induced inflammation and apoptosis in cardiomyocytes and the development of diabetic cardiomyopathy. Diabetes. 2014;63(10):3497-511. Epub 2014/05/23. doi: 10.2337/db13-1577. PubMed PMID: 24848068.
131. Mitchell S, Ota A, Foster W, Zhang B, Fang Z, Patel S, Nelson SF, Horvath S, Wang Y. Distinct gene expression profiles in adult mouse heart following targeted MAP kinase activation. Physiol Genomics. 2006;25(1):50-9. Epub 2005/12/22. doi: 10.1152/physiolgenomics.00224.2005. PubMed PMID: 16368875.
132. Garg D, Ng SSM, Baig KM, Driggers P, Segars J. Progesterone-Mediated Non-Classical Signaling. Trends Endocrinol Metab. 2017;28(9):656-68. Epub 2017/06/28. doi: 10.1016/j.tem.2017.05.006. PubMed PMID: 28651856.
133. Hester J, Ventetuolo C, Lahm T. Sex, Gender, and Sex Hormones in Pulmonary Hypertension and Right Ventricular Failure. Compr Physiol. 2019;10(1):125-70. Epub 2019/12/20. doi: 10.1002/cphy.c190011. PubMed PMID: 31853950; PMCID: PMC7338988.
134. Asavasupreechar T, Saito R, Miki Y, Edwards DP, Boonyaratanakornkit V, Sasano H. Systemic distribution of progesterone receptor subtypes in human

tissues. J Steroid Biochem Mol Biol. 2020;199:105599. Epub 2020/01/29. doi: 10.1016/j.jsbmb.2020.105599. PubMed PMID: 31991170.
135. Boonyaratanakornkit V, Scott MP, Ribon V, Sherman L, Anderson SM, Maller JL, Miller WT, Edwards DP. Progesterone Receptor Contains a Proline-Rich Motif that Directly Interacts with SH3 Domains and Activates c-Src Family Tyrosine Kinases. Molecular Cell. 2001;8(2):269-80. doi: 10.1016/s1097-2765(01)00304-5.
136. Lee HW, Eghbali-Webb M. Estrogen enhances proliferative capacity of cardiac fibroblasts by estrogen receptor- and mitogen-activated protein kinase-dependent pathways. J Mol Cell Cardiol. 1998;30(7):1359-68. Epub 1998/08/26. doi: 10.1006/jmcc.1998.0699. PubMed PMID: 9710804.
137. Molero L, Garcia-Duran M, Diaz-Recasens J, Rico L, Casado S, Lopez-Farre A. Expression of estrogen receptor subtypes and neuronal nitric oxide synthase in neutrophils from women and men Regulation by estrogen. Cardiovascular Research. 2002;56(1):43-51. doi: 10.1016/s0008-6363(02)00505-9.
138. You Y, Tan W, Guo Y, Luo M, Shang FF, Xia Y, Luo S. Progesterone promotes endothelial nitric oxide synthase expression through enhancing nuclear progesterone receptor-SP-1 formation. Am J Physiol Heart Circ Physiol. 2020;319(2):H341-H8. Epub 2020/07/04. doi: 10.1152/ajpheart.00206.2020. PubMed PMID: 32618512.
139. Mahmoodzadeh S, Dworatzek E, Fritschka S, Pham TH, Regitz-Zagrosek V. 17beta-Estradiol inhibits matrix metalloproteinase-2 transcription via MAP kinase in fibroblasts. Cardiovasc Res. 2010;85(4):719-28. Epub 2009/10/29. doi: 10.1093/cvr/cvp350. PubMed PMID: 19861308; PMCID: PMC2819834.
140. Spinale FG. Myocardial matrix remodeling and the matrix metalloproteinases: influence on cardiac form and function. Physiol Rev. 2007;87(4):1285-342. Epub 2007/10/12. doi: 10.1152/physrev.00012.2007. PubMed PMID: 17928585.
141. O'Hagan RC, Tozer RG, Symons M, McCormick F, Hassel JA. The activity of the Ets transcription factor PEA3 is regulated by two distinct MAPK cascades Oncogene. 1996;13(6):1323-33.
142. Chang WC, Hung JJ. Functional role of post-translational modifications of Sp1 in tumorigenesis. J Biomed Sci. 2012;19(1):94. Epub 2012/11/15. doi: 10.1186/1423-0127-19-94. PubMed PMID: 23148884; PMCID: PMC3503885.
143. Ghio S, Guazzi M, Scardovi AB, Klersy C, Clemenza F, Carluccio E, Temporelli PL, Rossi A, Faggiano P, Traversi E, Vriz O, Dini FL, all i. Different correlates but similar prognostic implications for right ventricular dysfunction in heart failure patients with reduced or preserved ejection fraction. Eur J Heart Fail. 2017;19(7):873-9. Epub 2016/11/20. doi: 10.1002/ejhf.664. PubMed PMID: 27860029.
144. Ghio S, Temporelli PL, Klersy C, Simioniuc A, Girardi B, Scelsi L, Rossi A, Cicoira M, Tarro Genta F, Dini FL. Prognostic relevance of a non-invasive evaluation of right ventricular function and pulmonary artery pressure in patients with chronic heart failure. Eur J Heart Fail. 2013;15(4):408-14. Epub 2013/01/12. doi: 10.1093/eurjhf/hfs208. PubMed PMID: 23307814.

145. Guazzi M, Naeije R, Arena R, Corra U, Ghio S, Forfia P, Rossi A, Cahalin LP, Bandera F, Temporelli P. Echocardiography of Right Ventriculoarterial Coupling Combined With Cardiopulmonary Exercise Testing to Predict Outcome in Heart Failure. Chest. 2015;148(1):226-34. Epub 2015/01/31. doi: 10.1378/chest.14-2065. PubMed PMID: 25633590.
146. Olver TD, Edwards JC, Jurrissen TJ, Veteto AB, Jones JL, Gao C, Rau C, Warren CM, Klutho PJ, Alex L, Ferreira-Nichols SC, Ivey JR, Thorne PK, McDonald KS, Krenz M, Baines CP, Solaro RJ, Wang Y, Ford DA, Domeier TL, Padilla J, Rector RS, Emter CA. Western Diet-Fed, Aortic-Banded Ossabaw Swine: A Preclinical Model of Cardio-Metabolic Heart Failure. JACC Basic Transl Sci. 2019;4(3):404-21. Epub 2019/07/18. doi: 10.1016/j.jacbts.2019.02.004. PubMed PMID: 31312763; PMCID: PMC6610000.
147. Emter CA, Tharp DL, Ivey JR, Ganjam VK, Bowles DK. Low-intensity interval exercise training attenuates coronary vascular dysfunction and preserves Ca(2)(+)-sensitive K(+) current in miniature swine with LV hypertrophy. Am J Physiol Heart Circ Physiol. 2011;301(4):H1687-94. Epub 2011/08/16. doi: 10.1152/ajpheart.00610.2011. PubMed PMID: 21841018; PMCID: PMC3197434.
148. Fleenor BS, Ouyang A, Olver TD, Hiemstra JA, Cobb MS, Minervini G, Emter CA. Saxagliptin Prevents Increased Coronary Vascular Stiffness in Aortic-Banded Mini Swine. Hypertension. 2018;72(2):466-75. Epub 2018/06/13. doi: 10.1161/HYPERTENSIONAHA.118.10993. PubMed PMID: 29891647.
149. Marshall KD, Muller BN, Krenz M, Hanft LM, McDonald KS, Dellsperger KC, Emter CA. Heart failure with preserved ejection fraction: chronic low-intensity interval exercise training preserves myocardial O2 balance and diastolic function. J Appl Physiol (1985). 2013;114(1):131-47. Epub 2012/10/30. doi: 10.1152/japplphysiol.01059.2012. PubMed PMID: 23104696; PMCID: PMC3544520.
150. Olver TD, Edwards JC, Ferguson BS, Hiemstra JA, Thorne PK, Hill MA, Laughlin MH, Emter CA. Chronic interval exercise training prevents BKCa channel-mediated coronary vascular dysfunction in aortic-banded miniswine. J Appl Physiol (1985). 2018;125(1):86-96. Epub 2018/03/30. doi: 10.1152/japplphysiol.01138.2017. PubMed PMID: 29596016; PMCID: PMC6086974.
151. Olver TD, Hiemstra JA, Edwards JC, Schachtman TR, Heesch CM, Fadel PJ, Laughlin MH, Emter CA. Loss of Female Sex Hormones Exacerbates Cerebrovascular and Cognitive Dysfunction in Aortic Banded Miniswine Through a Neuropeptide Y-Ca(2+)-Activated Potassium Channel-Nitric Oxide Mediated Mechanism. J Am Heart Assoc. 2017;6(11). Epub 2017/11/02. doi: 10.1161/JAHA.117.007409. PubMed PMID: 29089345; PMCID: PMC5721796.
152. Olver TD, Klakotskaia D, Ferguson BS, Hiemstra JA, Schachtman TR, Laughlin MH, Emter CA. Carotid Artery Vascular Mechanics Serve as Biomarkers of Cognitive Dysfunction in Aortic-Banded Miniature Swine That Can Be Treated With an Exercise Intervention. J Am Heart Assoc. 2016;5(5). Epub 2016/05/22. doi: 10.1161/JAHA.116.003248. PubMed PMID: 27207966; PMCID: PMC4889197.

153. Ouyang A, Olver TD, Emter CA, Fleenor BS. Chronic exercise training prevents coronary artery stiffening in aortic-banded miniswine: role of perivascular adipose-derived advanced glycation end products. J Appl Physiol (1985). 2019;127(3):816-27. Epub 2019/07/12. doi: 10.1152/japplphysiol.00146.2019. PubMed PMID: 31295062; PMCID: PMC6766711.
154. Olver TD, Edwards, J.C., Jurrissen, T.J., Veteto, A.B., Jones, J.L., Gao, C., Rau, C., Warren, C.M., Klutho, P.J., Alex, L., Ferreira-Nichols, S.C., Ivey, J.R, Thorne, P.K., McDonald, K.S., Krenz, M., Baines, C.P., Solaro, R.J., Wang, Y., Ford, D.A., Domeier, T. L., Padilla, J., Rector, R.S., and Emter, C.A. . Western Diet-fed, Aortic-Banded Ossabaw Swine: A Pre-Clinical Model of Cardio-Metabolic Heart Failure. Journal of the American College of Cardiology - Basic to Translational Science. 2019;4(3):404-21. Epub Feb. 2019. doi: 10.1016/j.jacbts.2019.02.004.
155. Olver TD, Grunewald ZI, Jurrissen TJ, MacPherson REK, LeBlanc PJ, Schnurbusch TR, Czajkowski AM, Laughlin MH, Rector RS, Bender SB, Walters EM, Emter CA, Padilla J. Microvascular insulin resistance in skeletal muscle and brain occurs early in the development of juvenile obesity in pigs. American journal of physiology Regulatory, integrative and comparative physiology. 2018;314(2):R252-R64. Epub 2017/11/17. doi: 10.1152/ajpregu.00213.2017. PubMed PMID: 29141949; PMCID: PMC5867673.
156. Padilla J, Jenkins NT, Lee S, Zhang H, Cui J, Zuidema MY, Zhang C, Hill MA, Perfield JW, 2nd, Ibdah JA, Booth FW, Davis JW, Laughlin MH, Rector RS. Vascular transcriptional alterations produced by juvenile obesity in Ossabaw swine. Physiol Genomics. 2013;45(11):434-46. Epub 2013/04/18. doi: 10.1152/physiolgenomics.00038.2013. PubMed PMID: 23592636; PMCID: PMC3680784.
157. Panasevich MR, Meers GM, Linden MA, Booth FW, Perfield JW, 2nd, Fritsche KL, Wankhade UD, Chintapalli SV, Shankar K, Ibdah JA, Rector RS. High-fat, high-fructose, high-cholesterol feeding causes severe NASH and cecal microbiota dysbiosis in juvenile Ossabaw swine. Am J Physiol Endocrinol Metab. 2018;314(1):E78-E92. Epub 2017/09/14. doi: 10.1152/ajpendo.00015.2017. PubMed PMID: 28899857; PMCID: PMC5866386.
158. Toedebusch RG, Roberts MD, Wells KD, Company JM, Kanosky KM, Padilla J, Jenkins NT, Perfield JW, 2nd, Ibdah JA, Booth FW, Rector RS. Unique transcriptomic signature of omental adipose tissue in Ossabaw swine: a model of childhood obesity. Physiol Genomics. 2014;46(10):362-75. Epub 2014/03/20. doi: 10.1152/physiolgenomics.00172.2013. PubMed PMID: 24642759; PMCID: PMC4042183.
159. Vieira-Potter VJ, Lee S, Bayless DS, Scroggins RJ, Welly RJ, Fleming NJ, Smith TN, Meers GM, Hill MA, Rector RS, Padilla J. Disconnect between adipose tissue inflammation and cardiometabolic dysfunction in Ossabaw pigs. Obesity (Silver Spring). 2015;23(12):2421-9. Epub 2015/11/03. doi: 10.1002/oby.21252. PubMed PMID: 26524201; PMCID: PMC4701582.
160. Hiemstra JA, Veteto AB, Lambert MD, Olver TD, Ferguson BS, McDonald KS, Emter CA, Domeier TL. Chronic low-intensity exercise attenuates

cardiomyocyte contractile dysfunction and impaired adrenergic responsiveness in aortic-banded mini-swine. J Appl Physiol (1985). 2018;124(4):1034-44. Epub 2018/01/24. doi: 10.1152/japplphysiol.00840.2017. PubMed PMID: 29357490; PMCID: PMC5972453.
161. Olver TD, Hiemstra JA, Edwards JC, Ferguson BS, Laughlin MH, Emter CA. The protective role of sex hormones in females and exercise prehabilitation in males on sternotomy-induced cranial hypoperfusion in aortic banded mini-swine. J Appl Physiol (1985). 2017;122(3):423-9. Epub 2016/12/03. doi: 10.1152/japplphysiol.00817.2016. PubMed PMID: 27909230; PMCID: PMC5401953.
162. Olver TD, Klakotskaia D, Ferguson BS, Hiemstra JA, Schachtman TR, Laughlin MH, Emter CA. Carotid Artery Vascular Mechanics Serve as Biomarkers of Cognitive Dysfunction in Aortic-Banded Miniature Swine That Can Be Treated With an Exercise Intervention. Journal of the American Heart Association. 2016;5(5). doi: 10.1161/jaha.116.003248.
163. Hayward GC, LeBlanc PJ, Emter CA, Nyarko JNK, Mousseau DD, MacPherson REK, Olver TD. Female Sex Hormones and Cardiac Pressure Overload Independently Contribute to the Cardiogenic Dementia Profile in Yucatan Miniature Swine. Front Cardiovasc Med. 2019;6:129. Epub 2019/09/26. doi: 10.3389/fcvm.2019.00129. PubMed PMID: 31552273; PMCID: PMC6746895.
164. Ouyang A, Olver TD, Emter CA, Fleenor BS. Chronic exercise training prevents coronary artery stiffening in aortic-banded miniswine: Role of perivascular adipose-derived advanced glycation end products. J Appl Physiol (1985). 2019. Epub 2019/07/12. doi: 10.1152/japplphysiol.00146.2019. PubMed PMID: 31295062.
165. Alvino VV, Fernandez-Jimenez R, Rodriguez-Arabaolaza I, Slater S, Mangialardi G, Avolio E, Spencer H, Culliford L, Hassan S, Sueiro Ballesteros L, Herman A, Ayaon-Albarran A, Galan-Arriola C, Sanchez-Gonzalez J, Hennessey H, Delmege C, Ascione R, Emanueli C, Angelini GD, Ibanez B, Madeddu P. Transplantation of Allogeneic Pericytes Improves Myocardial Vascularization and Reduces Interstitial Fibrosis in a Swine Model of Reperfused Acute Myocardial Infarction. J Am Heart Assoc. 2018;7(2). Epub 2018/01/24. doi: 10.1161/JAHA.117.006727. PubMed PMID: 29358198; PMCID: PMC5850145.
166. Lee JH, Gao C, Peng G, Greer C, Ren S, Wang Y, Xiao X. Analysis of transcriptome complexity through RNA sequencing in normal and failing murine hearts. Circ Res. 2011;109(12):1332-41. Epub 2011/10/29. doi: 10.1161/CIRCRESAHA.111.249433. PubMed PMID: 22034492; PMCID: 3243366.
167. Gao C, Ren S, Lee JH, Qiu J, Chapski DJ, Rau CD, Zhou Y, Abdellatif M, Nakano A, Vondriska TM, Xiao X, Fu XD, Chen JN, Wang Y. RBFox1-mediated RNA splicing regulates cardiac hypertrophy and heart failure. J Clin Invest. 2016;126(1):195-206. Epub 2015/12/01. doi: 10.1172/JCI84015. PubMed PMID: 26619120; PMCID: PMC4701548.
168. Gao C, Howard-Quijano K, Rau C, Takamiya T, Song Y, Shivkumar K, Wang Y, Mahajan A. Inflammatory and apoptotic remodeling in autonomic

nervous system following myocardial infarction. PLoS One. 2017;12(5):e0177750. Epub 2017/05/26. doi: 10.1371/journal.pone.0177750. PubMed PMID: 28542617; PMCID: PMC5436752.
169. Patro R, Duggal G, Love MI, Irizarry RA, Kingsford C. Salmon provides fast and bias-aware quantification of transcript expression. Nat Methods. 2017;14(4):417-9. Epub 2017/03/07. doi: 10.1038/nmeth.4197. PubMed PMID: 28263959; PMCID: PMC5600148.
170. Vincent Q. Vu. ggbiplot: A ggplot2 based biplot. R package version 0.55. http://github.com/vqv/ggbiplot 2011. Available from: http://github.com/vqv/ggbiplot.
171. Love MI, Huber W, Anders S. Moderated estimation of fold change and dispersion for RNA-seq data with DESeq2. Genome Biol. 2014;15(12):550. Epub 2014/12/18. doi: 10.1186/s13059-014-0550-8. PubMed PMID: 25516281; PMCID: PMC4302049.
172. Ben-Ari Fuchs S, Lieder I, Stelzer G, Mazor Y, Buzhor E, Kaplan S, Bogoch Y, Plaschkes I, Shitrit A, Rappaport N, Kohn A, Edgar R, Shenhav L, Safran M, Lancet D, Guan-Golan Y, Warshawsky D, Shtrichman R. GeneAnalytics: An Integrative Gene Set Analysis Tool for Next Generation Sequencing, RNAseq and Microarray Data. OMICS. 2016;20(3):139-51. Epub 2016/03/18. doi: 10.1089/omi.2015.0168. PubMed PMID: 26983021; PMCID: PMC4799705.
173. Jenkins NT, Padilla J, Thorne PK, Martin JS, Rector RS, Davis JW, Laughlin MH. Transcriptome-wide RNA sequencing analysis of rat skeletal muscle feed arteries. I. Impact of obesity. J Appl Physiol (1985). 2014;116(8):1017-32. Epub 2014/01/18. doi: 10.1152/japplphysiol.01233.2013. PubMed PMID: 24436298; PMCID: PMC4035791.
174. Emter CA, Bowles DK. Store-operated Ca(2+) entry is not essential for PDGF-BB induced phenotype modulation in rat aortic smooth muscle. Cell Calcium. 2010;48(1):10-8. Epub 2010/07/14. doi: 10.1016/j.ceca.2010.06.001. PubMed PMID: 20619453; PMCID: PMC2929302.
175. Livak KJ, Schmittgen TD. Analysis of relative gene expression data using real-time quantitative PCR and the 2(-Delta Delta C(T)) Method. Methods. 2001;25(4):402-8. Epub 2002/02/16. doi: 10.1006/meth.2001.1262. PubMed PMID: 11846609.
176. Hiemstra JA, Gutierrez-Aguilar M, Marshall KD, McCommis KS, Zgoda PJ, Cruz-Rivera N, Jenkins NT, Krenz M, Domeier TL, Baines CP, Emter CA. A new twist on an old idea part 2: cyclosporine preserves normal mitochondrial but not cardiomyocyte function in mini-swine with compensated heart failure. Physiol Rep. 2014;2(6). Epub 2014/06/26. doi: 10.14814/phy2.12050. PubMed PMID: 24963034; PMCID: PMC4208639.
177. Emter CA, Baines CP. Low-intensity aerobic interval training attenuates pathological left ventricular remodeling and mitochondrial dysfunction in aortic-banded miniature swine. Am J Physiol Heart Circ Physiol. 2010;299(5):H1348-56. Epub 2010/09/08. doi: 10.1152/ajpheart.00578.2010. PubMed PMID: 20817828; PMCID: PMC2993221.

178. Du B, Ouyang A, Eng JS, Fleenor BS. Aortic perivascular adipose-derived interleukin-6 contributes to arterial stiffness in low-density lipoprotein receptor deficient mice. American Journal of Physiology-Heart and Circulatory Physiology. 2015;308(11):H1382-H90.
179. Toth M, Fridman R. Assessment of Gelatinases (MMP-2 and MMP-9 by Gelatin Zymography. Methods Mol Med. 2001;57:163-74. Epub 2001/01/01. doi: 10.1385/1-59259-136-1:163. PubMed PMID: 21340898; PMCID: PMC3845455.
180. de Winter JCF. Using the Student's t-test with extremely small sample sizes. Practical Assessment, Research & Evaluation. 2013;18:1-12.
181. Silva KAS, Leary EV, Olver TD, Domeier TL, Padilla J, Rector RS, Emter CA. Tissue-specific small heat shock protein 20 activation is not associated with traditional autophagy markers in Ossabaw swine with cardiometabolic heart failure. Am J Physiol Heart Circ Physiol. 2020;319(5):H1036-H43. Epub 2020/09/19. doi: 10.1152/ajpheart.00580.2020. PubMed PMID: 32946285.
182. Curran-Everett D, Benos DJ. Guidelines for reporting statistics in journals published by the American Physiological Society. American journal of physiology Regulatory, integrative and comparative physiology. 2004;287(2):R247-9. Epub 2005/03/25. doi: 10.1152/ajpregu.00346.2004. PubMed PMID: 15789454.
183. Williams JL, Hathaway CA, Kloster KL, Layne BH. Low power, type II errors, and other statistical problems in recent cardiovascular research. Am J Physiol. 1997;273(1 Pt 2):H487-93. Epub 1997/07/01. doi: 10.1152/ajpheart.1997.273.1.H487. PubMed PMID: 9249522.
184. Frangogiannis NG. The Extracellular Matrix in Ischemic and Nonischemic Heart Failure. Circ Res. 2019;125(1):117-46. Epub 2019/06/21. doi: 10.1161/CIRCRESAHA.119.311148. PubMed PMID: 31219741; PMCID: PMC6588179.
185. Wang J, Chen H, Seth A, McCulloch CA. Mechanical force regulation of myofibroblast differentiation in cardiac fibroblasts. Am J Physiol Heart Circ Physiol. 2003;285(5):H1871-81. Epub 2003/07/05. doi: 10.1152/ajpheart.00387.2003. PubMed PMID: 12842814.
186. Yin FC, Spurgeon HA, Rakusan K, Weisfeldt ML, Lakatta EG. Use of tibial length to quantify cardiac hypertrophy: application in the aging rat. Am J Physiol. 1982;243(6):H941-7. Epub 1982/12/01. doi: 10.1152/ajpheart.1982.243.6.H941. PubMed PMID: 6216817.
187. Chirinos JA, Segers P, De Buyzere ML, Kronmal RA, Raja MW, De Bacquer D, Claessens T, Gillebert TC, St John-Sutton M, Rietzschel ER. Left ventricular mass: allometric scaling, normative values, effect of obesity, and prognostic performance. Hypertension. 2010;56(1):91-8. Epub 2010/05/12. doi: 10.1161/HYPERTENSIONAHA.110.150250. PubMed PMID: 20458004; PMCID: PMC3121539.
188. Litwin SE. Cardiac "Morphomics": Do We Need to Measure LV Mass and Geometry in Everyone? JACC Cardiovascular imaging. 2015;8(9):1016-8. Epub 2015/09/19. doi: 10.1016/j.jcmg.2015.06.008. PubMed PMID: 26381764.
189. Shi F, Sottile J. MT1-MMP regulates the turnover and endocytosis of extracellular matrix fibronectin. J Cell Sci. 2011;124(Pt 23):4039-50. Epub

2011/12/14. doi: 10.1242/jcs.087858. PubMed PMID: 22159414; PMCID: PMC3244985.
190. Arpino V, Brock M, Gill SE. The role of TIMPs in regulation of extracellular matrix proteolysis. Matrix Biol. 2015;44-46:247-54. Epub 2015/03/26. doi: 10.1016/j.matbio.2015.03.005. PubMed PMID: 25805621.
191. Brew K, Nagase H. The tissue inhibitors of metalloproteinases (TIMPs): an ancient family with structural and functional diversity. Biochim Biophys Acta. 2010;1803(1):55-71. Epub 2010/01/19. doi: 10.1016/j.bbamcr.2010.01.003. PubMed PMID: 20080133; PMCID: PMC2853873.
192. Hahn VS, Knutsdottir H, Luo X, Bedi K, Margulies KB, Haldar SM, Stolina M, Yin J, Khakoo AY, Vaishnav J, Bader JS, Kass DA, Sharma K. Myocardial Gene Expression Signatures in Human Heart Failure with Preserved Ejection Fraction. Circulation. 2020. Epub 2020/10/30. doi: 10.1161/CIRCULATIONAHA.120.050498. PubMed PMID: 33118835.
193. Zieman SJ, Melenovsky V, Kass DA. Mechanisms, pathophysiology, and therapy of arterial stiffness. Arteriosclerosis, thrombosis, and vascular biology. 2005;25(5):932-43.
194. Garner T, Ouyang A, Berrones AJ, Campbell MS, Du B, Fleenor BS. Sweet potato (Ipomoea batatas) attenuates diet-induced aortic stiffening independent of changes in body composition. Applied Physiology, Nutrition, and Metabolism. 2017;42(8):802-9.
195. Wagenseil JE, Nerurkar NL, Knutsen RH, Okamoto RJ, Li DY, Mecham RP. Effects of elastin haploinsufficiency on the mechanical behavior of mouse arteries. American Journal of Physiology-Heart and Circulatory Physiology. 2005;289(3):H1209-H17.
196. Srivaratharajah K, Coutinho T, deKemp R, Liu P, Haddad H, Stadnick E, Davies RA, Chih S, Dwivedi G, Guo A, Wells GA, Bernick J, Beanlands R, Mielniczuk LM. Reduced Myocardial Flow in Heart Failure Patients With Preserved Ejection Fraction. Circ Heart Fail. 2016;9(7). Epub 2016/07/15. doi: 10.1161/CIRCHEARTFAILURE.115.002562. PubMed PMID: 27413034.
197. Shah SJ, Lam CSP, Svedlund S, Saraste A, Hage C, Tan RS, Beussink-Nelson L, Ljung Faxen U, Fermer ML, Broberg MA, Gan LM, Lund LH. Prevalence and correlates of coronary microvascular dysfunction in heart failure with preserved ejection fraction: PROMIS-HFpEF. Eur Heart J. 2018;39(37):3439-50. Epub 2018/08/31. doi: 10.1093/eurheartj/ehy531. PubMed PMID: 30165580; PMCID: PMC6927847.
198. Taqueti VR, Solomon SD, Shah AM, Desai AS, Groarke JD, Osborne MT, Hainer J, Bibbo CF, Dorbala S, Blankstein R, Di Carli MF. Coronary microvascular dysfunction and future risk of heart failure with preserved ejection fraction. Eur Heart J. 2018;39(10):840-9. Epub 2018/01/03. doi: 10.1093/eurheartj/ehx721. PubMed PMID: 29293969; PMCID: PMC5939665.
199. Gui P, Chao JT, Wu X, Yang Y, Davis GE, Davis MJ. Coordinated regulation of vascular Ca2+ and K+ channels by integrin signaling. Adv Exp Med Biol. 2010;674:69-79. Epub 2010/06/17. doi: 10.1007/978-1-4419-6066-5_7. PubMed PMID: 20549941.

200. Wu X, Yang Y, Gui P, Sohma Y, Meininger GA, Davis GE, Braun AP, Davis MJ. Potentiation of large conductance, Ca2+-activated K+ (BK) channels by alpha5beta1 integrin activation in arteriolar smooth muscle. J Physiol. 2008;586(6):1699-713. Epub 2008/01/26. doi: 10.1113/jphysiol.2007.149500. PubMed PMID: 18218680; PMCID: PMC2375690.
201. Venstrom K, Reichardt L. Beta 8 integrins mediate interactions of chick sensory neurons with laminin-1, collagen IV, and fibronectin. Mol Biol Cell. 1995;6(4):419-31. Epub 1995/04/01. doi: 10.1091/mbc.6.4.419. PubMed PMID: 7542940; PMCID: PMC301201.
202. Ozawa A, Sato Y, Imabayashi T, Uemura T, Takagi J, Sekiguchi K. Molecular Basis of the Ligand Binding Specificity of alphavbeta8 Integrin. J Biol Chem. 2016;291(22):11551-65. Epub 2016/04/02. doi: 10.1074/jbc.M116.719138. PubMed PMID: 27033701; PMCID: PMC4882426.
203. Hayashido Y, Kitano H, Sakaue T, Fujii T, Suematsu M, Sakurai S, Okamoto T. Overexpression of integrin alphav facilitates proliferation and invasion of oral squamous cell carcinoma cells via MEK/ERK signaling pathway that is activated by interaction of integrin alphavbeta8 with type collagen. Int J Oncol. 2014;45(5):1875-82. Epub 2014/09/06. doi: 10.3892/ijo.2014.2642. PubMed PMID: 25190218.
204. Petrich BG, Wang Y. Stress-activated MAP kinases in cardiac remodeling and heart failure; new insights from transgenic studies. Trends Cardiovasc Med. 2004;14(2):50-5. Epub 2004/03/20. doi: 10.1016/j.tcm.2003.11.002. PubMed PMID: 15030789.
205. Wang Y, Su B, Sah VP, Brown JH, Han J, Chien KR. Cardiac hypertrophy induced by mitogen-activated protein kinase kinase 7, a specific activator for c-Jun NH2-terminal kinase in ventricular muscle cells. J Biol Chem. 1998;273(10):5423-6. Epub 1998/04/16. doi: 10.1074/jbc.273.10.5423. PubMed PMID: 9488659.
206. Guazzi M. Pulmonary hypertension in heart failure preserved ejection fraction: prevalence, pathophysiology, and clinical perspectives. Circ Heart Fail. 2014;7(2):367-77. Epub 2014/03/20. doi: 10.1161/CIRCHEARTFAILURE.113.000823. PubMed PMID: 24643889.
207. Medzikovic L, Aryan L, Eghbali M. Connecting sex differences, estrogen signaling, and microRNAs in cardiac fibrosis. J Mol Med (Berl). 2019;97(10):1385-98. Epub 2019/08/27. doi: 10.1007/s00109-019-01833-6. PubMed PMID: 31448389.
208. Mori T, Kai H, Kajimoto H, Koga M, Kudo H, Takayama N, Yasuoka S, Anegawa T, Kai M, Imaizumi T. Enhanced cardiac inflammation and fibrosis in ovariectomized hypertensive rats: a possible mechanism of diastolic dysfunction in postmenopausal women. Hypertens Res. 2011;34(4):496-502. Epub 2011/01/21. doi: 10.1038/hr.2010.261. PubMed PMID: 21248760.
209. Kelly SC, Rau CD, Ouyang A, Thorne PK, Olver TD, Edwards JC, Domeier TL, Padilla J, Grisanti LA, Fleenor BS, Wang Y, Rector RS, Emter CA. The right ventricular transcriptome signature in Ossabaw swine with cardiometabolic heart failure: implications for the coronary vasculature. Physiol Genomics. 2021;53(3):99-115. Epub 2021/01/26. doi:

10.1152/physiolgenomics.00093.2020. PubMed PMID: 33491589; PMCID: PMC7988741.
210. Jurrissen TJ, Olver TD, Winn NC, Grunewald ZI, Lin GS, Hiemstra JA, Edwards JC, Gastecki ML, Welly RJ, Emter CA, Vieira-Potter VJ, Padilla J. Endothelial dysfunction occurs independently of adipose tissue inflammation and insulin resistance in ovariectomized Yucatan miniature-swine. Adipocyte. 2018;7(1):35-44. Epub 2017/12/29. doi: 10.1080/21623945.2017.1405191. PubMed PMID: 29283284; PMCID: PMC5915048.
211. Deschamps AM, Yarbrough WM, Squires CE, Allen RA, McClister DM, Dowdy KB, McLean JE, Mingoia JT, Sample JA, Mukherjee R, Spinale FG. Trafficking of the membrane type-1 matrix metalloproteinase in ischemia and reperfusion: relation to interstitial membrane type-1 matrix metalloproteinase activity. Circulation. 2005;111(9):1166-74. Epub 2005/02/23. doi: 10.1161/01.CIR.0000157149.71297.3A. PubMed PMID: 15723986.
212. Spinale FG, Escobar GP, Mukherjee R, Zavadzkas JA, Saunders SM, Jeffords LB, Leone AM, Beck C, Bouges S, Stroud RE. Cardiac-restricted overexpression of membrane type-1 matrix metalloproteinase in mice: effects on myocardial remodeling with aging. Circ Heart Fail. 2009;2(4):351-60. Epub 2009/10/08. doi: 10.1161/CIRCHEARTFAILURE.108.844845. PubMed PMID: 19808359; PMCID: PMC2743030.
213. Grisanti LA, Talarico JA, Carter RL, Yu JE, Repas AA, Radcliffe SW, Tang HA, Makarewich CA, Houser SR, Tilley DG. beta-Adrenergic receptor-mediated transactivation of epidermal growth factor receptor decreases cardiomyocyte apoptosis through differential subcellular activation of ERK1/2 and Akt. J Mol Cell Cardiol. 2014;72:39-51. Epub 2014/02/26. doi: 10.1016/j.yjmcc.2014.02.009. PubMed PMID: 24566221; PMCID: PMC4037368.
214. Tanner MA, Grisanti LA. A Dual Role for Death Receptor 5 in Regulating Cardiac Fibroblast Function. Front Cardiovasc Med. 2021;8:699102. Epub 2021/09/17. doi: 10.3389/fcvm.2021.699102. PubMed PMID: 34527710; PMCID: PMC8437145.
215. Curran-Everett D, Benos DJ, American Physiological S. Guidelines for reporting statistics in journals published by the American Physiological Society. Am J Physiol Endocrinol Metab. 2004;287(2):E189-91. Epub 2004/07/24. doi: 10.1152/ajpendo.00213.2004. PubMed PMID: 15271643.
216. Kubow KE, Vukmirovic R, Zhe L, Klotzsch E, Smith ML, Gourdon D, Luna S, Vogel V. Mechanical forces regulate the interactions of fibronectin and collagen I in extracellular matrix. Nat Commun. 2015;6:8026. Epub 2015/08/15. doi: 10.1038/ncomms9026. PubMed PMID: 26272817; PMCID: PMC4539566.
217. McDonald JA, Kelley DG, Broekelmann TJ. Role of fibronectin in collagen deposition: Fab' to the gelatin-binding domain of fibronectin inhibits both fibronectin and collagen organization in fibroblast extracellular matrix. J Cell Biol. 1982;92(2):485-92. Epub 1982/02/01. doi: 10.1083/jcb.92.2.485. PubMed PMID: 7061591; PMCID: PMC2112086.
218. Paten JA, Martin CL, Wanis JT, Siadat SM, Figueroa-Navedo AM, Ruberti JW, Deravi LF. Molecular Interactions between Collagen and Fibronectin: A

Reciprocal Relationship that Regulates De Novo Fibrillogenesis. Chem. 2019;5(8):2126-45. doi: 10.1016/j.chempr.2019.05.011.
219. Ghosh AK. Factors involved in the regulation of type I collagen gene expression: implication in fibrosis. Exp Biol Med (Maywood). 2002;227(5):301-14. Epub 2002/04/27. doi: 10.1177/153537020222700502. PubMed PMID: 11976400.
220. Vogel C, Marcotte EM. Insights into the regulation of protein abundance from proteomic and transcriptomic analyses. Nat Rev Genet. 2012;13(4):227-32. Epub 2012/03/14. doi: 10.1038/nrg3185. PubMed PMID: 22411467; PMCID: PMC3654667.
221. Ebeling PR, Atley LM, Guthrie JR, Burger HG, Dennerstein L, Hopper JL, Wark JD. Bone turnover markers and bone density across the menopausal transition. J Clin Endocrinol Metab. 1996;81(9):3366-71. Epub 1996/09/01. doi: 10.1210/jcem.81.9.8784098. PubMed PMID: 8784098.
222. Scariano JK, Garry PJ, Montoya GD, Wilson JM, Baumgartner RN. Critical differences in the serial measurement of three biochemical markers of bone turnover in the sera of pre- and postmenopausal women. Clin Biochem. 2001;34(8):639-44. Epub 2002/02/19. doi: 10.1016/s0009-9120(01)00273-9. PubMed PMID: 11849624.
223. Takahashi M, Kushida K, Hoshino H, Ohishi T, Inoue T. Biochemical markers of bone turnover do not decline after menopause in healthy women. Br J Obstet Gynaecol. 1999;106(5):427-31. Epub 1999/08/03. doi: 10.1111/j.1471-0528.1999.tb08295.x. PubMed PMID: 10430192.
224. Zile MR, Desantis SM, Baicu CF, Stroud RE, Thompson SB, McClure CD, Mehurg SM, Spinale FG. Plasma biomarkers that reflect determinants of matrix composition identify the presence of left ventricular hypertrophy and diastolic heart failure. Circ Heart Fail. 2011;4(3):246-56. Epub 2011/02/26. doi: 10.1161/CIRCHEARTFAILURE.110.958199. PubMed PMID: 21350055; PMCID: PMC4071931.
225. Mani SK, Oyola MG. Progesterone signaling mechanisms in brain and behavior. Front Endocrinol (Lausanne). 2012;3:7. Epub 2012/06/01. doi: 10.3389/fendo.2012.00007. PubMed PMID: 22649404; PMCID: PMC3355960.
226. Tsai CF, Yang SF, Lo CH, Chu HJ, Ueng KC. Role of the ROS-JNK Signaling Pathway in Hypoxia-Induced Atrial Fibrotic Responses in HL-1 Cardiomyocytes. Int J Mol Sci. 2021;22(6). Epub 2021/04/04. doi: 10.3390/ijms22063249. PubMed PMID: 33806765; PMCID: PMC8004875.
227. Ye N, Ding Y, Wild C, Shen Q, Zhou J. Small molecule inhibitors targeting activator protein 1 (AP-1). J Med Chem. 2014;57(16):6930-48. Epub 2014/05/17. doi: 10.1021/jm5004733. PubMed PMID: 24831826; PMCID: PMC4148154.
228. Dixon JA, Spinale FG. Large animal models of heart failure: a critical link in the translation of basic science to clinical practice. Circ Heart Fail. 2009;2(3):262-71. Epub 2009/10/08. doi: 10.1161/CIRCHEARTFAILURE.108.814459. PubMed PMID: 19808348; PMCID: PMC2762217.

229. Douglas WR. Of pigs and men and research: a review of applications and analogies of the pig, sus scrofa, in human medical research. Space Life Sci. 1972;3(3):226-34. doi: 10.1007/BF00928167.
230. Dyson MC, Alloosh M, Vuchetich JP, Mokelke EA, Sturek M. Components of metabolic syndrome and coronary artery disease in female Ossabaw swine fed excess atherogenic diet. Comp Med. 2006;56(1):35-45. Epub 2006/03/09. PubMed PMID: 16521858; PMCID: PMC2930329.
231. Neeb ZP, Edwards JM, Alloosh M, Long X, Mokelke EA, Sturek M. Metabolic syndrome and coronary artery disease in Ossabaw compared with Yucatan swine. Comp Med. 2010;60(4):300-15. Epub 2010/09/08. PubMed PMID: 20819380; PMCID: PMC2930329.
232. Lowe R, Shirley N, Bleackley M, Dolan S, Shafee T. Transcriptomics technologies. PLoS Comput Biol. 2017;13(5):e1005457. Epub 2017/05/26. doi: 10.1371/journal.pcbi.1005457. PubMed PMID: 28545146; PMCID: PMC5436640.
233. Wang Z, Gerstein M, Snyder M. RNA-Seq: a revolutionary tool for transcriptomics. Nat Rev Genet. 2009;10(1):57-63. Epub 2008/11/19. doi: 10.1038/nrg2484. PubMed PMID: 19015660; PMCID: PMC2949280.
234. Khan MA, Yang EY, Nguyen DT, Nabi F, Hinojosa J, Jabel M, Nagueh SF, Graviss EA, Shah DJ. Examining the Relationship and Prognostic Implication of Diabetic Status and Extracellular Matrix Expansion by Cardiac Magnetic Resonance. Circ Cardiovasc Imaging. 2020;13(7):e011000. Epub 2020/07/17. doi: 10.1161/CIRCIMAGING.120.011000. PubMed PMID: 32673493; PMCID: PMC7384549.
235. Shah RV, Abbasi SA, Neilan TG, Hulten E, Coelho-Filho O, Hoppin A, Levitsky L, de Ferranti S, Rhodes ET, Traum A, Goodman E, Feng H, Heydari B, Harris WS, Hoefner DM, McConnell JP, Seethamraju R, Rickers C, Kwong RY, Jerosch-Herold M. Myocardial tissue remodeling in adolescent obesity. J Am Heart Assoc. 2013;2(4):e000279. Epub 2013/08/22. doi: 10.1161/JAHA.113.000279. PubMed PMID: 23963758; PMCID: PMC3828806.
236. van Hoeven KH, Factor SM. A comparison of the pathological spectrum of hypertensive, diabetic, and hypertensive-diabetic heart disease. Circulation. 1990;82(3):848-55. Epub 1990/09/01. doi: 10.1161/01.cir.82.3.848. PubMed PMID: 2394006.
237. Grinnan D, Farr G, Fox A, Sweeney L. The Role of Hyperglycemia and Insulin Resistance in the Development and Progression of Pulmonary Arterial Hypertension. J Diabetes Res. 2016;2016:2481659. Epub 2016/07/05. doi: 10.1155/2016/2481659. PubMed PMID: 27376089; PMCID: PMC4916286.
238. Nunoda S, Genda A, Sugihara N, Nakayama A, Mizuno S, Takeda R. Quantitative approach to the histopathology of the biopsied right ventricular myocardium in patients with diabetes mellitus. Heart Vessels. 1985;1(1):43-7. doi: 10.1007/BF02066486.
239. Tadic M, Ivanovic B, Celic V, Kocabay G. The impact of metabolic syndrome, recently diagnosed diabetes and hypertension on right ventricular remodeling. Is there difference between risk factors? Clin Exp Hypertens. 2014;36(5):295-301. Epub 2013/07/20. doi: 10.3109/10641963.2013.810235. PubMed PMID: 23865506.

240. Paneni F, Gregori M, Tocci G, Palano F, Ciavarella GM, Pignatelli G, Marra A, Sciarretta S, Ferrucci A, Volpe M. Do diabetes, metabolic syndrome or their association equally affect biventricular function? A tissue Doppler study. Hypertens Res. 2013;36(1):36-42. Epub 2012/09/07. doi: 10.1038/hr.2012.137. PubMed PMID: 22951523.
241. Serrano-Ferrer J, Walther G, Crendal E, Vinet A, Dutheil F, Naughton G, Lesourd B, Chapier R, Courteix D, Obert P. Right ventricle free wall mechanics in metabolic syndrome without type-2 diabetes: effects of a 3-month lifestyle intervention program. Cardiovasc Diabetol. 2014;13:116. Epub 2014/11/20. doi: 10.1186/s12933-014-0116-9. PubMed PMID: 25407698; PMCID: PMC4149206.
242. Calamaras TD, Baumgartner RA, Aronovitz MJ, McLaughlin AL, Tam K, Richards DA, Cooper CW, Li N, Baur WE, Qiao X, Wang GR, Davis RJ, Kapur NK, Karas RH, Blanton RM. Mixed lineage kinase-3 prevents cardiac dysfunction and structural remodeling with pressure overload. Am J Physiol Heart Circ Physiol. 2019;316(1):H145-H59. Epub 2018/10/27. doi: 10.1152/ajpheart.00029.2018. PubMed PMID: 30362822; PMCID: PMC6383356.
243. Cook SA, Sugden PH, Clerk A. Activation of c-Jun N-terminal kinases and p38-mitogen-activated protein kinases in human heart failure secondary to ischaemic heart disease. J Mol Cell Cardiol. 1999;31(8):1429-34. Epub 1999/07/29. doi: 10.1006/jmcc.1999.0979. PubMed PMID: 10423341.
244. Craige SM, Chen K, Blanton RM, Keaney JF, Jr., Kant S. JNK and cardiometabolic dysfunction. Biosci Rep. 2019;39(7). Epub 2019/07/05. doi: 10.1042/BSR20190267. PubMed PMID: 31270248; PMCID: PMC6639461.
245. Miksztowicz V, Muzzio ML, Royer M, Prada M, Wikinski R, Schreier L, Berg G. Increased plasma activity of metalloproteinase 2 in women with metabolic syndrome. Metabolism. 2008;57(11):1493-6. Epub 2008/10/23. doi: 10.1016/j.metabol.2008.06.001. PubMed PMID: 18940384.
246. Yadav SS, Singh MK, Dwivedi P, Mandal RK, Usman K, Khattri S, Pant KK. Significance of impaired serum gelatinases activities in metabolic syndrome. Toxicol Int. 2014;21(1):107-11. Epub 2014/04/22. doi: 10.4103/0971-6580.128818. PubMed PMID: 24748744; PMCID: PMC3989907.
247. Shvedova M, Anfinogenova Y, Atochina-Vasserman EN, Schepetkin IA, Atochin DN. c-Jun N-Terminal Kinases (JNKs) in Myocardial and Cerebral Ischemia/Reperfusion Injury. Front Pharmacol. 2018;9:715. Epub 2018/07/22. doi: 10.3389/fphar.2018.00715. PubMed PMID: 30026697; PMCID: PMC6041399.
248. Messoussi A, Feneyrolles C, Bros A, Deroide A, Dayde-Cazals B, Cheve G, Van Hijfte N, Fauvel B, Bougrin K, Yasri A. Recent progress in the design, study, and development of c-Jun N-terminal kinase inhibitors as anticancer agents. Chem Biol. 2014;21(11):1433-43. Epub 2014/12/03. doi: 10.1016/j.chembiol.2014.09.007. PubMed PMID: 25442375.
249. Simpson ER. Sources of estrogen and their importance. The Journal of Steroid Biochemistry and Molecular Biology. 2003;86(3-5):225-30. doi: 10.1016/s0960-0760(03)00360-1.

VITA

Shannon Christine Kelly was born March 27, 1991, in Saint Louis, Missouri. After growing up in Saint Peters, Missouri, Shannon attended Furman University in Greenville, South Carolina where she graduated cum laude with a Bachelor of Science degree in Biology. While at Furman, she conducted organic chemistry research with Dr. Greg Springsteen. Following graduation, she was an administrative assistant at Greenwood Genetic center handling the appointment schedule and insurance claims. After ten months, Shannon re-located back to the Saint Louis area after accepting a position at Washington University School of Medicine in St. Louis as a research technician in the Nutritional Science department under the supervision of Dr. Jun Yoshino. In 2016, Shannon began her graduate education at Saint Louis University studying muscle physiology in the laboratory of Dr. Jon Fisher. She graduated with a Master of Science degree in Biology in May 2018. Shannon then relocated to Columbia, MO to complete her doctoral degree in Biomedical Science in the laboratory of Dr. Craig Emter where she is studying cardiac remodeling in swine models of heart failure. She is in anticipation of a Doctor of Philosophy degree in Biomedical Science in July 2022.